

Middlesex University Research Repository:

an open access repository of
Middlesex University research

<http://eprints.mdx.ac.uk>

Lewis, Jeremy, 1996.
A steady state tip control strategy for long reach robots.
Available from Middlesex University's Research Repository.

Copyright:

Middlesex University Research Repository makes the University's research available electronically.

Copyright and moral rights to this thesis/research project are retained by the author and/or other copyright owners. The work is supplied on the understanding that any use for commercial gain is strictly forbidden. A copy may be downloaded for personal, non-commercial, research or study without prior permission and without charge. Any use of the thesis/research project for private study or research must be properly acknowledged with reference to the work's full bibliographic details.

This thesis/research project may not be reproduced in any format or medium, or extensive quotations taken from it, or its content changed in any way, without first obtaining permission in writing from the copyright holder(s).

If you believe that any material held in the repository infringes copyright law, please contact the Repository Team at Middlesex University via the following email address:

eprints@mdx.ac.uk

The item will be removed from the repository while any claim is being investigated.

MX 9901226 X



A Steady State Tip Control Strategy for Long Reach Robots

*Thesis submitted to Middlesex University in partial fulfilment
of the requirements for the degree of Doctor of Philosophy*



Jeremy Lewis BSc, MSc, PGCE

*School of Mechanical and Manufacturing Engineering
Middlesex University
London*

January 1996

Sore Christa

ABSTRACT

The work presented in this thesis describes the development of a novel strategy for the steady state tip position control of a single link flexible robot arm. Control is based upon a master/slave relationship. Arm trajectory is defined by through 'master' positioning head which moves a laser through a programmed path. Tip position is detected by an optical system which produces an error signal proportional to the displacement of the tip from the demand laser spot position. The error signal and its derivative form inputs to the arm 'slave' controller so enabling direct tip control with simultaneous correction for arm bending. Trajectory definition is not model-based as it is defined optically through movement of the positioning head alone.

A critical investigation of vacuum tube and solid state sensing methods is undertaken leading to the development of a photodiode quadrant detector beam tracking system. The effect of varying the incident light parameters on the beam tracker performance are examined from which the optimum illumination characteristics are determined.

Operational testing of the system on a dual-axis prototype robot using the purpose-built beam tracker has shown that successful steady state tip control can be achieved through a PD based slave controller. Errors of less than 0.05 mm and settling times of 0.2 s are obtained. These results compare favourably with those for the model-based tip position correction strategies where tracking errors of ± 0.6 mm are recorded.

Table of Contents

Abstract	i
Acknowledgements	viii
Table of Figures	ix
List of Symbols	xviii
Glossary of Terms	xix

Chapter 1 Introduction

1.1	Robot Deficiencies	1
1.2	Robot Requirements	4
1.3	Potential Solutions	5
	1.3.1 Flexible Arms	5
	1.3.1.2 <i>Implementation difficulties</i>	6
	1.3.2 Flexible Arm Control	6
	1.3.3 Control System Requirements	7
1.4	The Novel Flexible Arm Control Concept	9
	1.4.1 Principle of Operation	10
	1.4.2 The Master Position Control System	11
	1.4.3 The Arm Slave Position Control System	12
	1.4.3.1 <i>Beam tracking</i>	12
	1.4.3.2 <i>Deflection compensation</i>	13
	1.4.4 Additional Systems	13
1.5	Research Aims and Objectives	14
1.6	Proposed System Advantages and its Applications	14
	Declaration	16
	Summary	16
	References	18

Chapter 2 A Review of Optically Based Arm Position Correction Methods

2.1	Introduction	21
2.2	Post-Correction for Bending Errors - Micromanipulators	22
	Micromanipulators - Summary	29
2.3	Systems to Maintain Arm Tip Position	30
2.3.1	Active Stiffness Control	31
2.3.2	Active Position Correction	34
	2.3.2.1 <i>Link local deflection measurements</i>	35
	2.3.2.2 <i>Direct end-point deflection measurement</i>	37
2.4	Direct End-point Position Control Systems	42
2.4.1	Remotely Positioned Control Systems	43
2.4.2	Internally Positioned Systems	51
	Summary	56
	References	59

Chapter 3 Robot Construction

3.1	Introduction	62
3.2	Description	63
3.2.1	The Endoskeleton	64
	3.2.1.1 <i>Resolution, accuracy and repeatability</i>	67
	3.2.1.2 <i>Improvements to the positioning head elevation monitoring system</i>	68
3.2.2	The Exoskeleton	69
3.2.3	Prototype Limitations	71
3.3	The Dual-Axis, Single Link Robot	71
3.3.1	Endoskeleton Modifications	71
	3.3.1.1 <i>The mirror galvanometer positioning head</i>	73
	3.3.1.2 <i>The DC servomotor driven positioning head</i>	74
	3.3.1.3 <i>The stepper motor driven dual-axis positioning head</i>	75

3.3.1.4	<i>Positioning head performance testing</i>	76
3.3.2	Exoskeleton Modifications	80
3.4	Arm Joints	81
3.5	Revolute Joints - Designs and Operating Principles	81
3.5.1	Multiple Laser/Sensor Combinations	82
3.5.2	Single Laser Designs	82
3.5.2.1	<i>An 'in-line' joint using fibre optics</i>	82
3.5.2.2	<i>An 'in-line' joint using a beam splitting cube</i>	83
3.5.2.3	<i>The 'off-set' revolute joint</i>	87
3.5.3	The Prismatic Joint	89
	Summary	90
	References	91

Chapter 4 The Design and Development of the Beam Tracking System

4.1	Introduction	92
4.2	A Comparison of Position Detecting Devices	92
4.2.1	Vacuum Tube Devices	92
4.2.2	Silicon Photodiodes	94
4.2.2.1	<i>Multi-element arrays</i>	94
4.2.2.2	<i>Position sensing photodetectors</i>	95
4.3	Beam Tracker Design Specifications	100
4.3.1	The Photodiode Position Detecting Sensor Used	101
4.3.2	Important Considerations when using Photodiodes	101
4.4	The Linescan Camera Based Beam Tracker	103
4.4.1	Requirements	103
4.4.2	Camera Description and Position Monitoring Sensitivity	104
4.4.3	Camera Operation for Beam Tracking	105
4.4.4	The Camera Output Signals and Signal Conditioning Circuitry	106
4.4.5	Disadvantages Associated with using the Linescan Camera	109
4.5	Dual-Axis, Quadrant Detector Based Beam Tracker	110
4.5.1	Construction	110
4.5.2	The Detector	111

4.5.3	Coarse/Fine Position Detecting Beam Tracker	111
4.5.4	Coarse/Fine Detector Spacing	115
4.6	Beam Tracker Miniaturisation	115
4.6.1	Construction Details	116
	Summary	117
	References	119

Chapter 5 Beam Tracker Performance

5.1	Introduction	121
5.2	Test Apparatus and Methodology	121
5.3	Results	123
5.3.1	The Quadrant Detector Dual-Axis Beam Tracker - Theoretical Performance	123
5.3.2	Performance Testing - Experimental	124
5.3.3	A Comparison of Theoretical and Experimental Results	125
5.3.4	Light Intensity Effects	125
5.3.5	The Effect of Light Spot Size	128
5.3.6	The Effect of Light Source Distance	129
5.3.7	Spectral Matching	129
5.3.8	The Effect of Spot Shape	130
5.4	Light Source Improvements	131
5.5	Quadrant Detector and Bi-Cell Beam Trackers	134
5.5.1	A Comparison of Quadrant Detector and Bi-Cell Performance	134
	Summary	135
	References	137

Chapter 6 Control Methods and Results

6.1	Introduction	138
6.2	The 'Proof of Concept' Robot	138
6.2.1	Robot Performance	140
6.2.2	Performance Analysis	143

6.3	The Improved Single-Axis Robot	145
6.3.1	Direct Analogue Proportional Control	145
6.3.2	PD Control	148
6.3.3	PID Control	149
6.4	The Improved Prototype - Performance	151
6.4.1	PID Performance	151
6.4.2	PD Performance	153
6.4.3	A Comparison of PID and PD Tracking Performance	154
6.4.4	The Improved Robot - Summary	155
6.5	The Dual-Axis Robot	156
6.5.1	Control System Hardware	156
6.6	Step Response Tests	158
6.6.1	PDF Control	158
6.6.2	Step Response - Implementation	159
6.6.3	Step Response - Conclusions	163
6.7	Simulation	166
6.7.1	Simulation Results	168
6.8	Operational Performance	171
6.8.1	Deflection Compensation	172
6.8.2	Tracking Response	176
	6.8.2.1 <i>Tracking response - squares</i>	177
	6.8.2.2 <i>Tracking response - circles</i>	179
6.8.3	Tracking Results - Analysis	183
	Summary	185
	References	186

Chapter 7 Conclusions

7.1	The Tip Position Control Strategy	188
7.2	Robot Design and Construction	189
7.3	The Beam Tracking Systems	190
7.4	Robot Performance Testing	190
	Summary	191

Chapter 8 Future Work

8.1	Mechanical Modifications	192
8.2	Optical System Improvement	192
8.3	Slave Controller Development	194
8.4	Tip Six Degree of Freedom Measurement	194
8.4.1	Z-Axis Rotation	195
8.4.2	X and Y Axis Rotations	196
8.4.3	Z-Axis Extension	197
8.4.4	Simultaneous Six Degree of Freedom Measurement	198
	Summary	200
	References	201

Appendices

A	Mechanical Inaccuracies in Robots	202
B	The DC Motor Driven Positioning Head Circuitry	203
B	The Stepper Motor Driven Positioning Head Program	204
C	The Fast Laser Tracking/Deflection Compensation Program for Operating the Linescan Camera as a Beam Tracker	209
	The Linescan Camera/Computer Interfacing Electronics	210
	(1) The Clock Pulse Spreader Circuit	210
	(2) The Camera Signal Squaring/TTL Conversion Circuit	211
D	The Beam Tracker Performance Testing Apparatus	212
	(1) The Interferometer/PC Interfacing Electronics	212
	(2) The Interfacing Software	213
	(3) The Beam Tracker to Lab-PC Plus Attenuating Circuits	217
E	The Modified Single Axis Robot - Slave Control Software	218
F	The Dual-Axis Robot Slave Control Algorithms	224
	(1) Matlab simulation programs	229
G	Published Work	231
	'Heavy load robot', Industrial Robot, Vol.19, No.4, 1992	228

Acknowledgements

I would like to thank my Director of Studies, Dr R.Gill and my supervisor, Mr A.S.White, for their advice and guidance during the course of this research. Other members of the staff who have willingly and consistently helped me are Dr M.Karamanoglu, Dr S.D.Prior and Dr M.Stoker.

Very many thanks for the support and assistance given me by my fellow researchers in the Advanced Manufacturing and Mechatronics Centre at Middlesex University - Mr J.S.Surdhar, Mr J.Valls-Miro, Mr S.Okrongli, Mr B.Parsons and Mr A.Lasebe.

Worthy of special mention are my good friends Mr J.Korhonen and Mr A.G.Scott. Without their consistent enthusiasm, progress on this project would have been considerably slower.

I am grateful to the Mechanical Engineering workshop team - Mr C.Ablett, Mr P.Burn, Mr R.Brick and Mr N.Salam - for their excellent tuition and help during the many hours I spent in the workshop. I would also like to thank the other technicians within the Faculty - Mr I.Siman, Mr I. Bhaiji and Mr C.Cardozo - for all their help.

Thanks to British Nuclear Fuels plc for funding the purchase of the robot actuators and for their continued interest in pursuing this research in the future.

Table of Figures

Chapter 1 Introduction

Figure 1.1 -	The effect on positioning accuracy of load-induced arm deformation	2
Figure 1.2 -	Payload-to-weight ratios of industrial robots	3
Figure 1.3 -	The inertia handling capacity of electrically and hydraulically driven robots	4
Figure 1.4 -	Schematic diagram of conventional robot control system - actuator and position sensor collocated at arm hub	7
Figure 1.5 -	Schematic diagram of non-collocated control scheme with tip position sensing	8
Figure 1.6 -	Schematic diagram showing the operating principle of the optical tip sensing strategy	10
Figure 1.7 -	The control system 'master/slave' relationship	11
Figure 1.8 -	Schematic diagram illustrating the beam tracking component of the optical tip sensing system	12

Chapter 2 A Review of Optically Based Arm Position Correction Methods

Figure 2.1 -	An overview of methods using optical systems for the correction of positioning errors in flexible link robots	21
Figure 2.2 -	The macro/micro manipulator concept	23
Figure 2.3 -	Response of macro/micro manipulator to step position command	24
Figure 2.4 -	The experimental micromanipulator wrist	25
Figure 2.5 -	Step response with (a) collocated sensor for hub motor control, (b) with lead compensator and (c) with position and rate feedback	26
Figure 2.6 -	The dual-axis micromanipulator positioning system	27

Figure 2.7 -	The horizontal transverse deflections at the end of the beam and at the gripper in response to RBC and MMC	28
Figure 2.8 -	Active feedback control for flexible link robots	30
Figure 2.9 -	Schematic diagram of the twin beam link with active hydraulic 'straightness servo'	31
Figure 2.10 -	Schematic diagram of the apparatus for the active correction of link horizontal deflections	33
Figure 2.11 -	Effect of retroreflector rotation on the reflected laser beam position	34
Figure 2.12 -	Arm deflection detection system	35
Figure 2.13 -	Schematic diagram showing the laser beam path	36
Figure 2.14 -	Block diagram of the control system	36
Figure 2.15 -	Method for determining three end-point deformations along a flexible link	38
Figure 2.16 -	Schematic diagram of apparatus used for the correction of horizontal link end-point deflections	39
Figure 2.17 -	The adaptive control system	39
Figure 2.18 -	Time response of the flexible arm (a) without and (b) with end-point position stabilisation	40
Figure 2.19 -	The single axis link end-point deflection measurement system	40
Figure 2.20 -	Block diagram of the control system with active compensating controller	41
Figure 2.21 -	Experimental tracking control results (a) with and (b) without end-point position correction	42
Figure 2.22 -	The experimental end-point optical control system	43
Figure 2.23 -	Block diagram of the overall control system	44
Figure 2.24 -	The measured arm response to a step-command tip position of 10 cm	44
Figure 2.25 -	The Lasertrace robot performance testing apparatus	45
Figure 2.26 -	End-point position tracking	46

Figure 2.27 - Functional architecture of the manipulator tip stabilisation system	46
Figure 2.28 - 3-D tip position measurement system	48
Figure 2.29 - Flexible link control scheme	48
Figure 2.30 - X-Y tip coordinate errors for following trajectory under encoder based control	49
Figure 2.31 - Error in X-Y tip position	50
Figure 2.32 - Errors for X-Y tip position under Jacobian control	50
Figure 2.33 - Schematic diagram of the 5-axis optical end-point position orientation and measurement system	51
Figure 2.34 - Link structural deflections	52
Figure 2.35 - Horizontal displacement tracking error signals	53
Figure 2.36 - The twin gimbal laser tracking system	54
Figure 2.37 - The beam angle detecting system	55
Figure 2.38 - Controller configuration	55

Chapter 3 Robot Construction

Figure 3.1 - The initial experimental prototype	63
Figure 3.2 - Frequency response measurement of the endoskeleton column	64
Figure 3.3 - Frequency response of the endoskeleton column as measured with the column fixed within the exoskeleton frame	65
Figure 3.4 - Details of the positioning head	65
Figure 3.5 - Schematic diagram showing positioning head operation	66
Figure 3.6 - The modified positioning head with optical encoder	69
Figure 3.7 - Frequency response measurement of the Perspex arm	70
Figure 3.8 - Controllable current source motor power amplifier	70
Figure 3.9 - Front view of the dual-axis robot	72

Figure 3.10 - Details of the dual axis mirror galvanometer positioning head	73
Figure 3.11 - The original positioning head modified for dual-axis operation	74
Figure 3.12 - Velocity command versus actual velocity for the dual axis DC motor driven positioning head	74
Figure 3.13 - An exploded view of the stepper motor dual-axis positioning head	76
Figure 3.14 - Undamped and damped positioning head performance	77
Figure 3.15 - Step response with both friction dampers and low-pass filters	78
Figure 3.16 - Scatter graph showing the repeatability and accuracy of the stepper motor driven dual-axis positioning head	79
Figure 3.17 - Schematic diagram of the laser/detector combination revolute joint	82
Figure 3.18 - Details of the in-line fibre optic joint	83
Figure 3.19 - Details of joint design using a beam splitting cube	84
Figure 3.20 - Displacement of the deflected beam caused by vertical movement of the beam splitting cube	85
Figure 3.21 - The major axes about which twist occurs	86
Figure 3.22 - Details of the 270° off-set revolute joint using mirrors	87
Figure 3.23 - Details of the 360° off-set revolute joint	88
Figure 3.24 - Schematic diagram showing prismatic joint details	89
 Chapter 4 The Design and Development of the Beam Tracking System	
Figure 4.1 - Schematic of 'Optron' displacement tube showing single axis position monitoring system	93
Figure 4.2 - Quadrant detector electrical connector locations and formulae	96
Figure 4.3 - Duo-lateral and tetra-lateral configurations of lateral effect photodiodes	97
Figure 4.4 - Lateral-effect detector electrical connector locations and formulae	98
Figure 4.5 - Spatial variation of photodiode detector output	102

Figure 4.6 - Shift of the video output relative to the clock pulse as the laser beam is scanned across the array	105
Figure 4.7 - A typical camera output waveform	106
Figure 4.8 - The camera clock output pulses	106
Figure 4.9 - The stretched clock output pulse	107
Figure 4.10 - The camera video output using the laser beam as a light source	108
Figure 4.11 - The modified video output	108
Figure 4.12 - The laser spot intensity profile	109
Figure 4.13 - Construction details	110
Figure 4.14 - Principle of fine control operation	112
Figure 4.15 - Linearity plot for PIN photodiode	112
Figure 4.16 - Schematic of 'centroid' position sensing electronics	113
Figure 4.17 - Coarse position control ring	114
Figure 4.18 - Coarse positioning electronics	114
Figure 4.19 - Schematic of simplified position detecting electronics	115
Figure 4.20 - Miniature beam tracker construction	116

Chapter 5 Beam Tracker Performance

Figure 5.1 - Apparatus for beam tracker performance analysis	121
Figure 5.2 - Block diagram of the beam tracker performance test system	122
Figure 5.3 - Single-axis transfer function for 10 mm ϕ quadrant detector, 5 mm ϕ light spot	123
Figure 5.4 - The transfer function obtained experimentally for the beam tracker	124
Figure 5.5 - A comparison of theoretical and experimental summed outputs	125
Figure 5.6 - The effect of different intensity illumination on beam tracker performance	126

Figure 5.7 - Output clipping due to photodiode saturation	127
Figure 5.8 - Beam tracker output with and without a neutral density filter	127
Figure 5.9 - Outputs for spot diameters of 5 and 7.5 mm	128
Figure 5.10 - Comparison of simulated sensor outputs with different spot diameters	129
Figure 5.11 - The normalised spectral response of the quadrant detector compared with wavelength of laser light used showing good spectral match	130
Figure 5.12 - The laser diode spot profile	130
Figure 5.13 - Beam tracker output as the laser diode beam was scanned horizontally across the detector with the slit in both the horizontal and vertical positions	131
Figure 5.14 - The output from the beam tracker using the variable focus laser diode - with and without the No 1 neutral density filter	132
Figure 5.15 - Simulated beam tracker output for a square and circular spot	133
Figure 5.16 - Beam tracker outputs for diffused and undiffused filtered spots - exploded view of central region only	133
Figure 5.17 - Theoretical quadrant detector and bi-cell performance	134
Figure 5.18 - Recorded quadrant detector and bi-cell outputs	135

Chapter 6 Control Methods and Results

Figure 6.1 - Generalised block diagram of the slave control system	138
Figure 6.2 - Proportional position control with linescan camera sensor	139
Figure 6.3 - Errors recorded on the addition of a 0.5 kg load to the tip of the stationary arm	140
Figure 6.4 - The error signal for low and high speed beam tracking	142
Figure 6.5 - Direct analogue proportional control through the new beam tracker	145
Figure 6.6 - Accuracy tests with a 2.5 m arm under analogue proportional control	146

Figure 6.7 - Beam tracker output verses load for the uncontrolled arm	147
Figure 6.8 - Block diagram of the modified robot position control system	148
Figure 6.9 - PD control	149
Figure 6.10 - PID control	150
Figure 6.11 - PID controller performance showing the lag of the control signal (stepped line) behind the demand signal at high k_d values	152
Figure 6.12 - PID controller-induced arm oscillation at high k_i values	152
Figure 6.13 - PD control - the control signal following the demand to ± 50 mV	153
Figure 6.14 - Steady-state error recorded at arm tip for PD control	154
Figure 6.15 - Unstable PID control response - arm tracking the moving laser	154
Figure 6.16 - PD control	155
Figure 6.17 - Unfiltered and filtered error and control signals	157
Figure 6.18 - PDF control	158
Figure 6.19 - Linear solenoid step showing excessive oscillations	160
Figure 6.20 - Slave response to step input - proportional control	161
Figure 6.21 - Slave response to step input - PD control	162
Figure 6.22 - Comparison of step response with PID and PDF control	163
Figure 6.23 - Simulated tip responses for P, PD, PID and PDF controllers	165
Figure 6.24 - The block diagram for the rigid arm system with tip feedback based control	166
Figure 6.25 - Simulated step response, $J_{\text{eff}} = 0.492$ and $\mu_{\text{eff}} = 0.39$, proportional control	169
Figure 6.26 - Simulated step response at $J_{\text{eff}} = 3$, proportional control	169
Figure 6.27 - Step response simulation, $k_d = 0.002$, PD control	170
Figure 6.28 - Step response simulation, $k_d = 0.002$, $J_{\text{eff}} = 4$, PD control	170
Figure 6.29 - Beam tracker output against laser positioning steps - 6 mm ϕ light spot	171

Figure 6.30 - Tip error in response to sudden release of a 4.2 kg load	172
Figure 6.31 - Error and control signals with small integral contribution	173
Figure 6.32 - Beam tracker tip position errors for gradual weight reduction with and without control	175
Figure 6.33 - Tracking response with and without integral control	176
Figure 6.34 - Tracking response at hub and tip for a 30° x 30° square	177
Figure 6.35 - Superimposed hub and tip angular positions - 10 data points	178
Figure 6.36 - Tracking response at hub and tip for a 3.5° circle	179
Figure 6.37 - Superimposed hub and tip angular positions for 3.5° circle - half circle shown for clarity	180
Figure 6.38 - Hub and tip positions superimposed for a section of the 3.5° circle	181
Figure 6.39 - Tracking response at hub and tip for a 17° circle	181
Figure 6.40 - Hub and tip positions superimposed - 100 data points	182
Figure 6.41 - Gearbox vibrations detected at the beam tracker	184

Chapter 8 Future work

Figure 8.1 - The six degrees of freedom of the point defined in space	194
Figure 8.2 - Apparatus to measure twist about the Z axis	195
Figure 8.3 - Proposed apparatus for simultaneous X and Y axis twist measurement	196
Figure 8.4 - Details of the astigmatic distance measuring system	198
Figure 8.5 - Proposed modification to the positioning head required to establish tip position in terms of six degrees of freedom	199
Figure 8.6 - The complete six degrees of freedom position detection system	199

Appendices

Figure A.1 - The DC motor driven positioning head circuitry	203
Figure A.2 - The clock pulse spreader circuit	210
Figure A.3 - The camera signal squaring/TTL conversion circuit	211
Figure A.4 - The 74AS151 multiplexer	212
Figure A.5 - Block diagram of the interferometer/PC interfacing circuitry	213
Figure A.6 - The beam tracker to Lab-PC Plus attenuating circuitry	217

List of Symbols

θ	Joint angle
θ_{ref}	Hub demand angle (polar coordinates)
x, y_{ref}	Demand tip position (Cartesian coordinates)
x, y	Tip position (Cartesian coordinates)
u	Control signal
k_p	Proportional constant
e	Error signal
θ''	Tip feedback parameter (beam tracker error signal)
k_i	Integral constant
k_d	Derivative constant
θ_d	Base joint desired angular displacement
T	Motor torque
J	Inertia
F	Friction
ϕ	Diameter
μ_{eff}	Effective friction
J_{eff}	Effective inertia
R	Motor armature resistance
k_A	Amplifier gain
k_t	Motor torque constant
k_{bemf}	Motor back EMF
N	Gearbox ratio

Glossary of Terms

BCD - Binary coded decimal

CAT - Combined actuator/transducer

CCD - Charge coupled device

DC - Direct current

DIN - Deutsche Industrie Norm

DMA - Direct memory access

Ga-As - Gallium arsenide

He-Ne - Helium/Neon

IR - Infra red

LED - Light emitting diode

LQG - Linear quadratic Gaussian

MMC - Micromanipulator controller

NC - Numerical control

P - Proportional control

PCB - Printed circuit board

PD - Proportional derivative control

PDF - Pseudo-derivative control

PID - Proportional, integral and derivative control

PIN - P-type, Intrinsic region, N-type photodiode

PSD - Position sensitive detector

PWM - Pulse-width modulated

RBC - Rigid body controller

RFMC - Rigid and flexible motion controller

Chapter 1

INTRODUCTION

The Robotic Industries Association of America (1974) defines a robot as "A reprogrammable, multi-functional manipulator designed to move material, parts, tools, or specialised devices through variable programmed motions for the performance of a variety of tasks". Programmable robotics were first developed in the 1950's by G.C. Devol and J.F. Engelberger leading to the first industrial robot, introduced by Unimation Inc in 1959.

Robots have evolved from machine tools. A key characteristic of these machines is that they are built to hold their position regardless of the forces applied to them. This is achieved by constructing the axis slides from strong carriages, layered one on top of the other, on a massive bed.

Unlike a machine tool, a robot arm consists of a *serial* arrangement of movable links and joints, the linked structure providing the wide range of motion characteristics required. In current robot control practice, to simplify the controller design, the joint angle sensors and actuators are collocated within the joint mechanisms at the unloaded side of the joints. Absolute end-effector position and orientation is then calculated using coordinate transformations from the set of joint angle measurements. High repeatability is based upon the assumption that, as with a machine tool, both the links and joints are rigid from a control view-point. As a result, one of the major limitations of this type of conventional hardware wired control system is that it is unable to detect, measure or account for any unpredictable behaviour 'downstream' of the sensors.

1.1 ROBOT DEFICIENCIES

The arm is invariably the longest part of a robot and it is the serial arrangement of the links and joints that produces a structure that is inherently low in stiffness. When large, long-reach arms are used to manipulate heavy payloads, end-point positioning accuracy is found to deteriorate rapidly as the limit of lifting capacity is approached, restricting

applications to tasks that are error tolerant or where passive compliant elements can be used to correct for errors (Sharon and Hardt, 1984). This lack of accuracy is due to the manner in which the position feedback is derived, the inability of the controller to account for deformation of the robot structure, cumulative play in the arm joints due to gear backlash, poor actuator servo resolution and thermal expansion.

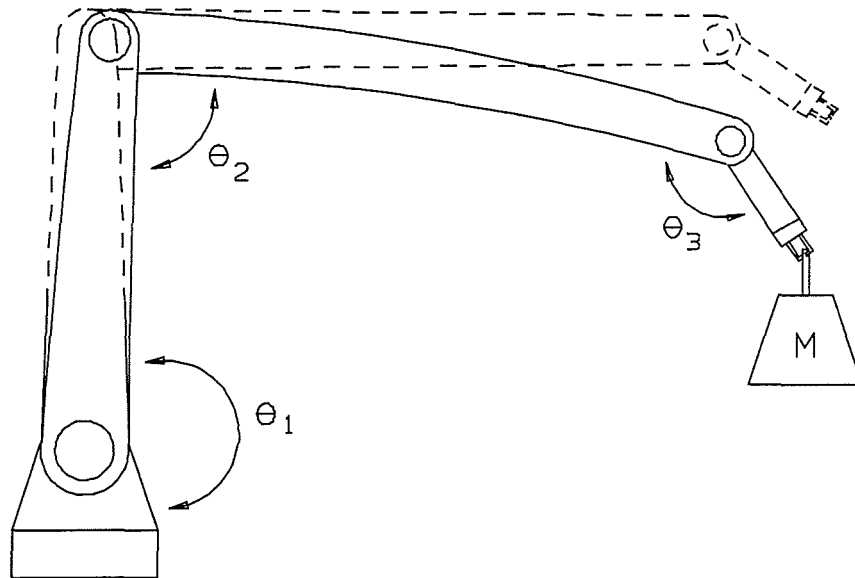


Figure 1.1 - The effect on positioning accuracy of load-induced arm deformation
- (Zalucky and Hardt, 1984)

Even in cases where the joints, position encoders and actuators are perfectly accurate and stiff to torque disturbances, the errors incurred through unmeasured link bending become greatly amplified through the link chain (Becquet, 1989), resulting in severe end-point positioning inaccuracies for both static and dynamic behaviour (see figure 1.1).

The effective payload capacity and arm reach of conventionally controlled robots is therefore limited by the flexibility of the links. Only with short reach arms carrying small payloads does the weight of the arm not cause significant positioning errors. Hence most robots used for industrial pick and place operations possess only a limited arm reach and can handle only small payloads of about 5 kg (Andeen, 1988).

Increasing link stiffness through design optimisation is not regarded as a satisfactory solution as it results in robots with massive arm sections (Harashima and Ueshiba, 1989). Fast manipulation requires extremely high torques. Arm weight introduces limitations in terms of speed, energy consumption, manoeuvrability and positioning accuracy resulting in a 'sloppy NC machine' (Zalucky and Hardt, 1984). Arm weight and stiffness are inversely related to the bandwidth and range of movement, accuracy is inversely proportional to the speed of robot movement (Driessen, 1988).

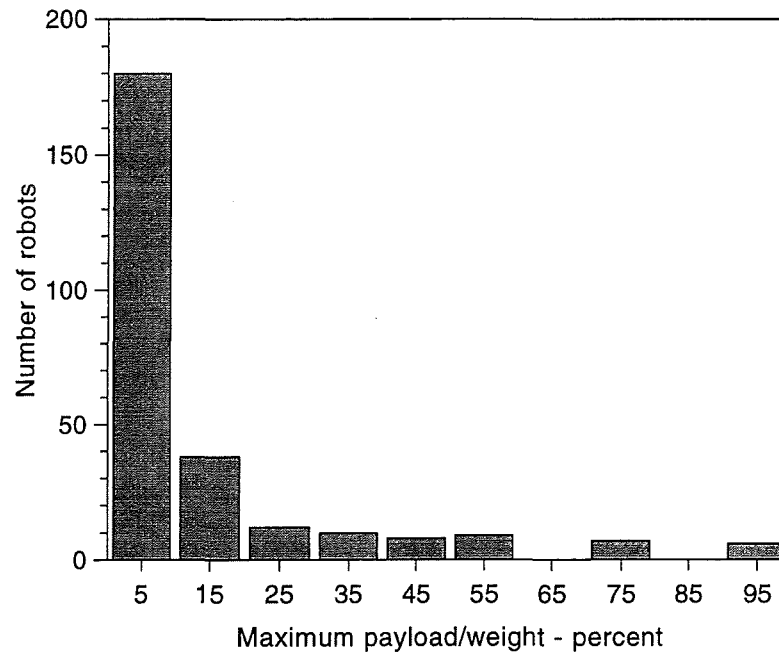


Figure 1.2 - Payload-to-weight ratios of industrial robots - (Andeen, 1988)

Present manipulators have low payload/weight ratios (see figure 1.2). Regardless of size, most manipulators fall in the less-than-10-percent category, i.e. they handle a payload that is small compared to their weight (Andeen, 1988). These low payload/weight ratios lead to robots that are expensive and heavy. These negative features have limited the use of robots to the factory environment, where they can be fed work regularly while being set on substantial foundations and isolated from human beings.

When choosing a robot for a particular application, arm inertia is found to be one of the most significant factors (see figure 1.3). Dynamic positioning errors increase significantly with extra load due to the inertia of the robot under acceleration and deceleration causing overshoot.

As an example, a large electric robot with a lifting capacity of 60 kg and a reach of 2.3 m (payload inertia of 317 kg m²) has a precision of 0.1 mm, together with a maximum speed of 3 m/s. At present, the application of heavy payload robots is restricted to situations where precision and high speed are not required.

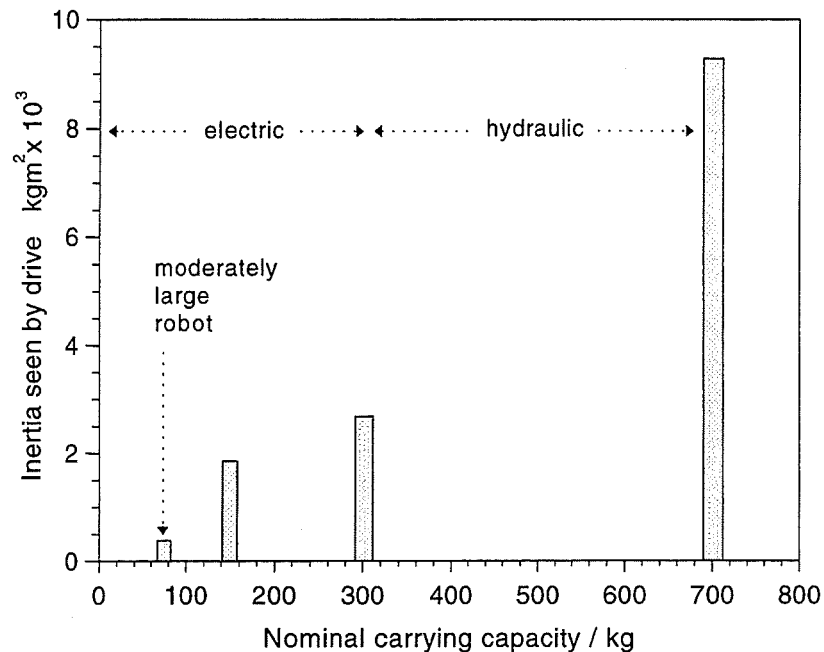


Figure 1.3 - The inertia handling capacity of electrically and hydraulically driven robots - (Walker, 1984)

1.2 ROBOT REQUIREMENTS

To broaden the scope of robot applications, new, highly versatile designs are required that can perform a variety of tasks, in uncertain environments, outside of the stable and predictable conditions found in a factory. To fulfil these requirements, robots must be designed to meet a set of demanding and difficult to achieve operating specifications. These main attributes are listed below.

- High payload capabilities
- Long reach
- Short dynamic response times
- Low energy consumption

- Light weight links
- High accuracy - the difference between the measured and command value of a specified position in the robot's workspace.
- Low inertia
- High acceleration
- Good repeatability - a *measure of the spread of positions* in a series of attempts to position the manipulator at a fixed location.
- Increased operational safety
- Low construction and maintenance costs

1.3 POTENTIAL SOLUTIONS

To increase arm reach and payload capacity, systems must therefore be devised that can give high end-point positioning accuracy whilst keeping arm weight to a minimum. Two approaches have been explored.

- Mechanical solutions in which link rigidity is maximised along with methods to accommodate for positioning errors - the reader is referred to the references listed in Appendix A.
- Mechatronic solutions in which link flexing is accepted and new control strategies are developed using end-point position sensing to correct for, or to directly control, arm bending.

Mechatronic strategies are those "which give appropriate integrated combinations of mechanical engineering, electronics and software applied to the design development and manufacture of a product to provide an optimum design solution" (Preston, 1989).

1.3.1 Flexible Arms

The use of flexible arm robots provides a potential solution, enabling the development of high speed, light weight, high payload precision manipulators with long reach (Usoro *et al*, 1984). Flexible arms have slender links which are considerably more rigid in compression than in flexure and therefore require less material, have less arm weight,

consume less power and are more manoeuvrable than traditional rigid arm manipulators. Furthermore, with the lower torque demand, smaller actuators can be used. Also the reduced arm weight and smaller manipulators lead to lower overall cost and less bulky design. Additionally, reduced weight enhances transportability, the robot could be moved around easily and set up at different locations, being particularly advantageous in small batch manufacturing.

1.3.1.2 *Implementation difficulties*

In spite of the potential advantages, flexible manipulators have not been much favoured in production industries. The use of lightweight, flexible arms is hindered by poor end-effector positioning accuracy since arm deflections affect position and orientation.

Reducing arm weight reduces rigidity even when advanced materials are used for construction and stiffness is enhanced by optimising the structural design (Kiderzynski, 1986). Whatever the design, structural flexibility is introduced, becoming more pronounced as arm length and payload are increased, producing the major source of inaccuracies in flexible manipulators. With a flexible robot arm, the position and attitude of the end-effector largely depends upon both link and joint elastic displacement.

Position accuracy is further deteriorated when the deformation is oscillatory. Traditionally, vibration effects have been reduced by increasing arm rigidity so that, for a constant damping ratio, vibrations die away more quickly. This solution is not available in the case of flexible manipulators if their basic advantages are not to be sacrificed.

1.3.2 Flexible Arm Control

The characteristics of flexible arm motion are far more complex than those of rigid arms (Uchiyama *et al*, 1990). Three major problems are introduced when attempting to control flexible structures

- link vibration suppression,
- accurate joint positioning, and
- compensation for tip displacement caused by gravity link deformation.

Link vibration can be effectively reduced through the use of appropriate control algorithms (White, 1991). The second problem occurs with rigid arms, yet is less severe than for the case of flexible arms as joint positioning and link vibration suppression are coupled. The third problem is not encountered, or is ignored, in potentially 'rigid' structures yet is the major cause of positioning errors in flexible arms.

1.3.3 Control System Requirements

The existence of elastic link deformation creates problems different from those of conventional arms with respect to modelling, control characteristics and control methods (Jiang *et al*, 1989). A major problem is that of controlling arm trajectory while simultaneously accounting for the manipulator characteristics - including structural deformations (Book *et al*, 1975), transmission mechanism inefficiencies and the problems inherent in the manipulator design (Book and Majett, 1982). The position controller must be able to suppress link vibration modes and compensate for the positioning errors of the end-effector caused by elastic link deformations (Wang *et al*, 1989).

In conventional systems (see figure 1.4) control is based entirely about the hub or joint of the arm - the error between the desired and actual hub angle being input to the control algorithm. These systems are designed specifically for use on rigid link robots because they do not have the facilities to sense, or correct for, errors caused by static or dynamic arm distortion (Parks and Pak, 1991).

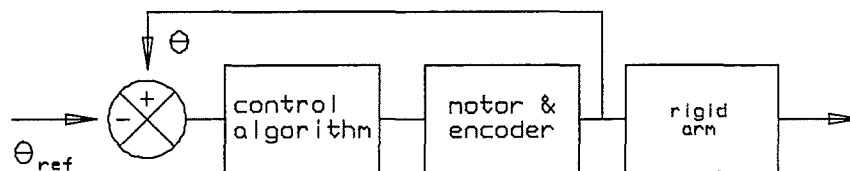


Figure 1.4 - Schematic diagram of conventional robot control system
 - actuator and position sensor collocated at arm hub

The usual control methods for industrial robots are therefore likely to be ineffective and are not applicable (Jiang *et al*, 1989). Control methods must therefore be developed that employ ways of actively determining the extent of link deflections, such as the use of

non-collocated end-point position sensors that can detect not only the position of the end-point, but the orientation as well.

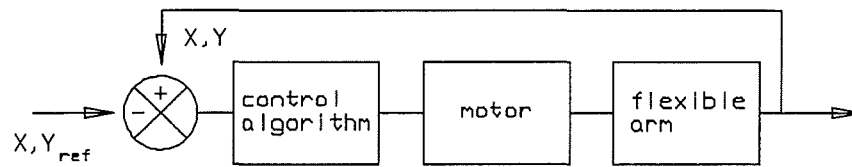


Figure 1.5 - Schematic diagram of non-collocated control scheme with tip position sensing

Externally sited systems measuring dynamically the position of the end-effector are difficult to develop (Cannon and Schmitz, 1984). Problems are introduced as arm vibrations which might destabilise the system, unless very frequent and high accuracy three-dimensional position and orientation measurements can be made over the whole operating volume.

Even if such a measurement system can be perfected, correction of small end-point errors requires the movement of several manipulator actuators. Each actuator must then be capable of handling two different tasks - it must provide high speed and good response or large range motion, whilst at the same time being capable of very accurate positioning for fine motion. This is particularly difficult with a serial link arrangement when the base actuators are located a considerable distance from the end effector.

It is clear that in order to realise the very attractive features of flexible manipulators, extensive research has to be performed in both the areas of design and control of the system (Usoro *et al*, 1984). New control strategies must be developed that provide high end-point stability under all speed and load conditions. These systems must provide the basis for the main operator controlled robot guidance system, provide position correction for load-induced static and dynamic structural deflections and be capable of stabilising the arm's tip by rejecting all unwanted disturbances (Manganas, 1993). Problems caused by low damping need to be addressed as these will have a significant effect on system stability. This will be particularly apparent when the robot changes direction if heavy loads are being manipulated.

The ability to precisely control flexible arms is regarded as an essential step towards the advancement of robotics. To date no truly effective method has been presented to solve it.

1.4 THE NOVEL FLEXIBLE ARM OPTICAL CONTROL CONCEPT

To control the position of flexible manipulators and to compensate for link structural deflections and vibrations, knowledge of the end-point position of the manipulator is desirable (Cannon and Schmitz, 1984). Optical systems for measuring deflections in conventionally controlled robots have been developed (see Chapter 2) but only limited research has been carried out on optically sensed direct end-point control strategies.

The following section describes the novel opto-electronic control strategy (Scott, 1989 and Lewis, 1991) which employs end-point position sensing to directly control overall robot movement. The inherently simple system forms a complete robot position controller, being unique in that it has the potential to define all six degrees of freedom at the end-point of the robot arm through optical means and to correct for mechanical inaccuracies caused by manufacturing imperfections, assembly misalignment, arm and joint flexibility.

The control system, in a global sense, includes trajectory generation, sensing and the method of control used to minimise errors between the desired and actual trajectories of the tip of the arm. The system can be subdivided into four distinct sections.

- A laser positioning system for trajectory generation.
- An optical sensor placed at the tip of the flexible arm for determining the deflection of the arm.
- A control algorithm used to minimise positioning errors between the desired position and the actual position of the arm tip.
- A manipulator system which includes the arm and drive motors.

1.4.1 Principle of Operation

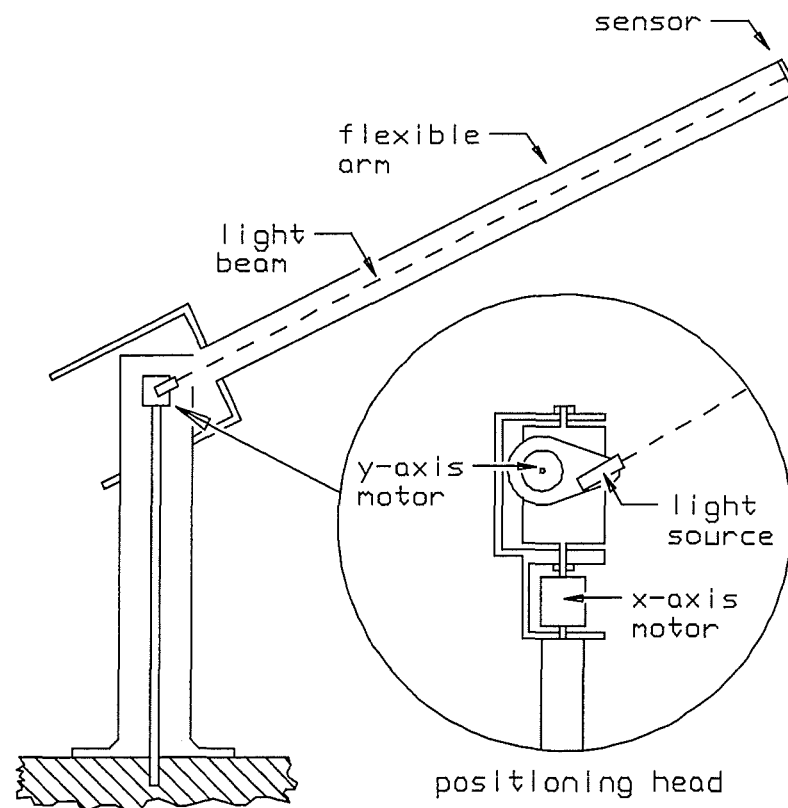


Figure 1.6 - Schematic diagram showing the operating principle of the optical tip sensing strategy

The beam, from a semiconductor laser light source, is directed via a high resolution positioning head along the desired trajectory, the beam passing up the centre of a hollow arm. The positioning head acts as a fixed reference point from which all arm base coordinates are calculated. Thus, the essence of the system is that the path of the light beam is unaffected by loads imposed upon the robot structure, the beam establishes an accurate position to which the end-point of the robot arm will travel. A sensor at the end of the arm detects the location of the light beam and this information is used to direct the arm to track the beam path. Positional accuracy is maintained because the end-point of the arm is always in the desired position when at rest, irrespective of arm deformations caused by varying loads or through flexing in the drive units; automatic deflection compensation is an integral part of the controller design. Both the beam tracking and arm deflection compensation components take place simultaneously.

Control is based upon a master/slave relationship (figure 1.7) between the trajectory defining laser and the hub controlled movement of the arm. Two closed loop systems govern the movement of the robot - an operator controlled master system for arm end-point positioning and orientation and an independent slave system to cause the arm to follow the desired path.

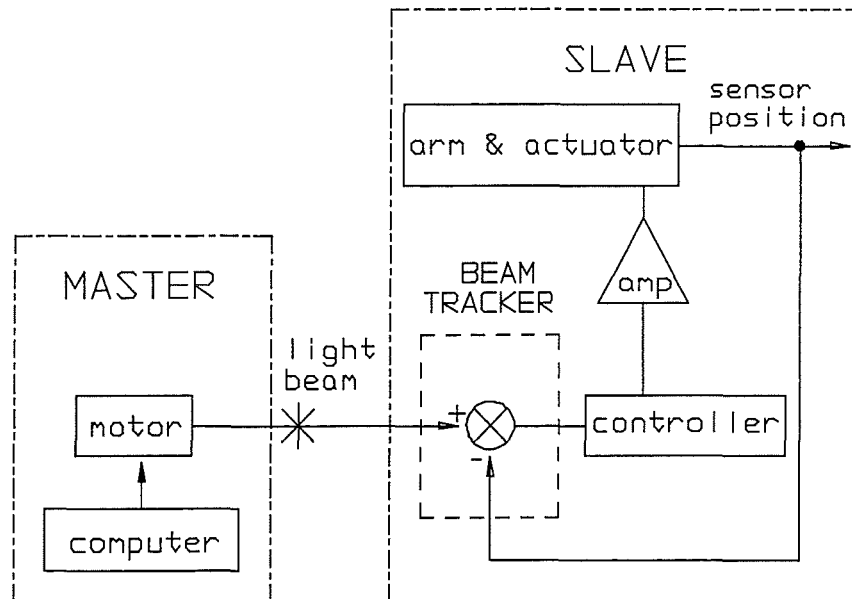


Figure 1.7 - The control system 'master/slave' relationship

1.4.2 The Master Position Control System

The purpose of the master position controller is to define a position in terms of azimuthal and elevational angular coordinates to which the end-point of the robot arm must travel. Desired end-point position is established through a positioning head. A closed loop feedback control system ensures the accuracy of the light beam's azimuth and elevation. The drive motor positions, measured by position encoders, are fed back to the microprocessor so that the actual motor positions can be monitored and adjusted until they coincide with those desired. Hence the robot's path of motion is defined by the master positioning system. The desired position is input into a microprocessor interface and then fed to the positioning head motor driver circuits. The motors direct the light beam according to the programmed position or path.

1.4.3 The Arm Slave Position Control System

Arm position is controlled by a closed loop independent of the master. A dual function optical sensor configuration both registers the position demand signal (for beam tracking) and generates the arm position error signal (for both beam tracking and deflection compensation). Positioning is achieved by the use of an error signal, corresponding to the distance between the centre of the sensor and the centre of the laser spot, which is fed into a controller to cause the hub motors to move the arm in the direction required to minimise the error.

1.4.3.1 Beam tracking

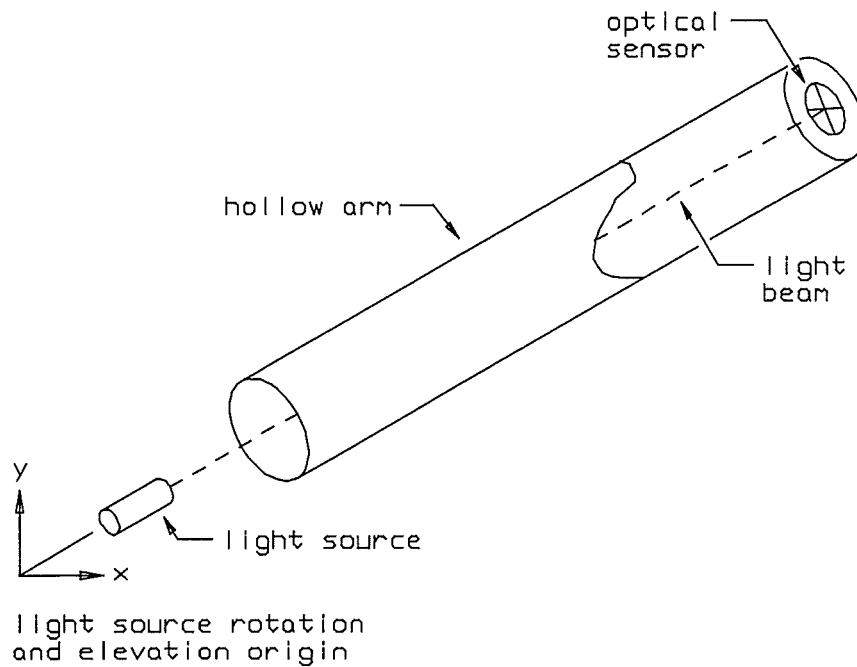


Figure 1.8 - Schematic diagram illustrating the beam tracking component of the optical tip sensing system

The beam emitted from the positioning head passes up inside the hollow arm and impinges upon the sensor at its far end. As the light source trajectory is changed, the sensor registers a tip position error. The optically generated error signal can be used directly in a feedback control loop causing the actuators to move the arm so that the sensor is again centred upon the light spot - the arm therefore slaves to the master controller.

For simple proportional control, the control signal u will be :-

$$u = k_p e \quad (1.1)$$

where the error (e) is defined as :-

$$e = \text{command input} - \theta \quad (1.2)$$

θ is the actual tip angle, corresponding to the *tip position error*, measured at the hub. The error signal is further modified by the inclusion of a second parameter, the *tip deflection control parameter* (θ'') also derived from the sensor output. The error quantity can now be represented as :-

$$e = \text{command input} - (\theta - \theta'') \quad (1.3)$$

Using the tip feedback parameter, the position of the arm tip can be directly accounted for in the control algorithm. The effect of the algorithm is to make corrections at the hub of the arm in response to position errors sensed at the tip. The quantity $(\theta + \theta'')$ may be physically interpreted as the position of the sensor. Tip feedback sensor control differs from encoder based control in that the state of the tip of the flexible arm is encoded in angular coordinates and then used directly in the control loop.

1.4.3.2 Deflection compensation

This is, in effect, the reverse of the beam tracking principle. Loading the arm will cause it to deform, deflecting the centre of the sensor off the light spot. A position error signal is produced that causes the arm to return to its original position.

1.4.4 Additional Systems

An optical distance measuring system is incorporated into the design allowing the length of the arm to be varied, the required extension being controlled so that any flexural extension of the robot is compensated for automatically (see Chapter 3). Methods of detecting and correcting for torque-induced arm twist have been devised which work in conjunction with that used to determine the desired end-point, thus fixing all six degrees of freedom at the end-point (see Chapter 8). Joints have been incorporated into the design to increase the number of degrees of freedom of the robot (see Chapter 3, Section 3.4).

1.5 RESEARCH AIMS AND OBJECTIVES

The aims are to develop and investigate the feasibility and performance of the opto-electronic control system. Research objectives are listed below.

- Investigation of the background literature.
- Prototype robot construction. The identification and development of the control strategy hardware and software systems.
- The design and testing of high performance beam tracking systems.
- The development, construction and testing of revolute and prismatic joints.
- System performance testing using a variety of control algorithms.
- Comparison of results.
- Investigations into methods of optically fixing the end-point position in terms of all six degrees of freedom.
- Recommendations for further work.

1.6 PROPOSED SYSTEM ADVANTAGES AND ITS APPLICATIONS

If successful, it is envisaged that the scope of robot applications will be increased dramatically, restrictions imposed by the necessarily rigid construction of conventional robot links will be lifted as structural flexing will no longer be a problem as far as positional accuracy, reach and payload are concerned. Potential advantages to be derived from the successful implementation of the proposed system are listed below.

- High end-point position stability under all speed and load conditions.
- A reduction in production costs since arm deformation, joint and actuator flexing can be accommodated without loss of accuracy. Specifically this means that less exotic materials can be used together with larger tolerances.
- A high degree of positioning accuracy since the arm will 'self-centre' on the laser beam thus maintaining the desired end-point position, irrespective of payload size - end-point position feedback enables the introduction of artificial stiffening at strategic points along the beam, namely the tip and actuator ends (Cannon and Schmitz, 1984).

- The system will accommodate for arm component assembly misalignment as the arm tip always slaves to the demand laser spot position.
- Providing the system response time is sufficiently fast the problem of overshoot should be significantly reduced.
- An increase in robot operational speeds, payload capacity and arm reach. The robot should be able to actively manipulate varying and cyclic loads.
- As the guidance system is internal to the robot structure it can be protected from all types of environmental damage and interference. The complete control system may be hermetically sealed so that the robot can be employed in hazardous and difficult conditions, e.g. in welding and paint spraying applications where externally mounted optical guidance systems suffer from problems caused by sparks and paint overspray.
- Being lighter, it will be easier to transport. Smaller actuators can be used as the arm inertia is decreased and so energy demand will be reduced.
- Safer operation as the flexibility in the robot structure provides a degree of damage protection during collisions, the control strategy allowing time to respond to the effects of impacts. Lightweight manipulators are also less hazardous since they carry less momentum.
- Widespread application outside of the conventional robotics field.
- Flexibility of installation.
- Modular construction - different links can be inserted for different tasks and repairs can be made more easily.

The robot could be used in applications where the use of manual or tele-operated devices has, up until now, been the norm or where the size and non-uniformity of payloads excludes the use of conventional designs.

The civil engineering and construction industries - research is currently being carried out into the development of robotic arms for lifting and positioning cladding directly onto the sides of high rise buildings (Editor, 1989, and Wanner, 1987).

The process industries - for example, in foundry operations where the ability of the control system to automatically accommodate for varying payloads will enable accurate pouring of molten metal to be carried out safely.

The nuclear industry - provided the electronics are shielded from radiation, this method of control could be used as there are requirements for robots with long reach, high payload capabilities in decommissioning and inspection of reactors.

Space - specifications for space arms are very demanding, requirements include long reach, large payload capabilities, low mass so as to be cost effective to transport, small diameter, low energy consumption, quick response and high accuracy. These, along with the added difficulties in handling objects in zero gravity conditions, require that a method of end-point position control is used (Book, 1993).

Applications outside the robotics field - The control system can be used on cranes where tip stabilisation techniques are required to compensate for the effects of wind buffeting on long jibs.

Declaration

The material in this thesis is my original work. Contributions made by both researchers and undergraduate students were under my supervision following my ideas and project concepts.

Summary

This chapter has introduced the difficulties encountered in increasing the reach and payload capacity of robots whilst still maintaining speed and precision. Although the use of slender, lightweight arms provides a potential solution, a major problem to be overcome is that of how to account for positioning errors incurred through arm bending as reach is increased.

A novel position control system has been described, designed specifically for use on flexible arm robots. The system is unique in that it controls arm position whilst simultaneously correcting automatically for load-induced arm bending.

The next chapter reviews other methods using optical measuring devices for the correction and control of bending in arms. The principle elements of these systems are compared and contrasted with the novel control method proposed.

An account is then given in Chapter 3 of each stage of the design and fabrication of the robots on which the controller was tested. Three variants are described, from an initial 'proof of concept' prototype through to a dual-axis model with high performance actuation. The inclusion of joints along the arm is also considered - details of four revolute and one prismatic design are included.

Chapter 3 is followed by two chapters describing the development of the laser beam tracking systems. The first begins with a review and performance comparison of optical position sensing devices, leading to the selection of a linescan camera and then later a photodiode quadrant detector as beam tracking sensors. The mode of operation of the linescan camera is discussed, along with its limitations for this particular application. An account then follows of the design of a dual-axis beam tracker with details of the associated electronics. Testing and performance of the quadrant detector beam tracker is discussed in the second chapter. A purpose built rig was produced on which to test the behaviour of the beam tracker under different light conditions. From the results of these experiments the optimum light spot size, shape and intensity are defined.

The operational performance of all three prototype variants under a series of control algorithms is given in Chapter 6. Initial results demonstrate the validity of the control concept, yet show clearly the weaknesses present in the first prototype design. Improved performance was seen with a modified single-axis prototype, yet the results from the dual-axis robot with high performance actuators verify the choice of a PD based controller for optimum control performance.

Following the conclusions, suggestions are given for a range of improvements which could be made to the dual-axis robot and the beam tracking system along with proposed methods to enable all six degrees of freedom of the arm end-point to be measured simultaneously.

References

Andeen, G.B. (ed), (1988) 'Robot Design Handbook', SRI International, Chapter 15, pp. 15.1-15.10.

Becquet, M., (1989) 'Analysis of flexibility sources in robot structure', Distributed Parameter Systems: Modelling and Simulation, IMACS 1989, pp. 375-380.

Book, W.J., Neto, O.M. and Whitney, D.E., (1975) 'Feedback control of two beam, two joint systems with distributed flexibility', Journal of Dynamic Systems Measurement and Control - Transactions of the ASME, pp. 424-431.

Book, W.J., (1993) 'Structural flexibility of motion systems in the space environment', IEEE Transactions on Robotics and Automation, Vol. 9, No. 5, October 1993, pp. 525-530.

Book, W.J. and Majett, M., (1982) 'Controller design for flexible, distributed parameter mechanical arms via combined state space and frequency domain techniques', Book, W.J. ed., Robotics Research and Advanced Applications, ASME booklet, pp. 101-120.

Cannon, R.H. and Schmitz, E., (1984) 'Initial experiments on the end-point control of a flexible one-link robot', The International Journal of Robotics Research, Vol. 3, No. 3, August 1984, pp. 62-75.

Driessen, F.P.G, Lucassen, F.H.R. and van der Ven. H.H., (1988) 'A three dimensional position measuring system', In IFAC Theory of Robots, IFAC Proceedings Series 1988 No. 3, Edited by Kopacek, P., Troch, I. and Desoyer, K., pp. 309-313.

Editor, (1989) 'Robots move in to tackle heavier weights on building sites', New Scientist, Vol.123, No. 1680, September 1984, p. 36.

Harashima, F. and Ueshiba, T., (1986) 'Adaptive control of flexible arm using the end-point position sensing', Japan - U.S.A Symposium on Flexible Automation from Distributed Parameter Systems: Modelling and Simulation, IMACS 1989, pp. 225-229.

Jiang, Z-H., Uchiyama, M and Hakomori, K., (1989) 'Active compensating control of the flexural error of elastic robot manipulators', Distributed Parameter Systems: Modelling and Simulation, IMACS 1989, pp. 369-373.

Kiedrzynski, A., (1986) 'Mass-stiffness analysis of robot links', Proceedings of the 16th ISIR, Brussels, pp. 151-158.

Lewis, J., (1991) 'The design, construction and testing of a laser guided robot arm', MSc dissertation, Middlesex Polytechnic, 1991.

Manganas, A., (1993) 'The stability of manipulator tip motions in response to low frequency, high magnitude manipulator base disturbances', Report, Advanced Robotics Research Ltd, Salford, U.K.

Manganas, A., (1993) 'Tip stabilisation of base compliant manipulators', Report, Advanced Robotics Research Ltd, Salford, U.K.

Parks, T.R. and Pak, H.A., (1991) 'Effect of payload on the dynamics of a flexible manipulator - modelling and control', Journal of Dynamic Systems Measurement and Control - Transactions of the ASME, Vol. 113, No. 3, pp. 409-418.

Preston, M.E., (1989) 'Mechatronics, the new design integrator', Proceedings of SEFITALI 1989 Annual Conference, Naples, Italy, 17-19 September 1989, pp. 263-268.

Robotic Industries Association, 1 SME-Drive, 20501 Ford Road, PO Box 1366, Dearborn, Michigan 48121, USA.

Scott, A.G., (1989) 'Position control for machines', U.K. Patent Application No. 8908755, April 1989.

Sharon, A. and Hardt, D., (1984) 'Enhancement of robot accuracy using endpoint feedback and a macro-micro manipulator system', Proceedings of the American Control Conference, San Diego, pp. 1836-1842.

Uchiyama, M., Jiang, Z-H. and Hakomori, K., (1990) 'Compensating control of a flexible robot arm', Journal of Robotics and Mechatronics, Vol. 2, No. 2, pp. 97-106.

Usoro, P.B., Nadira, R. and Mahil, S.S., (1984) 'Control of lightweight flexible manipulators: a feasibility study', Proceedings of the 1984 ACC, Vol. 2, pp. 1209-1216.

Walker, D.G.W., (1984) 'The development of high powered robots', U.K. Robots Research 1984, IMechE 1984, pp. 121-129.

Wang, W-J., Lu, S-S. and Hsu, C-F., (1989) 'Experiments on the position control of a one-link flexible robot arm', IEEE Transactions on Robotics and Automation, Vol. 5, No. 3, June 1989, pp. 373-377.

Wanner, M.C., (1987) 'Design of a manipulator with very large reach for applications in civil engineering', Robomatrix Reporter Annual 1988, pp. 259-267.

White, A.S., (1991) 'Vibration control in robots and other automation', 6th International Conference on CAD/CAM, Robotics and Factories of the Future 1991, Southbank Press, pp. 550-555.

Zalucky, A. and Hardt, D.E., (1984) 'Active control of robot structure deflections', Journal of Dynamic Systems Measurement and Control - Transactions of the ASME, Vol. 106, March 1984, pp. 63-69.

Chapter 2

A REVIEW OF OPTICALLY BASED POSITION CORRECTION METHODS

2.1 INTRODUCTION

Before the advantages of flexible arms can be exploited, the problem of how to control and maintain end-point position must be addressed. Various approaches have been investigated, of which those using optical systems can be divided into three categories

- where link *bending is accepted* and micromanipulators *correct* for arm position errors - (post-bending correction),
- methods that *artificially increase arm stiffness* to *maintain* arm tip position,
- methods employing *direct end-point position sensing*.

These categories can be subdivided as shown in figure 2.1.

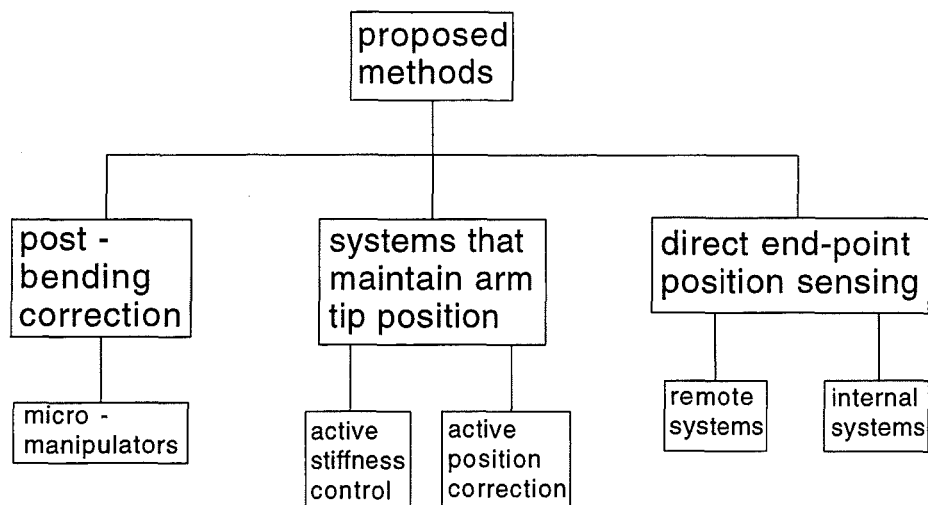


Figure 2.1 - An overview of methods using optical systems for the correction of positioning errors in flexible link robots

This chapter gives details of past and present research that falls under each of the three major categories, with the emphasis being on descriptions of relevant optical measurement systems, how they are integrated within the overall control strategy and of how these strategies compare and contrast with the novel method described in Chapter 1.

2.2 POST-CORRECTION FOR BENDING ERRORS - MICROMANIPULATORS

One approach that has attracted much interest is the use of add-on end-effector position correcting devices to industrial robots. The advantage of these post-bending error correction systems is that they can be attached between the arm tip and end-effector of conventionally controlled robots to provide a means of fine end-effector positioning.

These secondary devices, known as micromanipulators (Taylor *et al*, 1984), act independently of the host arm and reduce the sensitivity of the end-effector to arm structural deformations, therefore isolating the problem of end-of-arm deflections from the overall control problem and reducing the requirement for the arm link actuators to provide fine motion for accurate positioning.

A dual control system is required - the conventional 'macro' arm position controller and a micromanipulator 'micro' system for fine end-effector positioning and orientation. The 'micro' control system must be designed such that it can actively control micromanipulator positioning yet not hinder or limit free movement or orientation of the host robot arm. 'Non-contact' optical position sensing systems offer a potential solution.

One such system (Sharon and Hardt, 1984; Sharon *et al*, 1993) uses an optical end-point positioning 'micro' system on a five degree of freedom hydraulic micromanipulator. Their aim was to design a system that could offer all the features of a small high precision robot for local operations, whilst at the same time retaining the flexibility, speed and range of motion of the larger robot (Lin and Lee, 1992).

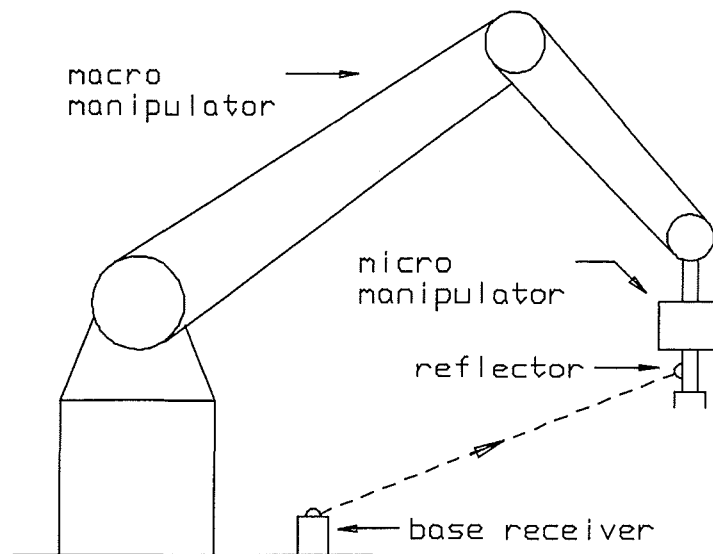


Figure 2.2 - The macro/micro manipulator concept - (Sharon and Hardt, 1984)

The micromanipulator is moved to the area of interest by the host robot, the optical positioning system then controlling fine movements to correct for end-effector errors caused by arm bending.

A compensating controller was implemented for the correction of static errors along one translational axis of the micromanipulator which was mounted on the end of a cantilever beam. The design was based upon the assumption that there was no dynamic coupling between the micro and macro systems. A multi-input, multi-output linear quadratic analysis was performed on the micromanipulator to examine the coupling between the various degrees of freedom. The dynamics of the host robot could be ignored as most industrial robots have relatively stiff links and are massive compared to the micromanipulator. Experiments with a single-input, single-output compensator showed that stable control was difficult to achieve under proportional control and gave inconsistent results at bandwidths above the structural frequency of the robot.

The system was improved by Sharon *et al* through implementation of a full state feedback control system. This enabled an end-point position bandwidth of 28 Hz to be achieved - being 15 times higher than the first structural mode of the robot. Model analysis showed that the system was stable at gains that would result in operating bandwidths that are below as well as above the resonant frequency caused by the structural dynamics of the

macromanipulator. Only at operating bandwidths close to the structural resonance of the macromanipulator did the system become unstable. Again, only the behaviour of one of the five micromanipulator axes was tested, end-point position being measured using an optical sensor (not described).

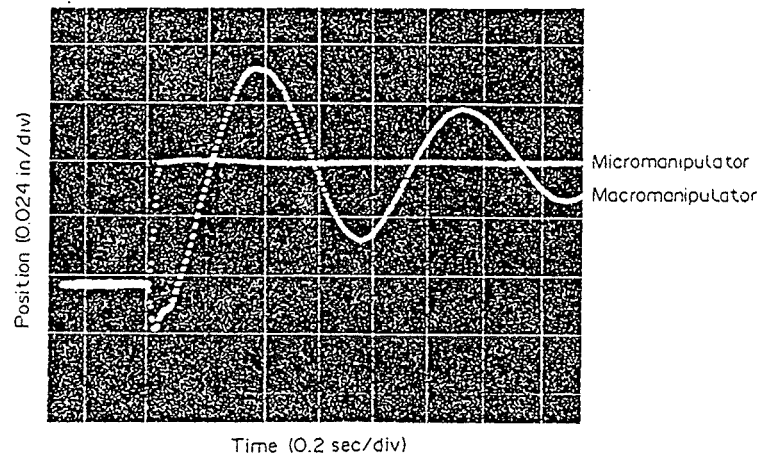


Figure 2.3 - Response of macro/micro manipulator to step position command
- (Sharon *et al*, 1993)

The micromanipulator reached its target quickly and locked in on it while the macromanipulator was still moving, showing that it was capable of compensating for the macro's undesirable motion. The macro/micro combination settled in 40 ms, the macro alone in 1.2 s.

A key factor for any practical implementation of the concept as conceived is the design of the optical base receiver for micromanipulator control. The authors concluded that a system does not exist capable of tracking and measuring end-effector position and orientation whilst simultaneously sending position correction signals to all five independent micromanipulator actuators. Such a high accuracy three-dimensional control mechanism would be complex to perfect, especially as high sampling rates are required as it will form part of the control loop. As with all such externally mounted devices, it would be susceptible to control breakdown caused by the end-effector and structures in the workspace shielding the tip reflector from view.

The micromanipulator concept was also explored by Chiang *et al* (1991) with the addition of a wrist to the experimental flexible arm used by Cannon and Schmitz (see Section 2.4.1). An end-point optical position sensor was used on the wrist tip to demonstrate the feasibility of controlling the end-effector position of a flexible macro/micro system at a bandwidth higher than the structural flexibility of the arm.

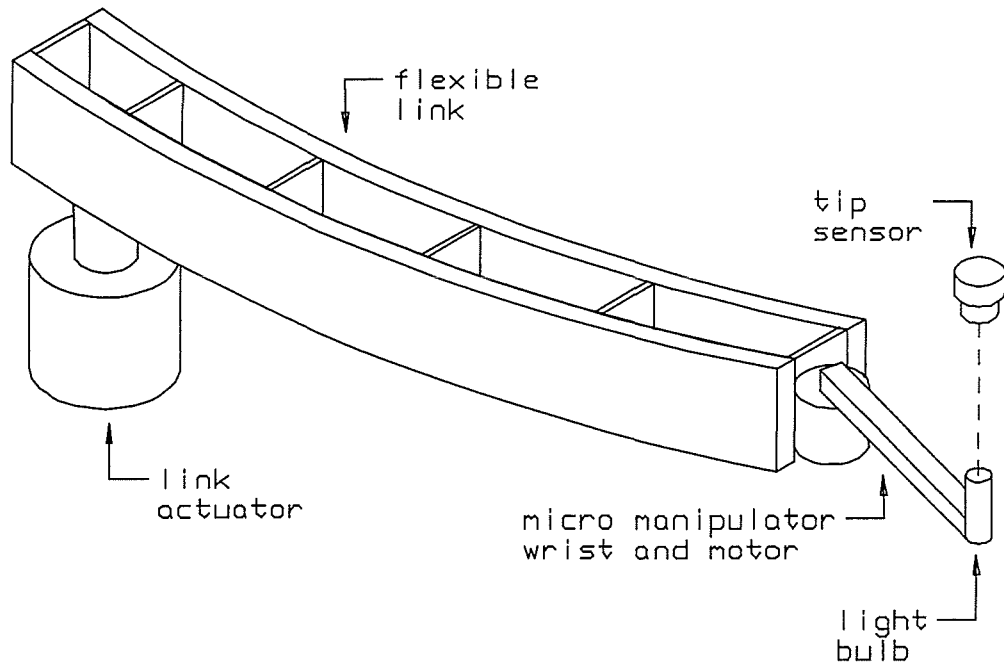


Figure 2.4 - The experimental micromanipulator wrist - (Chiang *et al*, 1991)

The host 96.8 cm long single link flexible arm and 16.5 cm long wrist were designed to move through the horizontal plane only. A 4.5 W incandescent bulb was attached to the wrist tip to indicate the end-point position which was sensed by a planar photodiode suspended on a fixture above the wrist. Movement of the wrist was controlled by a DC motor attached to the end of the host arm.

The optical system could not measure the amount of wrist positioning error, it merely indicated the desired horizontal end-point. If the host arm were to move too quickly, the bulb would swing out of range of the position demand photodiode and micromanipulator control would be lost.

Wrist motion was controlled using feedback from the tip position sensor when the wrist tip was in the vicinity of its target position. A digital lead compensator was used to control the tip position, a sample rate of 100 Hz being needed to achieve a bandwidth close to the second structural resonance frequency of the main flexible manipulator (3.9 Hz). Macro arm system dynamics were measured experimentally. The hub sensor was used to implement a simple and robust collocated feedback controller for the main beam. Two types of control were tested - a digital lead compensator and a position and rate feedback system, resulting in slightly different performances for the main beam, yet the tip motion had essentially the same response. The flexible main beam controller achieved a closed loop bandwidth of 1.2 Hz, which was higher than the first cantilever natural frequency of 0.55 Hz.

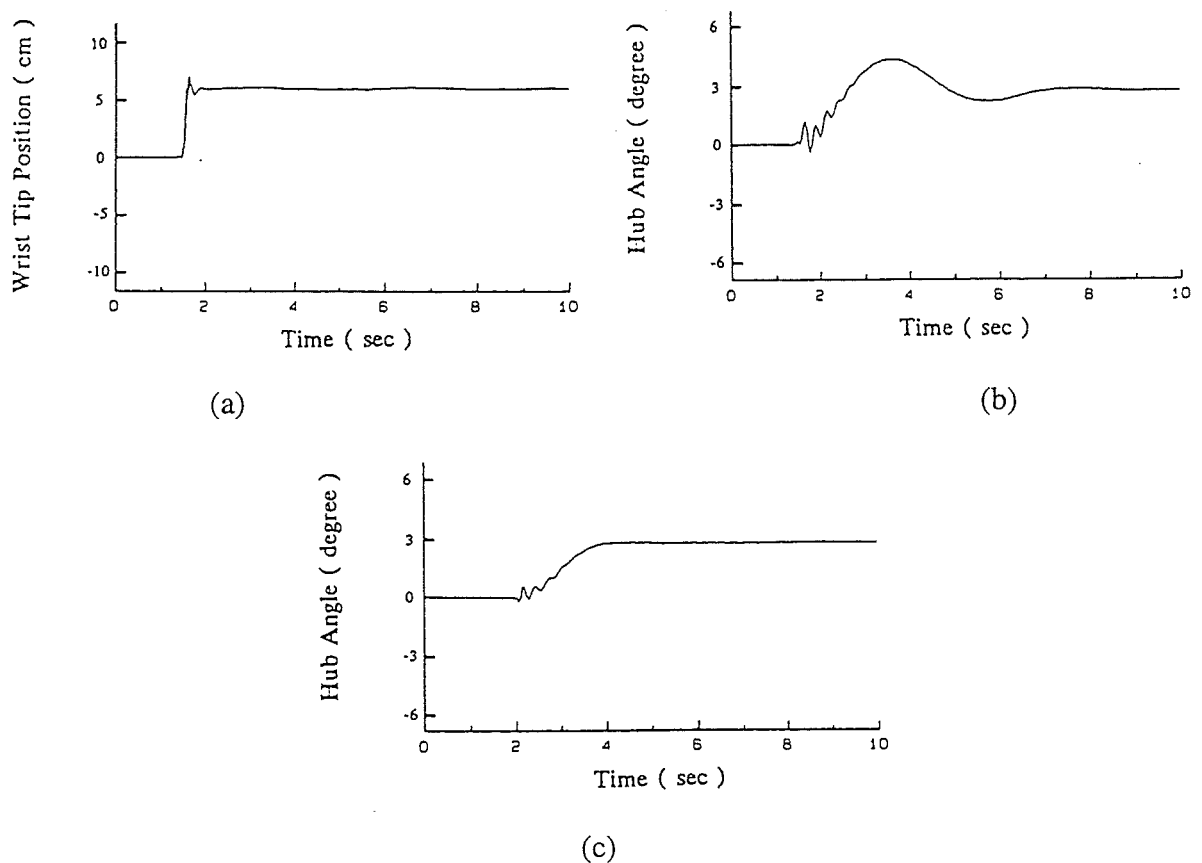


Figure 2.5 - Step response with (a) collocated sensor for hub motor control, (b) with lead compensator and (c) with position and rate feedback - (Chiang et al, 1991)

A more advanced system was that developed by Chalhoub and Zhang (1993). A two axis cartesian micromanipulator counteracted transverse deflections along a single host link.

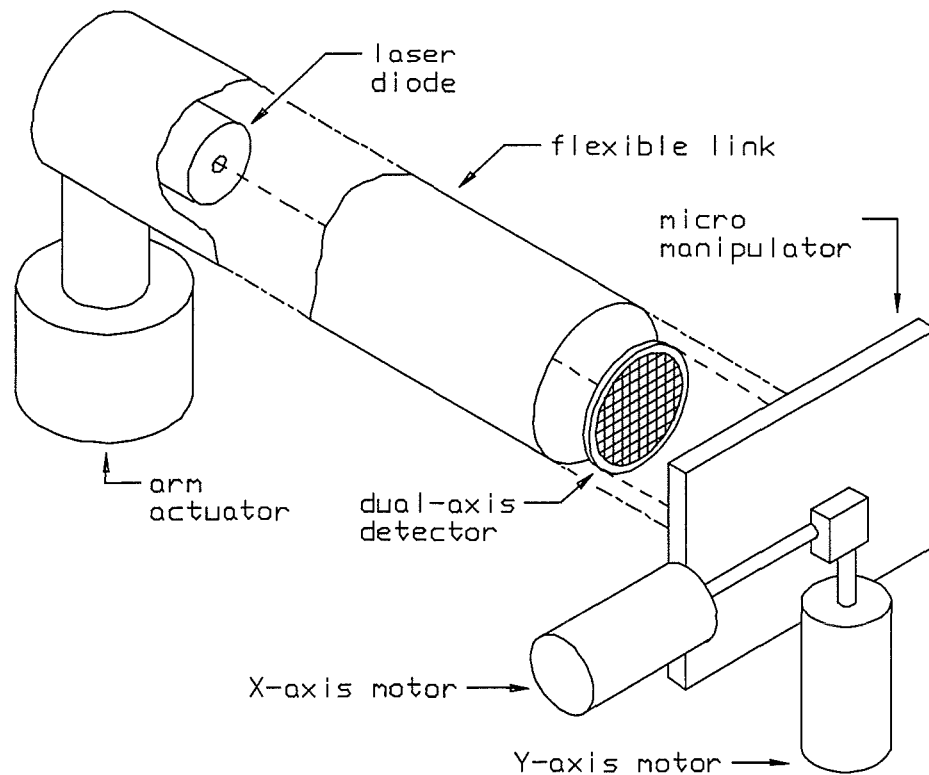


Figure 2.6 - The dual-axis micromanipulator positioning system
 - (Chalhoub and Zhang, 1993)

The beam from a laser diode, fixed at the pivot end of a 2.3 m long hollow arm, impinged upon a dual-axis photodiode array detector attached to the back of the micromanipulator at the link free end.

Measurements of link end-point transverse static deflections were obtained directly from the rectangular coordinates of the beam spot on the detector. It provided continuous analog outputs which were proportional to the coordinates of the centroid of the light spot as it moved within the active area, position sensitivity being within 0.01 mm. The detector was calibrated to yield zero analog outputs when the centroid of the light spot coincided with the origin of the grid, this position corresponded to the ideal straight beam configuration that was free of any static or dynamic deflections. The micromanipulator servo motors were equipped with encoders, the resolution in measuring linear displacement of each axis was 0.0254 mm. The servo motors responded to the measured position errors by re-centering the detector on the laser spot, thus correcting the attached end-effector position.

For controller design, a dynamic model of the system was derived, including all the coupling terms between the rigid and flexible motions of the compliant beam. Two separate control systems were tested on the compliant link. The first, a 'rigid body controller' (RBC) was used to simulate controllers used in existing industrial robots and followed a PID design, the control torque at the base joint can be represented by :

$$Torque = k_1\theta_1 - k_2\dot{\theta}_1 - k_3 \int (\theta_1 - \theta_d) dt \quad (2.1)$$

The second controller, the 'rigid and flexible motion controller' (RFMC), was an integral plus state feedback controller which added specified active damping to counteract vibrations in the beam.

For experimental testing, the control strategies were modified to include the dynamics of the joint actuators, a pure inertial load being assumed to be exerted on the motor shafts. A micromanipulator controller (MMC) was used, the purpose of which was to make the gripper insensitive to the end-of-arm deflections, the MMC working independently of the controller of the flexible link.

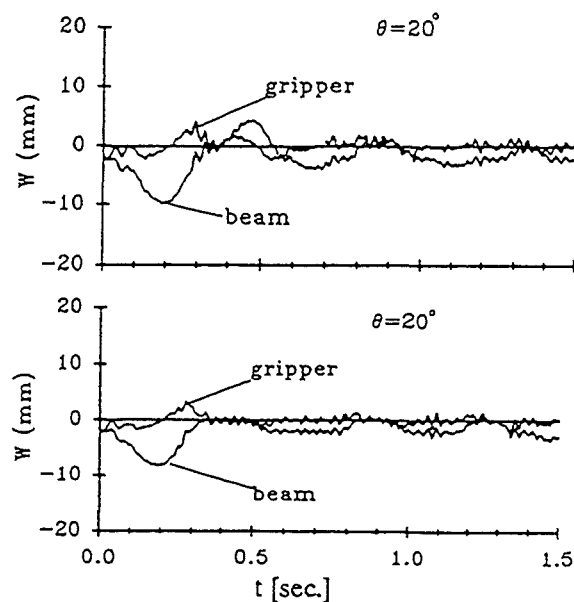


Figure 2.7 - The horizontal transverse deflections at the end of the beam and at the gripper in response to RBC and MMC - (Chaloub and Zhang, 1993)

Performance of the micromanipulator was evaluated by comparing the deflections at the free end of the link to those at the gripper - figure 2.7.

When the macro link was rotated through 10° , with the micromanipulator inactive, a maximum gripper horizontal deflection of 7.91 mm was recorded along with a vertical offset from the zero line of -1.9 mm caused by assembly misalignment. Oscillations were also observed, due to interaction between backlash in the gear head and flexible motion of beam. With the micromanipulator activated, the maximum horizontal deflection was reduced to 2.81 mm at gripper and vertical misalignment was corrected to within 0.5 mm. The micromanipulator significantly improved the positioning accuracy of the end-effector, it complemented rather than duplicated the efforts exerted by the host beam controller. This system showed distinct advantages over those described earlier. Accurate dual-axis control of the end-effector position was obtained. With the optical system mounted inside the arm, its position and orientation was no longer restricted and the light beam and detector were shielded from external interference. The major limitation is that errors produced by detector tilt, through bending of the loaded host arm, could not be detected.

The concept compares directly with the new control system described in Chapter 1. Both employ a laser source mounted inside the arm with a position detector at the arm far end. Operational strategies differ in that this device is a secondary system which acts so as to correct for static arm bending errors - initial arm positioning being through a conventional primary controller. The new system uses the laser source for both primary position control and dynamic end-point position correction.

Micromanipulators - Summary

Provided the micromanipulator is small in weight, it can significantly improve the accuracy of the motion of the end effector when carried by a very heavy, rigid robot arm moving at slow speed. It becomes more difficult to obtain a fast and stable control when the micromanipulator is carried by a beam that is lightweight and flexible or when the micromanipulator contributes significantly to the arm tip mass, increasing arm inertia and reducing the useful robot payload. With flexible arms, a fundamental ultimate limit on control bandwidth is shown to exist (Cannon and Schmitz, 1984), the limit arising from the time it takes a bending wave to travel the length of the arm. Dynamic interaction between the micromanipulator and the structural flexibility of the host arm destabilises the system, making controller design difficult and sensitive to parameter variations.

For successful micromanipulator control it has been shown that there are two essential requirements. Firstly, a parameter adaptive controller is required which must be based on accurate system modelling and accommodate the fact that the beam dynamics of the host robot are position dependent. Secondly, a direct multi-axis end-point micromanipulator position feedback system, which is difficult to achieve without the astute use of a highly sophisticated optical end-point position sensing. Such a system has not been developed.

2.3 SYSTEMS TO MAINTAIN ARM TIP POSITION

The second category (see figure 2.1) is that of developing optical systems to determine the amount of structural deflection at the end-point of flexible arms and using these measurements as the basis of feedback error signals to cause active arm tip repositioning through actuators applying torque in the direction required to oppose the bending force. Arm tip position is therefore *maintained* irrespective of the loading upon it.

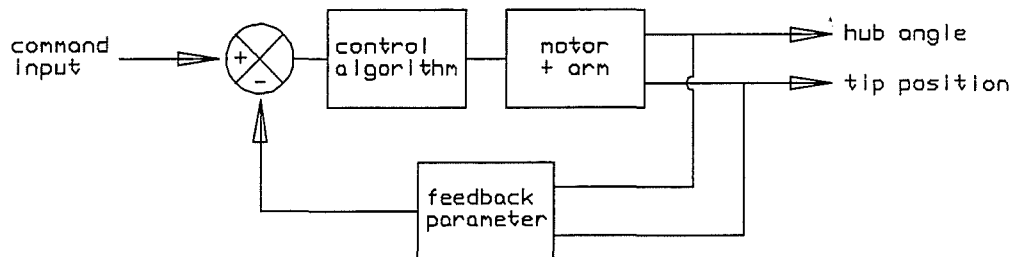


Figure 2.8 - Active feedback control for flexible link robots

This type of control, shown in figure 2.8, can be divided into three main tasks

- measurement of the state of the arm,
- use of the measured state in the control algorithm to minimise errors between the desired and measured states,
- physical realisation of the desired actuation using either using *secondary actuators for active arm stiffness control* or the *primary arm hub actuators to maintain end-point position*.

Again, primary arm position control is governed through a conventional robot controller.

2.3.1 Active Stiffness Control

Arm stiffness can be artificially increased by using beam straightness servos which operate so as to counteract bending in flexible links, so rendering the end-point position of a flexible link insensitive to load disturbances. This active correction strategy is based upon the inclusion of secondary control and actuating mechanisms which operate independently of the primary arm positioning mechanisms and controller. The strategy requires the comparison of the output from two sensors - position error signals are generated by an optical system and the arm pivot position is measured by shaft encoders collocated with the arm actuators. Bending error signals are fed to the secondary servo mechanisms which straighten the link to counteract for the load-induced deflections.

A twin-beam active stiffness controller was demonstrated by Zalucky and Hardt, (1984). The end-point position of a 1.5 m long square channel flexible load-bearing beam was controlled through a double-acting hydraulic actuator acting as a 'straightness servo'. The actuator, mounted at the end of the flexible beam, was supported between the outer beam and an inner rigid member.

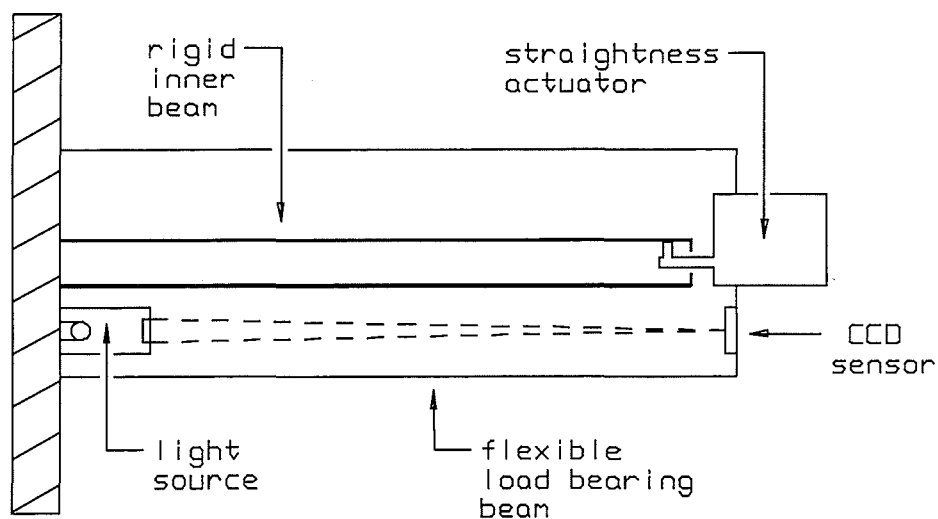


Figure 2.9 - Schematic diagram of the twin beam link with active hydraulic 'straightness servo' - (Zalucky and Hardt, 1984)

Bending in the outer link was sensed by an optical straightness measurement system consisting of a laser and CCD (charge coupled device) sensor - the laser was fixed internally to the base of the beam, the sensor at the tip of the load-bearing beam. As the

outer beam was loaded it deflected downwards, the amount of deflection being detected as a change in output from the sensor as the light spot moved across it. This error signal was then fed to the straightness servo which acted so as to straighten the load bearing beam so maintaining the original end-point position - the outer beam being, in effect, 'artificially stiffened' by the servo. Experimental results, for a 100 N load, gave a static error of 0.01 mm with a proportional controller and a reduced error of only 0.0085 mm when a lag compensator was added.

A potential advantage of this system is that as the actuator and measurement device are collocated, problems commonly encountered in controlling the compliance in flexible structures are mitigated.

Operational limitations are that the system measured and counteracted for vertical deflections only, no account could be made of horizontal deflections or beam torsion. The inner beam must be stiff for successful operation since accurate repositioning of the flexible outer beam is caused by the hydraulic servo acting against the far end of the inner beam. Therefore loading forces are transmitted through to the inner beam which will cause it to deflect upwards. To make the small diameter inner beam as rigid as possible, its wall thickness must be considerable which would add greatly to the overall weight, thus reducing the possible advantages to be gained over using a conventional single load-bearing beam.

A second beam straightness system (Mulders *et al*, 1986) made use of piezo-electric actuators to counteract the horizontal deflections in a single flexible link. The deflection measurement system consisted of a 2 mW collimated laser diode and a photodiode array sensor mounted beneath the fixed end of the 1000 mm long arm, the beam being reflected back from the end-point of the link by a retroreflector. This was chosen as it has special properties in that only translations in the X or Y directions and not the rotation of the retroreflector affects the position of the beam. The use of a flat mirror was rejected as tilt effects the direction of the reflected beam (see figure 2.11).

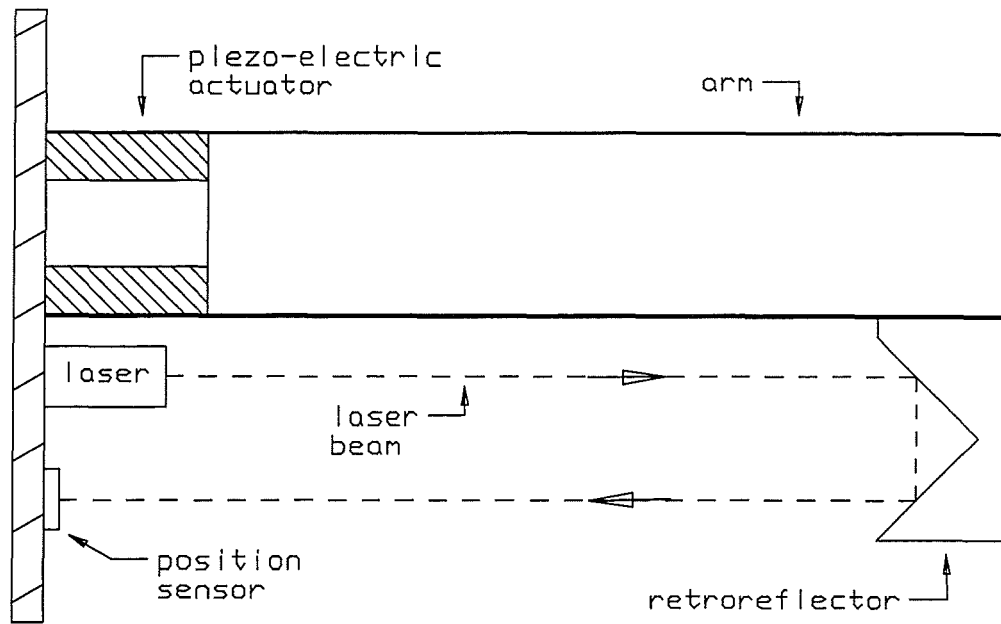


Figure 2.10 - Schematic diagram of the apparatus for the active correction of link horizontal deflections - (Mulders *et al*, 1986)

End-point position error was detected by the independent optical sensor. The error signal was fed back to the control unit which, operating independently of the main position controller through a PID algorithm, caused the stiffness actuators to return the free-end of the arm to its original position. The PID algorithm in discretised form is :-

$$Signal = k_p e(nT) + k_i \sum_{k=1}^n e(kT) + k_d (e(nT) - e(n-1)T) \quad (2.2)$$

where e is the error signal as measured by the sensor.

The 200 x 300 pixel resistive gate sensor was found not to be the ideal choice for this particular application. Detecting the laser beam in the matrix of pixels was time consuming - the sampling rate was 20 ms at 50 Hz which restricted control loop times such that the size of the usable PID control parameters (k_p , k_i and k_d) was restricted to ensure control stability.

When an external 50 N load was applied to the end of the arm, a deflection of 0.17 mm was recorded (no corrective action). With the actuators applying a force of 222 N this error could be counteracted successfully giving zero end-point position error.

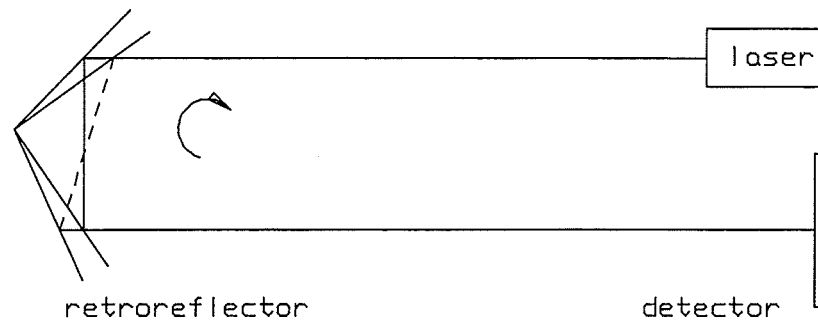


Figure 2.11 - Effect of retroreflector rotation on the reflected laser beam position
 - (Mulders *et al*, 1986)

This system had distinct advantages over that devised by Zalucky and Hardt. A single link beam is used, keeping arm weight to a minimum. The positioning accuracy of piezo-electric actuators is greater than can be obtained using hydraulics, being easily controllable and stiff in operation. If two pairs of orthogonally positioned actuators were used, torsion correction could be achieved by actuating the four actuators separately. The actuators were sited at the base end of the link such that they operate against only a short rigid inner beam. Advantages derived from piezo-electric actuators are their small time constant, good linearity between the electrical and mechanical characteristics, high stiffness and high mechanical stability; drawbacks include that high voltages necessary for actuation, limitations in terms of power output (small strain), thermal instability and an inability to cope with steady-state deformation.

The types of stiffness control described are effective in that they allow conventional control systems to be used for primary arm positioning, yet rely upon secondary systems to correct for link deformations. As a result, overall control has been shown to prove complex because the two systems must work simultaneously, yet independently, of one another (deflection compensation being carried out in a separate control loop from position control) and the problem of achieving stability becomes severe.

2.3.2 Active Position Correction

Active end-point position correction differs from active stiffness control. Stiffness control relies upon secondary actuators to cause straightening of loaded links whereas active position correction strategies attempt to maintain the desired arm tip position irrespective

of the load-induced link bending - primary arm positioning and secondary tip corrective movements being actioned through the link hub actuators alone.

Primary positioning is through a conventional control system. Load-induced deflections are measured using an optical means of position sensing, with the position errors fed back to the main controller to cause active link tip repositioning through the link hub actuator. End-point deflection is either calculated from measurements taken at points along the link or by measuring the end-point position directly.

2.3.2.1 Link local deflection measurements

Figure 2.12 shows details of a horizontal 'slope sensor' measurement system developed by Wang *et al* (1989). Arm deflections were detected as a shift in light spot position across the surface of a lateral effect photodiode. The beam from a laser light source was reflected back towards the sensor by a mirror attached towards the hub end of the link. The slope detector was positioned close to the hub for a stable response.

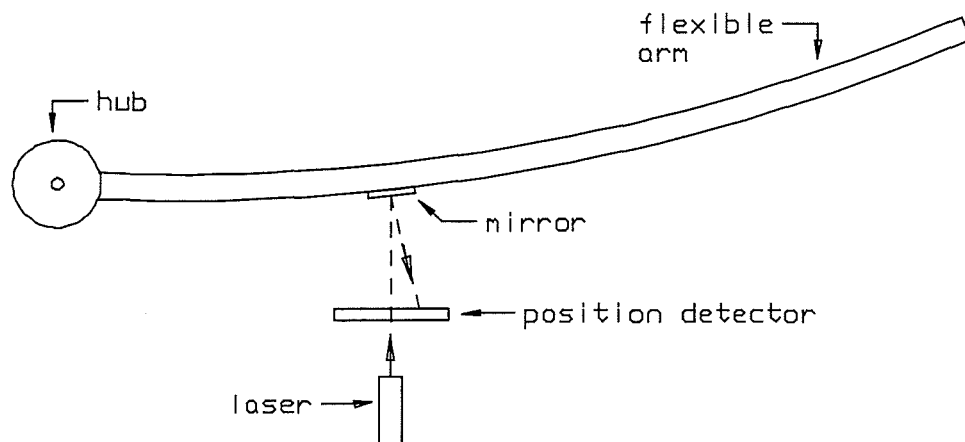


Figure 2.12 - Arm deflection detection system - (Wang *et al*, 1989)

The output from the slope sensor was fed to the main controller which, in conjunction with hub angle measurements from an optical shaft encoder, caused link repositioning such that $\delta(s)$ (displacement of the light spot from the neutral axis of the photodetector) was reduced to zero.

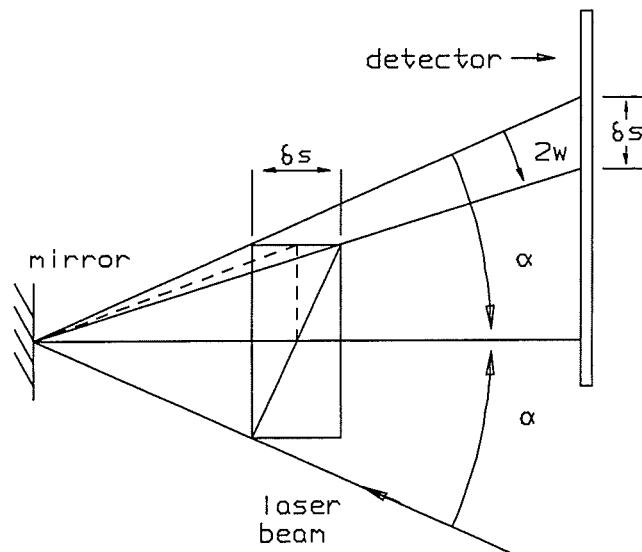


Figure 2.13 - Schematic diagram showing the laser beam path

The slope of the arm deflection being calculated from :-

$$w = \frac{\cos\alpha}{2l} \quad (2.3)$$

where w = the arm slope;

l = the laser to mirror distance;

α = the angle of incidence on the detector.

Figure 2.14 shows how the deflection sensor was incorporated into the controller design.

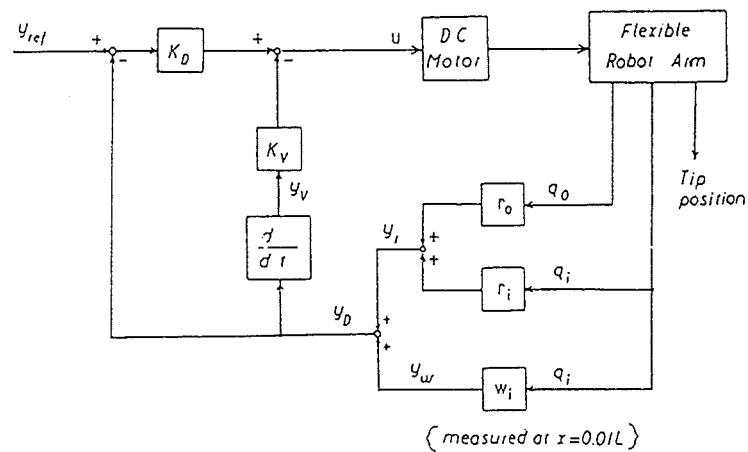


Figure 2.14 - Block diagram of the control system - (Wang *et al*, 1989)

The encoder position signal q_0 and its derivative \dot{q}_i are multiplied by encoder constants r_0 and r_i . The encoder derivative signal is further modified by w_i , which is a constant computed from the measurement of the slope. The output signal y_D is composed of the feedback signals from the shaft encoder and the slope sensor :-

$$y_D = y_r + y_w \quad (2.4)$$

Derivative feedback is also used :-

$$y_v = \dot{y}_D \quad (2.5)$$

The control law is therefore :-

$$u = k_D(y_{ref} - y_D) - k_v y_v \quad (2.6)$$

Where k_D (0.396) and k_v (0.220) are the feedback gains and y_{ref} denotes the reference input. Experiments showed the feasibility of this system to reduce position overshoot and settling time - the settling time was 0.86 s with zero overshoot, as compared to 1.25 s settling time and 3% overshoot for control with *no* deflection feedback.

2.3.2.2 Direct end-point deflection measurement

"To control the structural deflections of flexible manipulators, knowledge of the end-point position of link is essential. Knowing the position of the end-effector, all deflections, backlash and other error sources can be compensated" (Cannon and Schmitz, 1984).

Absolute end-point positioning can best be obtained by measurement of the end-point rather than any other point on the robot. If the absolute end-effector position is measured, robot accuracy would theoretically be limited by the measurement device and servo resolution. Thus, if the position of the end-effector is fed back to the controller, the actuators can react to eliminate the error. Besides reducing static positioning errors dramatically, closed loop control about the end-point also provides greater application flexibility since the information obtained can be used for active position correction. The desired end-point position can be maintained in the presence of external loads, appearing to be an 'infinitely' stiff system.

A link deflection measurement system that compares directly with that of Wang *et al* (see Section 2.3.2.1) was described by Wang and Shekhar (1991). A mirror was attached vertically to the end-point of a single flexible link. A laser and a photodiode two-dimensional array sensor were attached to the fixed end of the link, the laser beam being reflected back to the sensor.

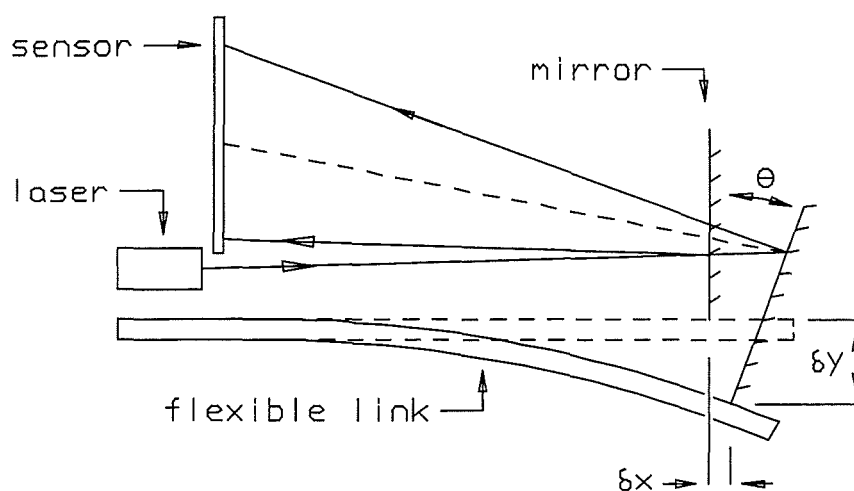


Figure 2.15 - Method for determining three end-point deformations along a flexible link - (Wang and Shekhar, 1991)

The spot position on the sensor gave information which, through geometric calculations, could be used to determine the link deflection δ_y , the tip bend angle θ and link elongation δ_x . As yet, this measurement system has not been implemented as part of a flexible arm control system.

Harashima *et al* (1986, 1989) used a CCD camera and a reflective target as a tip displacement measuring system for the adaptive control of flexing in a single link (link torsion and gravitational deflection being ignored). The camera was mounted at the base of the arm with the target at the far end (see figure 2.16). The system used visible light reflected from the target to measure *horizontal* end-point displacements. The camera image was processed by an image processor, then output to an on-line control loop.

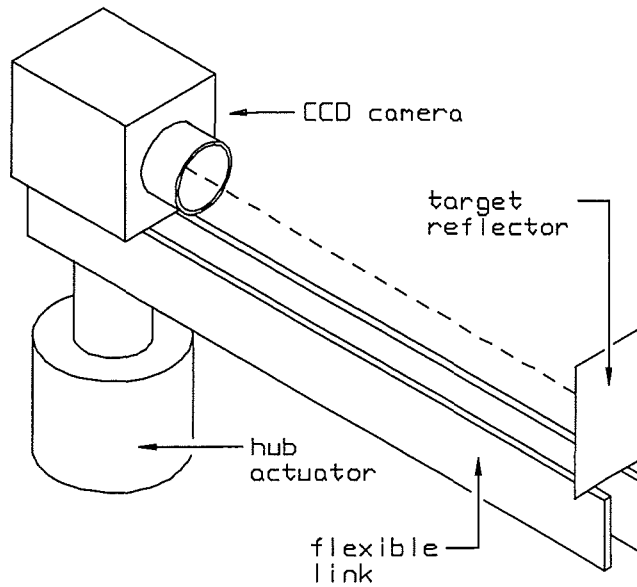


Figure 2.16 - Schematic diagram of apparatus used for the correction of horizontal link end-point deflections - (Harashima *et al*, 1989)

For active tip repositioning an adaptive control method was used. Three feedback signals were recorded - the amount of end-point deflection, $w(t)$, (as measured by the camera), the rate of hub angle change, $\dot{\theta}(t)$, (as measured by the hub tachogenerator) and the hub angle, $\theta(t)$, (as measured by the hub position encoder). The feedback signals were fed to an adaptive pole placement controller with on-line parameter estimation - figure 2.17. The control signal then causing arm repositioning such that the end-point displacement was reduced to zero.

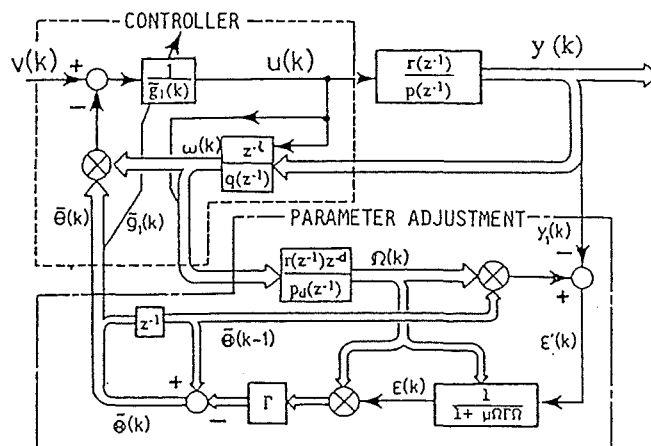


Figure 2.17 - The adaptive control system - (Harashima *et al*, 1989)

Fast response (< 1.5 s) was reported with minimal overshoot or link vibration - the tip vibrating continuously when the end-point position detector was not used, vibration being successfully suppressed when the measuring system was implemented.

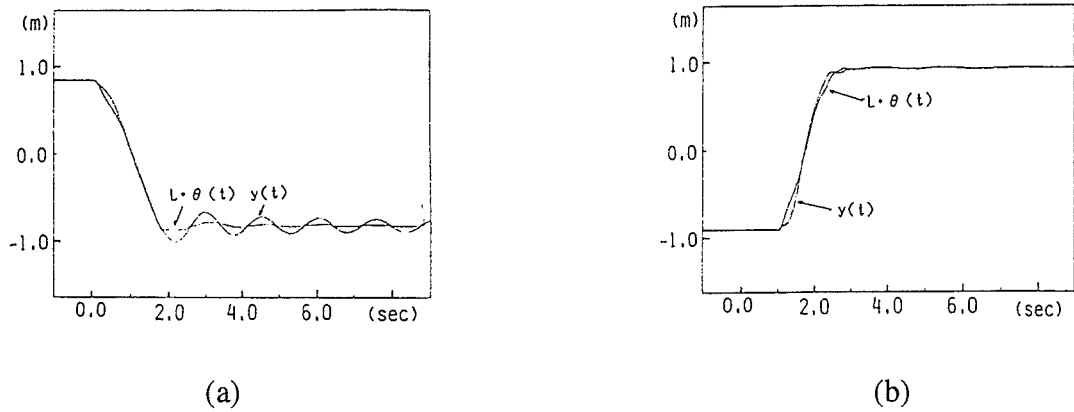


Figure 2.18 - Time response of the arm (a) without and (b) with end-point stabilisation

In contrast Jiang *et al* (1989) and Uchiyama *et al* (1990) developed a link displacement sensor for measuring *vertical* deflections (i.e. gravitational distortion). Tip displacement was detected as a laser spot position on the surface of a 100 mm long PSD (position sensitive detector) attached to the far end of each link. A laser diode was fixed to the hub end such that the light beam was directed towards the detector.

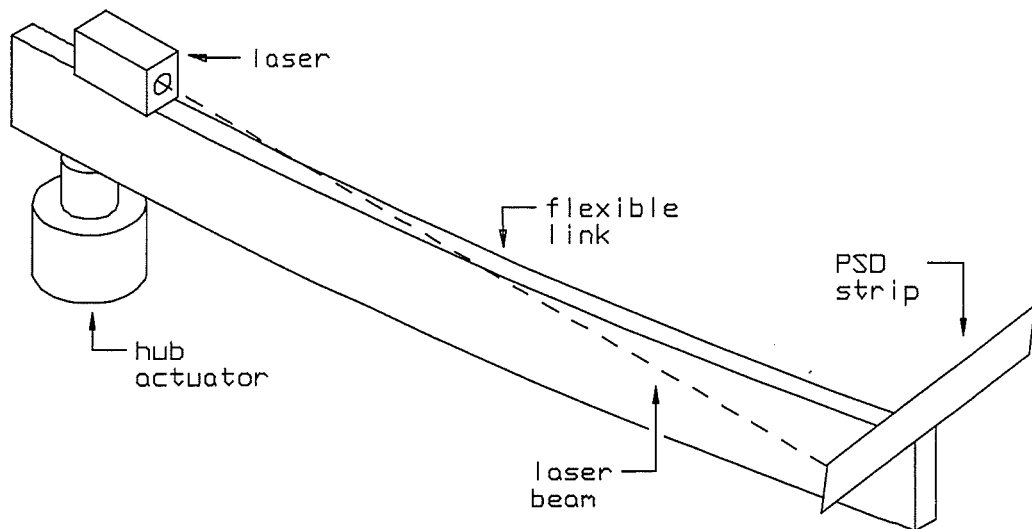


Figure 2.19 - The single axis link end-point deflection measurement system
- (Uchiyama *et al*, 1990) - one link only shown

The link control system was designed around a hierarchical structure with three control functions - a positioning function to achieve accurate joint positioning, a link vibration-suppressing function and a compensating function for errors resulting from link elastic displacement. Interconnections between the functions are shown in the block diagram.

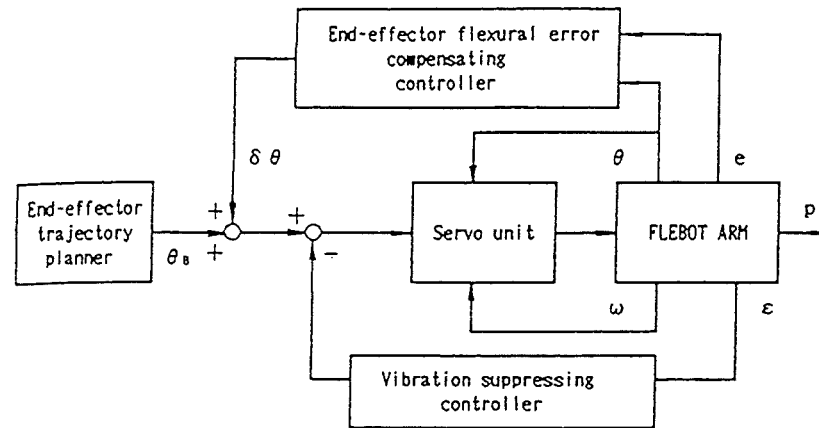


Figure 2.20 - Block diagram of the control system with active compensating controller
- (Jiang et al, 1989)

For joint positioning PI control was used : -

$$\text{Control signal} = (k_p + k_i / s) (\theta_r - \theta) \quad (2.7)$$

where θ_r represents the demand position.

The actual hub joint angle (θ) and the hub angular velocity (ω) were detected by a potentiometer and tachogenerator respectively. Vibration suppressing control was performed by measuring the strain (ϵ) on each link using strain gauges, and feeding back velocity commands to the corresponding joints. Tip deflection (e), as measured by the optical position sensor, formed the input for the compensating controller - the purpose of which was to cause active tip repositioning via the hub actuator to *compensate* for low frequency flexural errors caused by link elastic displacement.

To demonstrate the effectiveness of the system, the ability of the arm to track a planned circular trajectory was tested, the tracking time being 26.4 s. Without compensation, poor tracking ability was seen.

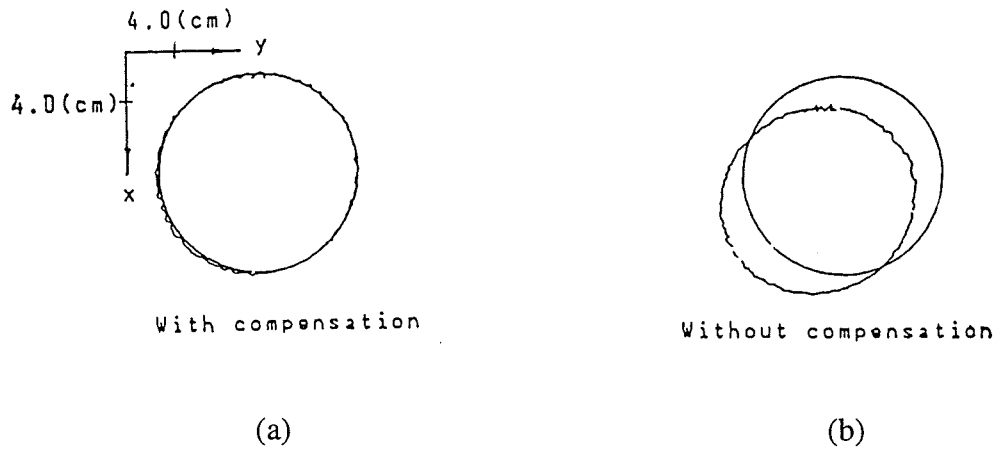


Figure 2.21 - Experimental tracking control results (a) with and (b) without end-point position correction - (Jiang *et al*, 1989)

The displacement sensor was reported to suffer from precision problems, resolution being ± 1 mm. The sensitivity of the PSD was affected by both the laser spot diameter and the precision of the analogue electronic circuitry.

Systems employing direct end-point deflection measurement have been successfully shown to reduce tip displacement errors, yet overall arm position control is complicated as the hub actuator has to actively respond to competing position demand signals from the primary controller and the secondary active position correction system. To overcome this problem, whilst still maintaining the advantages to be gained from direct end-point position measurement, experiments have been conducted into the use of single optical systems for primary arm end-point position control.

2.4 DIRECT END-POINT POSITION CONTROL SYSTEMS

In the methods previously described, primary arm positioning was governed by a conventional robot controller. End-point positioning error was measured by a subsidiary system which produced, or caused active correction for, the required end-point repositioning. Described below are methods in which arm position is controlled via a single optical end-point position sensing system. The optical systems may be positioned remotely from or attached directly to the arm (see figure 2.1).

2.4.1 Remotely Positioned Control Systems

Early generic investigations into the end-point control of a 1 m long single flexible link were conducted by Cannon and Schmitz (1984). Horizontal link tip position was determined through an optical position sensing means.

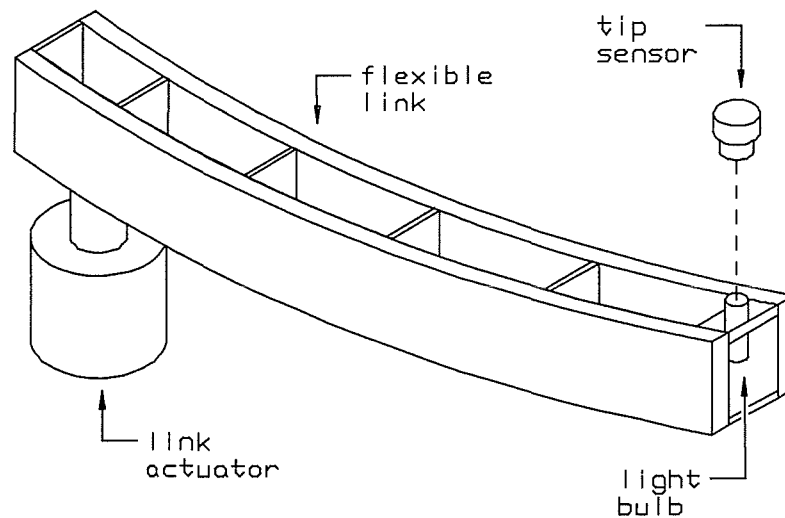


Figure 2.22 - The experimental end-point optical control system
- (Cannon and Schmitz, 1984)

The tip positioning system consisted of a small light bulb fixed to the far end of the arm. The light bulb illuminated, through a lens, a small section of a dual-axis position sensing photodetector suspended 1 m above the arm. Two analogue output voltages were obtained, corresponding to the X and Y arm tip position coordinates. The sensor's field of view was $\pm 20^\circ$ providing for measurement motions of the arm ± 40 cm about the centre line. The accuracy of the system was better than ± 0.5 mm.

Controller design, following a linear quadratic Gaussian (LQG) approach, was based upon a mathematical model of the system. The control loop is relatively simple in that just the position of the tip and hub are used in the feedback loop. Advantages of this method are that it could handle easily more than one sensor and it permitted trade-offs between the end-point speed of response, damping and available actuator power. Disadvantages are that accurate modelling is difficult: the process can be viewed as a complex, distributed-parameter system whose parameters are uncertain and change with time.

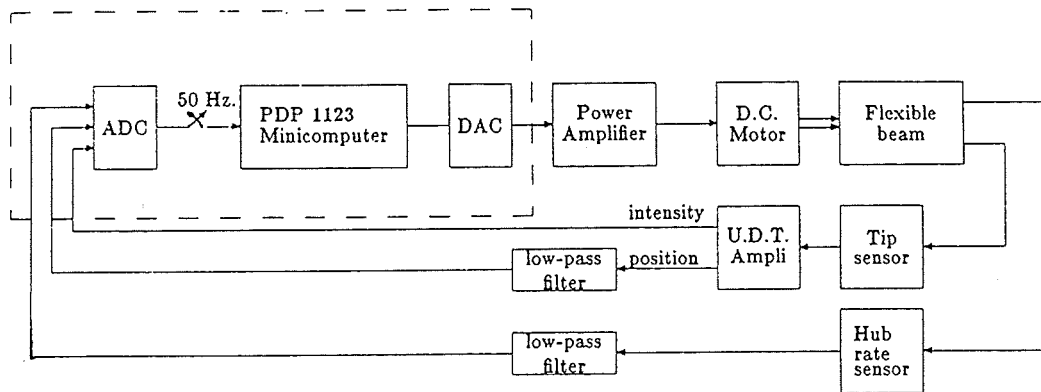


Figure 2.23 - Block diagram of the control system - (Cannon and Schmitz, 1984)

Successful operation of the system is shown by reference to figure 2.24. A typical response to a step-command tip position of 10 cm is shown, arm tip response being stable with little overshoot and fast (1 s) settling time.

Arm flexing caused the tip to whip to the desired position rather than move smoothly. Torque was applied through the hub actuator at time $t=0$. Despite the continuous change in hub angle, the arm tip remained stationary until 130 ms had passed (point A). This reflects the time taken for the bending wave to propagate along the arm.

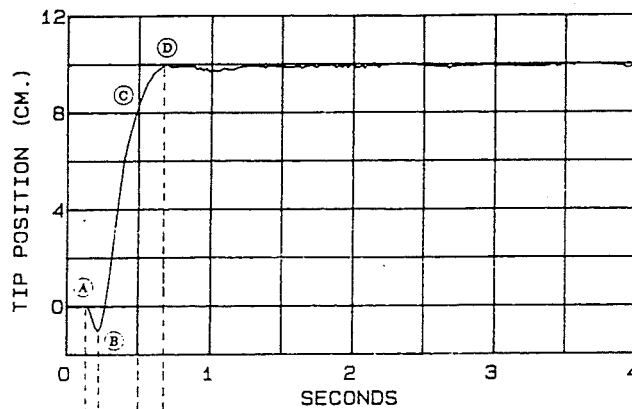


Figure 2.24 - The measured arm response to a step-command tip position of 10 cm
- (Cannon and Schmitz, 1984)

As torque was applied, the initial effect on the arm was to deflect the tip in the wrong direction (point B), whereupon the arm tip swung back rapidly and moved towards the command position, which it reached in 450 ms after leaving point B.

This generic experimental work demonstrated the feasibility of directly controlling arm tip position and showed the potential effectiveness of optical end-point sensing systems.

Optical systems, using triangulation methods (Driessen *et al*, 1986; De Schutter and Van Brussel, 1992) or single tracking laser interferometers (Kyle, 1995) can be applied to the direct, dynamic, 3-D measurement position calibration of robot end-effectors in space. One example of a commercial product, called Lasertrace, is that supplied by Automatic Systems Laboratories Ltd, U.K. (Editor, 1993).

Each of two Lasertrace pods use two orthogonally mounted CAT's (Combined Actuator/Transducers) to steer a laser beam towards a target retroreflector attached to the robot arm tip.

Although primarily designed for robot performance analysis, Intelligent Systems Ltd (formerly Advanced Robotics Research Ltd, U.K.) modified a Lasertrace tracking system to enable six degrees of freedom tip stabilisation of a base compliant manipulator - the RD4 tip stabilisation project (Manganas, 1993).

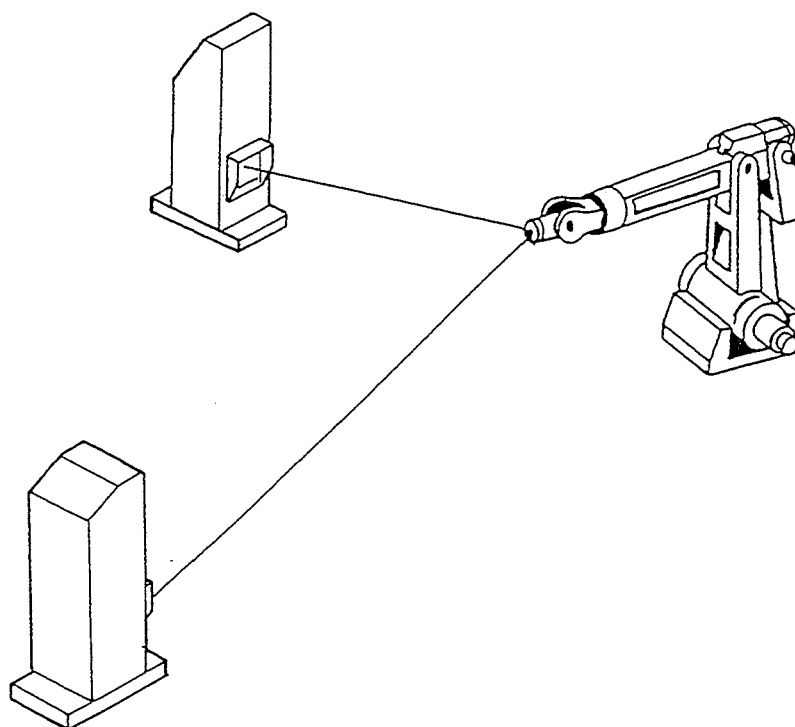


Figure 2.25 - The Lasertrace robot performance testing apparatus
- (Automated Systems Laboratories Ltd)

Triangulation techniques provide high integrity position data in three dimensions at rates between 100-1000 readings/s. Tip positional error is detected as an imbalance in the outputs from each quadrant of two detector pairs which detect the reflected laser beams.

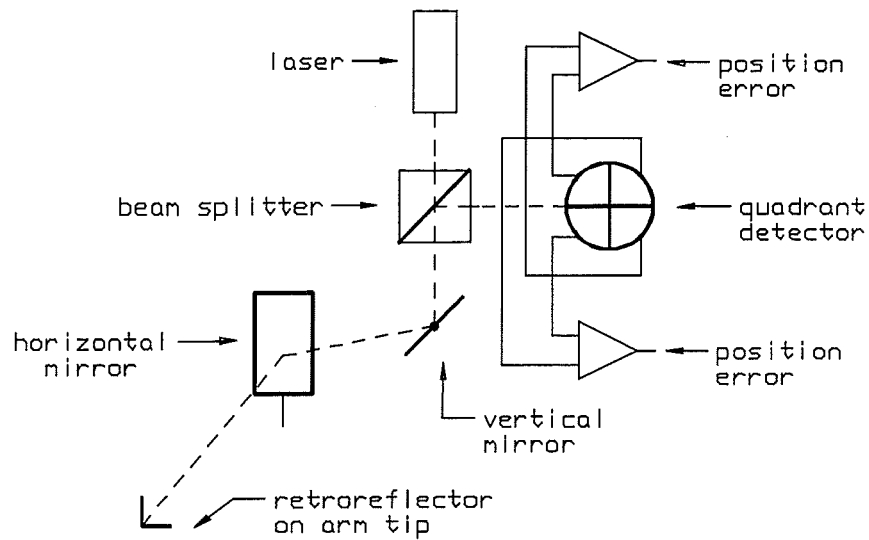


Figure 2.26 - End-point position tracking - (Automated Systems Laboratories Ltd)

End-point position error, as measured by the optical system, was introduced to a PI controller with a 28 ms sampling time, the output driving the manipulator's servo actuators through their own controller.

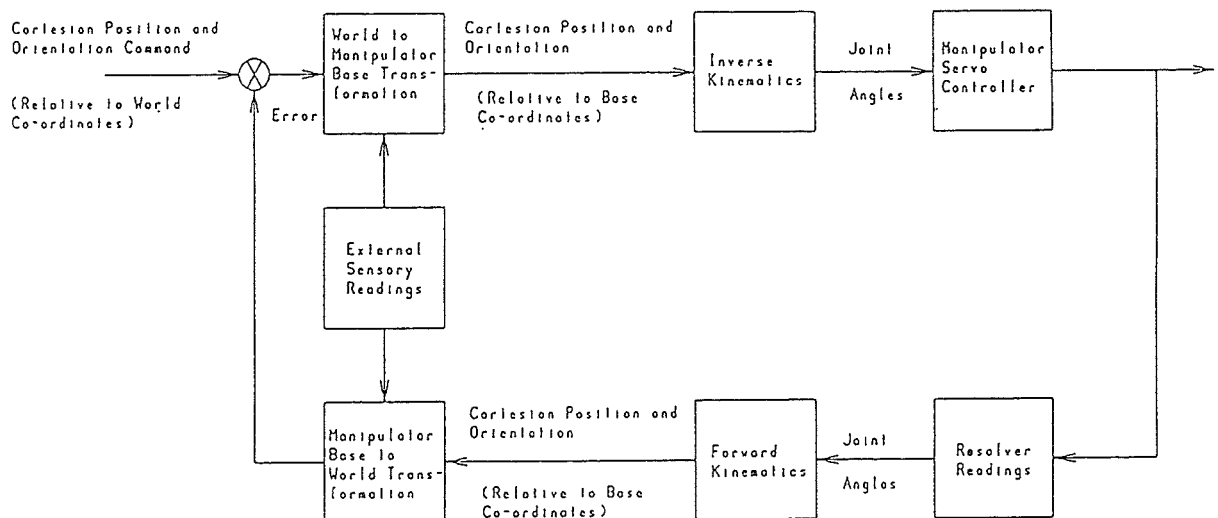


Figure 2.27 - Functional architecture of the manipulator tip stabilisation system - (Manganas, 1993)

The use of an external measuring system in this manner means that the effects of gear backlash, link flexing and inaccuracies in kinematic modelling can be largely bypassed. A high degree of positioning accuracy has been achieved (± 0.08 degrees with a resolution of ± 0.01 mm). The major drawback of this system is that it requires positioning at large, obstacle-free distances from the robot. Both laser pods must be well separated, thus creating a considerable 'dead volume' in front of the robot. In practice, applications are limited to purpose-built environments where the Lasertrace pods and robot can be permanently positioned such that the continuity of the reflected laser beams can be maintained. This means that the robot's working envelope, robot movements, configuration changes and payload sizes are restricted as the tip retroreflector must be continually exposed to both laser beams.

Smith (1995) describes a tracking system for military applications. A 'target' is moved in relation to a tracking platform, the object being to reduce the error between the line-of-sight of the tracking platform and the target in order to align the tracking platform with the target. In the experimental apparatus, the optical tracking platform determines the 2-D position (azimuth and elevation) of a target laser, the laser spot image is focused by the tracking platform optics onto a quadrant detector which, using signal conditioning electronics (see Chapter 4, figure 4.16) gives information as to the horizontal and vertical position of the image on the detector. Through a fuzzy logic controller, the tracking platform was moved such that the image of the laser is constantly centred upon the detector. This system compares directly with the twin gimbal laser tracking system of Furuta and Sampei (1984) described in the next section.

Grieco *et al* (1995) employ externally mounted cameras to detect the tip position of a flexible manipulator. True tip position, in Cartesian coordinates, is sensed using an LED attached to the link and measured with two 3-D infrared cameras (see figure 2.28). The strategy uses an internal PD loop to control the hub motor angle (θ), as measured by an incremental encoder, and an outer loop for tip position correction. A Jacobian transformation is used to convert the camera measured Cartesian coordinates of the tip to angular coordinates used in the control loop.

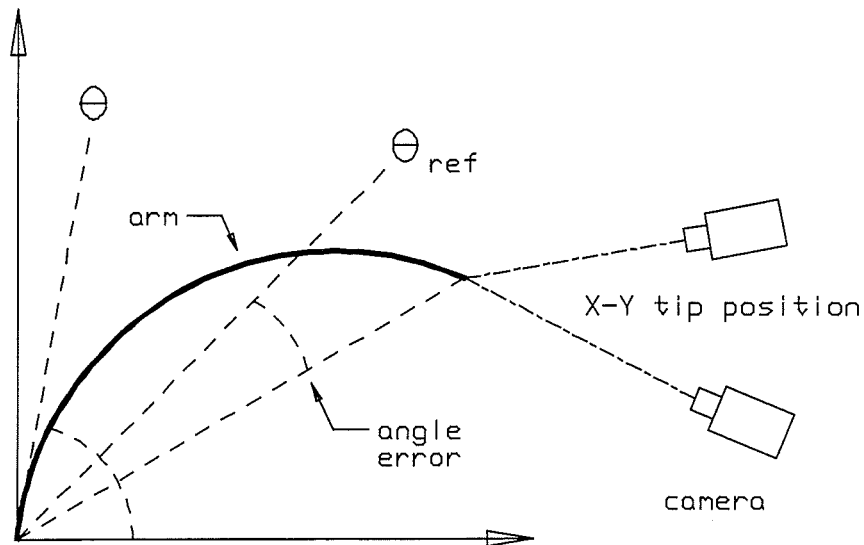


Figure 2.28 - 3-D tip position measurement system - (Grieco *et al*, 1995)

Figure 2.29 shows the layout of the controller design.

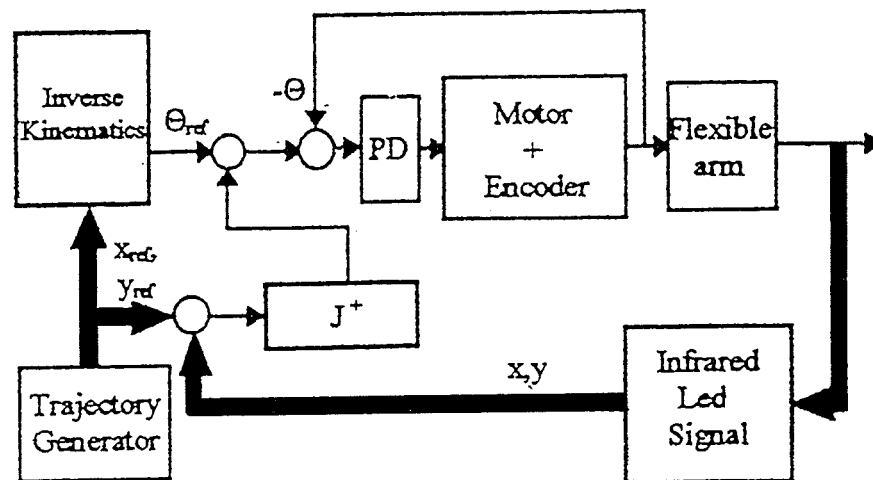


Figure 2.29 - Flexible link control scheme - (Grieco *et al*, 1995)

Tip position is compared with the reference trajectory, generating the X,Y space error with respect to the reference with the assumption that the beam located at the reference angle is rigid. This error is converted to joint space using a Jacobian inverse matrix transformation. The error is fed back to the internal loop, changing the set-point to correct for errors generated by vibrations or gravity effects on the tip position.

$$J^+(\dot{\theta}_{ref}) \times e_{x,y} = e_{\theta} \quad (2.8)$$

where J^+ donates the pseudo-inverse of J . The control signal is then given by :-

$$u = k_p(\theta_{ref} - \theta) + k_v(\dot{\theta}_{ref} - \dot{\theta}) + k_{PJ}(J^+e_{xy}) + k_{VJ}(J^+\dot{e}_{xy}) \quad (2.9)$$

Experiments were conducted on 0.6 m long arm moving through the horizontal plane - gravitational effects being ignored.

The arm was moved through an angle of π radians in 2 s, held in position for 2 s and then returned to the original angle in another 2 s. With conventional *hub angle (encoder based) control* considerable tip positioning errors were present. Maximum tip deviations from the reference position are up to ± 100 mm, with ± 20 mm for the steady state error (see figure 2.30).

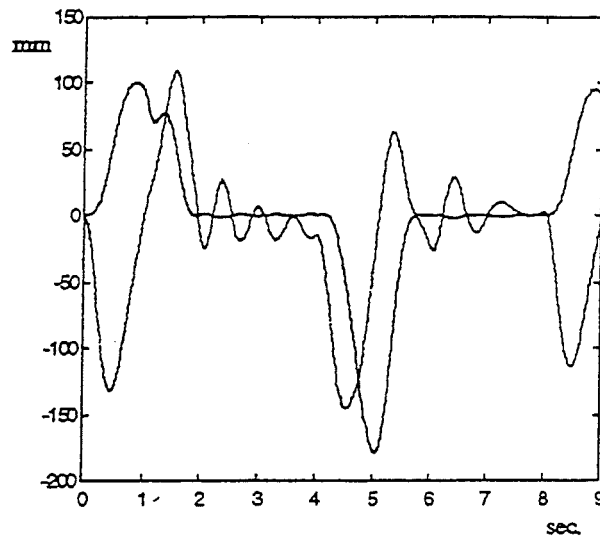


Figure 2.30 - X-Y tip coordinate errors for following trajectory under encoder based control - (Grieco *et al*, 1995)

With only *tip position control*, bigger following errors are observed - up to ± 400 mm (see figure 2.31). These are attributed to the non-collocated nature of the control as hub position is not corrected until a significant error signal is generated, occurring only after the delay transport of the deflection of the beam.

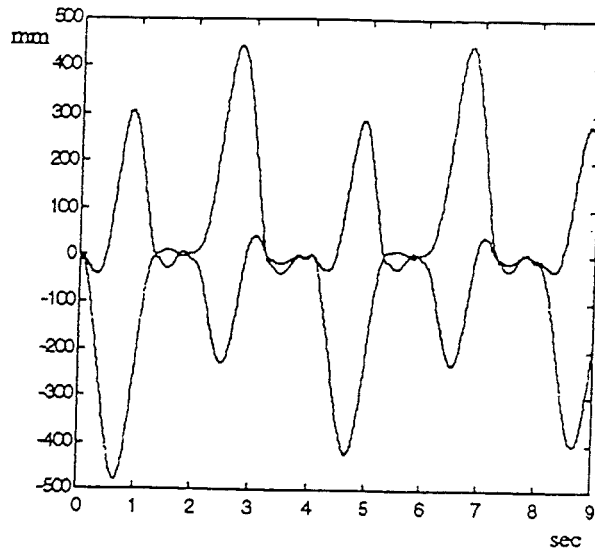


Figure 2.31 - Errors in X-Y tip position - (Grieco *et al*, 1995)

The *Jacobian control scheme* gave errors of less than 35 mm (steady state) with virtually no tracking delay (see figure 2.32). To work, in the steady state the beam must be completely undeformed and the hub angle must be aligned with the reference angle.

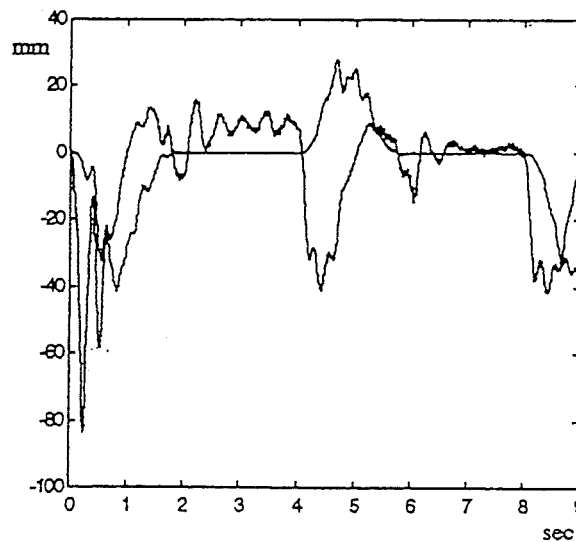


Figure 2.32 - Errors for X-Y tip position under Jacobian control - (Grieco *et al*, 1995)

The control method used does not use true non-collocated control as the measured tip position errors are used to correct the hub set-point rather than the hub position directly from the error signal coming directly from the tip.

2.4.2 Internally Positioned Systems

Demeester and Van Brussel (1991) developed a system for the real-time *measurement* of all spatial structural deflections of robot links (except elongation) to control deflections and vibrations in flexible arms. Three laser diodes were fixed to the low end of the link, each being aimed at a PSD attached to the far end of the link.

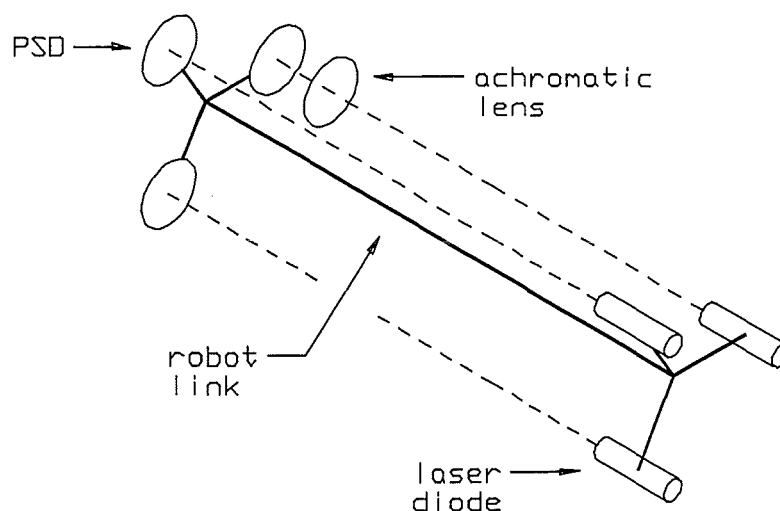


Figure 2.33 - Schematic diagram of the 5-axis optical end-point position orientation and measurement system - (Demeester and Van Brussel, 1991)

The system, called DIOMEDES (Laser DIode System for MEasuring Structural DEflectionS), measured the position coordinates of the spots on the sensor surfaces. The position of the spots on the PSD's contained the information for determining five structural deflections out of the six coordinates.

Figure 2.34 shows the link structural deflections. The frame $\{x_0, y_0, z_0\}$ represents the end of the straight link before deflection, the z -axis coinciding with the neutral axis of the undeformed link. The frame $\{x_0', y_0', z_0'\}$ represents the end of the link after deflection. The spatial structural deflection of the link is characterised by the translational deflections d_x, d_y, d_z (d_z unmeasured) and rotations a_x, a_y and a_z .

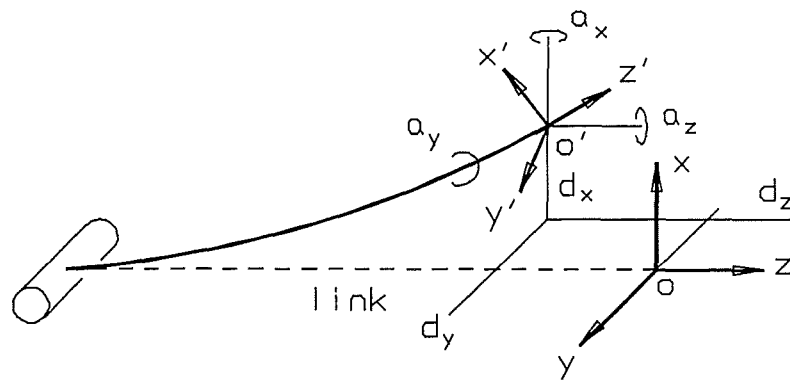


Figure 2.34 - Link structural deflections - (Demeester and Van Brussel, 1991)

The sensor system measured the structural deflections d_x and d_y and the rotations a_x , a_y and a_z . Deflections d_x and d_y , and rotation a_z , were calculated by combining the measurements of the PSD's *without* the lens. Rotations a_x and a_y were calculated from the measurements of the PSD mounted *in the focal plane of the lens*. With the lens in place, the structural deflections d_x and d_y had no effect on the position of the laser spot on the PSD. The relationship between the deflections and the coordinates of the spots on the PSD's can be represented as a series of coordinate frame, homogeneous coordinate and homogeneous transformation matrices to calculate the translations and rotations about the proper axes of the undeformed link frame $\{x_0, y_0, z_0\}$. Static and dynamic deformations could be measured within a range of ± 5 mm (resolution $3 \mu\text{m}$) for d_x and d_y and within a range of $\pm 0.8^\circ$ (resolution $7 \mu\text{rad}$) for bending angles a_x and a_y .

The use of this system for end-point *control* was later investigated by Swevers *et al* (1992). The system formed part of a tracking controller on a single flexible link.

The controller was based upon an experimentally identified discrete time state-space model and used the motor angle and the measurements of the optical link deflection sensor to determine the end effector position. An integral term was included to eliminate steady-state error :-

$$\text{Signal } u_i[k] = k_i \frac{T_s}{2} (e[k] + e[k-1]) + u_i[k-1] \quad (2.10)$$

with k_i the integral feedback gain, T_s the sampling period and $e[k]$ the tracking error.

The link was rigid in the vertical plane. Only the horizontal structural displacement d_y was measured to determine the link end-point position, tip rotation α_x was ignored. Due to the limited sensing range of optical system (± 5 mm), and as the beam deflections at the tip exceeded this range, the system was mounted half way along the link (c.f. the link local deflection system, Wang *et al*, Section 2.3.2.1). Tip position was calculated using a proportionality factor of 4, giving a maximum measurable tip deflection of ± 20.05 mm.

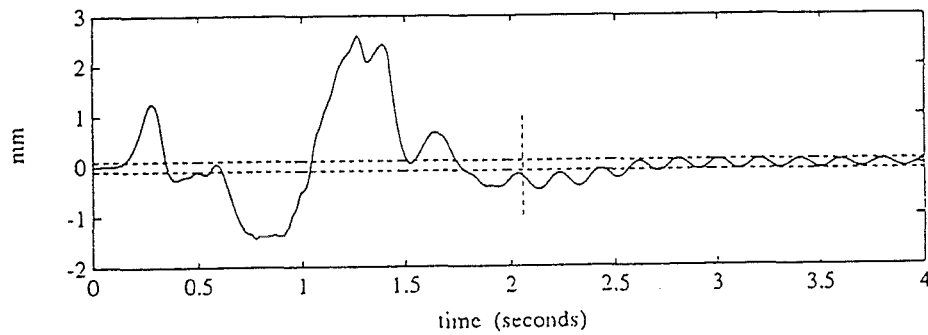


Figure 2.35 - Horizontal displacement tracking error signals
- (Swevers *et al*, 1992)

Figure 2.35 shows the horizontal tip displacement as measured by the optical system - the horizontal dashed line indicating the steady state error tolerance of ± 0.1 mm, the vertical dashed line indicating the time instant at which the final position should be reached. The maximum tracking error was less than 2 mm with a maximum overshoot of 0.48 mm.

Again, the optical system formed *only one part* of an overall end-point positioning system - primary arm position being measured by an encoder collocated with the arm hub actuator. Although capable of determining five end-point position coordinates, its use was limited to the measurement of one coordinate only.

A system that most closely resembles the novel position control strategy, as described in Chapter 1, was that described by Furuta and Sampei (1984) in which they proposed a method of controlling the movement and attitude of a robot using a laser and an optical sensor. The sensor means, shown in figure 2.36, consisted of a beam position sensor and a beam angle sensor. Both were supported on a common frame supported on a twin gimbal frame. The complete system was attached to a three-axis motorised table.

A lateral effect PSD was used as a beam position sensor. Output from the sensor determined the direction in which the sensing head should move (along the direction of the beam) and the deviation of the sensing head from the beam : by measuring the distance between the centre of the sensor and the irradiated point on the sensor surface.

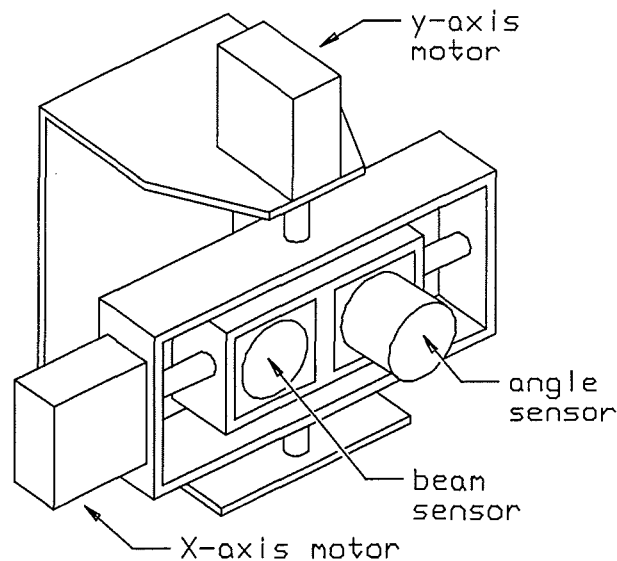


Figure 2.36 - The twin gimbal laser tracking system - (Furuta and Sampei, 1984)

A second sensor recorded the angle between the direction of the laser beam and the normal to the beam sensor surface. It differed from the position sensor in that a lens was used to focus the image of an IR laser diode onto a PSD such that the output from the PSD could be used to determine the angle between the centre line of the lens and a line connecting the centre of the lens and the PSD, as shown in figure 2.37.

Gimbal servo motors were controlled through the outputs from the angle sensor such that the normal to the sensor surface was automatically adjusted to correspond to the direction of the laser beam. Each was equipped with a position recording potentiometer. The angles recorded by the potentiometers gave the X and Y coordinates of the incoming beam.

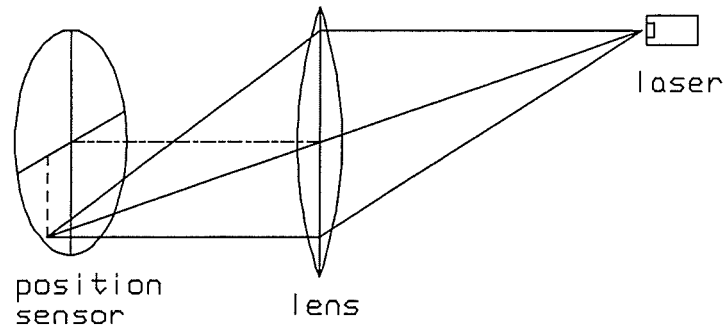


Figure 2.37

- The beam

angle detecting system - (Furuta and Sampei, 1984)

A PI controller with state feedback was employed (sampling interval 13 ms). The control configuration is shown in figure 2.38.

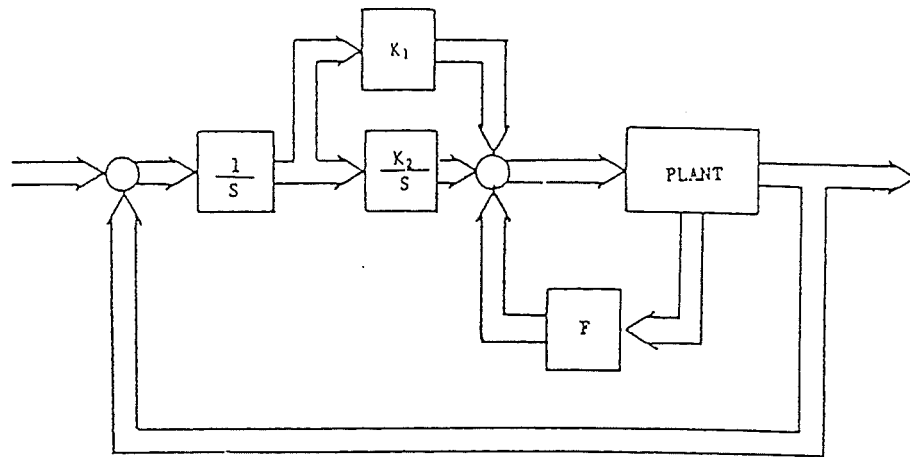


Figure 2.38 - Controller configuration - (Furuta and Sampei, 1984)

In contrast with the novel control system proposed in this thesis, that described by Furuta and Sampei was employed as a centering device, for position teaching purposes, such that an industrial robot equipped with the sensor was caused to move along the axis of a laser beam with minimal deviation from the beam path. The system was not designed for tracking control and trajectory control was restricted to movement along the axis of the beam. Robot control was model based in that, unlike that of the novel system proposed, an accurate mathematical prediction of the mechanical system dynamics was required, to enable robot movement to be actioned through the hub based controller.

Summary

A range of optical position sensing methods have been reviewed. As shown in figure 2.1, the strategies explored fall into one of three categories. No single system described can claim to provide a complete solution for end-point control of flexible link robots, each suffers from implementation difficulties which are summarised below.

Post-bending correction - micromanipulators

- Dual control system required due to dynamic interactions between the micro and macro systems lead to difficulties in obtaining a stable response on flexible arms.
- Static errors only compensated.
- Complex optical end-point position sensing and orientation system required.
- With external optical systems there are limitations on macro operating volume, arm configuration and payload size necessary to avoid restricting the optical sensor from view.

Systems that maintain arm tip position - Active stiffness control and active position correction

- Forms only one part of the overall robot control system.
- Secondary actuators and subsidiary controller required.
- Optical system for deflection measurement only, twist not detected.
- Stability problems - dynamic interaction between the independently operated, yet mechanically coupled, systems.
- Indirect measurement method demands time consuming calculation of end-point position.

Direct end-point position control

- *External optical position sensing* - restricts robot operating volume and arm orientation as optical beam path must be maintained.

- Open to interference from ambient light sources.
- Use limited to stable operating environments.
- *Internal optical systems* - Most restricted to the *measurement* of arm deflections.
- Form part only of a complex robot position control system.

The use of optics has been restricted to the *measurement* of link deflection errors, this measurement forming *only part* of the overall robot control strategy. A fundamental aspect of the system proposed in this thesis is that the output from an optical detector provides the sole input to the robot controller enabling flexible arm position control to be achieved. The control concept has been formulated to overcome the limitations inherent in the systems described in this chapter. The advantages of the new system are listed below.

- Direct optical end-point position sensing.
- Optical system internal to the robot structure, therefore enabling robot movement within the full operating volume available.
- Single sensor for arm positioning and deflection compensation.
- Control system requiring input from the optical sensor only.
- Static error correction.
- Single actuators for both arm positioning and deflection compensation.
- As the optical system is inside the robot structure, it can be protected from mechanical damage and shielded from ambient light sources.

The fundamental difference between the method of control proposed in this thesis and those that have been reviewed in this section is that all other methods use a *model* of the flexible arm and actuator *to generate the desired trajectory* for the manipulator. This method of trajectory generation is prone to errors due to model parameters varying while the plant is in operation. Various methods of on-line parameter estimation techniques have been employed to overcome these problems but there is an additional computational complexity involved and the models are linearised to make them solvable.

The new method of control does not rely on any modelling of the system. This is because *the trajectory is generated as a separate entity from the arm control loop*. The accuracy of trajectory generation is dependent only on the accuracy of the positioning head. Also, the errors between the desired trajectory set by the laser and the actual trajectory of the tip are limited by the size of the tip detector. A closed loop control system via the hub actuator ensures that the tip of the arm, which corresponds to the centre of the detector, is as close as possible to the laser spot, i.e. the tip of the arm tracks the laser spot.

The next chapter gives details of the robot design and construction. The various stages in its development are discussed. Modifications and improvements made during development are described.

References

- Cannon, R.H. and Schmitz, E., (1984) 'Initial experiments on the end-point control of a flexible one-link robot', The International Journal of Robotics Research, Vol. 3, No. 3, Autumn 1984, pp. 62-75.
- Chalhoub, N.G. and Zhang, X., (1993) 'Reduction of the end effector sensitivity to the structural deflections of a single flexible link: theoretical and experimental results', Journal of Dynamic Systems Measurement and Control, Transactions of the ASME, Vol. 115, No. 4, Dec. 1993, pp. 579-740.
- Chiang, W.W., Kraft, R. and Cannon, R.H., (1991) 'Design and experimental demonstration of rapid, precise end-point control of a wrist carried by a very flexible manipulator', The International Journal of Robotics Research, Vol. 10, No. 1, Feb. 1991, pp. 30-40.
- De Schutter, J. and Van Brussel, H., (1992) '3-D laser tracking system', In Lecture Notes of the Short Course on Computer Controlled Motion, Third edition, Katholieke Universiteit Leuven 1992, pp. 237-242.
- Demeester, F. and van Brussel, H., (1991) 'Real-time optical measurement of robot structural deflections', Mechatronics, Vol. 1, No. 1, pp. 73-86.
- Driessen, F.P.G., Lucassen, F.H.R and Van de Ven, H.H., (1986) 'A three dimensional position measuring system', In Theory of Robots, edited by P. Kopacek, I. Troch and K. Desoyer. IFAC Proceedings Series 1988, No. 3, pp. 309-313.
- Editor, (1993) 'Lasertrace tracking laser system', Automatic Systems Laboratories Ltd, Milton Keynes, U.K.
- Furuta, K. and Sampei, M., (1984) 'Path control of three dimensional mechanical system using laser', Proceedings of IECON'84, pp. 189-193.

Grieco, J.C., Fernandez, G., Gammarra-Rosado, V.O. and Armada, M., (1995), 'Tip position control with hub corrections for a flexible manipulator', IFAC - Workshop on Human-Oriented Design of Advanced Robotic Systems, DARS'95, September 19-20, Vienna, Austria, pp. 215-220.

Harashima, F., Nishiyama, Y., Ueshiba, T. and Hashimoto, H., (1989) 'Adaptive control of a flexible arm with a variable payload', Distributed Parameter Systems:Modelling and Simulation - IMACS 1989, pp. 323-328.

Harashima, F. and Ueshiba, T., (1986) 'Adaptive control of flexible arm using the end-point position sensing', Proceeds of the Japan - U.S.A. Symposium on Flexible Automation 1986, pp. 225-229.

Jiang, Z-H., Uchiyama, M. and Hakamori, K., (1989) 'Active compensating control of the flexural error of elastic robot manipulators', Distributed Parameter Systems: Modelling and Simulation - IMACS 1989, pp. 369-373.

Kyle, S.A., (1995) 'Optical methods for calibrating and inspecting robots', Computing and Control Engineering Journal, Vol. 6, No. 4, August 1995, pp. 166-173.

Lin, Y-J. and Lee, T-S., (1992) 'Comprehensive dynamic modelling and motion/force control of flexible manipulators', Mechatronics, Vol. 2, No. 2, April 1992, pp. 129-148.

Manganas, A., (1993) 'Tip stabilisation of base compliant manipulators', Advanced Robotics Research Ltd, Salford, U.K.

Mulders, P.C., van der Wolf, A.C.H., Heuvelman, C.J. and Snijder, M.P., (1986) 'A robot-arm with compensation for bending', Annals of CIRP, Vol. 35, No. 1, pp. 305-308.

Sharon, A. and Hardt, D., (1984) 'Enhancement of robot accuracy using endpoint feedback and a macro-micro manipulator system', Proceedings of the American Control Conference, San Diego, pp. 1836-1842.

Sharon, A., Hogan, N. and Hardt., D.E., (1993) 'The macro/micro manipulator: an improved architecture for robot control', Robotics and Computer Integrated Manufacturing, Vol. 10, No. 3, pp. 209-222

Smith, E.S., (1995) 'An application of fuzzy-logic control to a classical military tracking problem', Naval Engineers Journal, Vol. 107, Part 1, pp. 99-108.

Swevers, J., Torfs, F., Demeester, F. and Van Brussel, H., (1992) 'Fast and accurate tracking control of a flexible one-link robot based on real-time link deflection measurements', Mechatronics, Vol. 2, No. 1, pp. 29-41.

Taylor, R.H., Hollis, R.L. and Lavin, M.A., (1984) 'Precise manipulation with endpoint sensing', IBM research report, IBM T.J. Watson Research Centre, Yorktown Heights, New York 10598.

Uchiyama, M., Jiang, Z.H. and Hakomori, K., (1990) 'Compensating control of a flexible robot arm', Journal of Robotics and Mechatronics, Vol. 2, No. 2, pp. 97-106.

Wang, W-J., Lu, S-S and Hsu, C-F., (1989) 'Experiments on the position control of a one-link flexible robot arm', IEEE Transactions on Robotics and Automation, Vol. 5, No. 3, June 1989, pp. 373-377.

Wang, C-C. and Shekhar, A., (1991) 'On-line acquisition of link deformation for the robot of accuracy', Computers and Industrial Engineering, Vol. 21, Nos. 1-4, pp. 529-533.

Zalucky, A. and Hardt, D.E., (1984) 'Active control of robot structure deflections', Journal of Dynamic Systems Measurement and Control - Transactions of the ASME, Vol. 106, March 1984, pp. 63-69.

Chapter 3

PROTOTYPE ROBOT CONSTRUCTION

3.1 INTRODUCTION

This chapter details the development of the robot from its earliest to final configuration. Special mention is made of critical component designs along with any alternatives tested.

Initially a 'proof of concept' single-axis robot was constructed to test the feasibility of the optically sensed position control system. Linescan cameras were used for both laser elevation and arm end-point control. The 1 m Perspex arm was driven by an electric linear actuator. Although successful for demonstrating the control principle, performance was hindered by low camera resolution and slow actuator speed.

The robot was later modified and refined considerably. The positioning head was redesigned with an optical encoder replacing the linescan camera for elevation control. An aluminium arm was used, a more powerful linear actuator was added along with a purpose-built beam tracker.

In the third version, horizontal movement was added to enable the dual-axis position detecting ability of the beam tracker to be tested. This necessitated a complete redesign of many of the major features, foremost being the positioning head and exoskeleton motor mounts. With the linear actuator replaced by two high performance servo drives, the speed of arm response increased dramatically, so allowing testing and analysis of the end-point control concept under a variety of control algorithms.

A series of joint designs are also described. In each case, the laser beam is deflected about the joint axis such that it continues to pass up inside the arm and impinge upon a beam tracker at its tip. With these designs, optically sensed end-point controllers can be used on multi-axis robots.

3.2 DESCRIPTION

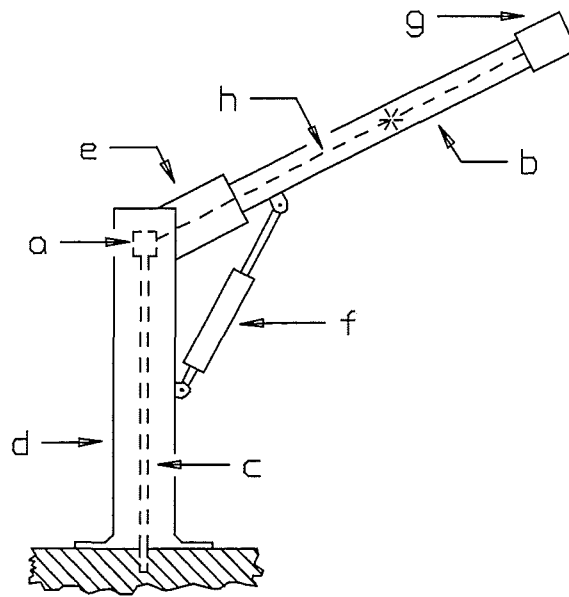


Figure 3.1 - The initial experimental prototype

As shown in figure 3.1, the beam from a laser diode was directed by a positioning head (a) along the desired trajectory, the beam passed up the centre of a hollow, flexible, single-link arm (b). The positioning head was housed co-axially with and inside the inboard arm pivot on a vibration resistant post - *the endoskeleton* (c) - positioned in the centre of the robot upright column. The column and arm constituted the robot's load bearing structures - *the exoskeleton* (d). The endoskeleton was firmly fixed to the robot support plate so that it was mechanically isolated from the exoskeleton and therefore not subject to the load-induced deflections experienced by the exoskeleton.

A U-frame assembly (e), which supported the arm, pivoted about the upper most part of the robot upright column. Arm elevation was controlled through an electric linear actuator (f) - Absac model ELM 1024. A linescan camera (g), located at the extremity of the arm, tracked the position of the laser beam (h) (see Chapter 4, Section 4.4). Camera signals were fed back to the computer to monitor arm position. As the laser beam moved to a new position, the camera gave a change in output which was processed and fed to the arm actuator to cause repositioning of the arm so that the camera was continuously centred on the beam spot.

3.2.1 The Endoskeleton

The endoskeleton consisted of two parts :- a column and a positioning head.

The column - The magnesium/aluminium alloy column served two purposes. It formed an independent support for the positioning head and acted as a means of insulating the positioning head from vibrations transmitted through the exoskeleton. The magnesium alloy tube was packed with lead shot to act as a damping medium. Magnesium alloy has exceptional ability to absorb vibrational energy and is thermally stable. It is commonly used in applications where impact concerns are critical.

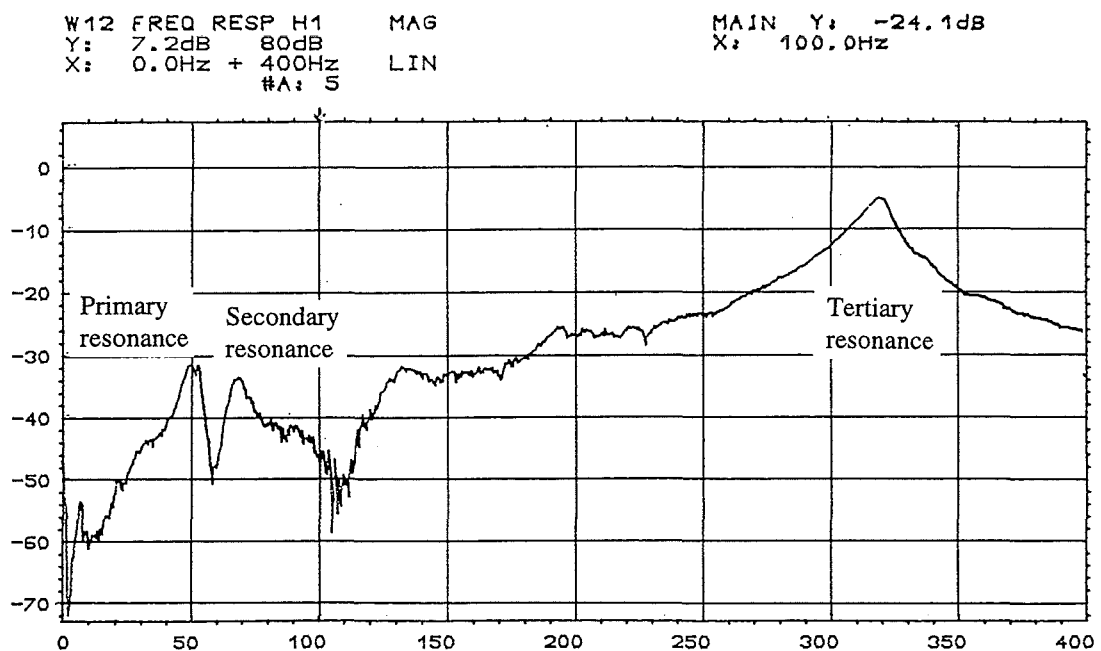


Figure 3.2 - Frequency response measurement of the endoskeleton column

The frequency response of the column was measured on a Bruel and Kjaer real-time frequency analyser, the column being bolted vertically on a concrete block and struck at various points along its length with a Bruel and Kjaer type 8202 impact hammer. The lowest natural frequency of the column was 50 Hz. This can be compared directly with the frequency response of the endoskeleton column and exoskeleton fitted with a 1 m long arm (again recorded at the column) showing that the frequencies at which the column vibrates remain unaffected by vibration disturbances of the main robot structure (see figure 3.3).

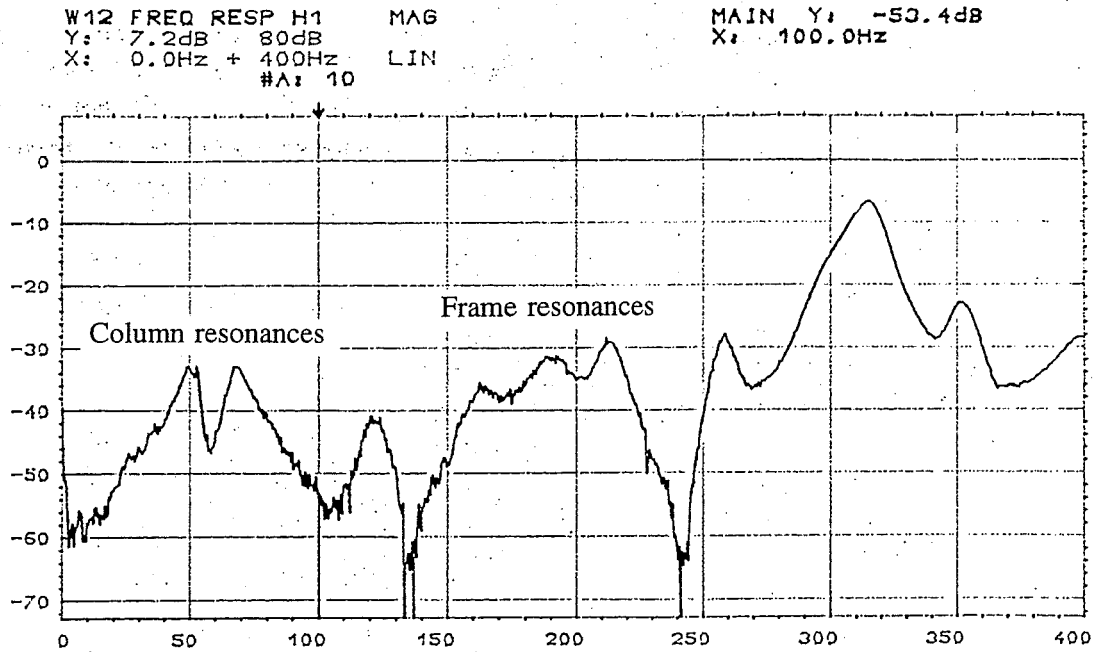


Figure 3.3 - Frequency response of the endoskeleton column as measured with the column fixed within the exoskeleton frame

The positioning head - The purpose of the positioning head was, through operator control, to cause elevation of the laser beam through the desired programmed path. A positioning head was constructed which enabled accurate elevation of the laser beam (a) through angles between 0° and 45° to the horizontal. To produce finely controlled and smooth rotation of the laser (b) a precision DC motor (c) was used along with a 15000:1 ratio gearbox (d). The motor provided sufficient torque through a range of voltages (2-12 V). Its speed (0-3000 rev/min) and direction of rotation could be easily controlled. The high gearbox reduction ratio gave precise control over laser positioning so that small angular corrective movements, in the order of 10 arc", were achievable.

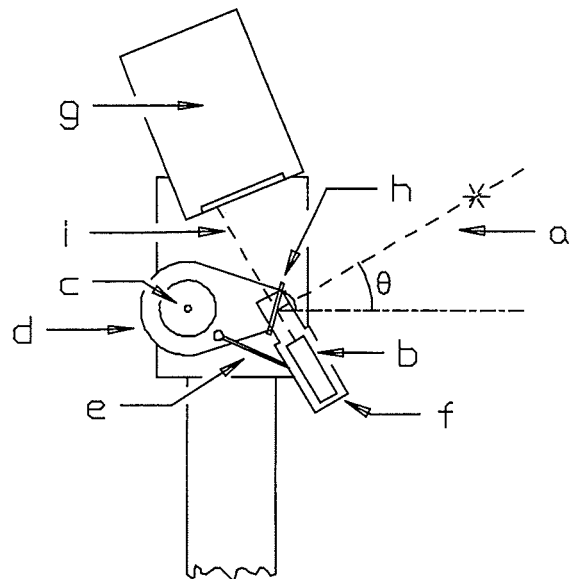


Figure 3.4 - Details of the positioning head

An anti-backlash spring (e), attached between the laser head (f) and gearbox casing, minimised the delay that occurred on changing direction and eliminated backlash on the

final drive. A linescan camera (g) was used for non-contact laser position detection. It was mounted above a beam splitter (h) and the laser and indicated the position along the array of the light (i) transmitted through the beam splitter, enabling the angle of elevation of the reflected portion of the laser beam (a) to be monitored and controlled. The camera was mounted at an angle of 22.5° to the horizontal so as to maintain the angle of incidence of the laser beam on the array as near to the normal as possible throughout the 45° sweep, so minimising light scatter into neighbouring photosites along the array. Arm movement was limited to 45° to enable the bulky linescan camera to be incorporated into the design.

An important design feature was that both the laser and beam splitter were rotated as one unit about a common pivot. This ensured that the transmitted light was caused to scan across the endoskeleton mounted, elevation monitoring camera as the angle of elevation of the laser beam was changed. This would not have been the case if the laser had been fixed and only the mirror had been driven. Therefore only a laser source of small physical size could be used since it was to form one of the moving components of the positioning head. The light needed to be visible, to enable it be aimed at the cameras by eye and produce a well defined, small area of illumination over a distance of up to 3 m.

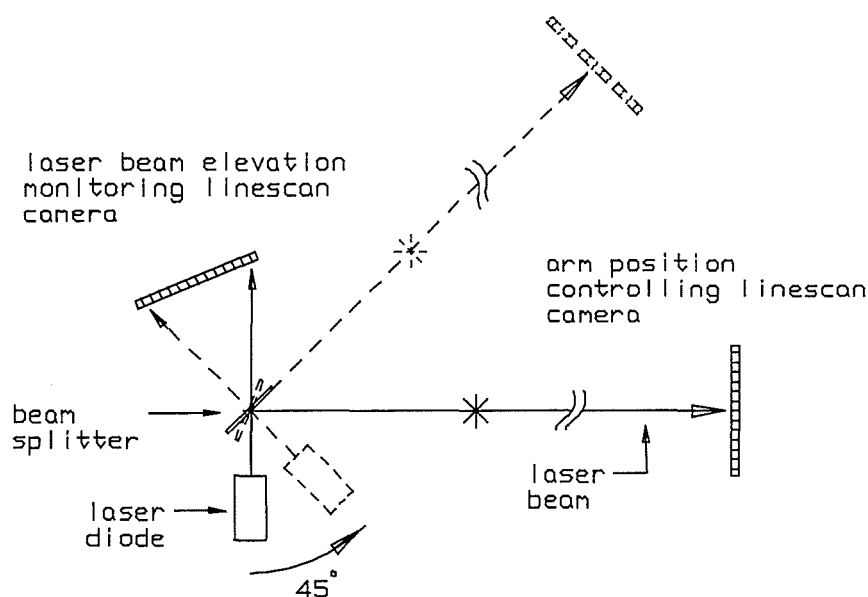


Figure 3.5 - Schematic diagram showing positioning head operation

A collimated laser diode was used. It, together with the collimating lenses and power supply, was housed in a 25 x 10 mm cylindrical brass body. The output power of the laser

was 1 mW, the wavelength of the light was in the 670 nm visible red region. It illuminated only a small section of the photodiode array - a necessary requirement for obtaining maximum position resolution with the linescan cameras.

The semi-silvered beam splitter had 50/50 transmission/reflection characteristics (when set at 45° to the incident beam) and therefore could be angled to provide both cameras with illumination of equal intensity. To enable elevations of up to 45° to be achieved, with an active photosite length of 26 mm, the centre of the photosite strip required positioning at a distance of 31 mm from the beam splitter pivot.

3.2.1.1 *Resolution, accuracy and repeatability*

System performance was determined by :

- the length and resolution of the photosite array,
- the maximum angle through which the arm was designed to move, and
- the accuracy of the laser drive mechanism.

Resolution of the linescan camera elevation detector depended upon the number of photosites per unit length on the photodiode strip. The 26 mm long linescan camera array had 256 photosites, and so the resolution was 0.176° of laser rotation per photosite, equivalent to an end-of-arm movement of 3.14 mm (for a 1 m arm) per photosite scanned. The accuracy of the system could have been increased using a higher resolution camera yet this would have incurred a substantial increase in cost.

The speed at which the elevation monitoring system worked depended upon :

- the speed of computation (see Chapter 6, Section 6.2.2.) and
- the rate at which the laser beam was scanned over the photosite array.

Speed of laser rotation could be varied between 0-1 rev/min by controlling the voltage across the drive motor. Maximum scanning speed was determined by the rate of operation of the laser driving gearbox/motor combination. The motor, rated at 3000 rev/min at 12 V input, caused the output shaft of the 15000:1 gearbox to rotate the laser through the

maximum arm elevation angle of 45° in 37.5 s, this being the time taken to traverse the whole array. Each photosite would therefore be scanned in 0.15 s.

System accuracy was determined by the resolution of the optics and the tolerances to which the laser drive system was built. Removal of end and side float in the gearbox output shaft ensured that the laser beam would track along the desired path through all angles of elevation. The anti-backlash spring removed backlash from the gear train. A certain amount of error was inevitable as both the laser and mirror were aligned by eye, yet this was not thought to be a serious problem as this error would always be constant. Repeatability of angle setting was within $\pm 0.26^\circ$ of the desired angle.

3.2.1.2 Improvements to the positioning head elevation monitoring system

The camera was replaced by an optical encoder to increase the resolution of the laser elevation control system. A non-contacting incremental encoder was used (Hewlett Packard HEDS-6000) which did not burden the system with added inertia and friction. It was reliable, maximum velocity and encoding speed were high (12,000 rev/min and 200 kHz respectively) and was tolerant to shaft axial play (max 0.58 mm), shaft eccentricity and radial play (max 0.25 mm).

Replacement of the linescan camera by the optical encoder eliminated the need for the beam splitter as the encoder was attached directly to the output shaft of the gearbox. Position monitoring errors that could occur as a result of backlash in the gear train were eliminated as both the laser and encoder were driven from the same shaft. The encoder contained a pair of integrated detectors which produced an output as two square wave signals in quadrature form, there being a phase difference of 90° between the outputs from each channel. The output gave the necessary information to determine shaft position, speed and direction of rotation. Phase shift between the pair of signals produced a four-fold increase in the position detecting sensitivity of the device which gave a maximum resolution possible of 4096 counts per revolution. This produced 512 counts over an angle change of 45° which corresponded to 0.088° per count, being equivalent to an end-of-arm travel (for a 1 m arm) of 1.5 mm per encoder count.

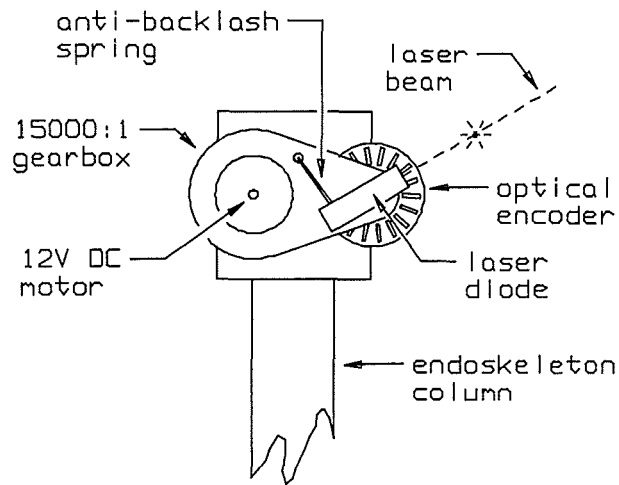


Figure 3.6 - The modified positioning head with optical encoder

The optical encoder was connected to a motion control microprocessor (Hewlett Packard HCTL-1000). The microprocessor was configured to output pulse-width modulated (PWM) signals enabling velocity control of the DC motor through H-bridge amplifiers. The microprocessor was interfaced to a computer through a PC-30B I/O board. A program, written in 'C' code, controlled the motor position (Waki, 1992).

3.2.2 The Exoskeleton

The exoskeleton constituted the load bearing elements of the robot structure. It consisted of the upright support and the arm.

The upright support - This consisted of a base and a hollow stand which provided the support for a U-frame about which the arm pivoted.

The U-frame and arm - A 32 x 15 x 8 mm U-frame supported the arm and allowed it to pivot on plain bearings mounted on the exoskeleton upright. The frame was designed to be sufficiently rigid to prevent sideways movement about the pivot points which could cause the arm mounted camera to be deflected out of the path of the laser beam. The arm was constructed from a 1 m length of 45 mm ϕ Perspex tube, being sufficiently flexible (lowest natural frequency of 10 Hz) to enable the operation of the guidance and position correcting systems to be tested with the arm under loads of up to 1 kg.

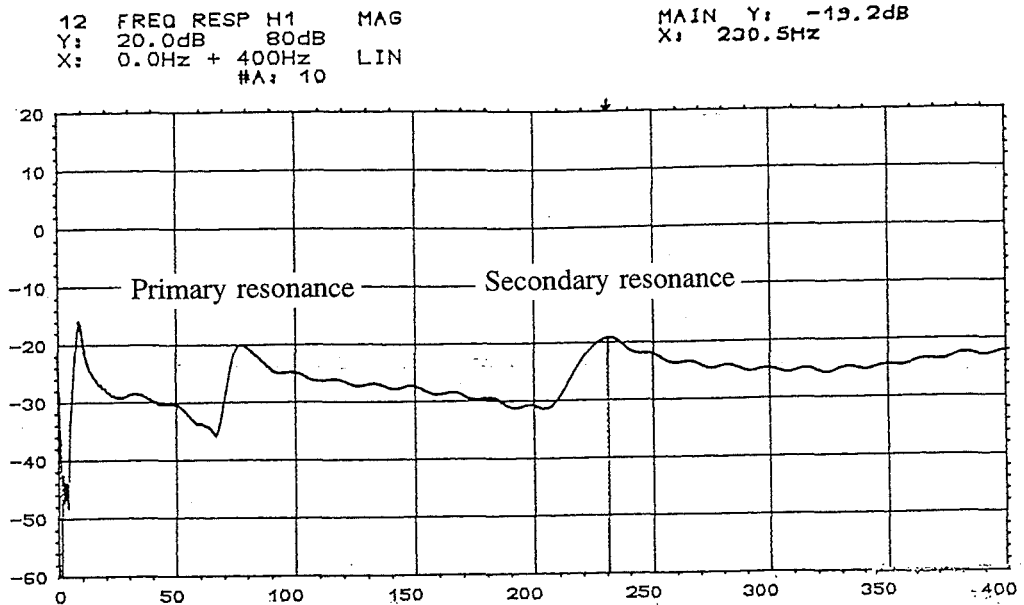


Figure 3.7 - Frequency response measurement of the Perspex arm

The Perspex arm was later replaced by a 2 m, 33 mm ϕ , extruded aluminium tubular arm of 1.5 mm wall thickness. Doubling arm length gave a more flexible structure and an increase in the amount of load induced deflection. Aluminium tube was chosen as it was sufficiently strong, yet still possessed the necessary degree of flexibility to enable the deflection correcting component, of the control system, to be tested thoroughly. Due to the increased weight of the arm, a more powerful electrical linear actuator was used (Absac model ELM 5012) driven by a current rather than voltage amplifier (Editor, 1994). Since torque in a DC motor is proportional to current, modifications shown in figure 3.8 were made to the power amplifier circuitry such that the motor drive current was proportional to the drive voltage signal (Snyder, 1985). This direct control of motor torque improved tracking ability.

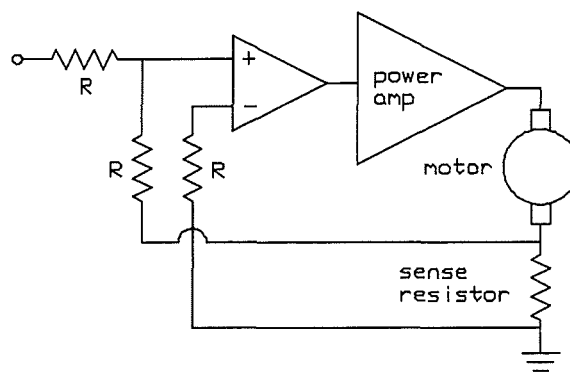


Figure 3.8 - Controllable current source motor power amplifier

3.2.3 Prototype Limitations

The prototype suffered from mechanical faults which limited its performance. Lack of damping in the positioning head caused it to vibrate, sluggish actuator response restricting the speed of arm movement, as shown by the recorded results in Chapter 6. A radical re-design of the major components was undertaken, leading to the development of the dual-axis robot described in the following sections.

3.3 THE DUAL-AXIS, SINGLE LINK ROBOT

To enable further development of the control strategy the original robot was modified for two axis movement so that the arm could move simultaneously in both the horizontal and vertical directions. Faster and more responsive actuators were used allowing the behaviour of the position control system to be tested further.

The linescan camera was replaced by a dual-axis beam tracker (see Chapter 4). The arm vertical drive, linear actuator was replaced by a geared servo motor attached directly to the arm at the pivot point. A similar actuator was added for horizontal arm movement (see figure 3.9).

3.3.1 Endoskeleton Modifications

The original endoskeleton column was retained, yet the positioning head was redesigned to enable the laser to be moved about both the horizontal and vertical axes. A variety of commercial motorised two-axis positioning devices are available (see Chapter 8), yet all are very expensive and physically too large to be incorporated within the existing robot frame. It was therefore necessary to custom build a positioning head of small dimensions (no greater than 80 x 80 x 140 mm). Three designs were considered, each using different methods of actuation. The design details are described in the next sections.

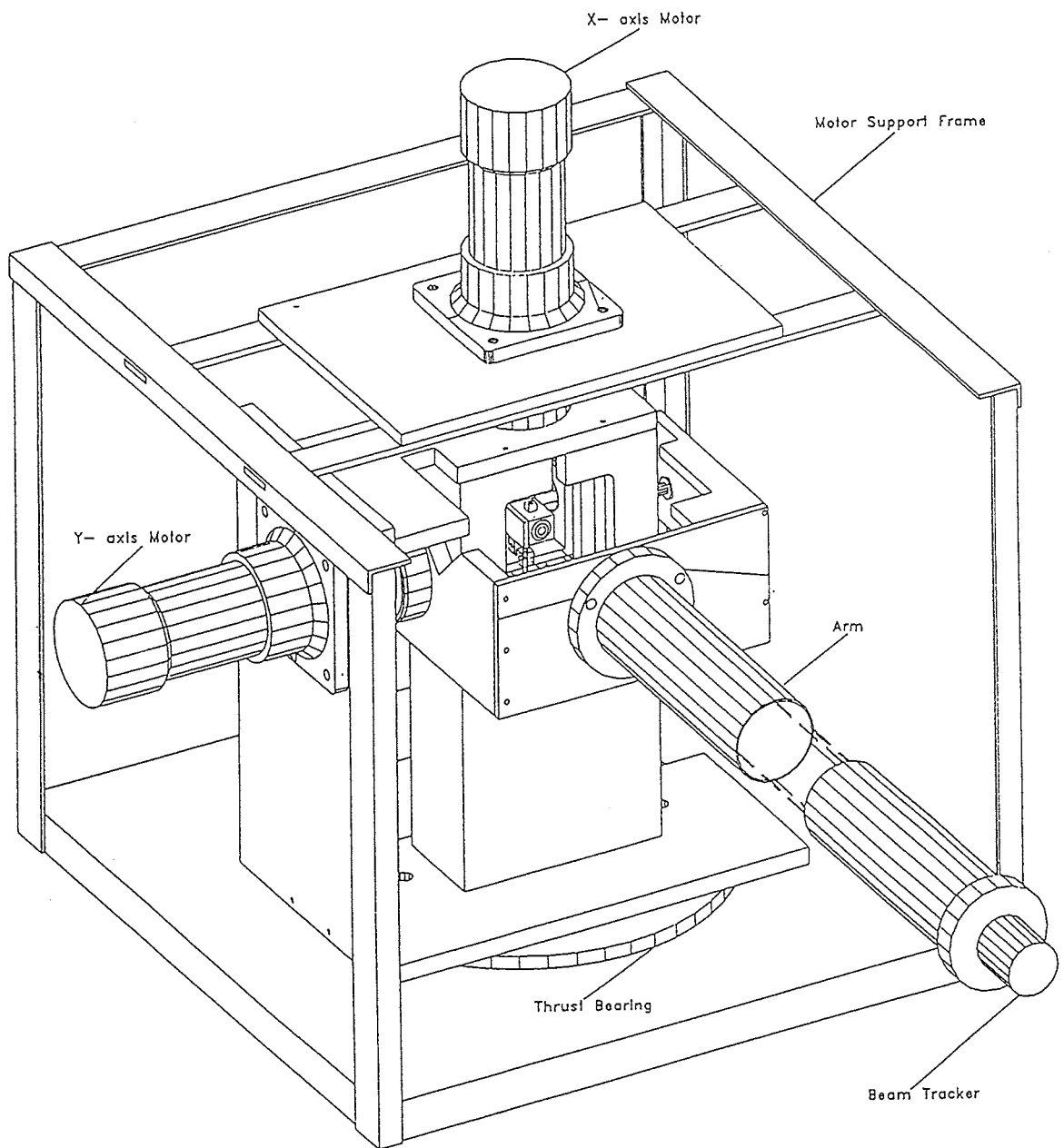


Figure 3.9 - Front view of the dual-axis robot
(Suuronen, 1994)

3.3.1.1 *The mirror galvanometer positioning head*

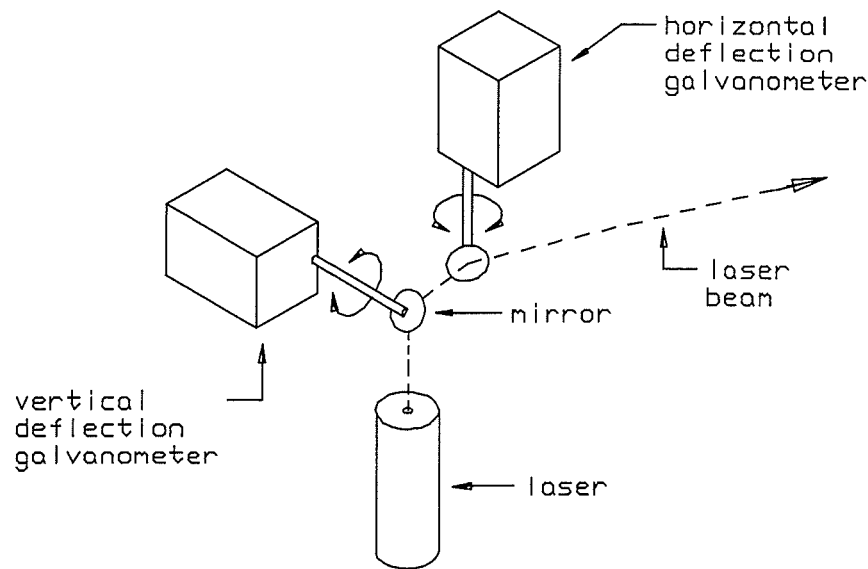


Figure 3.10 - Details of the dual-axis mirror galvanometer positioning head

A pair of mirror galvanometers (Editor, 1985 - model G120D) were set at right angles to each other and to the axis of the incident laser beam. One galvanometer controlled horizontal beam position, the other its vertical position. The advantages of this design were that a large laser unit could be used, e.g. a He-Ne laser which produces a well defined circular light spot and that, as the galvanometers were physically small, the head itself could be compact since the laser could be mounted independently of the head inside the support column.

Disadvantages with the design were primarily associated with the cost and operational behaviour of the galvanometers. These expensive devices (£350 each) work under open loop control, there being no means of verifying the actual angle of rotation of the mirrors. They are used conventionally to cause fast scanning of laser beams where scan speed is the main requirement. Testing showed that where steady positioning at a given target point was required, fluctuating demand signal voltages caused the galvanometers to oscillate and heating of the coils caused thermal drift. They were therefore not used as part of an operational positioning head, yet this approach has not been abandoned since upgraded versions are used in commercially available optical positioning mounts. The viability of this option is further discussed in Chapter 8.

3.3.1.2 The DC servomotor driven positioning head

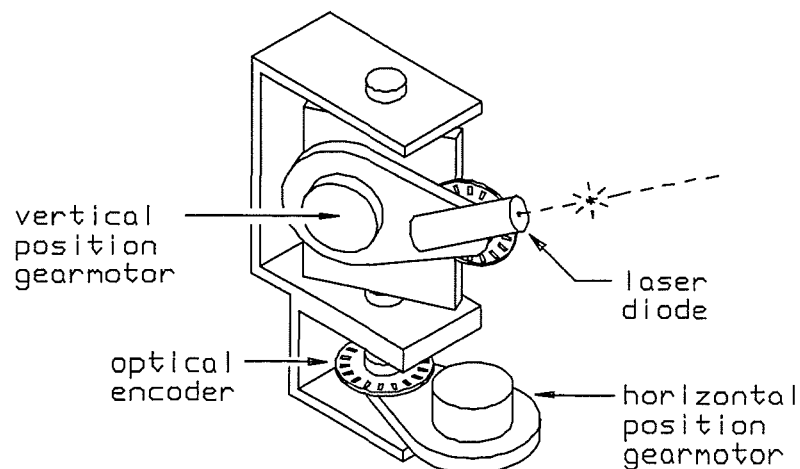


Figure 3.11 - The original positioning head modified for dual-axis operation

The original positioning head was converted to dual-axis functioning through the addition of a second gearmotor. Smooth movement of the laser was achieved, yet two problems became apparent. Firstly, the construction was too big to be incorporated within the exoskeleton. Secondly, the repeatability of the system was poor due to problems in reading data fast enough from the motion control microprocessor (Waki, 1992), resulting in an accumulation of positioning errors when operating the two axes simultaneously.

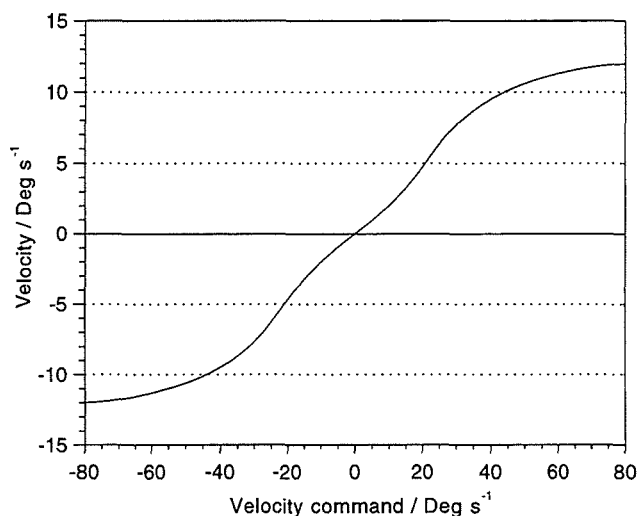


Figure 3.12 - Velocity command versus actual velocity for the dual axis DC motor driven positioning head

The relationship between the input command and the recorded velocity of the motors is shown in figure 3.12. A near linear relationship was found between command velocities of -40 - 40 °/s, above which the drive motors became saturated and were unable to match the demand. Therefore a third, simpler, design was produced.

3.3.1.3 *The stepper motor driven dual-axis positioning head*

An exploded view of this design is shown in figure 3.13. The DC motors were replaced with 12 V, 7.5° step unipolar stepper motors (RS 332-947), each attached to a 250:1 synchronous gearbox, producing at the output shaft a step angle of 0.03°, a torque of 0.8 Nm and a maximum output speed of 2 rev/min (Editor, 1987). Gearbox backlash (given as 2°) was reduced by attaching an anti-backlash spring between the output shafts and gearbox bodies. The motors have permanent magnet rotors and therefore braking torque when not energised. The residual torque was found to be a useful feature for maintaining position integrity. The small motor size meant that the positioning head fitted easily within the restricted space inside the robot upright support.

Position control was much simplified. An open loop controller was used as position feedback is not required for stepper motors providing they are not loaded excessively causing them to 'miss' steps. Positioning head accuracy and repeatability tests (see figure 3.16) showed that the motors operated successfully under open loop control alone.

The control algorithm was implemented in 'C' code - (see Appendix B), the angular position of the motors being controlled with signals from the computer's parallel port. Two types of stepper motor driver boards were tested. Initially SAA 1027 driver IC's were used along with a Hex non-inverting open-collector buffer (IC 7407) to interface them to the computer. A problem with this driver was that there was no half-step facility available. It was later replaced with a pair of RS 332-098 unipolar stepper motor driver boards with both fast stepping rate and half-step facilities.

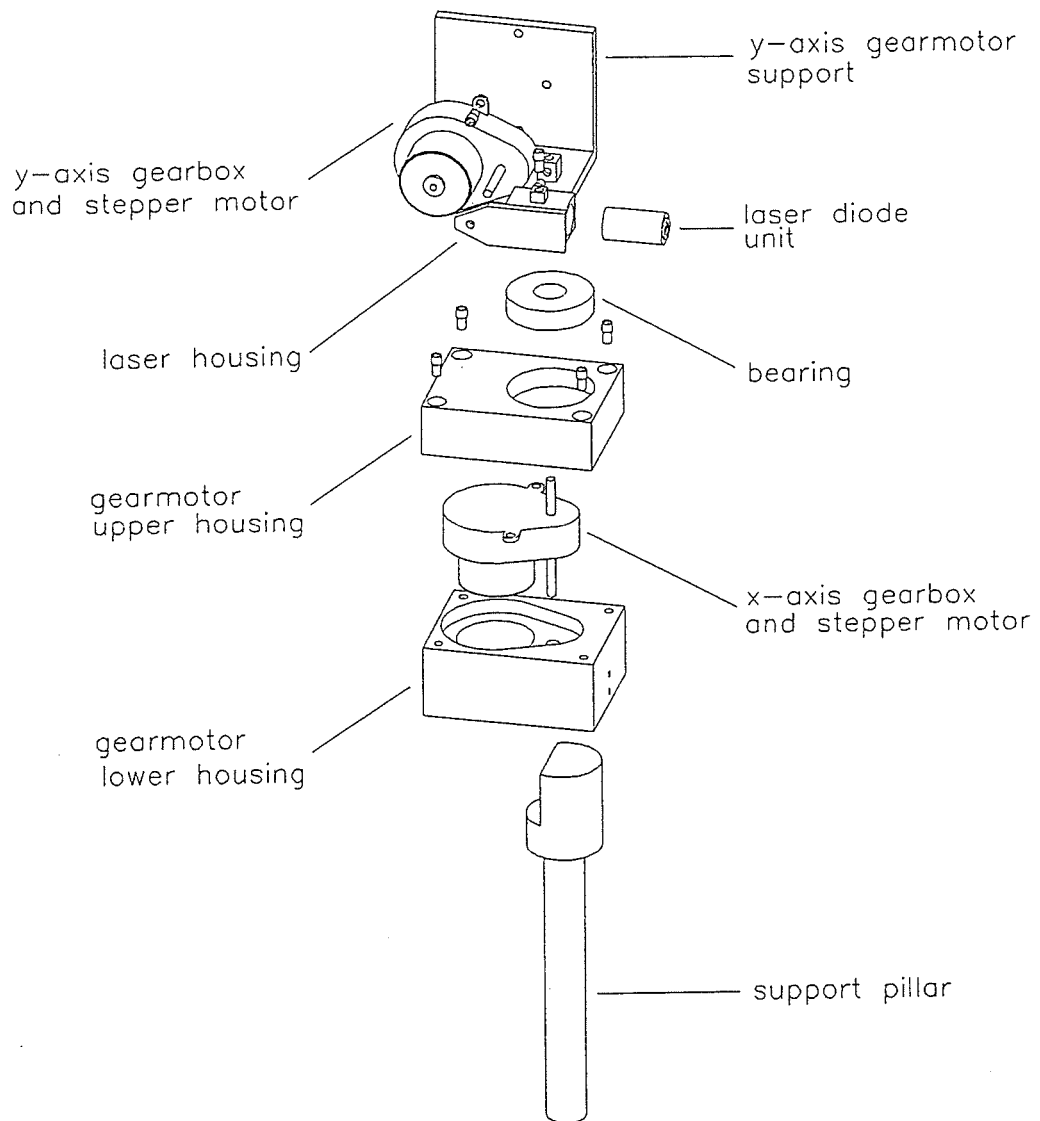


Figure 3.13 - An exploded view of the stepper motor dual-axis positioning head

3.3.1.4 Positioning head performance testing

Speed - Smoothest single-axis movement was obtained at a rotation rate of $6.9^\circ/\text{s}$. For dual-axis operation the maximum rotational speed of each axis was $5.4^\circ/\text{s}$, less than that for a single axis due to the throughput limitations of the slow PC used (360 control loops/s). A parabolic acceleration ramp was implemented in the software extending over the first and last 20 movement steps.

Overshoot and oscillations - Figure 3.14 shows the error signal, as detected by the beam tracker, produced when the positioning head vertical axis stepper motor was moved through a single step with and without friction damping.

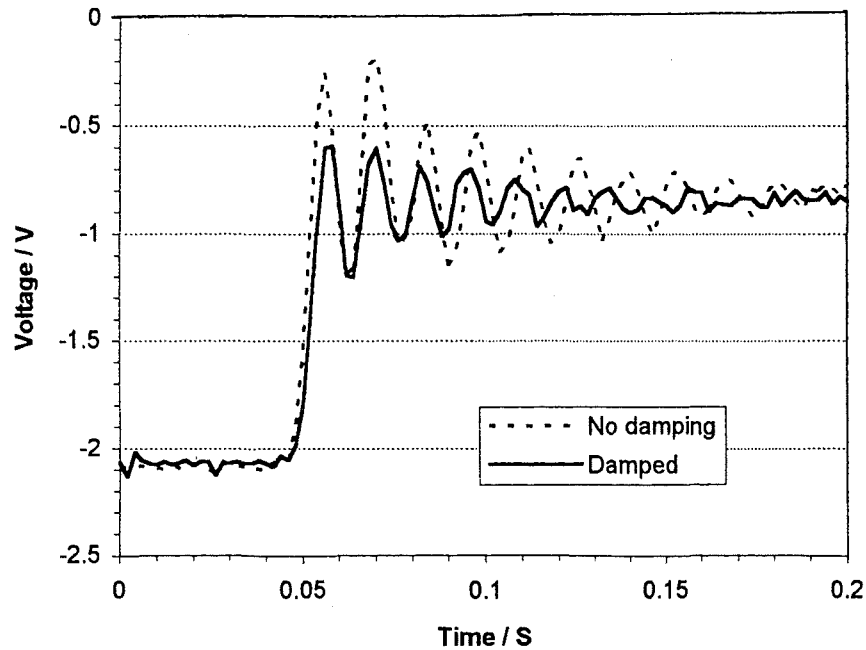


Figure 3.14 - Undamped and damped positioning head performance

Without damping, considerable overshoot (± 0.5 V) and poor settling time (0.15 s) is shown. The addition of oil-filled dampers improved the system, the maximum amplitude of the transient was reduced from 1.0 V to 0.6 V with a 20% reduction in settling time. Oscillations in the error signal were further reduced by introducing electronic low-pass filters to the error signal channels. These were designed to both damp the undesired oscillations produced by the positioning head and to reduce the effects of electronic noise produced by the actuator power amplifiers. The ratio between the input voltage V_{in} and the output voltage V_{out} of a first order low-pass filter can be represented as :

$$A = V_o / V_i = \frac{1}{(1 + (j\omega CR))} \quad (3.1)$$

where $\frac{1}{j\omega C}$ is the reactance of C and $\omega = 2\pi f$.

Comparing the magnitudes of the voltages and neglecting phase changes :

$$V_o/V_i = \frac{1}{\sqrt{(1+(\omega^2 C^2 R^2))}} \quad (3.2)$$

if $\omega^2 C^2 R^2 = 1$ then $V_o = \frac{V_i}{\sqrt{2}}$ which is equivalent to the -3dB point.

As shown in figure 3.15, filters with R and C values of 10 k Ω and 0.3 μ F successfully eliminated spurious transients and electronic noise.

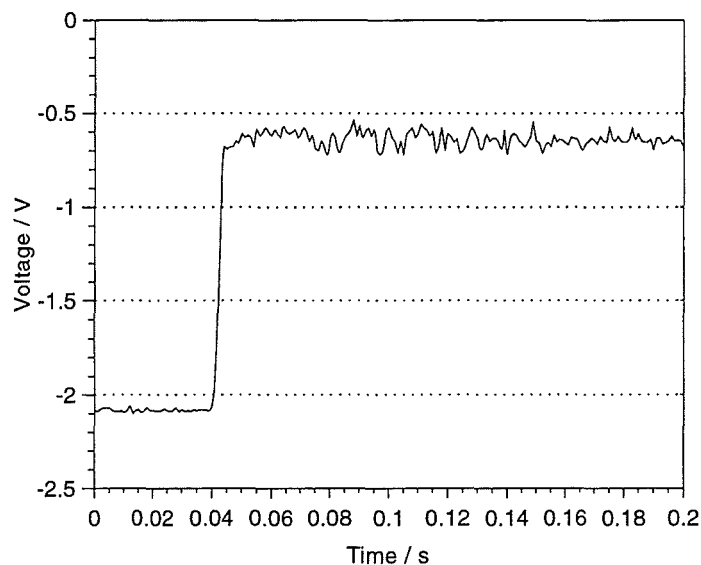


Figure 3.15 - Step response with both friction dampers and low-pass filters

Accuracy and repeatability - The laser was aimed at a target point 20 m from the positioning head. It was moved horizontally, vertically and through a series of compound movements before being returned to the datum point.

Four distinct point clusters (A, B, C and D) were formed as shown in figure 3.16. When moved horizontally to the left of the datum point, the beam spot returned to within area A, when moved horizontally to the right it returned to area B - the angle change A-B (0.085°) representing the horizontal positioning error caused by bias in the X-axis actuating circuitry.

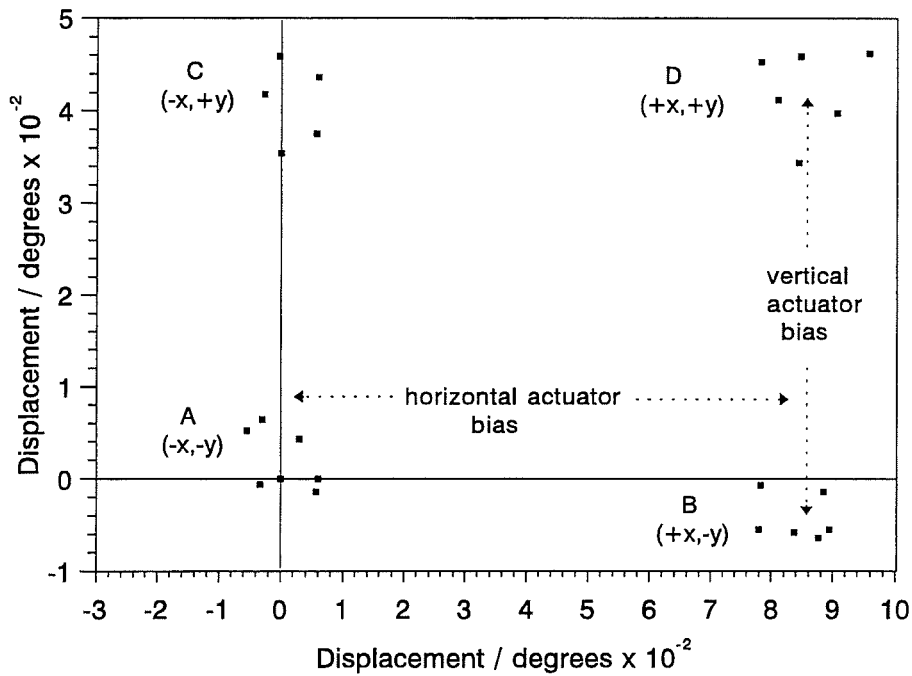


Figure 3.16 - Scatter graph showing the repeatability and accuracy of the stepper motor driven dual-axis positioning head

Bias was also present in the Y-axis, as shown by the angle change B-D of 0.04° , being only half that evident in the X-axis. This was because X-axis positioning required movement of both the laser and Y-axis mechanism - accumulative backlash within the horizontal and vertical axis gearboxes increasing the positioning error. Compound X-Y movements caused points to be clustered about all four areas, the area to which the spot returned being governed by whether positive or negative X or Y axis movements were actioned.

Table 3.1

Values for point sets on positioning head scatter graph / degrees				
Point set	A	B	C	D
Centroid value (x, y coordinates)	0.04, 0.32	8.43, -0.42	0.17, 4.08	5.43, 4.21

Positional accuracy for the stepper motors depends upon the tolerance of each angular step movement, the figure given being 5-10% of one step angle. This error is non-cumulative, i.e it remains constant regardless of the number of steps advanced. With these four phase motors this error averages to zero in 4 steps (corresponding to a full drive cycle). For high accuracy positioning, movement should be divided into multiples of 4 steps, corresponding to 0.12° changes in laser angle.

Resolution - The theoretical minimum step angle was 0.03° per axis. This was tested by moving the laser spot through single step increments about the target point. For the both axes, point separations of 10.5 mm were recorded over 20 m, being equivalent to an angle change (or resolution) of 0.03008° .

3.3.2 Exoskeleton Modifications

The exoskeleton upright was modified to accommodate both the horizontal and vertical axis drive actuators. A rigid aluminium frame surrounded the exoskeleton and acted as a support for the horizontal axis motor (see figure 3.9). The exoskeleton rotated about a 240 mm ϕ thrust bearing, fixed concentrically about the endoskeleton column.

Two Harmonic Drive (Editor, 1995) DC servo motors were used (model RFS 20-3007-EO50AL). They were fitted with 100:1 harmonic drive gearboxes, with the later addition of 10:1 planetary gearboxes to give an overall ratio of 1000:1 and an output shaft speed of 4 rev/min. Two pulse width modulation amplifiers were used (model HDEA-M-100-15-SADC), giving an 11.5 A peak current at 75 V and a theoretical maximum motor input power of 860 W.

3.4 ARM JOINTS

To increase the number of degrees of freedom of the robot, joints can be installed along the arm. Four revolute and a prismatic joint were developed, the merits and drawbacks of each being considered at the design stage and through observations of their performance.

The inclusion of revolute joints affects, considerably, the end-point position sensing concept as originally conceived. *Direct* end-point optical sensing, where the sensing means is *inside* the arm frame, is no longer possible - hence a major advantage of the *externally positioned* optical end-point sensing systems described in Chapter 2, Section 2.2.

Prismatic joints, on the other hand, do not effect the position sensing strategy as joint action does not obstruct the laser beam path between the positioning head and the arm end-point position detector.

3.5 REVOLUTE JOINTS - DESIGNS AND OPERATING PRINCIPLES

The problem in developing revolute joints is that of controlling link position without detracting from the concept of using a laser light spot to define the ultimate arm end-point position. To deflect the laser beam through the desired angle, optics are required at the joint pivot, where the optics must be supported on fixtures attached to the arm at the joint. This means that before a joint can be moved, the preceding link must firstly be fixed in its desired position to prevent movement of the optics, and that this position must be maintained until the link being controlled has completed its movement.

Each link therefore needs to be equipped with a sensing device which detects the beam position and keeps the end of the link located centrally about the incident beam while it is being deflected about the joint axis. A beam tracker at the end of the final link provides the information necessary to accurately establish the end-point position of this link on the laser spot. This control strategy makes each link act as a 'slave' to the 'master' positioning control system, resulting in not only end-of-link position sensing but also automatic active position correction for deformation in each link.

3.5.1 Multiple Laser/Sensor Combinations

The simplest revolute joint design uses a laser/detector combination on every link. Each link therefore formed a separate unit in which position and deflection was monitored and adjusted independently of the adjoining links.

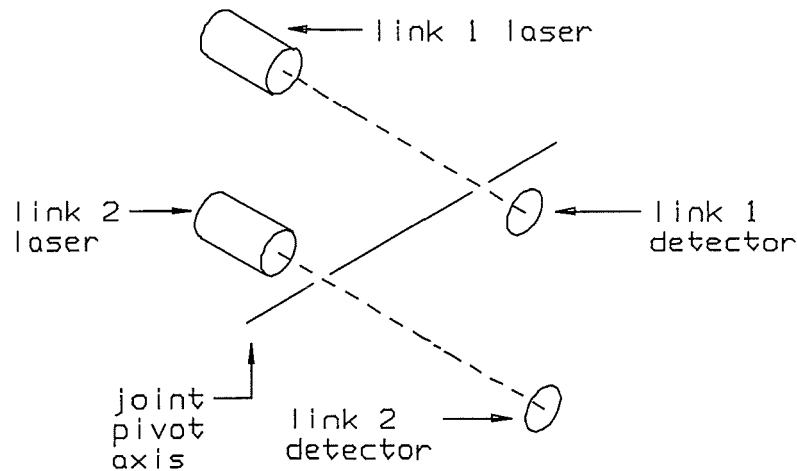


Figure 3.17 - Schematic diagram of the laser/detector combination revolute joint

The advantage of this design lies in its simplicity as complex optics are not needed since no deflection of the beam is required at the joint axis. The major disadvantage is that each link movement needs to be controlled independently of the others.

3.5.2 Single Laser Designs

Three, single laser designs were constructed, each employing different principles.

3.5.2.1 An 'in-line' joint using fibre optics

A flexible optical fibre connection was used as a transmission medium through which the laser beam could travel about the joint axis. This device could be used successfully in any form of rotary joint, the only limitation was that the position of the joint supporting link must be fixed prior to joint movement taking place. This was achieved using a beam splitting mirror and a dual-axis beam tracker arranged such that a portion of the incident beam was reflected towards the beam tracker mounted at the link joint. A Perspex cone

enabled the incoming beam to be funnelled into the optical fibre. This ensured that the beam was captured continuously irrespective of any flexing or bending of the joint supporting link. The emitting end of the optical fibre was aimed by a servomotor attached to the link such that the laser beam continued along the designated path at the desired angle.

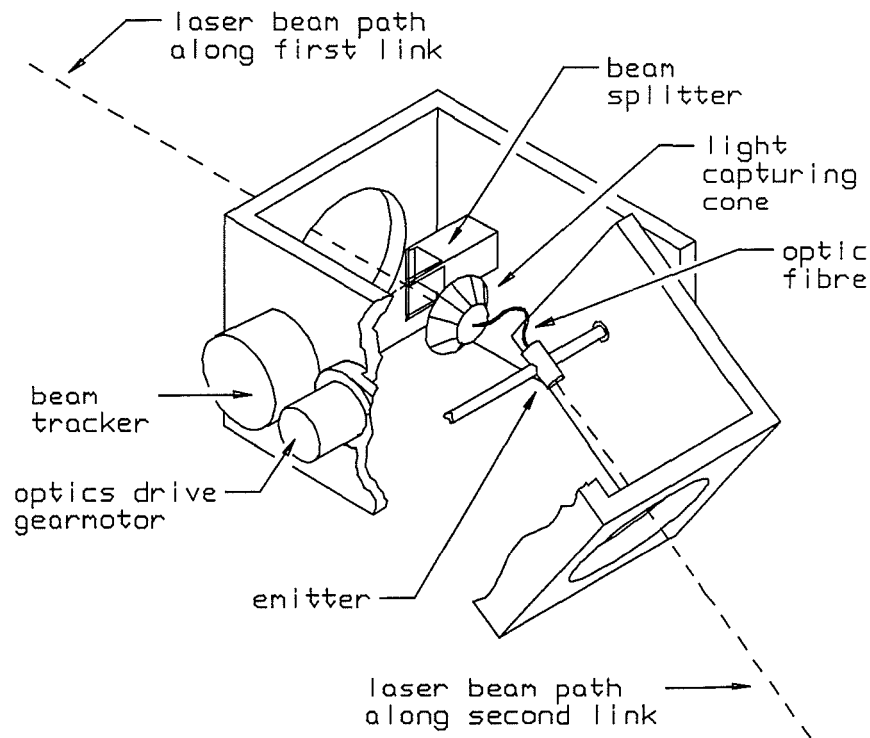


Figure 3.18 - Details of the in-line fibre optic joint

3.5.2.2 An 'in-line' joint using a beam splitting cube

The incident laser beam impinged upon a beam splitter mounted at the extremity of the first link at an angle of 45° to the link axis. The reflected portion (50%) of the laser beam impinged upon a beam tracker which controlled the vertical position of the first link. The transmitted portion was deflected about the joint axis by a beam splitting cube. As the cube was rotated the second link was caused to track the beam through a second beam tracker at the end of the link control the movement of the link actuator.

The prism was rotated by a DC gearmotor, the shaft running up the axis through the joint bearing. The angle of deflection of the light beam was twice that of the angle of rotation

of the prism. This could have had a profound effect on the overall accuracy of the positioning system as any errors incurred in controlling the position of the prism would result in an effective doubling of errors in the positioning of the light beam. To minimise these errors a high resolution optical encoder (Hewlett Packard HEDS-6000) was attached directly to the output shaft of the gearbox thereby giving the angle of rotation of the cube directly and eliminating the need to account for backlash in the gear train.

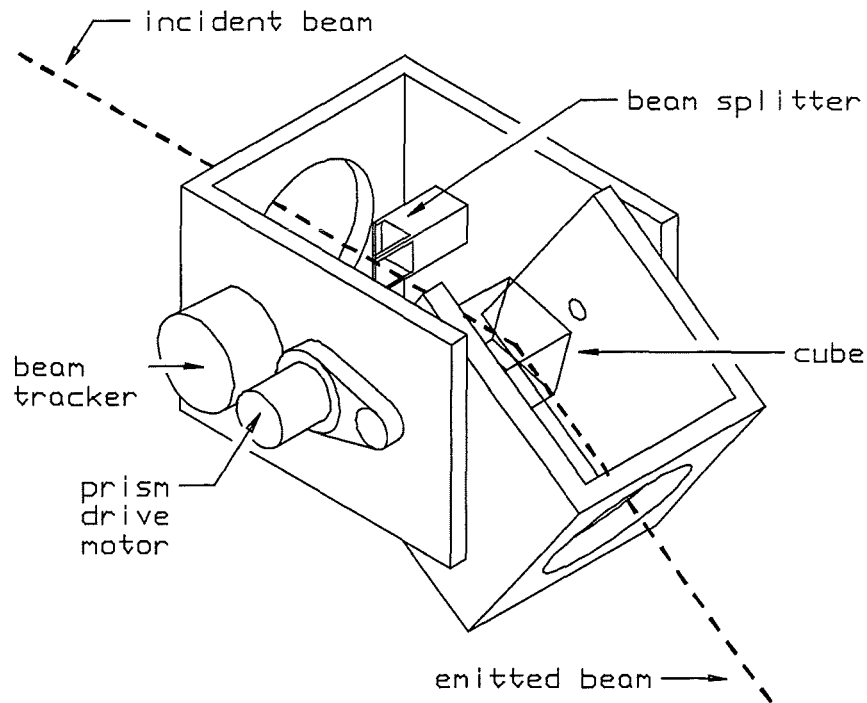


Figure 3.19 - Details of joint design using a beam splitting cube

The joint could be rotated through 90° using a linear actuator. If this had been replaced by a direct drive DC gearmotor angles of rotation of up to 270° could have been achieved.

Optical component characteristics - The cube size was 20 mm^3 , being large enough to ensure that the beam path was maintained even when the links were subject to extreme horizontal and vertical deflections. A plane mirror could have been used where restricted movement of the joint ($<135^\circ$) would satisfy requirements, yet for movements greater than this, the cube must be used as it could deflect light in both a positive and negative direction about the line of the incoming beam.

(i) *The effect of vertical arm deflection on the beam path through the cube*

Vertical bending of the first link caused the beam path along the second link to be displaced from its desired trajectory through a vertical distance equivalent to the amount of joint displacement.

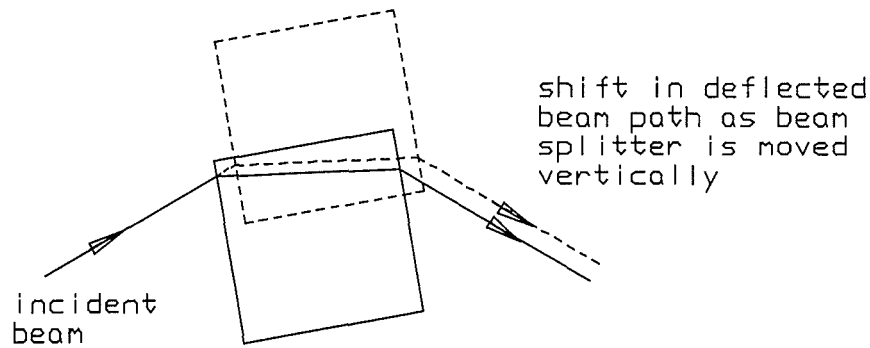


Figure 3.20 - Displacement of the deflected beam caused by vertical movement of the beam splitting cube

This had the effect of shifting the fixed reference beam which could have led to severe positioning errors for the second link. It was therefore essential that the first link carrying the joint was fixed in position prior to rotation of the joint. For this reason a beam tracker was located on the first link close to the joint.

(ii) *The effect of horizontal arm deflection on the beam path through the cube*

The beam path was unaffected by movement of the joint through the horizontal axis when the incident beam entered the cube normal to the cube face. The beam struck the face of the cube along the same horizontal plane irrespective of the horizontal displacement of the cube. This was advantageous as it gave one axis about which the joint could move without effecting the reference beam path. This was not the case for designs using either multiple laser/sensor combinations or optical fibres where movement of the joint about any axis caused deflection of the reference beam from the desired path.

As demonstrated, the vertical component required active correction to maintain the desired beam trajectory through the joint. Therefore only the vertical component of the first link position needed to be fixed, requiring the use of a single axis bi-cell beam tracker at the joint (see Chapter 5, Section 5.5). Monitoring of the horizontal displacement of the arm was performed by the dual-axis beam tracker mounted at the end of the arm.

(iii) *The effects of twist on the joint*

Load-induced joint twisting caused rotation of the cube about the major axes. Rotation of the cube about the horizontal axis caused a displacement of the beam from the vertical axis resulting in a link positioning error about the vertical plane.

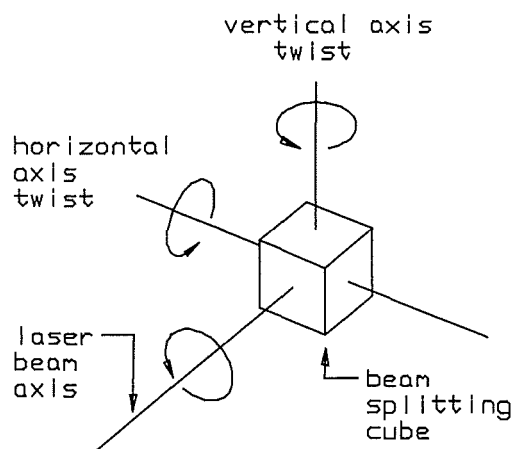


Figure 3.21 - The major axes about which twist occurs

Twist about the vertical axis produced a shift in the beam path along the horizontal axis. The shift produced a displacement of the beam to one or the other side of the desired path. These errors were produced by the displaced joint subscribing an arc about the robot base causing rotation of the cube face about the incident beam. This in turn displaced the deflected beam to the left or right of the desired path. In both cases the degree of deviation of the beam from the desired path depended upon both the amount of twist present in the joint and the angle of joint rotation.

During operation, effects of twist on the reference beam position were minimal because

- the joint was constructed to withstand considerable twisting of the torque tube with little distortion,
- twisting effects were more pronounced in the relatively flexible links than in the joints. These could be measured and counteracted for by the detection and corrective systems described in Chapter 8.

3.5.2.3 The 'off-set' revolute joint

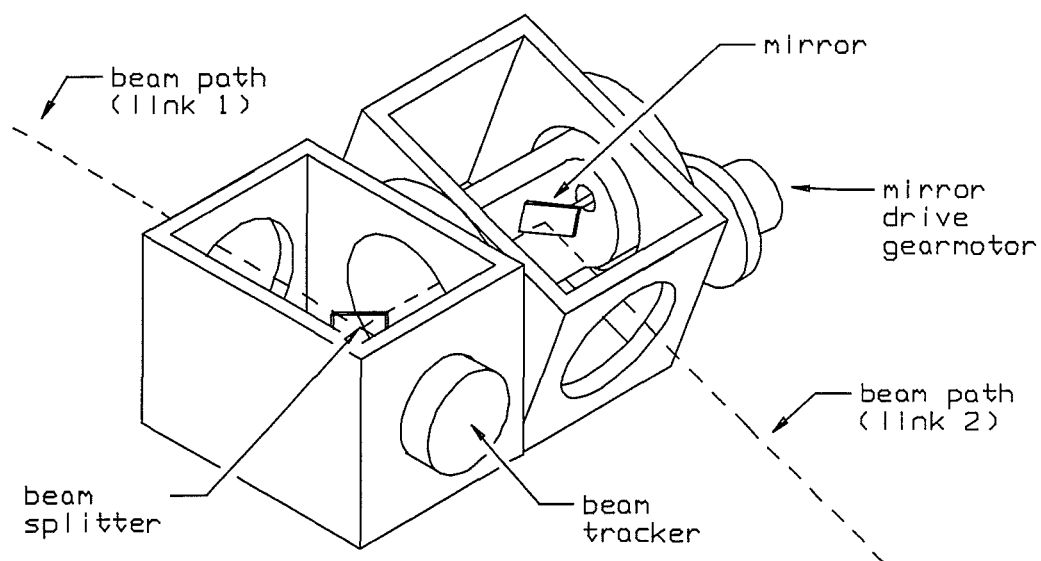


Figure 3.22 - Details of the 270° off-set revolute joint using mirrors

A beam splitter, supported at an angle of 45° to the incident beam, caused a portion of the beam to be reflected along the axis of rotation of the link, whilst the transmitted light impinged upon the link beam tracker. The reflected beam struck a mirror mounted on the output shaft of a gearmotor at an angle of 45° to the beam path. The mirror caused the beam to be reflected up the centre of the second link in a direction parallel to that of the original beam (Kleinwechter and Schroth, 1993).

An important feature of the design was that the beam splitter, mirror and gearmotor were housed in a common framework supported by the first link only. This framework was unaffected by flexing of the second link. This arrangement maintained the beam splitter

and mirror parallel to each other ensuring that the incident and reflected beams were parallel at all times. The second link was supported on a roller bearing that allowed it to rotate about the first link, the bearing being pre-loaded to take up lateral play. Joint actuation was through a 246:1, precision, 12 V, low backlash gearmotor. The gearmotor drove a 57 mm ϕ sprocket which, by means of a chain drive, was connected to a 170 mm ϕ sprocket attached directly to the bearing head. This produced an overall reduction of 733:1 to give a suitable maximum rotational speed of 10 rev/min.

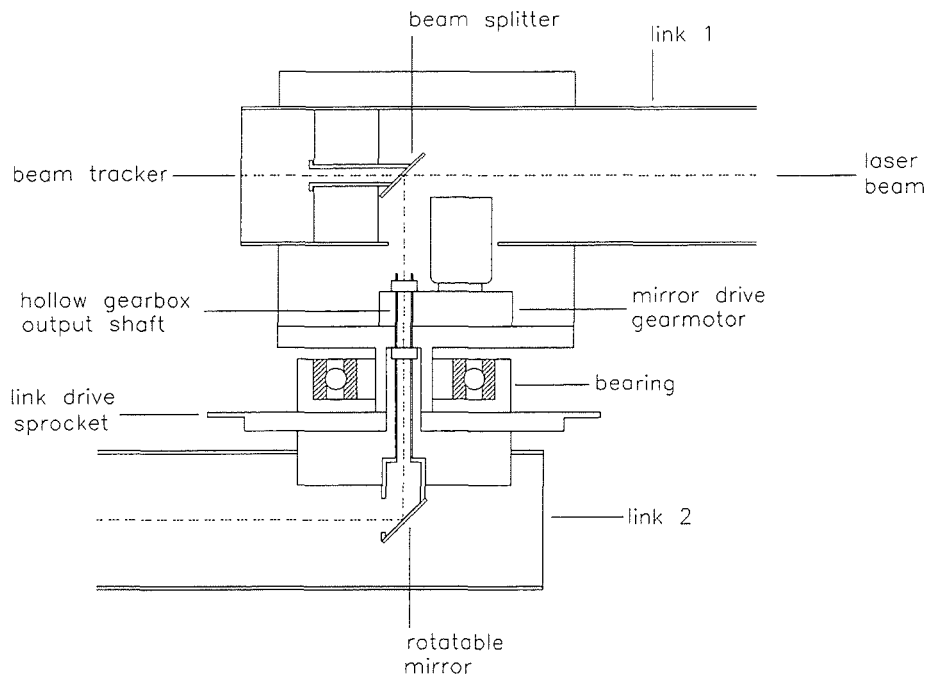


Figure 3.23 - Details of the 360° off-set revolute joint

The design was later modified for complete 360° joint rotation by repositioning the mirror drive motor so that the light beam passed through the centre of a tubular gearbox output shaft. Through rotation of the mirror the angle of elevation of the laser beam was changed. This in turn could produce complete 360° link movement. A beam tracker fixed to the end of the second link caused the link to follow the laser beam.

3.5.3 The Prismatic Joint

To account for load-induced arm extension, an experimental prismatic joint was developed (see figure 3.24). A system was devised that enabled the joint position to be automatically adjusted so that the required arm length could be maintained.

A laser metrology unit (Hewlett-Packard 5526A metrology unit and 5500C laser head) was positioned such that the emitted beam struck a retroreflector attached inside the far end of the joint, the reflected beam passing through a fixed interferometer unit before impinging upon the metrology unit sensor.

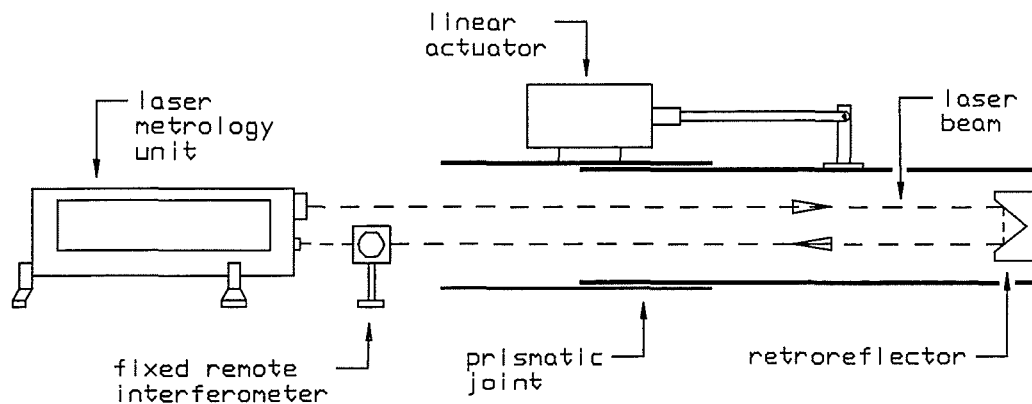


Figure 3.24 - Schematic diagram showing prismatic joint details

The phase shifts between the emitted and returned beam gave an accurate measure (to within $\pm 1 \times 10^{-4}$ mm) of the emitter to retroreflector distance. The measured distance was input to PC via a PC-30B I/O card. For maintaining a constant arm length, this distance was compared against a set reference value, the difference between the two forming a position error signal which was fed through an amplifier to the linear actuator which moved the joint in the direction required to reduce the error. The arm length could be increased or decreased as required by changing the length reference value. Further details of the hardware configuration are given in Chapter 5, Section 5.2 and in Appendix D.

Linear bearings provided smooth joint movement. Horizontal and vertical movement was minimised by pre-loading the bearings against the inner slide with springs. Any residual

tilt was automatically accommodated for by the deflection compensation component of the control system.

Although this joint positioning mechanism proved to be very accurate (± 0.05 mm), the very cost of the laser metrology unit itself (over £15,000) makes it impractical for use on a commercial basis. A cheaper, yet still optically sensed, alternative design is proposed in Chapter 8.

Summary

This chapter has dealt with the design and construction of the major mechanical parts of the robot. Descriptions are given of modifications made as the robot evolved from the initial single-axis 'proof of concept' design through to the more advanced dual-axis model.

A variety of optically controlled revolute joint designs are given with a discussion of the merits and drawbacks of each one proposed. A prismatic joint for controlling arm length is also described.

The next chapter describes the design of optical beam tracking systems for detecting the position of the laser spot at the end of the arm. The purpose of the beam tracker is to generate a position error signal which, via the arm slave control system, will cause the arm to track the laser spot movement so enabling end-point position control. A review is given of available sensors, leading to the selection of those used on the robot.

References

Editor, (1987) 'Stepper motors', RS data sheet No. 8199, Nov 1987.

Editor, (1985) 'User's manual for galvanometer scanners', General Scanning Inc, 500 Arsenal Street, Watertown, MA 02272.

Editor, (1995) 'Harmonic Drive User Manuals', Harmonic Drive Ltd, Claremont Lodge, Fontwell Avenue, Eastergate, Chichester, West Sussex, U.K.

Editor, (1994) 'Electric linear actuators - application notes', Abssac Ltd, Porton House, Birmingham Road, Stratford-Upon-Avon, U.K.

Kleinwechter, P. and Schroth, S., (1993) 'Design, constructing and testing of an optically controlled robot joint', BEng Honours in Mechanical Engineering, final year project, Middlesex University, 1993.

Snyder, W.E., (1985) 'Industrial robots: computer interfacing and control', Prentice Hall International.

Suuronen, J., (1994) Internal report, Middlesex University, 1994.

Waki, K., (1992) 'Development of a controller for a laser guided robot', IASTE exchange programme, undergraduate project, Middlesex University, 1992.

Chapter 4

THE DESIGN AND DEVELOPMENT OF THE BEAM TRACKING SYSTEM

4.1 INTRODUCTION

This chapter describes the development of the laser beam tracking systems. A review of position detecting devices is included, followed by a description of how a linescan camera was used as the initial experimental beam tracker. A new system was then developed based upon a photodiode quadrant detector. Full details of this design and of a miniaturised version are given, along with a description of their modes of operation.

4.2 A COMPARISON OF POSITION DETECTION DEVICES

Several light detecting transducers were considered for use in the beam tracker as position sensors. These consisted of both cathode ray tube and silicon photodiode based devices.

Optical position sensing can be used for the measurement of movement, angle, straightness, object location, height, centering, surface uniformity and distance. In this application the use of sensors for centering is the prime consideration.

4.2.1 Vacuum Tube Devices

Vacuum tube devices, such as the Optron displacement tube (Optron Corporation, Ya-Man Ltd), have been used successfully in position sensing applications for many years. An image of the light spot is focused on to the tube cathode. The rear surface of the photocathode generates electrons in relation to the light intensity striking the front surface, thus making an 'electron image' of the target. An applied electric field accelerates the electron image down the tube and focuses it on to an aperture plate with a tiny pinhole.

Only a small portion of the image is seen by the photomultiplier, which produces an output current proportional to the intensity of the light image.

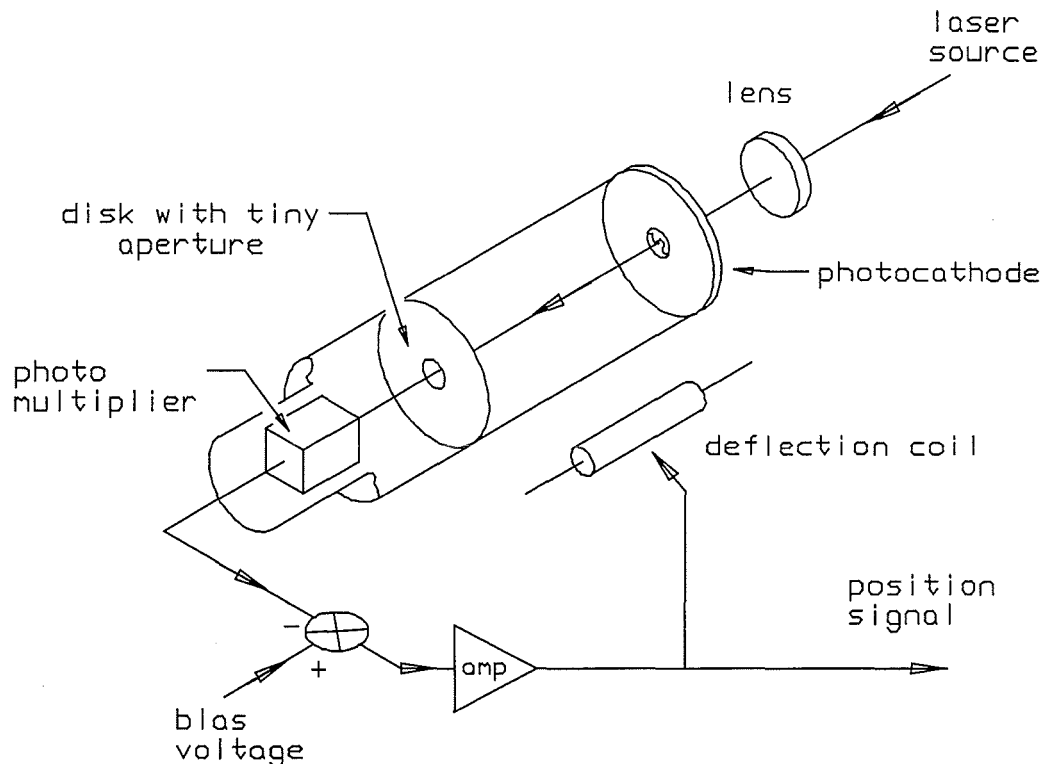


Figure 4.1 - Schematic of 'Optron' displacement tube showing single axis position monitoring system - (from Doebelin, 1990)

On subtracting the electron multiplier output from a pre-set bias voltage an error signal is generated which becomes positive or negative depending on the light intensity. The image-dissector tube has a deflection coil which can position the electron image. The amplified error signal is connected to this coil with polarity such that if there is 'too little light', the coil drives the image in the direction necessary to centre it on the light spot. Thus a feedback system is created which keeps the light spot centred on the aperture at all times. The output signal, proportional to the light target displacement in one axis, is obtained from the amplifier output.

Dual-axial motion detection is achieved by using a tube with two perpendicular deflection coils. As the electron multiplier has only one output signal, an electronic switching system

rapidly switches the output of the tube between the horizontal and vertical channels of the image deflection system, holding amplifiers in each channel rapidly preserve the most recent data while the other channel is being updated.

4.2.2 Silicon Photodiodes

Silicon photodiodes are solid state quantum detectors sensitive to light wavelengths from 200 to 1200 nm, which extends from X-rays through the visible to near infra-red region. They may therefore be used with a variety of light sources including light emitting diodes and lasers. Silicon photodetectors have been used for making quantitative light measurements (e.g photometers, radiometers, densitometers etc), they may also be used for optical position sensing (Light, 1982). The basic PIN (P-type, Intrinsic region, N-type) photodiode is common to all configurations used for optical positioning. The most significant difference between the types involve the juxtaposition of active areas to one another and the manner in which the substrate of the diode is contacted.

Photodiodes are capable of sensing extremely small motions (see table 4.1) and provide the high resolution necessary for precision positioning and alignment applications (Edwards, 1988). For optical position sensing applications two configurations are applicable - multi-element arrays and position sensing photodetectors.

4.2.2.1 Multi-element arrays

A silicon array consists of a series of discrete photodiode elements which are individually connected. They may be arranged in a one or two dimensional matrix, a series of annular rings, or other patterns. The intent is to produce an electrical analogue of the image incident on the array by monitoring the relative intensity from element to element.

A light spot on the array induces photocurrents in the illuminated elements. All elements are then scanned to determine the position of the image spot, corresponding to the pattern of radiation distributed on the units surface. Scanning requires the implementation of sophisticated circuitry which comprises the bulk of the cost of self-scanned array systems.

These devices are versatile as image sensors. They can be used to detect the position of a single light spot, multiple spots and complex patterns.

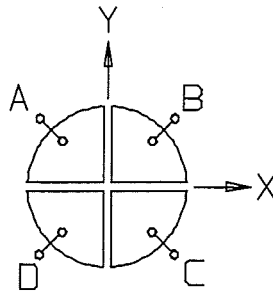
The chief limitation of these units is that the spatial resolution over the array surface is limited by the pixel spacing. Even devices with maximum resolution consist typically of 25.4 μm elements on 50.8 μm centres. The resolution as such cannot be expected to exceed this with a high degree of accuracy. Ideally the light spot should be smaller than the pixel size. If the spot is larger, the centroid centre must be obtained by measuring the output of several adjacent elements, which increases the complexity and cost of the analysing circuitry.

4.2.2.2 *Position sensing photodetectors*

These are designed for either single or dual-axis position measurement. They consist of single photodiodes or arrangements of two or more individual photodiodes on a single silicon wafer.

Bi-cells and quadrant detectors - These overcome the disadvantages of multi-element arrays for certain applications (Light, 1982). The bi-cell features two sensing elements on a single chip, the quadrant detector has four, the elements being separated by a small gap (typically 2-12 μm). The elements are masked onto a common substrate so that their cathode is shared. The anode, or active area of each element, is individually connected so that a light spot illuminating a single element may be electrically characterised as being only in that element. As this spot is translated across the detector, its energy is distributed between adjacent elements, and the difference in electrical contribution to each segment defines its relative position with respect to the centre of the device.

When a light beam is centred on the cells, output currents from each element are equal, indicating centering or nulling. As the beam moves, a current imbalance occurs indicating an off-centre position (Editor, 1993a). Analogue electronics automatically perform the algebraic functions that determine the horizontal and vertical position of the spot on the detector (see figure 4.15).



$$x \text{ position} = \frac{(A+D) - (B+C)}{A+B+C+D} \qquad y \text{ position} = \frac{(A+B) - (D+C)}{A+B+C+D}$$

Figure 4.2 - Quadrant detector electrical connector locations and formulae
- (Editor, 1993b)

With bi-cell and quadrant detectors, position resolution is excellent due to the high response uniformity from element to element and high sensitivity (due to low noise output which may approach 1-10 pW) but is dependent on the element size and spot diameter. For optimum resolution, the spot size should be as small as possible without being smaller than the gap between the cells. Also, the dynamic range is limited by the diode transfer function which is linear only around the centre of movement. With resolutions of 0.1 μm or better, bi-cells and quadrant cells are ideally suited for precise centering and nulling and for tracking position over narrow ranges. They behave as supersensitive null detectors only for small motions near the element gap since they give no change in output once the light spot is totally within one quadrant.

Because these detectors are best used as null indicators, the applications for which they are most often applied, fall into the category of optical alignment. The purpose is to align a direct or reflected light source. Their capabilities in this respect are unsurpassed and generally no front-end optics are required.

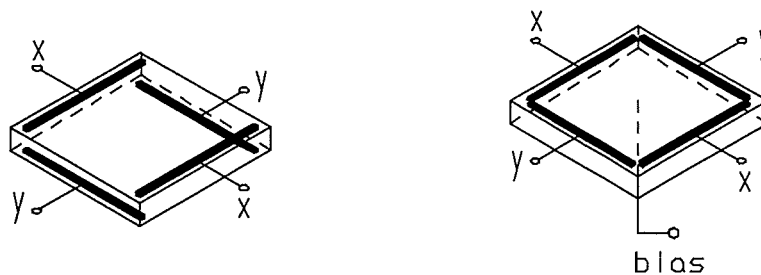
Lateral effect photodiodes - These sensitive position detectors operate on a different principle to quadrant detectors with resulting difference in characteristics. There is no 'dead' region as there is between the quadrants in a quadrant detector, since the detectors utilise just a single photodiode with continuous detection capability. Position indication is obtained even if all light is in one corner. No defocusing of the light spot is necessary

since overlap between quadrants is no longer required. The most striking difference between these and quadrant detectors is that they provide accurate position information independent of the light spot intensity, profile, symmetry or size.

Two types are in common use :-

(1) *Duo-lateral* - this has electrodes on both front and rear surfaces of the photodiode. Each position signal is only divided into two parts by the resistive layers and therefore this type has a high position detecting ability.

(2) *Tetra-lateral* - this has four electrodes on the front surface of the photodiode. The photocurrent is divided into four parts by the same resistive layer and then output as a position signal. When compared with duo-lateral the distortion is greater in the circumference yet the response time is faster. An improved version of the tetra-lateral type is known as the 'pin-cushion' type.



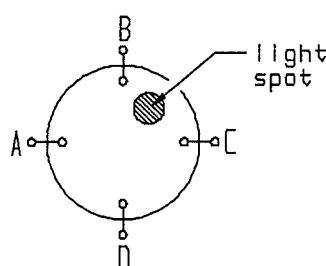
Duo-lateral
configuration

Tetra-lateral
configuration

Figure 4.3 - Duo-lateral and tetra-lateral configurations of lateral effect photodiodes
- (Editor, 1993c)

Lateral effect photodiodes can provide real-time analogue information relating the position and movement of a light spot over the active area. Position is derived by dividing photon-generated electrons within the substrate region of the device rather than profiling intensity distribution on the surface (Light, 1982). This is achieved by applying multiple ohmic contacts on the back layer of the device - two are made at opposite ends of the sensor for single axis versions, four for dual-axis versions.

When the light spot is exactly at the device centre, no electrical signals are generated. By moving the light spot over the active area continuous electrical signals are provided at the terminals, giving the exact light spot position at each instant of time. These electrical signals are proportionally related to the light spot position from the centre, and thus provide an analogue error signal proportional to displacement - In essence, the ratio of the output current difference to the summation of the output current is a near linear function of the position of the incident light spot. It is essentially the difference in current from each of the terminal feed-throughs to the centre terminal which gives the position indication. The input light beam to these detectors may be any diameter and have a varying intensity profile, since the position of the centroid of the light spot is indicated and provides an electrical output signal proportional to the position from the centre.



$$x \text{ position} = \frac{(A-C)}{(A+C)} \qquad y \text{ position} = \frac{(B-D)}{(B+D)}$$

Figure 4.4 - Lateral-effect detector electrical connector locations and formulae

These devices are not perfectly linear, the major contributor to this non-linearity being the sheet resistance. A shift in linear position of the light spot with relation to the centre of the device, is not linear with respect to the cartesian axes as defined by the four ohmic contacts. Yet the difference between the left and right currents give a nearly linear function of the shift from the centre if the currents are fed into low impedance amplifiers.

Resolution is not quite so good as it is for bi-cells and quadrant detectors because of the higher signal to noise ratio, nevertheless resolution is still excellent and far better than CCD (charge coupled device) arrays.

Table 4.1 (from Wendland, 1973)

A comparison of vacuum and solid state position sensing device characteristics		
Characteristic	Vacuum tube device	Photodiode
Spectral response	200-1200 nm range, yet requiring 'matched' detector	wide range, 200-1200 nm in one detector
Noise	sophisticated electronics to keep low	very low noise levels
Stability	Exhibit hysteresis and performance degradation	Long term, no hysteresis or degradation
Response time	less than 5 ns rise and decay, but up to several μ s delay in dynode transit	less than 5 ns response in the detector, 50 ns to 1 μ s in the op amp
Minimum detectable light level	can count single photons	10^{-13} W/cm ²
Power supply	600 to 3000 V, sensitive to power fluctuations	± 6 to ± 20 V, insensitive to power fluctuations
Cost	£25 - £250	£15 -£250
Power supply cost	£50 - £100	£10 - £35
Size and weight	large ($\phi > 50$ mm), heavy	compact and light weight
Mechanical strength	fragile	rugged
Associated electronics	sophisticated and expensive	simple, compact and cheap
Position resolution	high - better than 20 μ m	very high - better than 12.5 μ m
Spatial resolution	range limited	excellent over a wide range

A comparison of vacuum and solid state position sensing device characteristics (continued)		
Characteristic	Vacuum tube device	Photodiode
Light spot shape and intensity distribution	has marked effect on resolution	works on centroid of light spot
Linearity	very good	excellent
Geometry variation	glass envelope restricts large areas and small precision arrays	made in a variety of formats and sizes to suit specific applications

It can be concluded that on all key design factors photodiode position sensing devices have a clear advantage over photomultiplier tubes for use in this application.

4.3 BEAM TRACKER DESIGN SPECIFICATIONS

Performance

- The beam tracker must detect movements of the laser beam in real-time with a high degree of accuracy - ± 0.005 mm or better.
- The output signal from the beam tracker must be proportional to the displacement of the spot from a reference position on the detector.
- It must be adaptable for single and dual-axis link displacement detection.

Size and weight - The beam tracker must be small enough (< 100 mm³) so as not to obstruct link movement or restrict the method of end effector attachment to the robot arm. Beam tracker weight must be kept to a minimum (< 100 g) as it could significantly effect the vibration modes set up in the links during robot operation.

Robustness - It should be able to withstand collision shock. Its performance should not degrade with time, with fluctuations in ambient conditions or due to constant exposure to laser light.

Cost - As one beam tracker is required per link, unit costs should be kept as low as possible while still meeting the specifications.

4.3.1 The Photodiode Position Detecting Sensor Used

Three types of photodiode device were considered for use as position sensing detectors. Lateral effect photodiodes were rejected on the grounds of high unit cost. Initial experiments were carried out using a modified photodiode linescan camera as these are widely used in position sensing applications. A photodiode rather than a CCD based sensor was chosen as CCD's are static sensitive, delicate, more expensive than photodiode types and prone to permanent damage when exposed to high intensity light such as that from a laser source. An improved beam tracker was developed using quadrant detectors. This beam tracker, employing a direct measurement approach, was not only the least expensive but found to be simpler and more accurate than the alternatives considered.

4.3.2 Important Considerations when using Photodiodes

Although photodiodes have much better performance characteristics than comparable vacuum tube devices (Kelly & Duda, 1974), four factors can affect performance.

(1) *Temperature effects* - As the temperature increases there is an apparent shift of the responsivity curve towards higher wavelengths.

(2) *Responsivity non-uniformity* over the device active area - caused by a variety of device imperfections, the most significant of which is the junction profile within the photodiode.

Responsivity changes brought about through temperature fluctuations or caused by device non-uniformity should have no effect on the beam tracker performance when using array or quadrant detector configurations as in operation the proposed beam trackers will work by measuring the difference in output between two photodiodes rather than measuring absolute light values.

(3) Any *variation in responsivity with light intensity* represents a variation in linearity. At input light intensities greater than 0.1 mW/mm², major deviations in linearity begin to

occur. When laser light is condensed on an extremely small area, resistance increases and linearity deteriorates. The output power of the laser used is a continuous 1 mW, the spot size being 30 mm², giving a fixed intensity of 0.033 mW/mm² which is below the level required to cause major deviations in output linearity. Also the area over which the spot is localised is sufficiently large so as not to adversely affect output linearity.

(4) *Sensor optical properties* - Special attention has to be given to all optical interfaces, especially in the case of a laser where optical attenuation is usually required to prevent flux density saturation. The reflectivity of an uncoated silicon photodiode varies, according to the wavelength, from 47% to 32%. For protection, a glass window is incorporated into the sensor construction. These interfaces can become interference cavities when illuminated with coherent radiation which gives rise to additional spatial non-uniformities.

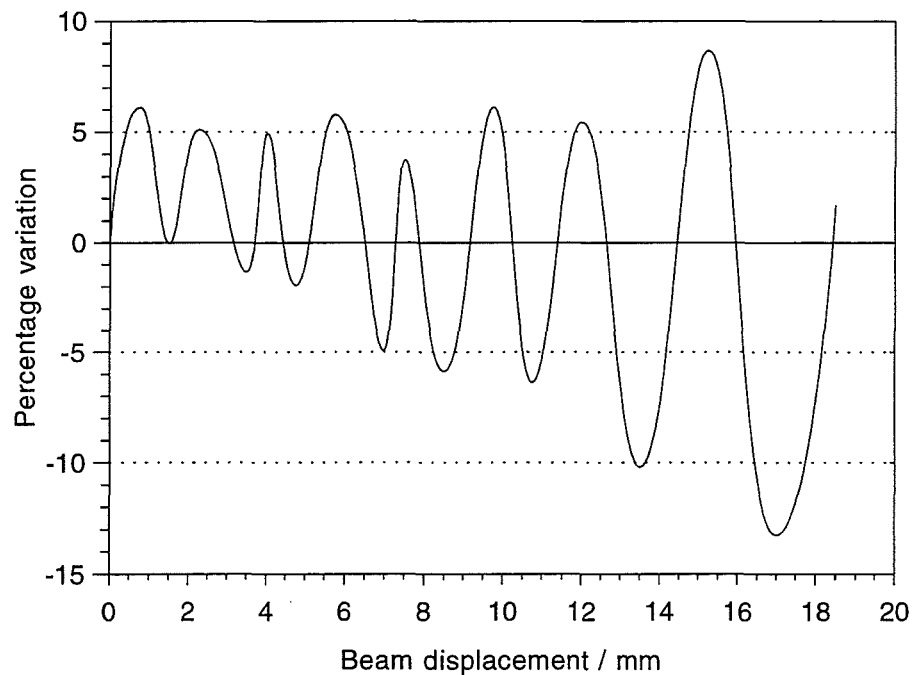


Figure 4.5 - Spatial variation of photodiode detector output - (Kelly & Duda, 1974)

To minimise the detrimental effects of beam scattering, front-end optics were not used on the beam trackers.

4.4 THE LINESCAN CAMERA BASED BEAM TRACKER

The prototype laser tracking system made use of a photodiode linescan camera (Lewis, 1991). The camera was used as a single axis position detecting device, the prototype arm moving in the vertical direction only.

4.4.1 Requirements

For the arm mounted beam tracker there were three requirements.

(1) The photosite array needed to be *of adequate length* to detect vertical movements of the laser beam and the deflections caused by a reasonable load range (0-4 kg) suspended from the end of the arm.

In both cases the length of the array would determine the range of angular movement of the laser for which arm positional information could be recorded. The length of the array was important as it needed to be great enough to ensure that the arm linear actuator had sufficient time to respond to the camera generated error signals and to re-centre the camera, via movement of the arm, on the laser beam (see table 4.2).

(2) The photosite array needed to be *of sufficiently high resolution* to detect small positional changes of the laser over its surface. This was necessary to cause rapid response in the arm motor drive feedback mechanism, so as to enable both vertical arm movement and deflection compensation to be actioned accurately with minimum time delay.

(3) Output signals *should give positional information* about where along the photosite array the laser beam was detected. A linescan camera was ideally suited for this purpose as measuring the time delay between the start of the clock pulse and the start of the camera video signal gave this information directly.

4.4.2 Camera Description and Position Monitoring Sensitivity

The camera used was an IPL series 2000 linescan camera (Editor, 1985). It has a 26 mm self-scanning photodiode array, containing a row of 256 individual photodiodes, each with its own charge storage capacitor and solid state multiplex switch. It contains a shift register for serial readout of the individual element signals. The array and processing circuitry is housed inside a 100 x 60 x 74 mm aluminium case, connections to the power supplies and external circuitry being made via a single connector. An M42 thread provides a means of attaching the camera to the robot arm adaptor. The camera mass is 447 g.

Table 4.2

The effect of arm length on the detectable laser angle change from the central photosite on the array and between adjacent photosites		
Arm length (mm)	Detectable laser spot angular displacement from central photosite on array / degrees	Detectable laser spot angle change between adjacent photosites / degrees
250	± 2.98	0.023
500	± 1.49	0.012
1000	± 0.74	0.006
1500	± 0.50	0.004
2000	± 0.37	0.003
2500	± 0.30	0.0023
3000	± 0.25	0.00195

The accuracy of the tracking system depends directly upon the length of the robot arm (see table 4.2) - the longer the arm the greater the overall position detecting accuracy. The resolution of the system was determined by the number of photosites per unit length along the array. The camera array was able to detect laser spot position changes equivalent to the distance between individual photosite centres, this distance being 0.102 mm.

The angle through which laser movement could be detected by the camera decreased proportionally with arm length since the detectable vertical arm displacement from the centre of the array remained constant at ± 13 mm.

4.4.3 Camera Operation as Beam Tracker

The camera was directly able to provide the positional information required for full functioning of the robot. By monitoring the camera clock and video outputs simultaneously information was obtained which related directly to the position along the array of those photosites being illuminated by the laser.

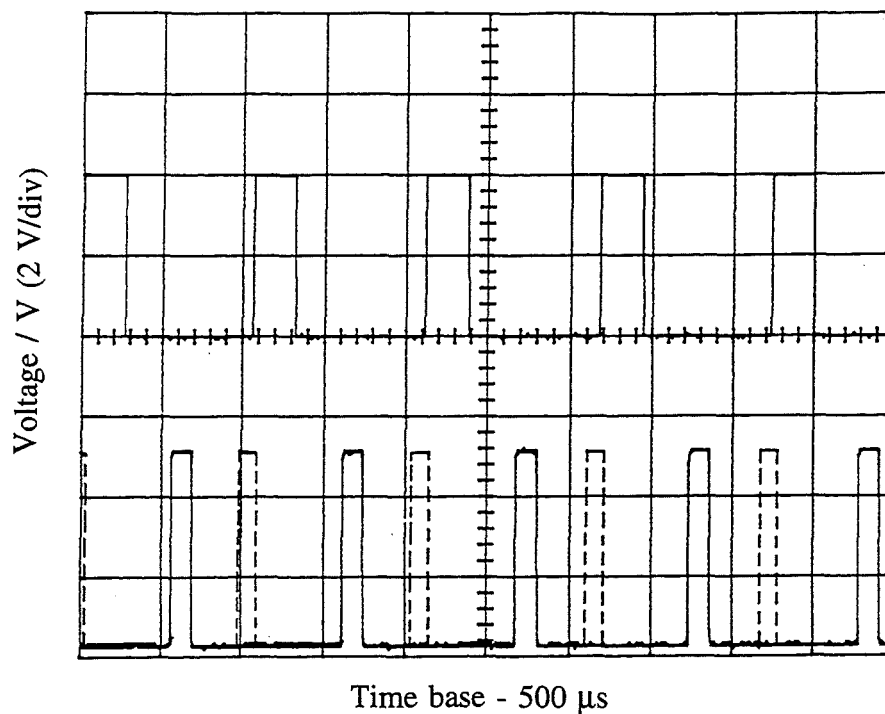


Figure 4.6 - Shift of the video output relative to the clock pulse as the laser beam is scanned across the array

A program, written in 'C' code, used the middle pixel as a reference null point (see Appendix C). Any deviation of the laser light from this point caused an error signal to be generated, the magnitude of the error signal being directly proportional to the displacement of the laser beam from the null point. This proportional signal was then used to drive the arm actuator via a power amplifier in the direction required to reduce the error.

4.4.4 The Camera Output Signals and Signal Conditioning Circuitry

The camera video signal showed the time-integrated illumination of each individual picture element over one scan cycle. A typical output waveform is shown in figure 4.7.

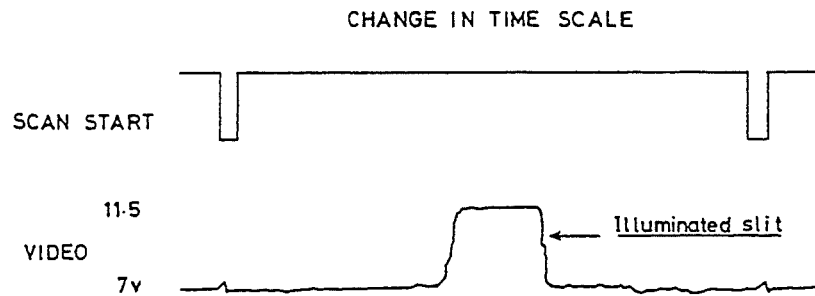


Figure 4.7 - A typical camera output waveform - (Editor, 1985)

(1) *The clock output*

The camera clock frequency was set at 2 kHz to give a relatively long time interval between clock pulses. This ensured that the computer would not 'miss' pulses as was the case if the frequency were too high.

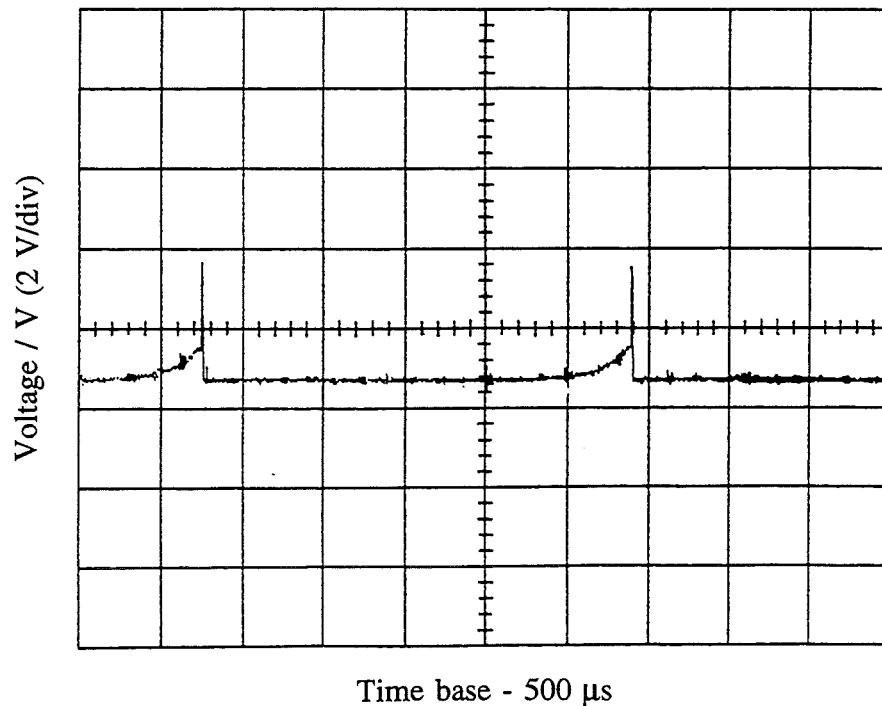


Figure 4.8 - The camera clock output pulses

Figure 4.8 shows the camera clock output. In this form it was not computer compatible as the clock pulses were of too short a duration to be detected by the computer and so the pulse width needed to be increased.

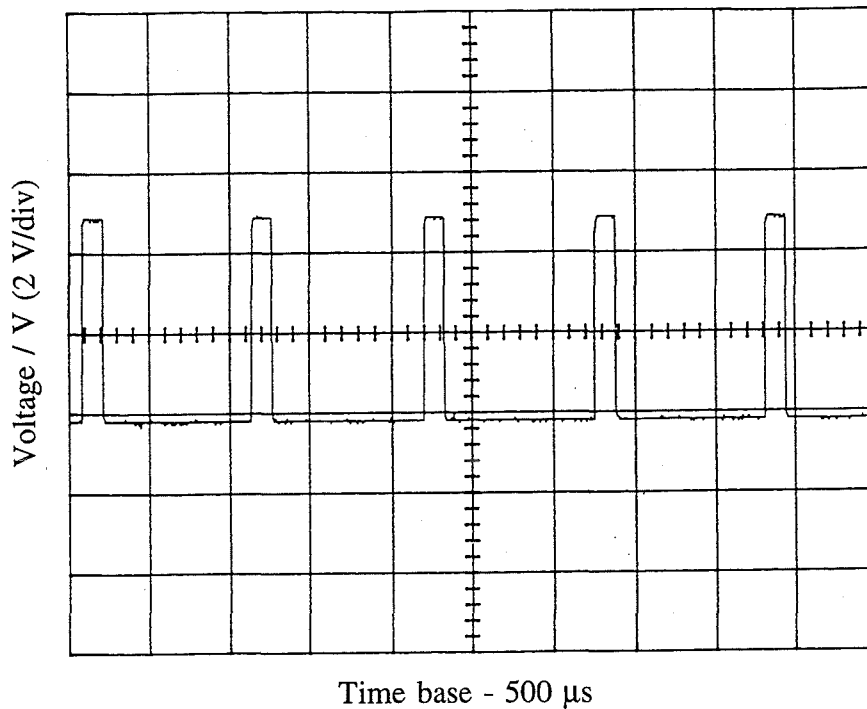


Figure 4.9 - The stretched clock output pulse

A monostable network formed the pulse stretching circuit (Jones, 1985). A $0.1 \mu\text{F}$ capacitor in conjunction with a $12 \text{ k}\Omega$ resistance produced sufficient stretching of the pulse (0.84 msec) for the computer to detect both the rising and falling edges (see Appendix C).

(2) *The video output*

The video output was an analogue signal as shown in figure 4.10. As with the clock signal this required modification to make it computer compatible as :-

- The output ranged between + 6 V (dark signal) and + 12 V (saturation) and therefore required conversion to TTL values for input to the computer.
- The waveform was 'squared' to enable the rising edge of the signal to be sharply defined and so detected easily.

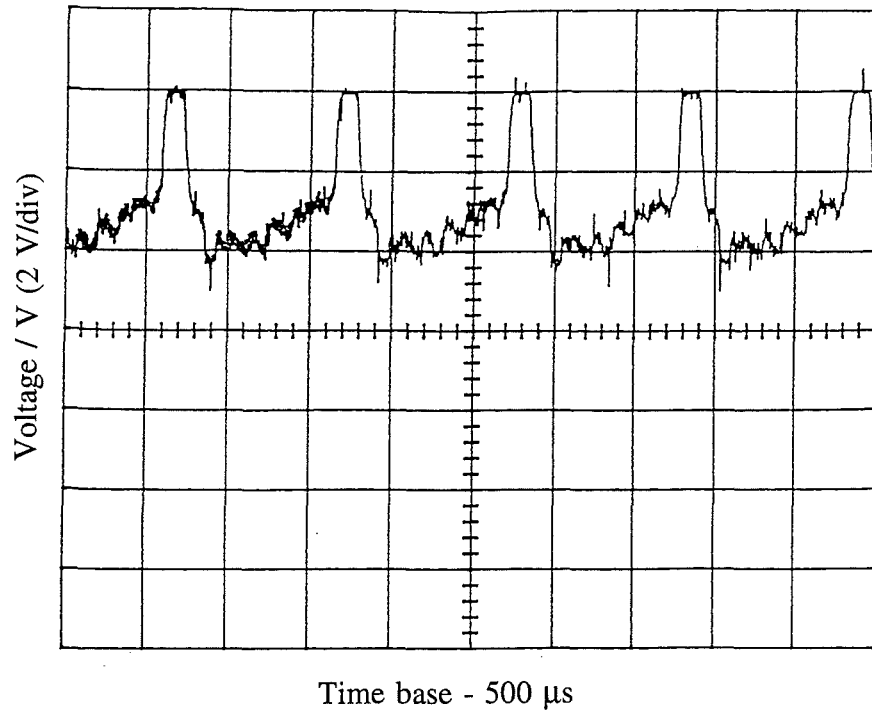


Figure 4.10 - The camera video output using the laser beam as a light source

A comparator converted the analogue output into a square wave. A voltage divider set the switching threshold level at 8.5 V. The squared video output signal was then fed into a second comparator to convert the input square wave to TTL values (see Appendix C).

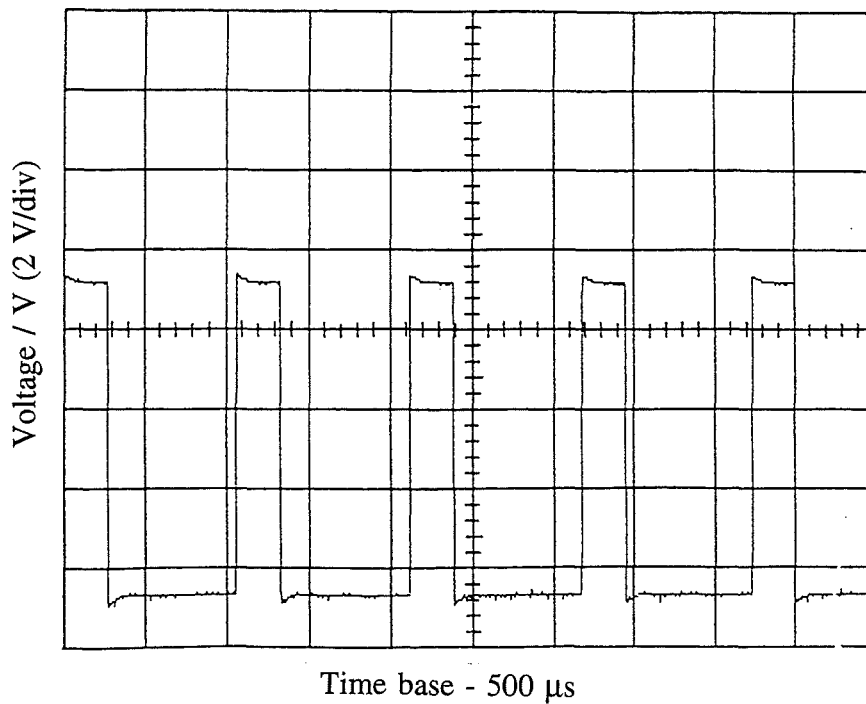


Figure 4.11 - The modified video output

There were two benefits derived from squaring the signal.

- The point at which the edge began to rise could be adjusted by varying the comparator threshold level setting. This meant that the sensitivity of the camera output could be adjusted so that only laser light over a certain intensity was recorded.
- The width of the laser spot over the photosite array became immaterial as only the rising edge of the signal was used for position monitoring.

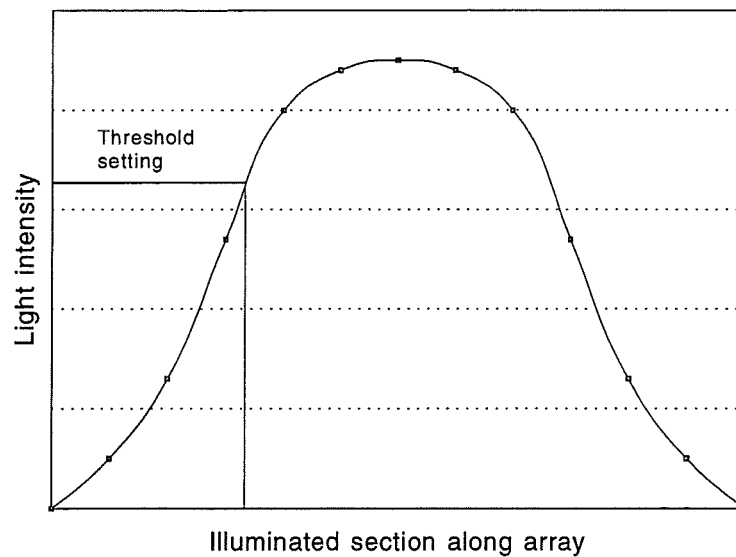


Figure 4.12 - The laser spot intensity profile - (Milne, 1983)

4.4.5 Disadvantages Associated with using the Linescan Camera

Although adequate for concept proving, various disadvantages were apparent.

- Size (100 x 60 x 74 mm) and mass (447 g) : both were difficult to reduce significantly as the signal processing electronics required positioning as close as possible to the diode array to minimise electronic noise.
- The need for signal post-processing circuitry : required since the video and clock signals were not computer compatible.
- Method of error determination : real-time, computer intensive calculations were required to set middle pixel as the null point and to generate the

position error signal.

- Single axis error detection only : dual axis detection could be achieved by using a two-dimensional diode array, yet this not only would increase unit cost considerably but also increase the complexity of the computer interfacing electronics and software required.
- Relatively low resolution : resolution could be increased by using a camera with more pixels per unit length (e.g. 1024 pixels per 26 mm row), yet this increase in performance would be reflected considerably in the cost of the device.

4.5 DUAL AXIS, QUADRANT DETECTOR BASED BEAM TRACKER

A new, dual axis beam tracking apparatus was designed using a photodiode quadrant detector as a 'fine' position sensor. The detector was surrounded by a ring of individual photodiodes which made up a 'coarse' position sensor.

4.5.1 Construction

The body (a) was built from a 75 mm length of 50 mm diameter aluminium tube. An M42 threaded tube (b) was secured to the front end to provide a ready means of attaching the apparatus to the robot arm. The back was sealed with an aluminium plate (c).

An electrically insulating former (d), was secured inside the apparatus at a distance of 45 mm from its front end.

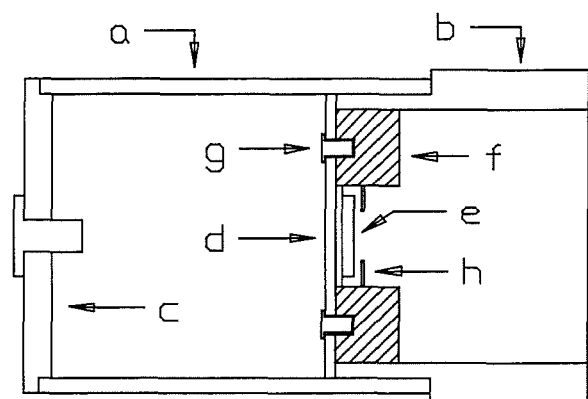


Figure 4.13 - Construction details

The quadrant detector (e) was glued with an epoxy resin to the centre of the former and surrounded by a ring of four light diffusers (f). The diffusers were made from machined Perspex, sand blasted to give a frosted surface. Single photodiodes (g) were fixed in

circular recesses drilled into the back of each diffuser. A matt black cardboard washer (h) was secured to the front of the quadrant detector, the internal hole was sufficiently large to expose the whole active area of the detector. All internal surfaces were painted with matt black paint. The beam tracker mass was 87 g.

4.5.2 The Detector

A Centronics QD 100 general purpose silicon photodiode quadrant detector was used (Editor, 1993d). It had a total active area of 100 mm^2 and a diameter of 11.3 mm, with separation between quadrants of 0.2 mm. An important consideration was the size of the device's active area (Editor, 1993e). Those with large active areas ($31\text{-}100 \text{ mm}^2$) are useful for applications requiring an extended field of view, or the measurement of expanded beams of light. However there is a trade-off with the increased noise. Photodiodes with small active areas ($0.1\text{-}3.1 \text{ mm}^2$) are less noisy ($<1 \text{ mV rms}$) and well suited for directional measurements, but usually require optics to focus the incoming light. As the beam tracker was designed to directly monitor link deflection over a reasonable range a relatively large device was chosen at the expense of noise.

The photodiode element was enclosed in a sealed metal can with a thin cover glass. This ensured ruggedness and reliable operation. The maximum responsivity was in the 780-950 nm range which closely matched the wavelength of the laser light used (see figure 5.11).

4.5.3 Coarse/Fine Position Detecting Beam Tracker - Principle of Operation

(1) Fine control

The beam tracker was mounted at the free end of the arm such that if the laser beam passed directly up the middle of the unloaded arm it would strike the centre of the quadrant detector. When the light beam was centred, the output currents from each element were equal. As the beam was moved, a current imbalance proportional to the displacement of the spot from the central position occurred, indicating off-centre position.

Current output from the quadrant detector was converted into a voltage using the circuit shown in figure 4.16. with quadrants connected together in pairs.

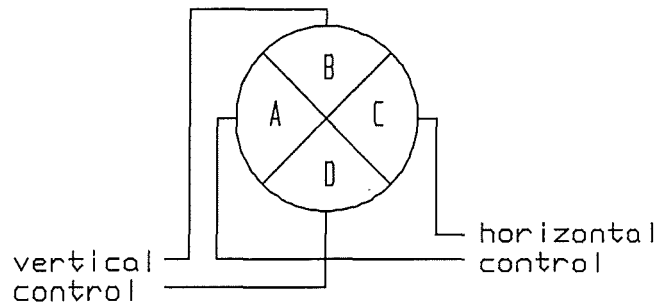


Figure 4.14 - Principle of fine control operation

A and C formed a pair of quadrants which detected the laser spot movement along the horizontal axis. B and D were similarly arranged to detect beam movements along the vertical axis. Circuits for horizontal and vertical arm movement functioned simultaneously yet independently of each other and controlled the movement of different actuators. As the position of the spot shifted across the face of the detector both the horizontal and vertical sensing systems operated to return the arm to the null position so that the beam was again centred on the detector.

Photodiodes operate by the absorption of light photons to generate a flow of current in an external circuit, i.e. they function as 'solar cells'. This photovoltaic mode of operation provides the optimum signal-to-noise ratio with good response linearity. A typical linearity plot for a silicon photodiode is shown in figure 4.15.

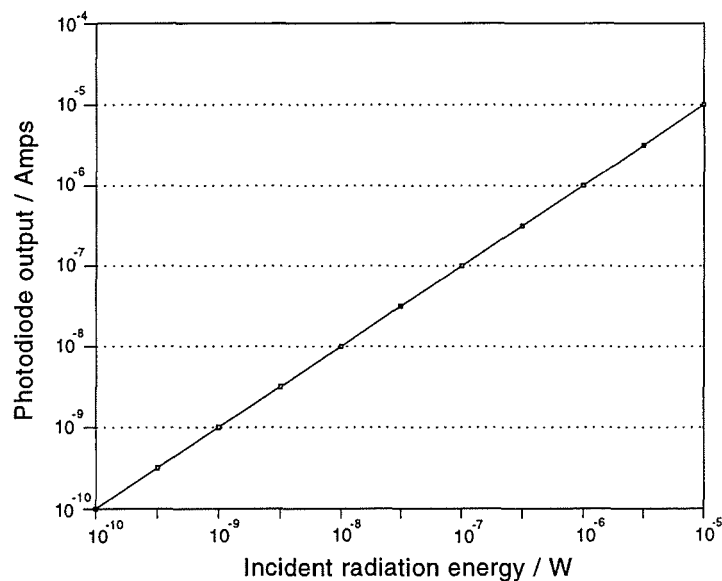


Figure 4.15 - Linearity plot for PIN photodiode - (Editor, 1994)

The lower limit of this input/output relationship is established by the noise in the photodiode, and has a value between 10^{-12} - 10^{-15} W depending upon the size of the active area and mode of operation. The upper limit of this input/output relationship is established by the maximum current that the photodiode can handle without becoming saturated. It varies between 10-500 mW depending upon the area of the incident spot of light, and the detailed construction features of the sensor.

Photodiodes may be operated with an applied reverse bias voltage (photoconductive mode), yet changes in responsivity can occur due to changes in the dark leakage current which doubles for every 10° rise in temperature. With the photovoltaic mode of operation these problems do not occur.

The external circuit to which the photodiode was connected contained a network of analog amplifiers and dividers.

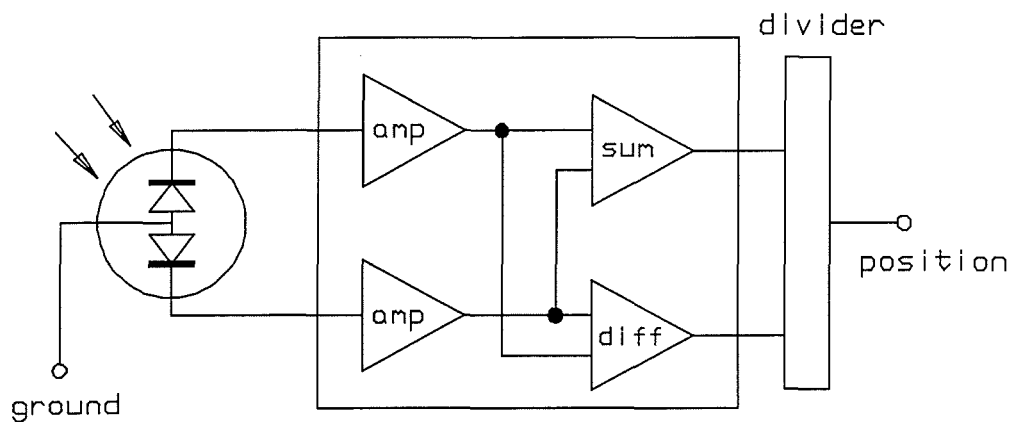


Figure 4.16 - Schematic of 'centroid' position sensing electronics

The first stage amplified the photodetector current and converted it to a voltage, the second stage performed the summing (proportional to the intensity) and differencing (proportional to the intensity and position) of the quadrant signals. A divider was used to divide the sum signals into the difference to determine the 'centroid' of the light spot (Feige & Clegg, 1983).

(2) *Coarse control*

If the light beam were to travel so rapidly that the arm was unable to track it, the light spot would have moved off the active area of the quadrant detector and arm control would have been lost. This was prevented by having a second series of detectors surrounding the quadrant detector such that when illuminated they caused rapid arm actuation in the direction required to re-centre the quadrant detector on the beam again.

This coarse controller consisted of individual photodiodes (a) mounted in each of four purpose-built light diffusing segments (b) surrounding the quadrant detector (c). Whenever and at whatever point the beam struck one of these segments the light was scattered internally and detected by the photodiode.

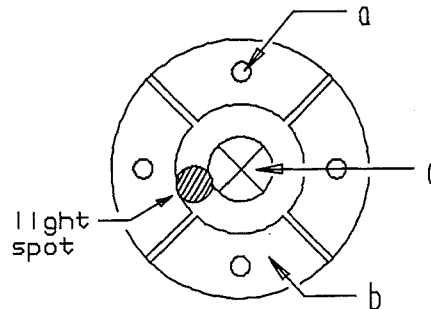


Figure 4.17 - Coarse position control ring

If the light spot passed across the junction of two segments both diodes were illuminated causing simultaneous horizontal and vertical corrective movements.

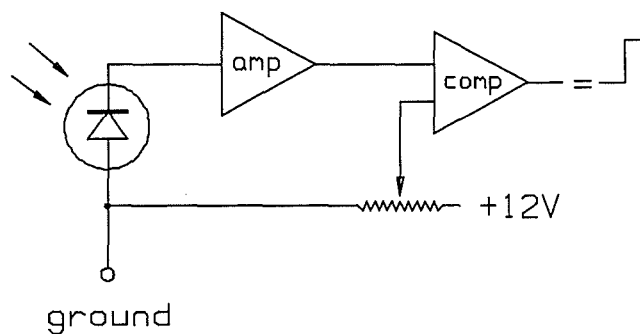


Figure 4.18 - Coarse positioning electronics

Each photodiode in the coarse position detecting system was connected to an operational amplifier/comparator circuit with adjustable switching threshold so that the sensitivity of this detection system could be adjusted. The full circuitry was housed in a shielded metal box connected to the beam tracker through a shielded cable.

4.5.4 Coarse/Fine Detector Spacing

To enable continuous beam tracking the coarse positioning segments were arranged concentrically around the quadrant detector at a distance no greater than the diameter of the spot (see figure 4.17). This ensured that control remained active when switching from coarse to fine control and vice versa.

4.6. BEAM TRACKER MINIATURISATION

During testing it became apparent that the beam tracker could be miniaturised considerably without reducing its performance.

(1) The slave position control system was found to be so responsive to shifts in the laser spot position that the coarse position control described in Section 4.5.3 was not required.

(2) The electronics could be simplified considerably as the summing and dividing circuitry is needed only in situations where the incident light varies in intensity and shape, which can be detected as an apparent shift in spot position. As the laser light source was stable and the spot profile did not vary, it was found sufficient to measure difference alone.

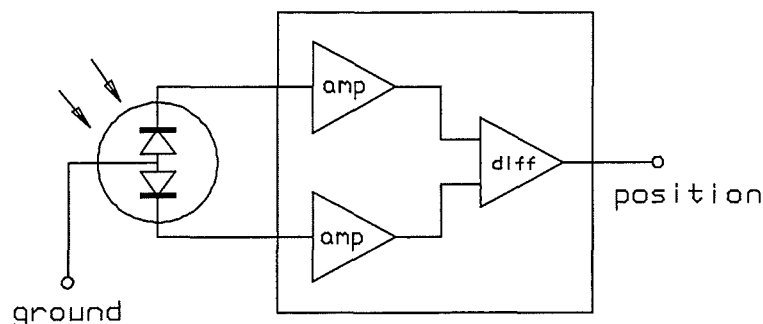


Figure 4.19 - Schematic of simplified position detecting electronics

AD165 programmable instrumentation amplifiers were used (Derenzo, 1990). These particular devices are very stable during operation. By modifying the gains the relative sensitivity of the tracker system could be varied (Hutcheson, 1976). The quadrant detector could then be used for both course and fine tracking, the sensitivity being increased as the detector centred on the spot. Two such devices were required for dual-axis functioning.

(3) Single axis position detection systems would be required to measure the vertical deflection of each link near the link joints. A bi-cell rather than quadrant detector could be used to reduce the size, weight, complexity and cost of the beam tracker even more.

4.6.1 Construction Details

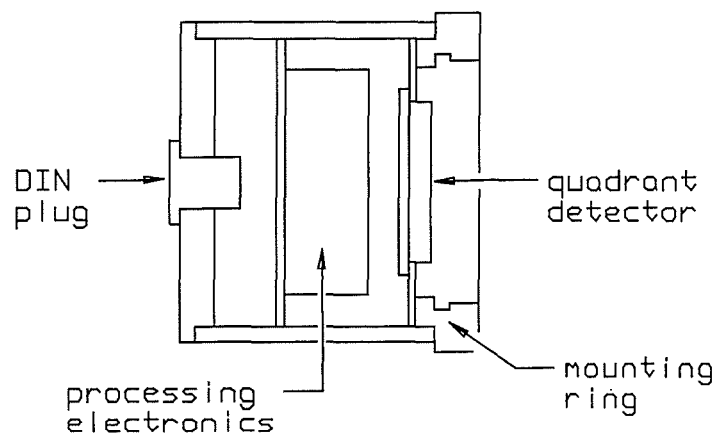


Figure 4.20 - Miniature beam tracker construction

The beam tracker was built up in a similar manner to the coarse/fine beam tracker described in Section 4.5.1. It differed in the following ways.

- the body length was shortened to 50 mm,
- the coarse positioning detector ring was not included,
- the anti-reflection washer was omitted,
- a 7 pin female DIN connector was added to the rear sealing plate,
- the signal processing electronics were mounted inside the beam tracker on a PCB behind the quadrant detector.

Summary

Table 4.3 gives a comparison between the linescan camera and quadrant detector based beam tracking systems. It shows that the miniaturised quadrant detector beam tracking system has distinct advantages over the linescan type in terms of both its physical and performance characteristics.

Table 4.3

A comparison of linescan camera performance with that of the quadrant detector type		
Characteristics	Linescan beam tracker	Q/D beam tracker
Cost (£)	£80 - 200	£50 - 180
Size (mm)	100 x 60 x 74 mm	42 mm ϕ x 50 mm
Weight (g)	approx 500 g	approx 100 g
Mechanical strength	electronics make it fragile	strong, robust
Associated electronics	must be sited adjacent to sensor	very simple, can be sited remotely
Position resolution	limited by pixel size	very high - < 0.1 μ m
Interfacing electronics	needed to make signal TTL compatible	none required
Method of error determination	requires computer calculation	direct reading
No of axes	single only	switchable between single and dual

The miniaturised beam tracker formed a 'stand alone' system. It more than adequately met the original specification and was versatile in that it was easily modified for single axis functioning. It was considerably cheaper, smaller, lighter and more accurate than the linescan beam tracker. It required only an external power supply to operate it, which can

be replaced by a battery fixed inside the beam tracker body as the current consumption was very small (30 mA).

The two output signals from the beam tracker, corresponding to the position of the spot over its surface, were in the form of proportional voltage swings between ± 10 V and were easily interfaced to the other parts of the position control feedback circuitry.

Testing methods and a comparison of the beam tracker simulated and measured performance are described in the next chapter, leading to a conclusion in which the optimum incident light spot parameters are defined.

References

Derenzo, S.E., (1990) 'Interfacing - a laboratory approach using the microcomputer for instrumentation, data analysis and control', London, Prentice-Hall, pp. 277-286.

Doebelin, E.O., (1990) 'Measurement systems - application and design', London, McGraw-Hill International, (Fourth edition), pp. 269-287.

Optron Corporation, Woodbridge, Conn. USA.

Ya-Man Ltd, San Jose, Calif, USA.

Editor, (1993a) 'Position sensing photodetectors', United Detector Technology.

Editor, (1993b) 'The guide to position sensing', UDT Instruments Incorporated.

Editor, (1993c) 'Photodiodes catalogue', Hamamatsu Photonics.

Editor, (1993d) 'High specification silicon photodetectors', Centronics Ltd.

Editor, (1993e) 'Detector guide', Melles Griot Incorporated.

Editor, (1994) 'Optoelectronic components catalogue', UDT Sensors Incorporated.

Editor, (1985) '2000 series linescan camera manual', Integrated Photomatrix Limited.

Edwards, I., (1988) 'Using photodetectors for position sensing', Sensors, Vol. 5, No. 12, December, pp. 3-7.

Feige, E. and Clegg, T.B., (1983) 'A new optical transducer to measure damped harmonic motion', The American Journal of Physics, Vol. 51, No. 10, October, pp. 954-955.

Hutcheson, L.D., (1976) 'Practical electro-optic deflection measurement system', Optical Engineering, Vol. 15, No. 1, January-February, pp. 61-63.

Jones, M.H., (1985) 'A practical introduction to electronic circuits', Cambridge University Press, pp. 220-221.

Kelly, B.O. and Duda, R., (1974) 'Suitability of silicon photodiodes for laser emission measurements', Proceedings of the Conference of Radiological Health, Gaithersburg, Maryland, June 4-7.

Lewis, J., (1991) 'The design, construction and testing of a laser guided robot arm', MSc project, Middlesex Polytechnic Report, April.

Light, W., (1982) 'Non-contact optical position sensing using silicon photodetectors', United Detector Technology, Hawthorne, Calif, USA, Application notes, 10 pp.

Milne, W.I., (1983) 'Lasers and their industrial applications', The Electricity Council.

Wendland, P.H., (1973) 'Silicon photodiodes come into their own', Optical Spectra, October.

Chapter 5

BEAM TRACKER PERFORMANCE

5.1 INTRODUCTION

This chapter begins with a description of the apparatus used to test the performance characteristics of the beam tracker. The response of the beam tracker to variations in the incident light spot parameters are discussed, leading to a conclusion in which the optimum light source specifications are derived.

5.2 TEST APPARATUS AND METHODOLOGY

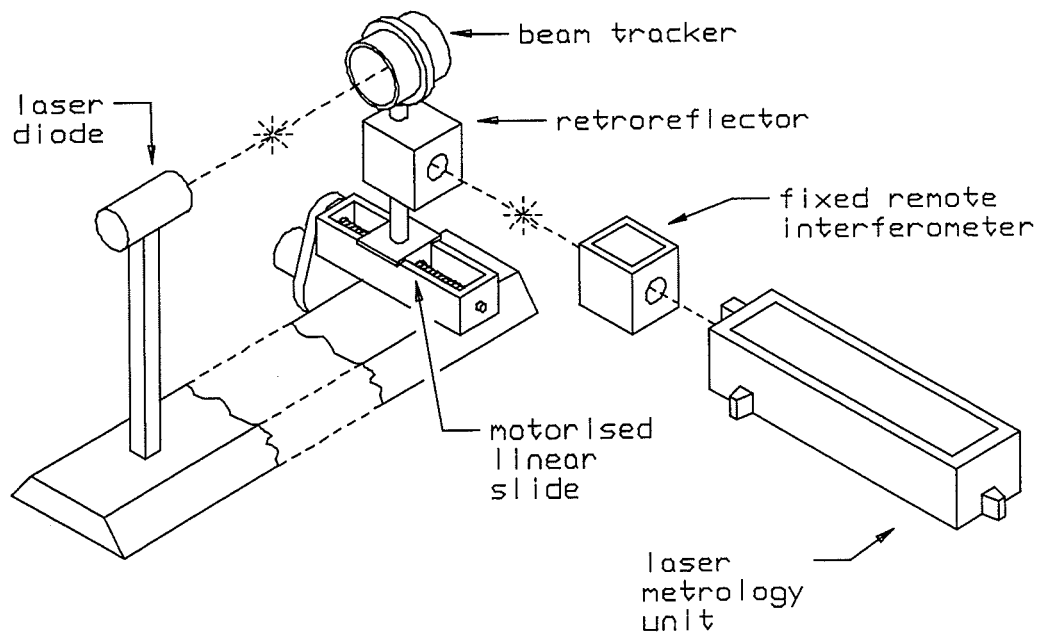


Figure 5.1 - Apparatus for beam tracker performance analysis

Figure 5.1 shows the arrangement of the apparatus used to determine, experimentally, the performance characteristics of the beam trackers. A laser was mounted at one end of an

optical bench. The beam tracker was fixed onto the uppermost section of a motorised optical slide at the opposite end of the bench such that it could be moved horizontally across the path of the laser beam. A laser measurement system (Hewlett-Packard metrology system 5526A and 5500C laser head (Editor, 1980)), accurately measured the linear distance through which the beam tracker moved - the retroreflector cube was fixed below the beam tracker on the moving portion of the slide and the remote interferometer cube interposed between the laser measurement system and the retroreflector. Filters and lenses could be supported on mounts between the laser and beam tracker.

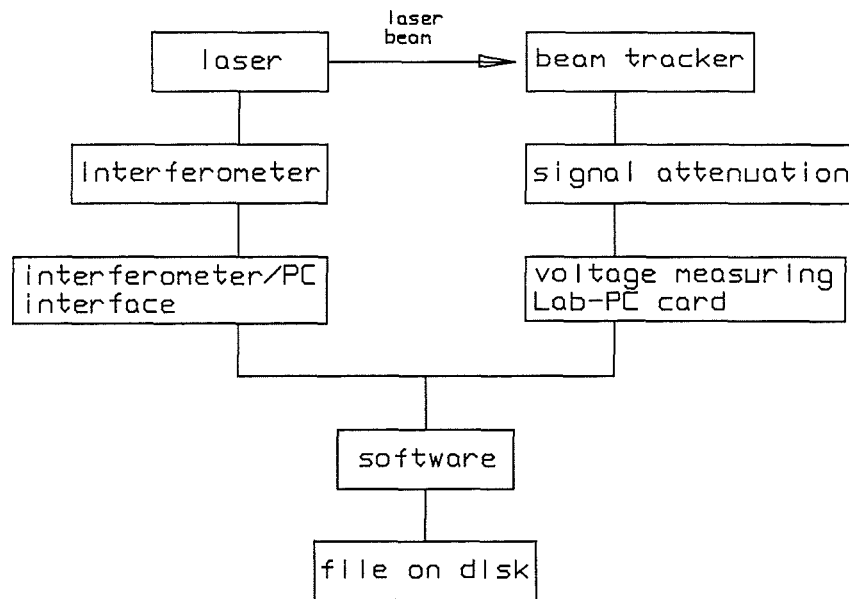


Figure 5.2 - Block diagram of the beam tracker performance test system

A Lab-Windows data acquisition package was used along with a Lab-PC Plus acquisition card to record the incoming data; additions were made to built-in Lab-Windows 'C' library functions to tailor the system to the specific requirement (Petit, 1994). Due to the incompatibility of the voltage levels between the beam tracker outputs (± 10 V) and the data acquisition card (± 5 V limit) signal conditioning attenuators were required. Interfacing circuitry was produced to convert the interferometer output (binary coded decimal or BCD) into a string of ASCII characters for compatibility with the data acquisition software (Korhonen, 1995). The data from the interferometer and that from the beam tracker were recorded as spreadsheet compatible files (see Appendix D).

Three separate beam tracker outputs were recorded :- the left and right quadrant signals and the summation of the two. A fourth channel recorded the distance information provided by the interferometer. The sampling rate could be varied (typically 5 samples/s) and the rate of travel of the optical slide could be pre-set (typically 0.1 mm/s). The beam tracker was moved initially so that the laser spot was at the extreme right of the quadrant detector. The slide drive motor was turned on and all four sets of data were recorded. Graphical representations of the results were then plotted.

5.3 RESULTS

5.3.1 The Quadrant Detector Dual-Axis Beam Tracker - Theoretical Performance

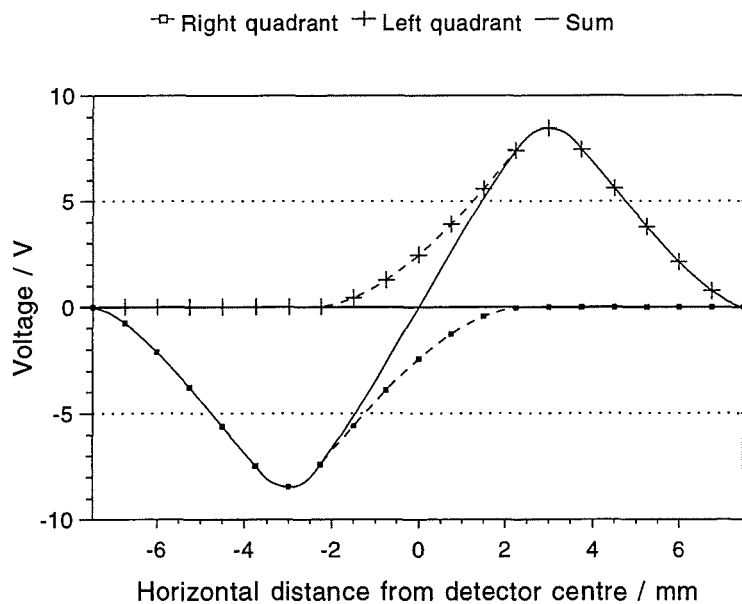


Figure 5.3 - Single-axis transfer function for 10 mm ϕ quadrant detector,
5 mm ϕ light spot

Figure 5.3 shows the single axis transfer function for opposing quadrants on the detector, the X-axis defining the spatial movement and the Y-axis the signal difference between the two elements and the individual outputs from each. The graph was constructed by calculating the area of overlap (using Autocad 12) between a 5 mm ϕ light spot and opposing quadrants on a 10 mm ϕ detector as the spot was moved incrementally from

right to left across the detector. Calculations were based on the assumptions that the spot profile and intensity were symmetrical and that the voltage generated was directly proportional to the area of the quadrant covered by the spot.

5.3.2 Performance Testing - Experimental

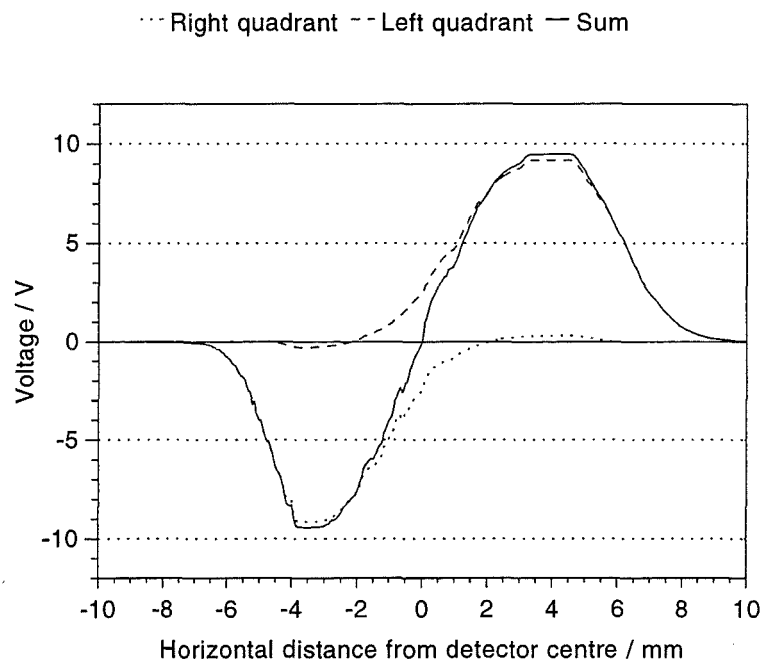


Figure 5.4 - The transfer function obtained experimentally for the beam tracker

The effect of the sensor is to map the actual position of the laser spot in X-Y space to a corresponding voltage signal in the X-Y plane. The voltage levels produced from the right and left quadrant amplifiers and the voltage sum produced from the output of the horizontal axis signal processing circuitry is shown in figure 5.4. As the beam scanned across the detector from right to left the voltage rapidly fell to the amplifier minimum of -10 V and remained at this level until 2 mm from the detector centre. This occurred as the amplifiers had been intentionally configured to give their greatest voltage output when the detector was noticeably off-centre of the spot so that maximum corrective action could be taken to restore the arm to the desired position. Proportional output was produced when two opposing quadrants were again exposed to the light spot. As the spot travelled across the apex of the right quadrant the strength of the signal diminished whilst that of the left quadrant increased to give a similar, yet opposite, output. In the region where both left and right quadrants were exposed a near linear output was produced.

5.3.3 A Comparison of Theoretical and Experimental Results

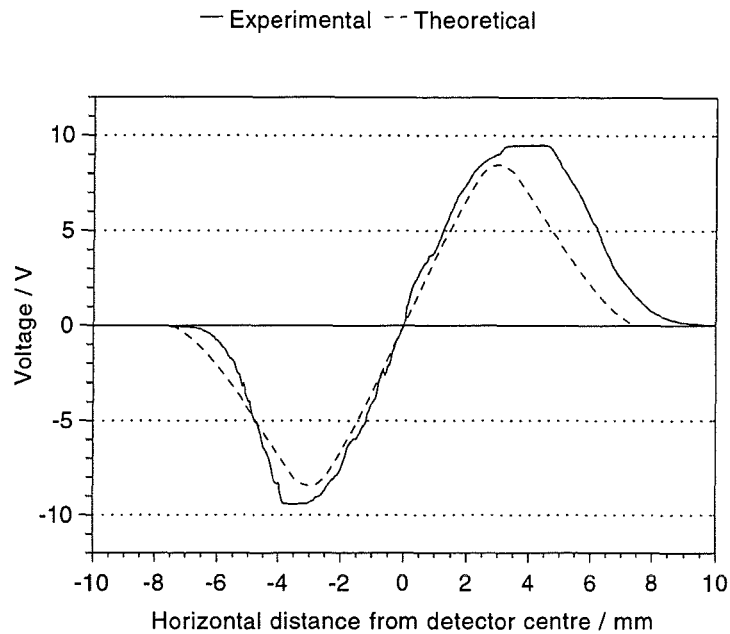


Figure 5.5 - A comparison of theoretical and experimental summed outputs

The experimental output profile of the beam tracker closely matched that of its theoretical performance. In the case shown, deviations from the theoretical performance are due to variations in intensity across the light spot and the high power of the light source used.

5.3.4 Light Intensity Effects

Figure 5.6 shows how the output profile from the beam tracker varied according to the intensity of the incident light. For low intensity illumination light emitting diodes (LED's) were used in place of the laser which caused photodiode saturation (see figure 5.7). A red LED, supported 50 mm from the detector, was operated from a 12 V supply with a 1 k Ω current limiting resistance (for bright illumination) and a 6 k Ω resistance (for dim illumination) wired in series. 3 mm ϕ light spots were produced in both cases.

At low intensity, a smooth curve was produced being similar in shape to that of the theoretical output, swinging between ± 6 V (see figure 5.3). With more powerful illumination, greater output voltage swings were produced (± 10 V) and the proportional region was longer with a steeper gradient. In this case, the gradient depended upon the degree of variation of light intensity across the spot and not the spot size as both spots

were of equal size. The low power spot had an intensely bright central but a weak peripheral region, the higher powered spot appeared to give equal illumination across its diameter. These observations are further supported by reference to the effects of variations in spot size and spot shape as discussed in Sections 5.3.5 and 5.3.8.

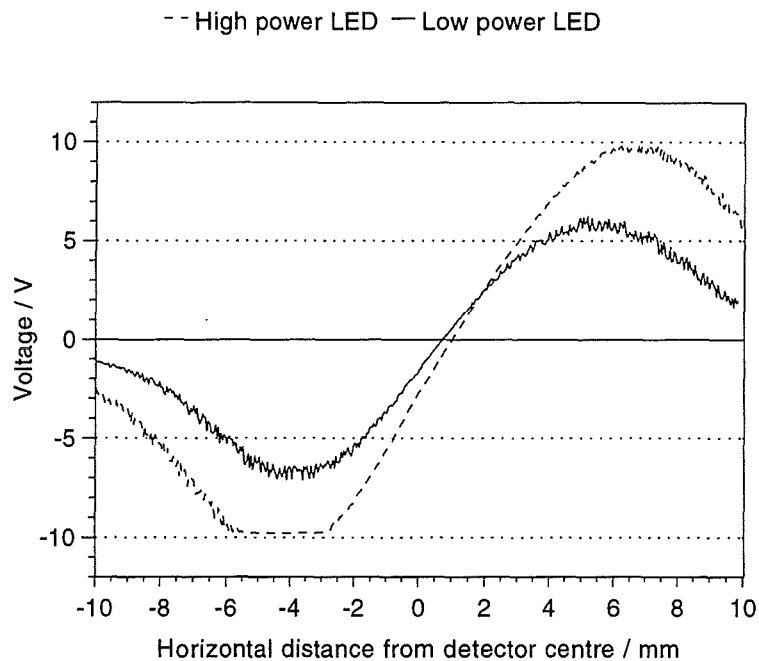


Figure 5.6 - The effect of different intensity illumination on beam tracker performance

With intense light, such as that from the laser, photodiode saturation occurred when large areas of individual diodes were directly exposed (see figure 5.7). The light power level at which the photodiodes begin to saturate depends upon light power density rather than the light power itself. The 1 mW laser produced a 2.5 mm ϕ spot, giving a density of 0.2 mW/mm² which caused saturation of the detector when virtually all of one quadrant was covered by the spot. Laser intensity was later attenuated with a neutral density filter.

The proportional region was maintained yet the output became saturated at ± 10 V as the laser was moved further than 1 mm either side of the central null point. For slave system operation this was found to be advantageous - if only one quadrant was illuminated, the output would be saturated and drive the arm at full power in the required direction until the spot again covered areas of opposing quadrants - thus restoring proportional control.

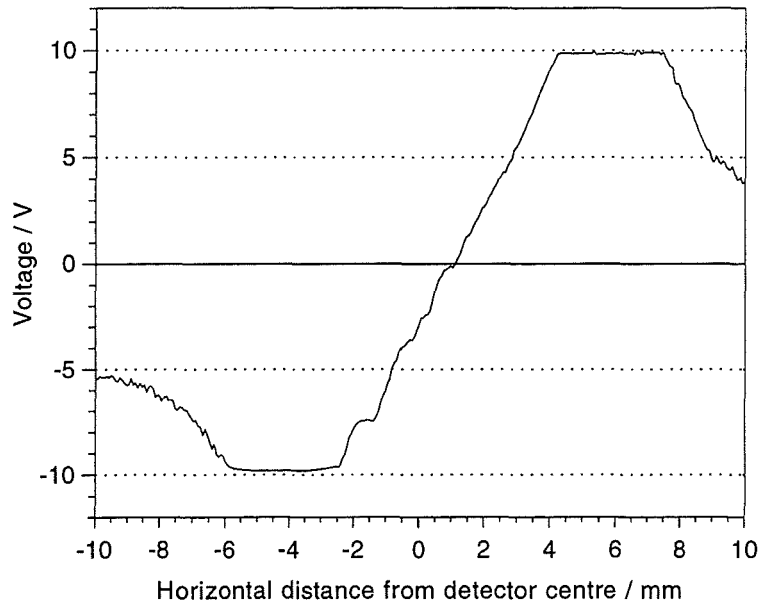


Figure 5.7 - Output clipping due to photodiode saturation

Figure 5.8 shows the effect of placing a No 1 neutral density filter between the He-Ne laser and the quadrant detector. The intensity of light on the quadrant detector is reduced giving an increased region of proportional output and reduced photodiode saturation.

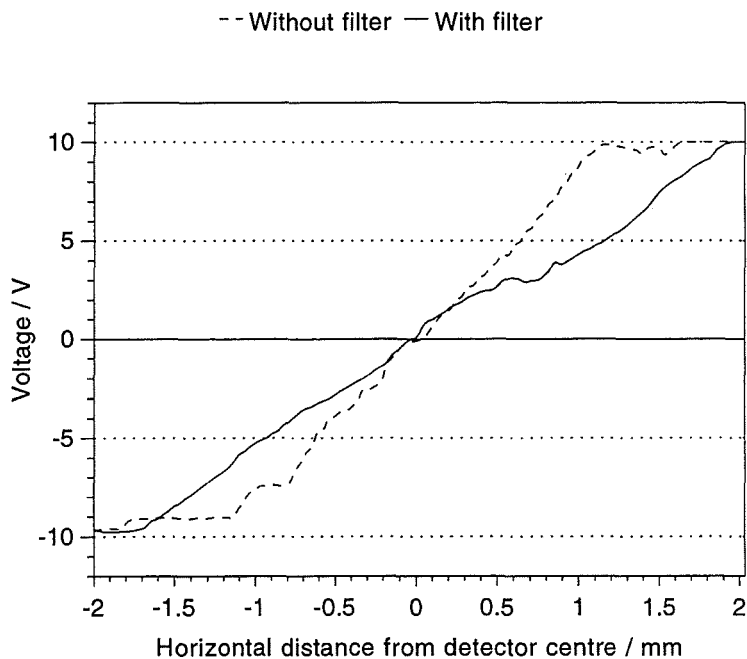


Figure 5.8 - Beam tracker output with and without a neutral density filter

5.3.5 The Effect of Light Spot Size

The detector provided position correction information as long as the spot illuminated any portion of a quadrant, giving an effective working range equivalent to the diameter of the detector plus the diameter of the spot. Proportional signals relating to the distance of the detector null point from the centre of the spot were produced only when portions of the spot covered opposing quadrants. This gives a proportionality region over a linear distance equivalent, in theory, to that of the spot diameter, i.e. until the edge of the spot had reached the gap separating individual quadrants.

Spot size was varied by placing appropriate diverging lenses in front of the laser. As the spot size was increased the light intensity over the spot decreased. The spot intensities were matched by adjusting the laser supply voltage and measuring the spot intensity using a single filtered photodiode - the generated photodiode voltage being proportional to the intensity of the incident light.

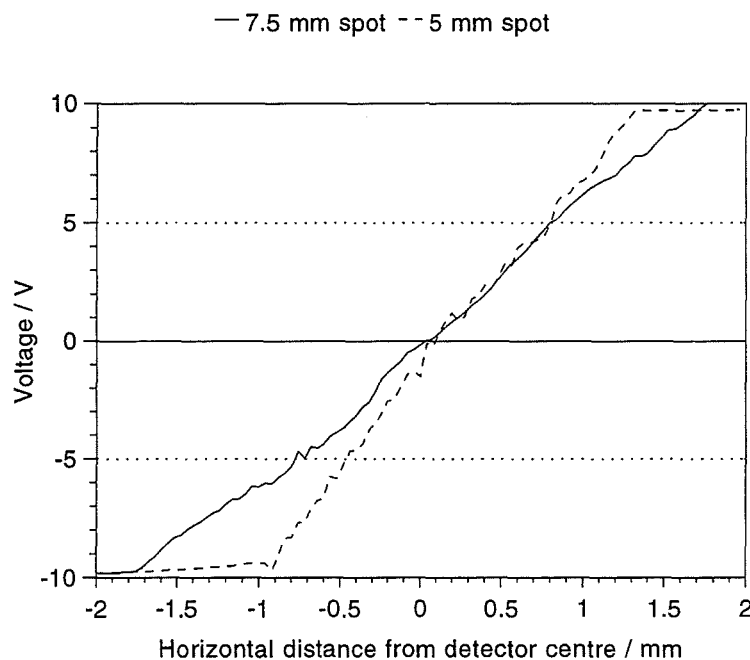


Figure 5.9 - Outputs for spot diameters of 5 and 7.5 mm

Figure 5.9 shows the results obtained experimentally for 5 mm and 7.5 mm ϕ light spots. A He-Ne laser was used producing a circular spot of uniform intensity. Experimental and

simulated results compare favourably, simulation showing that the greatest near-linear response range is obtained when the light spot diameter equals that of the sensor, yet greatest linearity is shown where the spot diameter is equal to half that of the sensor - in this case with the 5 mm ϕ spot as shown in figure 5.10.

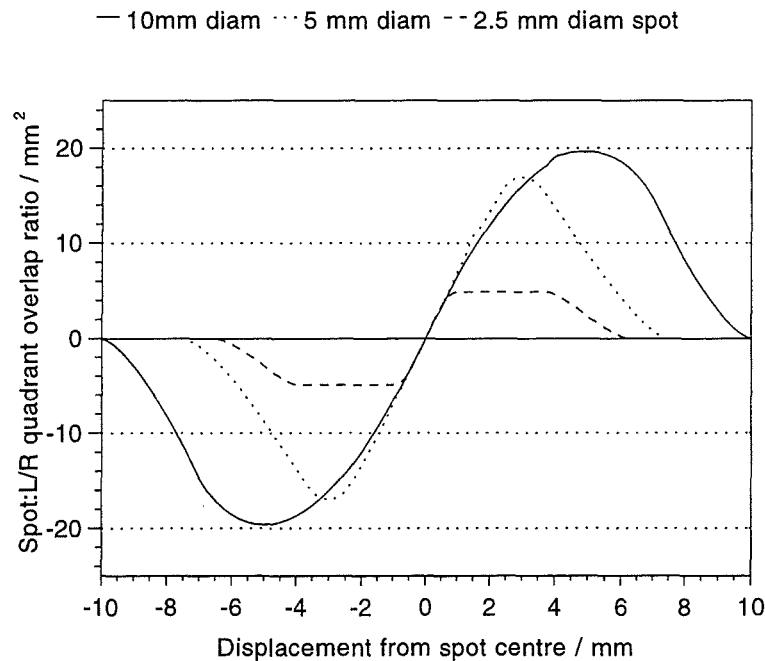


Figure 5.10 - Comparison of simulated sensor outputs with different spot diameters

For robot operation it was found through experimentation that a spot size between 1/2 - 3/4 the detector diameter gave best performance - a large central proportional region with substantial maximum positive and negative peripheral regions.

5.3.6 The Effect of Light Source Distance

Altering the distance between the laser source and beam tracker had no noticeable effect on performance as the laser was well collimated ensuring that both the spot shape and spot intensity profile remained constant over a long distance.

5.3.7 Spectral Matching

The peak sensitivity of the quadrant detector (the red to near I.R. part of the spectrum at 865 nm) closely matched that of the wavelength of laser light used - 670 nm.

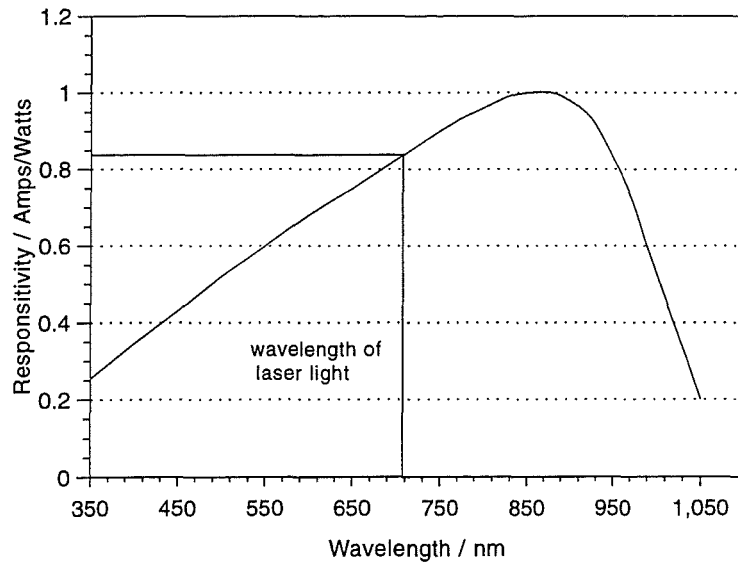


Figure 5.11 - The normalised spectral response of the quadrant detector compared with wavelength of laser light used showing good spectral match

5.3.8 The Effect of Spot Shape

A Ga-As laser diode was initially used on the positioning head, the beam spot profile is shown in figure 5.12. This profile was oval in shape with an intense central region. Attempt at modifying the spot shape by placing a plate containing a machined hole over the laser failed as it caused considerable diffraction and light scattering. The laser was later replaced by a focusable laser diode which produced a circular spot shape of variable size (see Section 5.4).

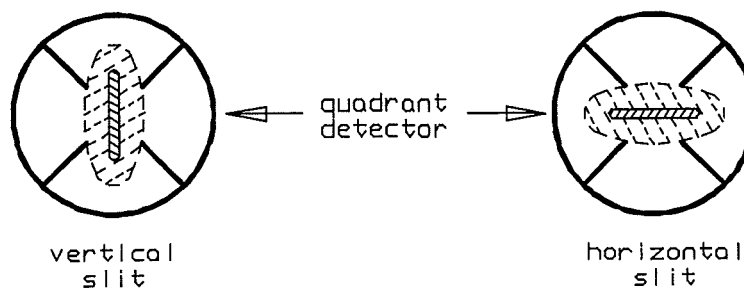


Figure 5.12 - The laser diode spot profile

Figure 5.13 shows the effects produced when the laser was scanned horizontally across the detector with the slit in both the horizontal and vertical positions. As can be seen, the longer, horizontal slit produced the greater region of proportionality. This is in agreement with the observations made regarding both spot intensity and spot size since both effect the resulting beam tracker output profile.

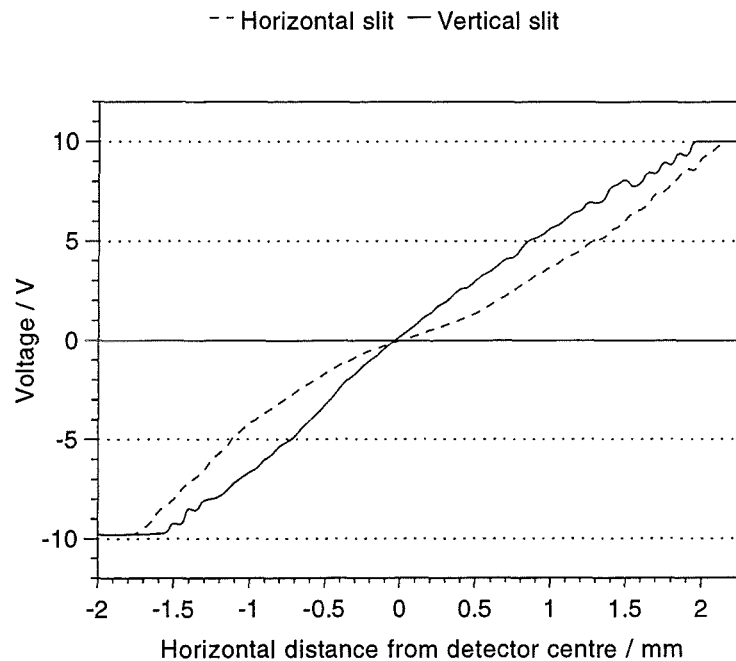


Figure 5.13 - Beam tracker output as the laser diode beam was scanned horizontally across the detector with the slit in both the horizontal and vertical positions

5.4 LIGHT SOURCE IMPROVEMENTS

Three factors were shown to have significant bearing on the quadrant detector based beam tracker performance. These were the spot shape, the spot size and the spot density profile. From these observations, modifications were made to the laser source in an attempt to improve and increase the range of output linearity from the beam tracker.

Reduction in spot intensity - The output power of the focusable laser was 1 mW. As shown in Section 5.3.4, direct illumination of the detector with a laser of this power produced photodiode saturation and clipping of the output signals. The incident laser spot density was reduced using a No 1 neutral density filter. Figure 5.14 shows the increase

in width of the linear output from 2 to 4 mm produced by using the filtered beam for both the horizontal and vertical scans. Irregularities in the plots were caused by non-uniformity across the spot due to dirt on the collimating lenses.

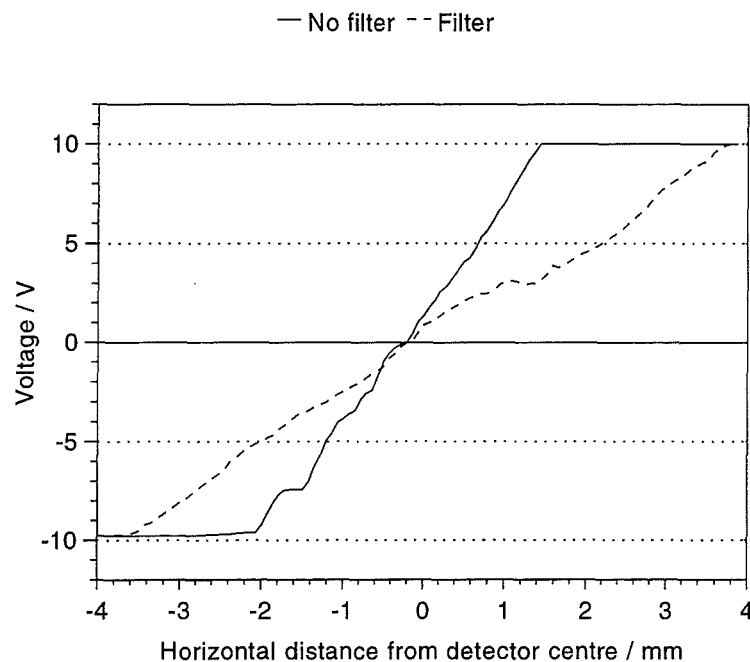


Figure 5.14 - The output from the beam tracker using the variable focus laser diode - with and without the No 1 neutral density filter

Optimising spot shape - The original laser was replaced by a focusable version which enabled the spot size to be adjusted from a pin-point through to a maximum of 12 mm ϕ over a distance of 2 m. By focusing the laser on the beam tracker face, the required 5 mm ϕ circular spot profile was produced. Similar responses were now obtained for both the horizontal and vertical beam tracker outputs. For a truly linear output response a square spot with a uniform intensity profile is required (Editor, 1993). The transfer function for a circular spot is not quite linear, mainly because its linear movement is not directly proportional to the percentage of its area which shifts between adjacent segments. For ease of attainment, a circular spot was used. As can be seen from figure 5.15, the use of a circular spot is justified as there is only a marginal difference between square and circular spot output profiles.

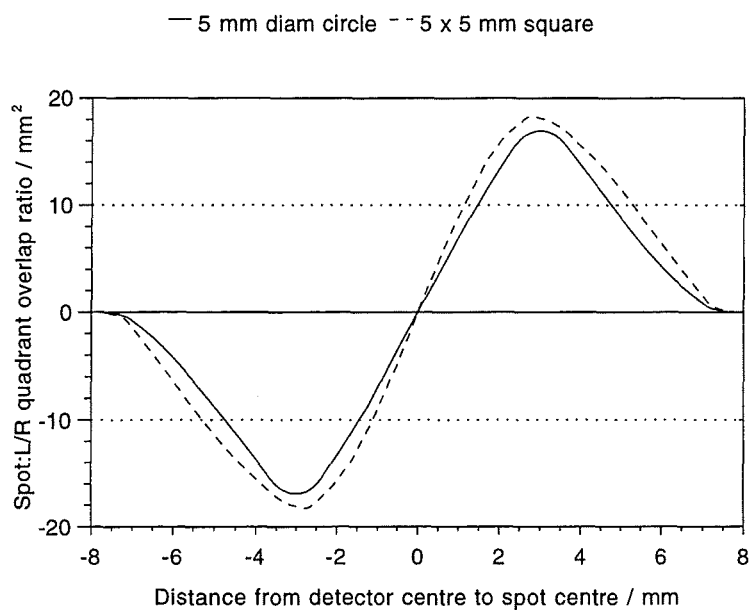


Figure 5.15 - Simulated beam tracker output for a square and circular spot

Improvements to the spot density profile - Spot profile was further improved with a diffusing screen of frosted acetate film attached directly to the quadrant detector face. It increased the width of the linear response region and prevented scattering of light from the surface of the detector glass, thus eliminating the major source of spurious signals.

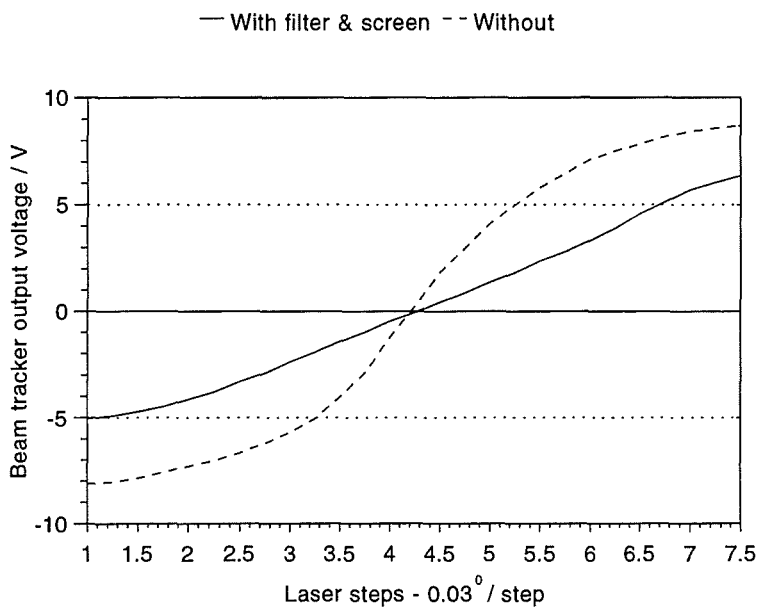


Figure 5.16 - Beam tracker outputs for diffused and undiffused filtered spots
- exploded view of central region only

Figure 5.16 shows the beam tracker output as the laser angle is changed by 0.03° increments over the central region of the beam tracker. It clearly shows the improved linear output obtained using the diffusing screen with the No 1 neutral density filter.

5.5 QUADRANT DETECTOR AND BI-CELL BEAM TRACKERS

Bi-cell based beam trackers were used for optical joint operation in instances where single-axis position tracking only was required (see Chapter 3, Section 3.5). The bi-cells were constructed by joining quadrant outputs in pairs prior to the signals being fed to a single AD165 instrumentation amplifier for amplification and summation.

5.5.1 A Comparison of Quadrant Detector and Bi-Cell Performance

Figure 5.17 shows a comparison of the theoretical transfer functions obtained from one axis of a 10 mm ϕ quadrant detector and bi-cell illuminated with a 5 mm ϕ light spot. Differences between outputs are caused by variation in the rate of change of overlap and the maximum achievable overlap between diode pairs.

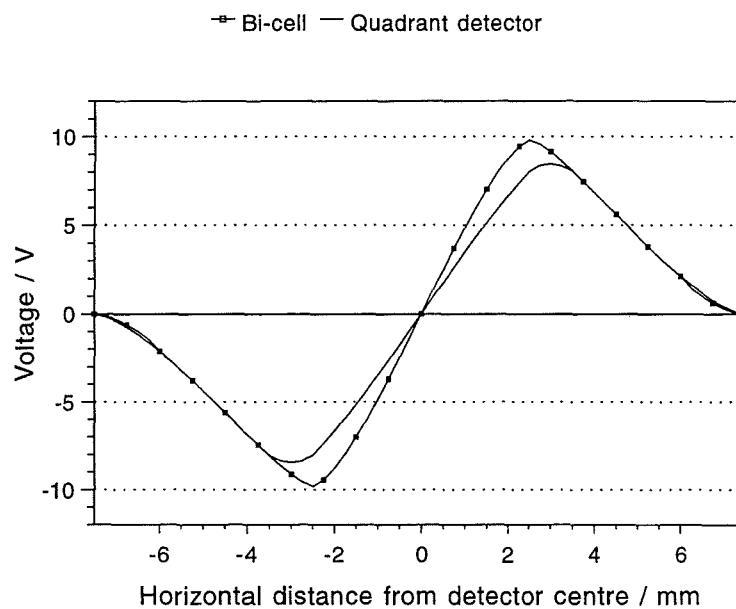


Figure 5.17 - Theoretical quadrant detector and bi-cell performance

The bi-cell configuration produced only a slightly smaller proportionality range than the comparable quadrant detector. There is therefore little loss in performance when switching the beam trackers from single to dual-axis position detection. Theoretical performance can be compared with the experimentally obtained outputs by reference to figure 5.18 : the experimental results matching closely those calculated showing that both the quadrant and bi-cell configurations function as predicted.

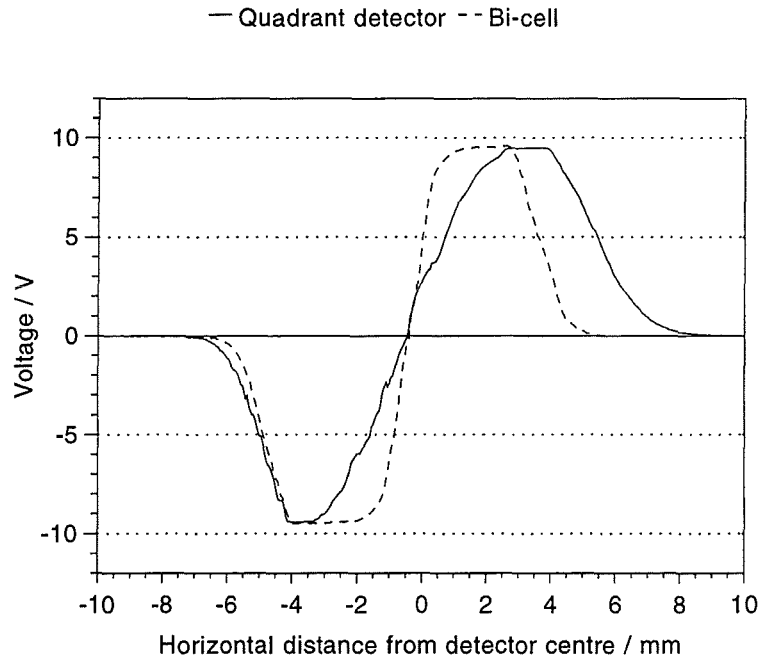


Figure 5.18 - Recorded quadrant detector and bi-cell outputs

Summary

The performance of the miniaturised dual-axis beam tracker under varying incident light parameters has been described. Tests were conducted on a purpose built rig to enable experimental and simulated behaviour to be compared. Beam tracker output under varying light source distance, intensity, spot shape and spot intensity profile were investigated.

- *Light source distance.* - This was shown to have little effect on beam tracker performance as, with the collimated laser light source, no variation in intensity or spot size was observed over distances up to 5 m.

- *Light intensity.* - Direct exposure to the laser caused saturation of individual photodiodes. A filter noticeably reduced this effect yet, for operational purposes, saturation at distances close to the quadrant detector perimeter was found to be advantageous.
- *Spot shape.* - Shape had a direct effect on the extent of linear response about the centre of the quadrant detector. Theoretically a square spot shape produces the most linear output. The light source initially used produced a oval spot, giving different output profiles for horizontal and vertical scans. This was replaced by a focusable laser which gave a circular spot, the output profile closely matching that of the theoretical ideal.
- *Spot intensity profile.* - A spot with a symmetrical intensity profile about its centre is required for most accurate position detection, this is difficult to achieve in practice as the laser collimating lenses cause spot intensity variations. Electronics can be used to determine the centroid of the spot (see Chapter 4, figure 4.16), thus accommodating for these variations. For operational purposes, due to the consistency of the spot profile, good performance was found when this additional circuitry was not included. A diffusion screen, placed in front of the detector, reduced intensity variations and light scattering from the detector glass window.

In conclusion, a focusable laser diode producing a 5 mm ϕ circular spot was shown to be the optimum light source for the photodiode quadrant detector based beam tracking systems. The original 1 mW source was too powerful as it caused excessive photodiode saturation. Its effective power was attenuated using a No 1 neutral density filter. A diffusing screen produced a considerable increase in performance by improving the uniformity of the spot intensity profile. Suggestions for beam tracker performance enhancement are given in Chapter 8.

In the next chapter, the performances of the initial and improved robot variants operating under a series of control algorithms are given. The chapter begins with results obtained for the 'proof of concept' robot operating with the linescan camera, leading to an in-depth analysis of the functioning of the dual-axis robot with miniaturised beam tracker.

References

Editor, (1993) 'Photodiodes catalogue', Hamamatsu Photonics.

Editor, (1980) 'Laser measurement system 5526A - users guide', Hewlett Packard company, 5305 Stevens Creek Blvd, Santa Clara, Calif.95050, October 1980, Part No. 05526-90066.

Korhonen, J., (1995) 'The control and testing of a laser guided robot arm', MSc project, Middlesex University, MSc Applied Computing Technology, Computers in Industry, July 1995.

Petit, B., (1994) 'The analysis, development and testing of aspects of a laser guided robot control system', BSc Industrial Engineering - Nuclear Option, Institute Gramme Liege, Belgium. ERASMUS exchange programme, Middlesex University project report - 1994.

Chapter 6

CONTROL METHODS AND RESULTS

6.1 INTRODUCTION

This chapter describes the operation of the 'slave' position control system, the purpose of which is to cause the arm tip sensor to centre upon the laser spot so minimising tip steady state errors. Laser beam positioning is controlled by the 'master' position controller, as described in Chapter 3. The slave system minimises steady state tip position error whether it is created by movement of the laser beam or by arm deflection.

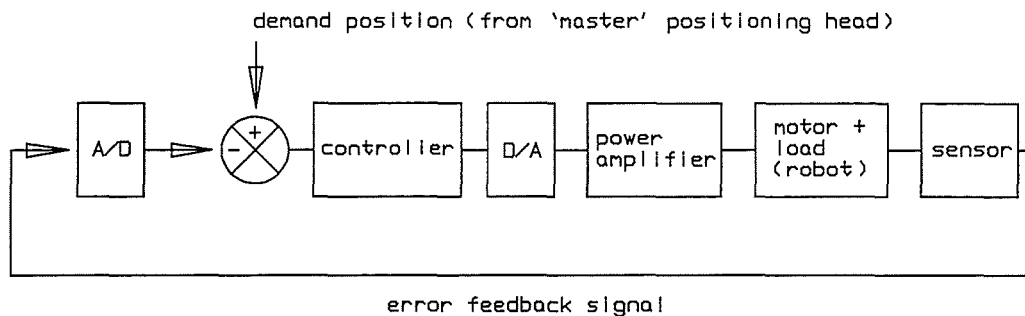


Figure 6.1 - Generalised block diagram of the slave control system

The chapter is divided into three sections: the first describes the performance of the 'proof of concept' prototype robot, the second the improved single-axis version and the third the dual-axis robot. For each case the applied slave control algorithms and operational results are given. The results show that the control strategy is efficient in controlling the steady state tip position of a 1 m flexible arm under a range of load conditions.

6.2 THE 'PROOF OF CONCEPT' ROBOT

The single-axis prototype robot used a modified linescan camera (see Chapter 4, Section 4.4) as an end-point position sensor. The camera signals were fed to a computer via an I/O card. The processed output position error signal, ranging from ± 10 V, was then fed through a power amplifier to the arm linear actuator.

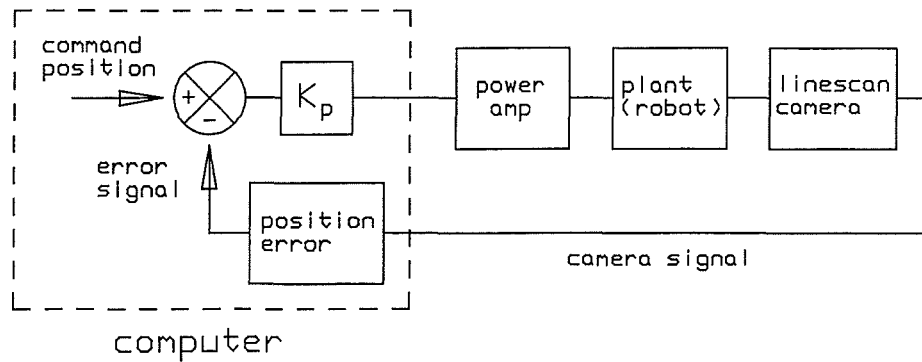


Figure 6.2 - Proportional position control with linescan camera sensor

The linescan camera output a signal from which end-point position error was determined. This was achieved through computation of both the distance and direction of the illuminated photosite from the centre of the camera array, i.e from the 'fixed' demand position : the central photosite No.128. The arm tip was at the desired position when the central photosite was centred upon the laser spot.

The camera signal processing algorithm was initially written in 'C' code (Holtzer, 1991) but found to be too slow to give a fast output response to variations in the input signal. The speed of error calculation was increased three-fold by reducing code length and translating much of it into nested turbo assembler (see Appendix C).

A simple proportional system was used to control arm movement, the control signal being directly proportional to the position error signal e :

$$e = (\theta_d - \theta) \quad (6.1)$$

where θ_d was the desired angular position (the set point as defined by the laser positioning head) and θ was the actual arm end-point position as detected by the linescan camera. The control signal can then be expressed as :-

$$\text{Control signal} = k_p \cdot e \quad (6.2)$$

where k_p is a proportionality constant. In operation, the proportionality constant was changed by adjusting the gain of the actuator power amplifier.

6.2.1 Robot Performance

Results are presented under two headings, each designed to test a specific aspect of the control concept, namely : tip deflection compensation and laser tracking.

Deflection compensation

The ability of the system to correct for positioning errors caused through load-induced arm bending was demonstrated by adding a loads to the arm tip and recording the position error signal from the camera as deflection compensation took place.

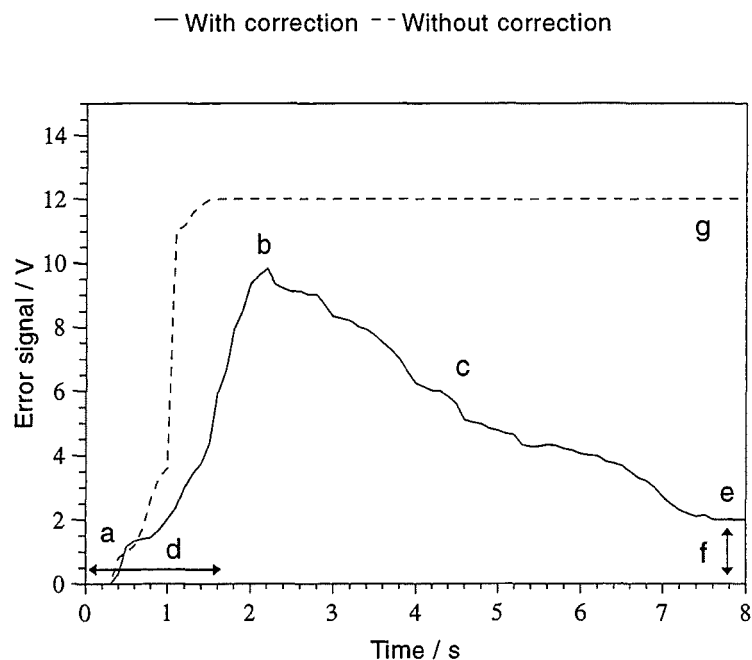


Figure 6.3 - Errors recorded on the addition of a 0.5 kg load to the tip of the stationary arm

Figure 6.3 shows that, from its stationary, unloaded position (a) the arm was deflected rapidly by the addition of the load (b) such that the tip was displaced downwards through a distance of 13 mm. The actuator responded and raised the arm to compensate for the load deflection (c). (d) is measure of the system response time : the time that elapsed between the addition of the load and the actuator beginning to respond (1.3 s). At (e) compensation was complete and the actuator was again at rest. (f) is a measure of the

steady state error, i.e. the error that exists between the original and final arm positions (see table 6.1). Adding loads to the arm produced a greater steady state error than is found when the arm was unloaded due to the requirement for a sufficient holding torque to hold the arm stationary against the force of gravity. (g) was the error signal produced with no load compensation, being equivalent to a vertical tip displacement of 15.6 mm.

The speed at which the arm corrected for load-induced deflections was found to be independent of the load applied. The size of the load had no effect on the speed of recovery of the arm as a proportional type of feedback system was used. The behaviour of the above system is analogous to that of a simple pendulum in that the size of the correcting force is directly proportional to the displacement of the laser spot from the central photosite : the tip displacement sensor acting as a force sensor. The recovery rate remained constant at 2.5 s for loads ranging from 0.5-2.5 kg.

Table 6.1

Steady state errors for deflection compensation		
	Maximum	Steady state
Control signal / V	10	2.00
Error at hub / degrees	0.74	0.15
Tip displacement / mm	13	2.6

Laser tracking

The ability of the arm to track the laser was demonstrated by recording the control signal as the 1 m long arm followed the laser beam. Slow and fast tracking (at a laser angle change of 15°/s and 30°/s respectively) are compared in figure 6.4 and table 6.2.

(a) The arm was initially stationary. The laser motor was turned on at $t = 1$ s (b). The error increased until sufficient voltage was supplied to the actuator to overcome stiction, the required voltage only being produced when the laser beam had moved a significant

distance from the centre of the array - i.e when the error signal was large enough. The delay before the arm moved was, in part, due to the time taken for the bending wave to propagate along the length of the arm (0.2 s). The arm began to track the laser spot (c). Nearly constant error signals were recorded (4 V for slow, 6 V for fast tracking), the arm lagging behind the moving laser. The laser drive motor was turned off at (d), the laser was again stationary (e) and the arm had caught up with the beam.

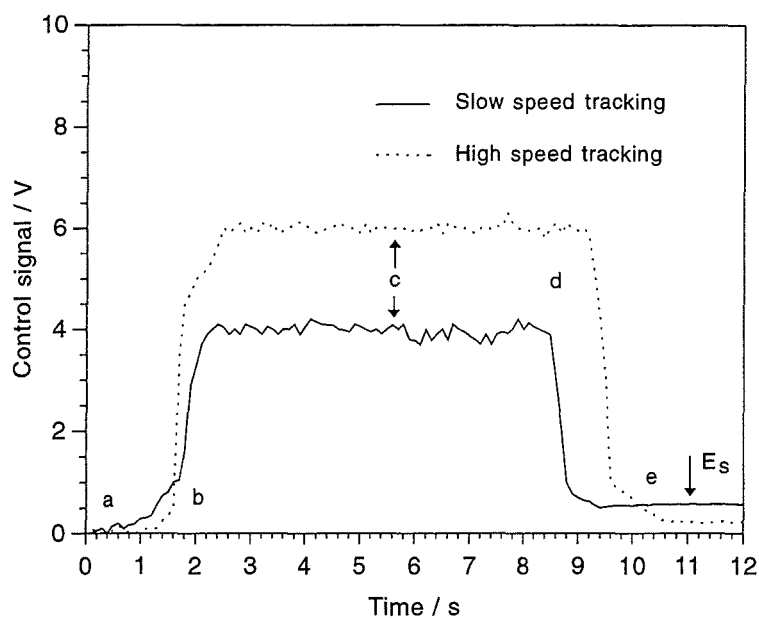


Figure 6.4 - The error signal for low and high speed beam tracking

At low speeds the arm followed the laser beam in an erratic manner, due to actuator friction. At fast speed the arm moved more smoothly. The maximum speed at which the arm was able to track the laser was 5 cm/s (measured as vertical movement at the tip). If the speed of the laser was increased further, arm control was lost as the laser no longer impinged upon the photosite array. It was found necessary to increase the speed gradually from rest to allow time (3 s) for the actuator speed to build up - the speed of response and sensitivity of the actuator determining the maximum rate of arm movement. The lag of the arm behind the moving laser depended on the speed laser rotation : the faster the laser movement the greater the lag. As the laser was started from rest the lag built up until an equilibrium was established between the error signal level and the rate of arm travel. Only as the laser was brought to rest did the arm re-centre upon the beam so reducing the position error.

Table 6.2

Tracking and steady state errors for slow/fast laser movement			
		Maximum	Steady state
Slow tracking	Control signal / V	4.10	0.57
	Error at hub / degrees	0.30	0.04
	Tip displacement / mm	5.33	0.74
Fast tracking	Control signal / V	6.03	0.22
	Error at hub / degrees	0.45	0.02
	Tip displacement / mm	7.84	0.29

Static positioning accuracy, as measured by the steady state error, depended upon the rate of arm travel. Fast arm travel with sudden deceleration produced the best positioning accuracy (0.29 mm) - the inertia of the arm overcoming the actuator friction. A worse positioning accuracy was recorded for slow arm travel (0.74 mm), friction having a significant effect at slow actuator speeds.

6.2.2 Performance Analysis

The results demonstrate that direct tip control of long reach arms is a viable proposition using the novel control strategy. The arm is shown both to track the laser beam, using end-point optical position detection, with the controller simultaneously correcting for arm deflections. The results shown have also highlighted limitations and weaknesses within the physical and control systems used.

- Poor actuator power and responsiveness

The inability of the arm to track the laser accurately, as evident in an average lag of the tip behind the travelling laser of 7.84 mm, was caused by a combination of poor actuator performance and the purely proportional nature of the control system employed.

Static actuator friction required that a minimum control voltage of ± 3 V was applied across the actuator before it would move, this was equivalent to a position error at the arm tip of ± 3.9 mm. This problem was exacerbated by the weight of the linescan camera (4.47 N) at the arm tip, adding to the required actuating effort. The maximum speed at which the actuator was able to move the arm (50 mm/s at the tip) proved to be another limiting factor; when operating at full speed, the actuator was unable to match the speed of arm movement to that of the laser.

- The applied control method

Limitations imposed by using proportional control are shown in both the tracking response (the difference between the actual and demand tip positions while the arm was in motion) and the steady state response. The steady state error for fast tracking (0.29 mm for the case shown) was always considerably less than that recorded for slow tracking (0.74 mm) as the faster actuator speed gave enough increase in momentum, to the arm system, to overcome the near-zero voltage input as the arm approached the demand position. Increasing the amplifier gain reduced the steady state error and the tracking lag. As the system was naturally highly damped a gain of 26-29.5 dB was acceptable before overshoot and tip oscillations became a problem.

- The speed of feedback computation

The maximum speed of control updates (50 ms) was limited by the relatively slow 12 MHz computer. The computer was used to determine the tip position error from the camera signal prior to calculating the control output. The maximum camera array scanning rate was 0.1 ms.

To alleviate many of these problems, the physical system was changed considerably through the addition of a more powerful and responsive linear actuator (Absbac model ELM 5012) operating through a combined voltage/current controlled amplifier. A new beam tracking system was developed in which the position error signal was determined directly through hardware. These improvements enabled the behaviour of the robot under a range of control algorithms to be explored, with the aim being to reduce steady state errors and improve the tracking ability of the arm.

6.3 THE IMPROVED SINGLE-AXIS ROBOT

The beam tracker (described in Chapter 4, Section 4.5) performed a dual function: it sensed the laser spot position and, through built-in electronics, gave both the magnitude and direction of the spot displacement from the centre of the sensor. It therefore produced a real-time position error signal, so relieving the computer of the task of calculating the error signal.

6.3.1 Direct Analogue Proportional Control

The beam tracker enabled experimental implementation of direct *analogue* proportional control : the output signal was input directly into the actuator power amplifier as shown in figure 6.5.

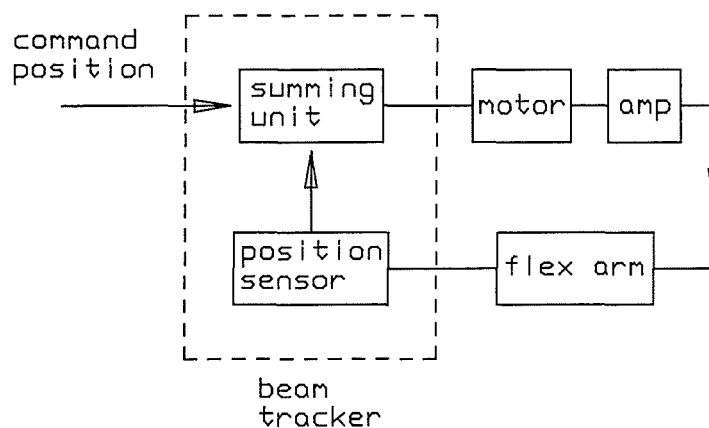


Figure 6.5 - Direct analogue proportional control through the new beam tracker

Experiments were conducted on a 2.5 m long arm to measure tip positioning accuracy under different load conditions with the beam tracker illuminated by a 7.5 mm ϕ light spot. Tip deflection was measured for both static and tracking tests using a dial test indicator suspended above the tip of the arm. For tracking, the DC motor driven positioning head was set to move the laser from the horizontal through to a pre-defined stop at the end of a 45° vertical arc. The speed of tip travel was 150 mm/s.

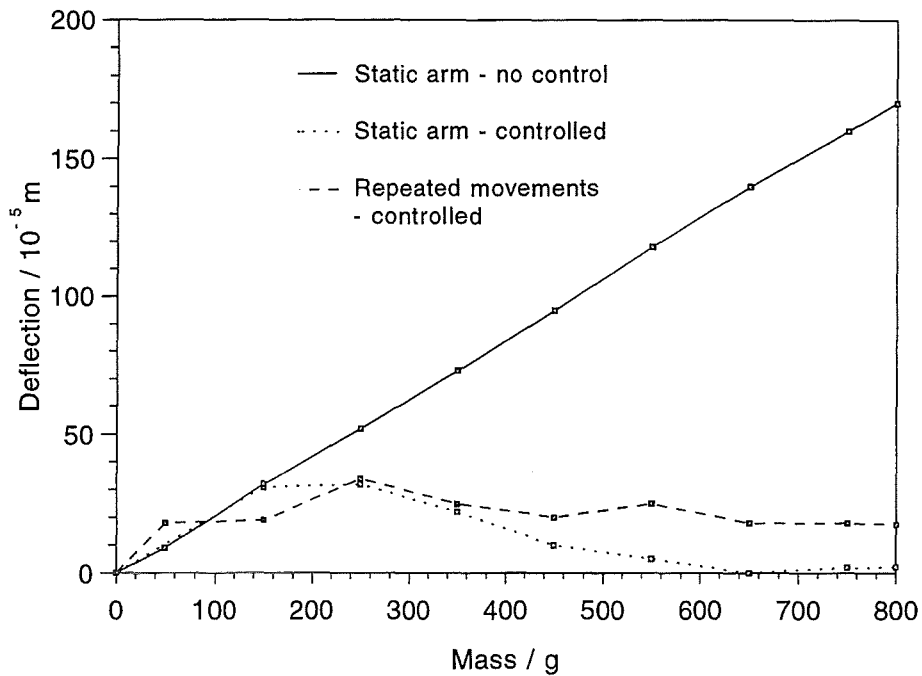


Figure 6.6 - Accuracy tests with a 2.5 m arm under analogue proportional control

From figure 6.6 it can be seen that, without control, tip deflection increased linearly with the applied load. Under control, but without tracking, the arm deflected downwards through a distance of 0.35 mm (equivalent to a 2.5 N load) before the error signal from the beam tracker was sufficient (2.25 V) to cause the actuator to respond. The addition of more weight produced a reduction rather than increase in positioning error since, as the tip deflection increased, so did the sensed position error - this in turn provided an increased voltage to the actuator. For the controlled static and tracking tests, the maximum steady state errors were 0.2 and 0.25 mm respectively.

Even solely with proportional arm control, high positioning accuracy was achieved as tracking and steady state errors were controlled to within the deflection range sensed by the beam tracker, as determined by its characteristics.

These results show an increase in performance, obtained with the new beam tracker and actuator, over the prototype in terms of tracking speed and reduced steady state error. On the prototype, steady state errors of up to 0.74 mm were recorded on a 1 m unloaded arm compared with 0.2 mm on the improved robot with a 2.5 m arm.

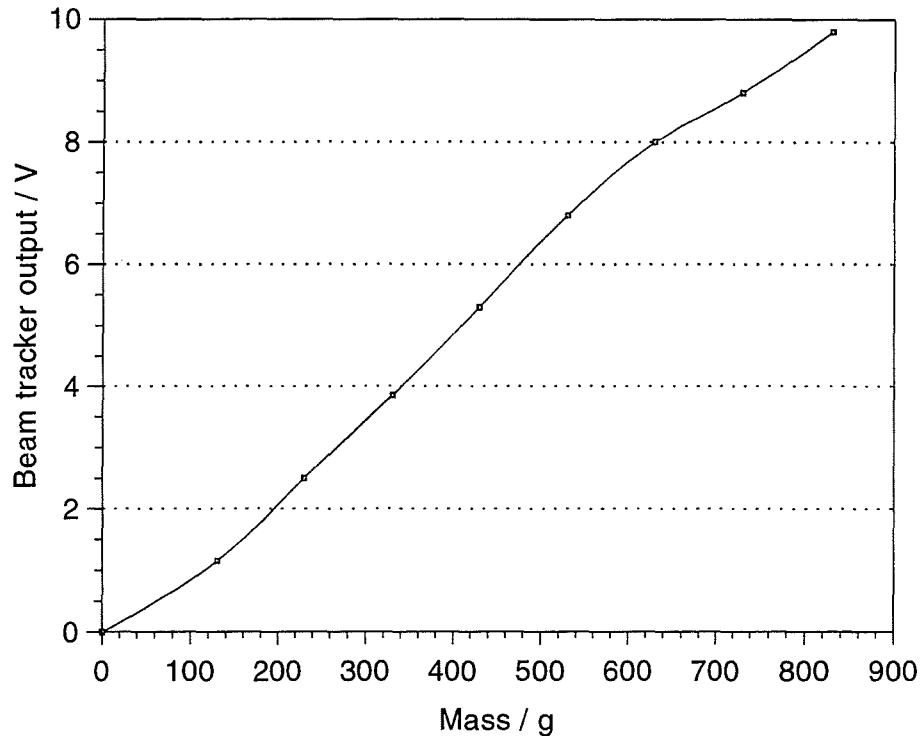


Figure 6.7 - Beam tracker output versus load for the uncontrolled arm

From figure 6.6 it can be seen that a mass of 800 g caused a tip deflection of 1.7 mm and, from figure 6.7, a corresponding 9.45 V beam tracker output when illuminated by the 7.5 mm ϕ light spot. This equates to an error signal of 5.6 V/mm displacement, which is in agreement with the results given in Chapter 5, section 5.3.5 for a spot of similar diameter, shape and intensity.

A major drawback of this direct control method was that the maximum speed of arm movement was 150 mm/s measured at the tip. For faster tracking speeds, proportional control gave poor performance as the unloaded arm overshoot and oscillated about the demand position, even at k_p values as low as 0.3. More sophisticated control methods were therefore required so that faster, yet stable, tip response could be achieved.

Algorithms with damping terms were implemented in software in an attempt to reduce tip oscillations. Those tested were proportional-integral-derivative (PID) and proportional-derivative (PD). The block diagram in figure 6.8 shows the modified setup.

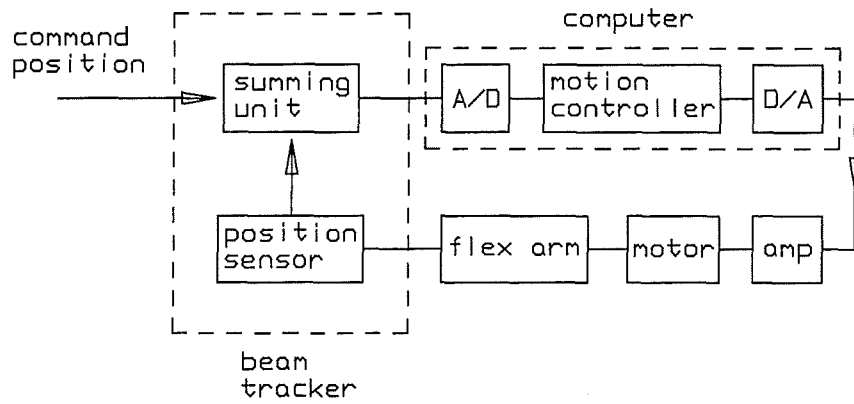


Figure 6.8 - Block diagram of the modified robot position control system

6.3.2 PD Control

With small friction and high inertia, the arm under proportional control tended to overshoot as it had nothing but its own friction to stop its movement. To eliminate overshoot, the drive torque can be made proportional to the derivative (rate of change) of the error, e , with respect to time :

$$T = k_p e + k_d \dot{e} \quad (6.3)$$

Equation 6.10 defines the evaluation of the derivative term.

Although the positional error decreases as the inflection point is neared, the derivative term is negative, having a maximum value as the error passes through the inflection point (N-Nagy and Siegler, 1986). The output torque will therefore reverse before output alignment occurs and effectively act as a brake which greatly reduces the transient. In qualitative terms, derivative control can be applied to control the slope of the position response, thus damping oscillations and reducing overshoot. The ability of this controller to handle overshoot depends upon the controller gains k_p and k_d , and the inertia and friction of the load. Increasing k_d is equivalent to increasing the friction (damping). Figure 6.9 shows the control scheme obtained if the derivative error is used instead :-

$$\text{Control signal} = k_d \frac{de}{dt} + k_p e \quad (6.4)$$

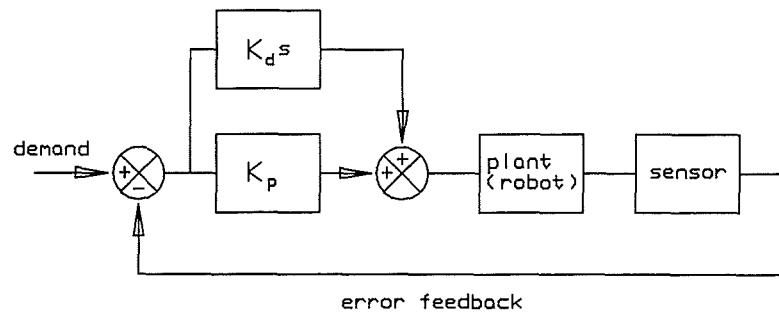


Figure 6.9 - PD control

Digital implementation of PD control in its simplest form is done by representing the rate of change of error by the difference of two sequentially sampled errors, scaled by the time interval, T , to repeat the control evaluations. The control derivative can also be calculated from a combination of several sampled errors, which have different weights. This method reduces the effect of noise in the error signal but reduces the instantaneousness of the derivative. Though noise was apparent in the error signals, best results were found with the simplest method. In digital implementation the PD signal becomes :-

$$\text{Control signal} = k_p e_0 + k_d (e_0 - e_1) / T \quad (6.5)$$

where k_p and k_d are weighting multipliers, e_0 the most recent and e_1 the previous error.

6.3.3 PID Control

A PID controller combines proportional, integral and derivative of error feedback : signals corresponding to the derivative and integral of the position error, are superimposed on the proportional error signal. The three parts composing the PID can control movement, steady state error and overshoot (De Schutter and Van Brussel, 1992; Fu *et al*, 1987). The overall expression for a PID control action can be represented as :-

$$u(t) = k_p e(t) + k_i \int e(t) dt + k_d \frac{de}{dt} \quad (6.6)$$

For digital implementation, the algorithm must be adapted for discrete time data sampling. If the sampling time is short (i.e. the sampling frequency > 20 times the highest frequency in the monitored signal), approximation methods may be applied without any appreciable loss in precision.

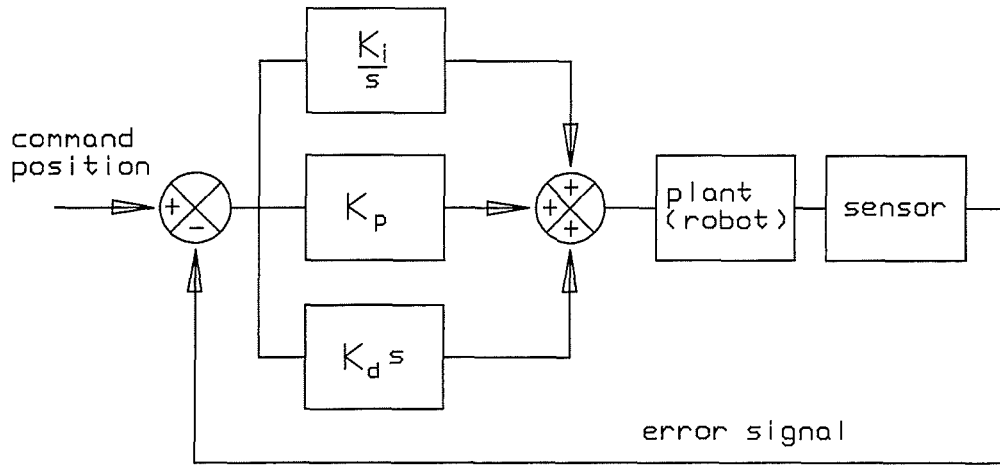


Figure 6.10 - PID control

The integration and the differentiation are performed by numerical approximation. If the sample time is kept constant in its simplest form, the integral may be represented as a sum and the derivative as a difference. The integral term becomes :-

$$f_i = \int e(t)dt \approx \sum_k e(k)\Delta T \quad (6.7)$$

and the derivative term becomes :-

$$f_d = de(t)/dt \approx [e(k) - e(k-1)]/\Delta T \quad (6.8)$$

However better approximations can be used if required; a trapezoidal approximation is used in the program for the integral action and the derivative action was replaced with one obtained from a four-point central difference technique (Korhonen, 1995). The integral term became :-

$$f_i(k) = f_i(k - 1) + \left[\frac{e(k) + e(k - 1)}{2\Delta T} \right] \quad (6.9)$$

and the derivative term :-

$$f_d(k) = [e(k) + 3e(k-1) - 3e(k-2) - e(k-3)]/6\Delta T \quad (6.10)$$

PID control trades off the possibility of overshoot against the speed of joint motion. Increasing k_d tends to slow the arm down since it increases the negative contribution to the torque due to velocity. Decreasing k_d decreases the damping of the system, thus increasing the likelihood of overshoot. Control gains were chosen by empirical methods,

yet with this three-term controller no ideal solutions could be found. Firstly critical damping can be obtained with an infinite number of values of k_p and k_d . Secondly as the arm angle was changed, the dependence of the solution on values of J (system inertia) and F (system friction) must be accounted for. The PID controller torque can be equated to the mechanical torque applied through the actuator :-

$$T = J\ddot{\theta} + F\dot{\theta} \quad (6.11)$$

A differential equation can be developed to characterise the performance (Snyder, 1985). Best choice of k_p , k_i and k_d can then be made for *specific* values of the loads J and F. Yet, as both J and F change rapidly in practice this simple optimisation technique fails. Control gains were therefore chosen through experimental observation of the robot behaviour.

6.4 THE IMPROVED PROTOTYPE - PERFORMANCE

Performance was measured as the ability of the computer generated actuator control signal to match the demand as sensed by the tip position sensor.

6.4.1 PID Performance

PID controllers are expected to give good performance when the position sensor is collocated with the arm actuator. In contrast, poor performance is expected when the sensor and actuator are separated by a large distance - as in this case. Under PID control the robot performed poorly, which agrees with the observations made by Swevers *et al* (1992). Problems were found in choosing the optimum gains to ensure stability. Figures 6.11 and 6.12 show the beam tracker and PID control algorithm outputs in response to a 0.5 Hz sine wave input to the positioning head drive motor. As shown in figure 6.11, increasing the damping, k_d , produce sluggish performance, increasing the integral gain, k_i , made the instability worse.

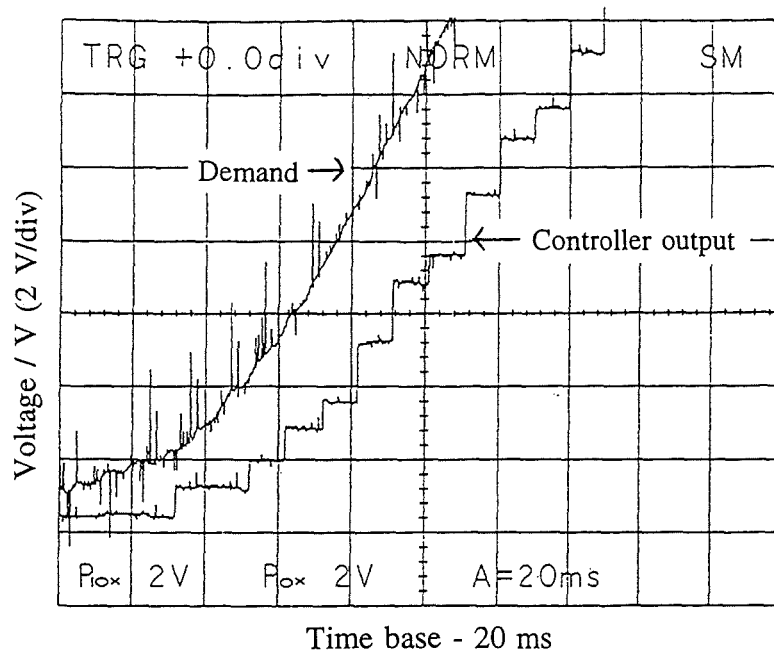


Figure 6.11 - PID controller performance showing the lag of the control signal (stepped line) behind the demand signal at high k_d values

Better behaviour was expected by the use of a more accurate approximation of the integral and derivative terms, so an attempt was made to speed up the computation rate of each and the signal sampling rate by using the DMA (Direct Memory Access) feature of the I/O board. Due to parity error problems and poor synchronisation between the computer and I/O board clocks, little improvement could be obtained.

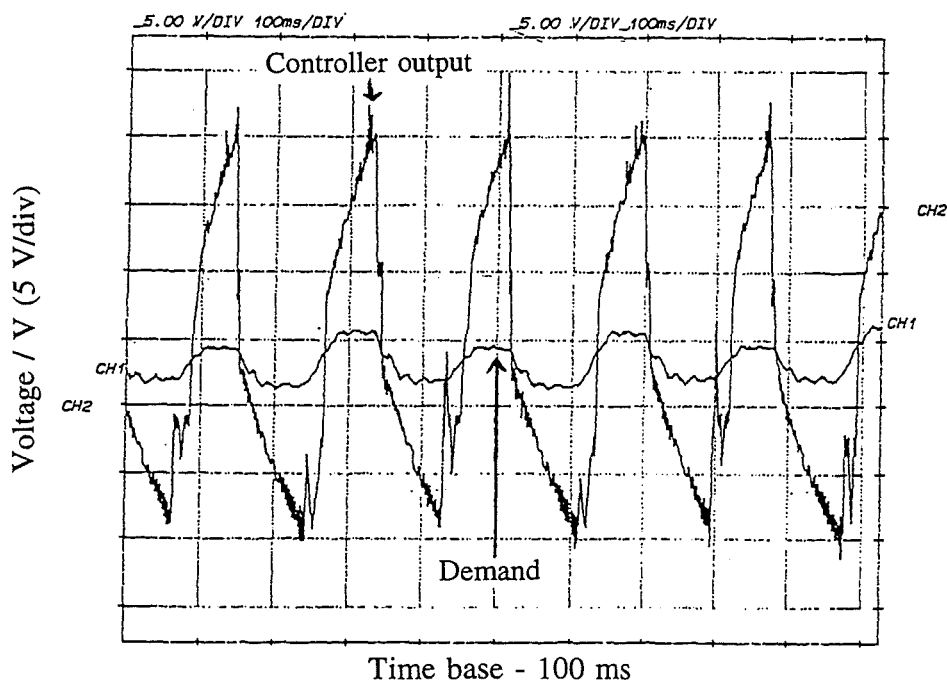


Figure 6.12 - PID controller-induced arm oscillation at high k_i values

At high k_i values the system is unstable, the PID output behaving erratically with random arm oscillations being induced in response to a regular input signal.

In general PID control showed poor performance. The integration time, represented by the number of samples in the integrative sum and the weight of the integral multiplying parameter, had to be reduced to near-zero to produce a system that did not oscillate uncontrollably. The integral parameter caused an increase in computation time which created a severe control lag and increased the response time of the system - in practice the PID system became an over-damped PD controller.

6.4.2 PD Performance

This controller offered good performance. As the following figures show, the output to the actuator followed closely the input from the beam tracker - no oscillations were present and motion-induced arm vibrations could be controlled. The results clearly show the improvement in performance over PID control.

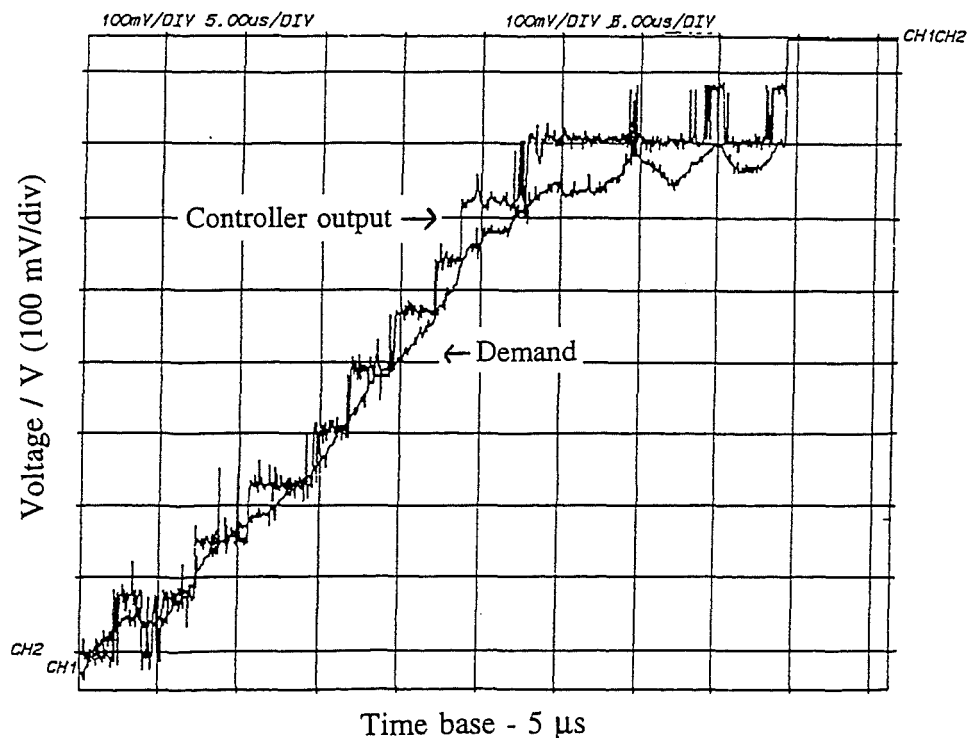


Figure 6.13 - PD control - the control signal following the demand to ± 50 mV

Figure 6.14 shows that a small steady state error was recorded (< 50 mV or 0.01 mm). This equates to an angular error of 0.003° as measured at the arm hub, showing the ability of the tip positioning system to control steady state arm positioning accurately.

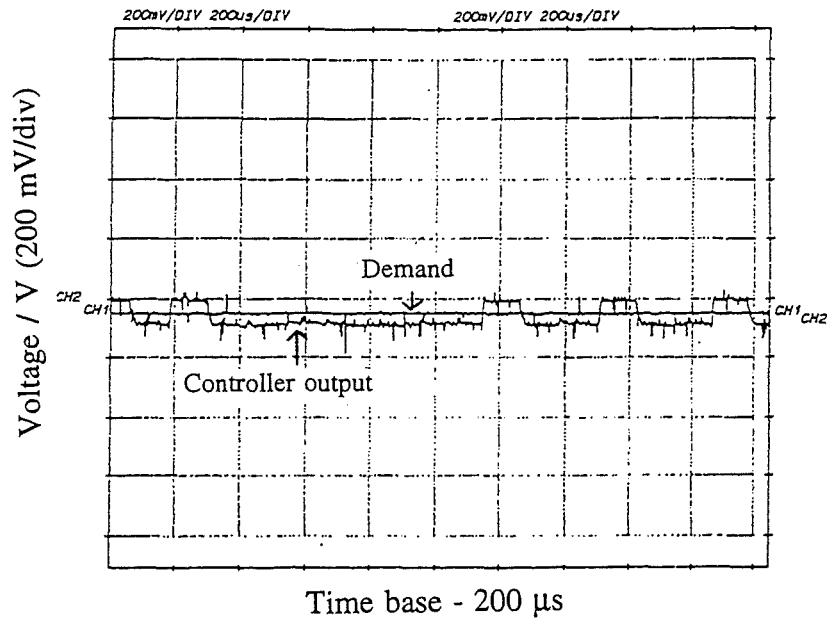


Figure 6.14 - Steady state error recorded at arm tip for PD control

6.4.3 A Comparison of PID and PD Tracking Performance

PID and PD controls were tested under similar conditions (2 m arm, $k_p = 0.3$, $k_d = 0.3$, $k_i = 0.025$), with the robot arm moving steadily upwards at a tip speed of 15 cm/s. The PID response is unstable with dramatic overshoot which increases arm oscillations.

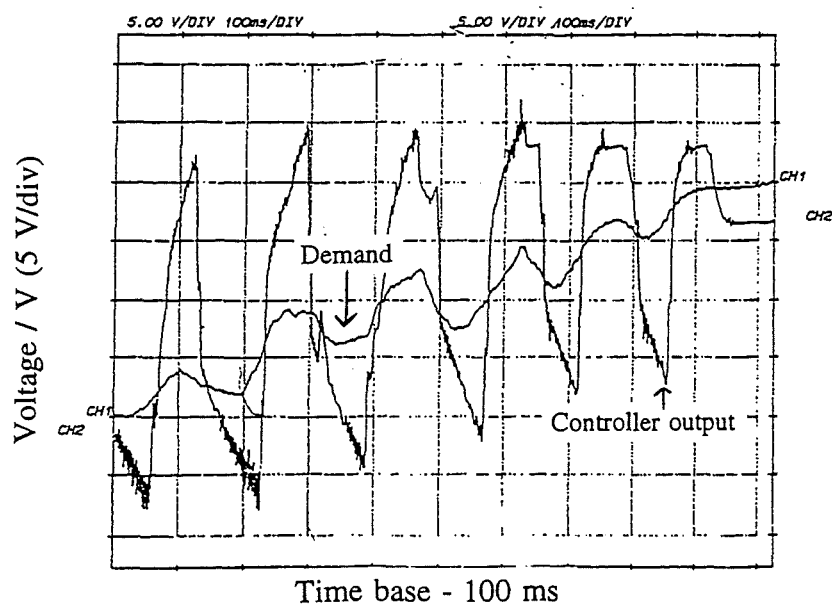


Figure 6.15 - Unstable PID control response - arm tracking the moving laser

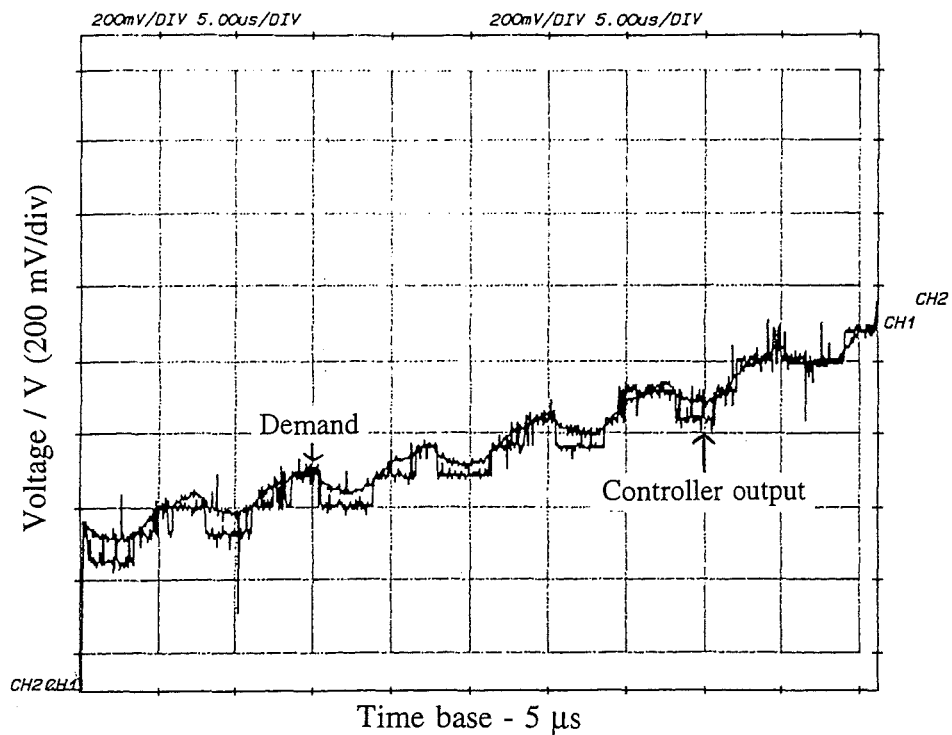


Figure 6.16 - PD control

With PD control, the control signal closely follows the demand.

6.4.4 The Improved Robot - Summary

Of the control algorithms tested, PD control gave the best performance - the additional derivative term producing the required damping at the tip for high speed motion. With PID control, the inclusion of even a minor integral influence caused the behaviour to degrade to the extent that oscillations were induced at the tip and arm movement became sluggish with noticeable trailing lag being introduced. These problems may be partly attributed to the decrease in sampling rate caused by the time-consuming integral calculations. Removal of the integral term altogether (i.e. the conversion of the algorithm from PID to PD) had little effect on the steady state error since the arm tip position error was measured directly at the tip by the beam tracker sensor where, for the specific light spot used, the maximum steady state error could be ± 1.8 mm. On average, steady state errors of less than 0.2 mm were recorded.

This version of the robot allowed for a better study of controller performance but suffered from excessively slow actuator response. As movement was restricted to the vertical direction, the dual-axis functioning of the beam tracker could not be tested. To overcome these limitations, a dual-axis robot with high performance actuation was constructed.

6.5 THE DUAL-AXIS ROBOT

Traditional testing methods examine a system's response to a step or constant velocity reference. When high inertia loads are manipulated, such tests give little idea of the true behaviour of the system unless the actuators are responsive enough to enable the robot to operate at high torques. The robot actuators were therefore replaced by high performance servo actuators, the closed loop bandwidth of the motors was 111 Hz, the time constant was 9 ms (see Chapter 3, Section 3.3).

For comparison of control types, two performance specifications were set.

1. End-point overshoot should not be greater than ± 2 mm.

Overshoot to within ± 2 mm equates to a ± 10 V output signal from the beam tracker with a 5 mm ϕ spot, i.e. the spot displacement limit from the centre of the detector before sensor saturation occurs (see Chapter 5, figure 5.4).

2. Steady state error should not exceed ± 0.1 mm.

The limit of ± 0.1 mm for steady state error reflects the resolution of the motor encoders with 100:1 gearboxes (± 0.07 mm). This equates to a ± 0.5 V position error sensed by the beam tracker at the arm tip.

6.5.1 Control System Hardware

For operation, the servo motors required a drive controller card (Harmonic Drive model HDEC-ES-D). The controller was programmable through its MINT (BASIC related) programming language and has built-in functions for different motor movement controls. It was designed to use the servo motor optical encoders as sensors, control being through its embedded PID and other algorithms.

To have good response and to avoid restricting permissible gains requires short sampling times, a 486-SX25 PC was used to compute the control signals. The PC-30B I/O card

input function execution time averaged 2×10^{-3} s - equivalent to one tenth of the PD control loop time. Maximum throughput rate (30 kHz) could only be obtained if the Direct Memory Access feature was used. Its complex implementation was not justified as the DMA would not have saved time in the case of interrupted sampling (Korhonen, 1995).

During initial testing with the Harmonic Drive controller, the slave system processor computation speed was found to be too slow. The loop frequency for a simple two-axis PID algorithm (including A/D and D/A conversions) was only 20 Hz. The controller was obviously not designed for this kind of control task.

An attempt was then made to retain the controller so that the motors could be driven with constant torque. It was interposed between the PC and servo amplifiers, signal input being through the analogue input ports. The controller digitised the signals and then applied its own proportional analogue control signals to the power amplifiers. Performance improvements were apparent, yet the controller created a delay which prolonged the system's response time excessively. In the final version, the Harmonic Drive controller was not used at all; the slave system control running on the PC alone.

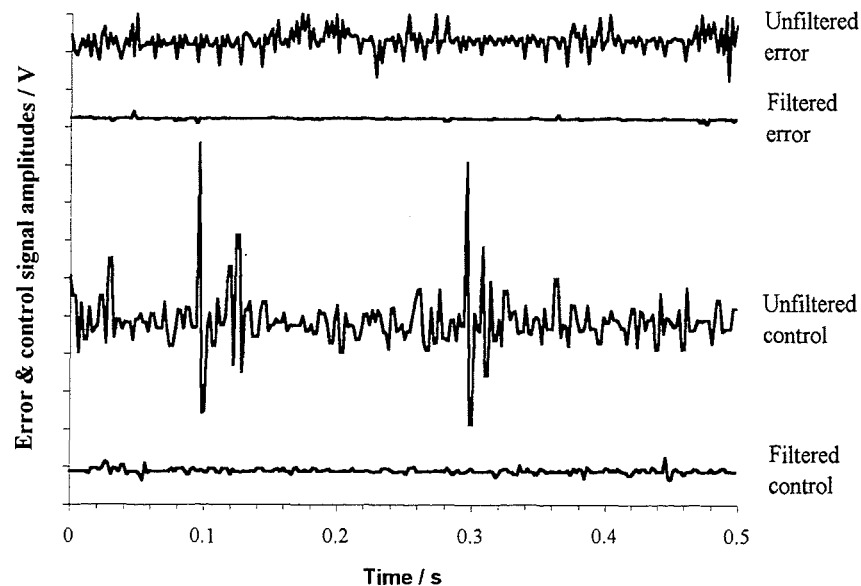


Figure 6.17 - Unfiltered and filtered error and control signals

The actuator PWM amplifiers introduced considerable noise into the beam tracker (error) signals (see figure 6.17). This noise was filtered out at the controller input using 30 Hz

passive low pass filters. The filters were built up from a 330Ω resistor and $100\ \mu\text{F}$ capacitor network, giving a time constant of $0.03\ \text{s}$. The upper limit of $30\ \text{Hz}$ was chosen following Shannon's sampling theorem (from Houpis and Lamont, 1985) such that the sampled signal frequency was at least twice that of the highest measured frequency of oscillation in the system under control; in this case the $14\ \text{Hz}$ natural frequency of the arm (see figure 6.30).

6.6 STEP RESPONSE TESTS

Tests were performed under a variety of algorithms - P, PD, PID and Pseudo-Derivative Feedback Control (PDF) to determine which produced best slave system response.

6.6.1 PDF Control

Pseudo-Derivative Feedback control (PDF) has been applied successfully to systems susceptible to random disturbances (White and Kelly, 1994) with the advantages that control loop time is decreased and overshoot is reduced. PDF control reduces vibration levels in comparison to other techniques and its performance compares well to controllers which use tip displacement or root bending moment feedback for single degree of freedom flexibilities (Phelan, 1977). In a PDF loop a simple integration is performed in the forward path, while the *effect of the differentiation* is carried out by the feedback without the necessity of a real-rate measuring sensor or numerical approximation.

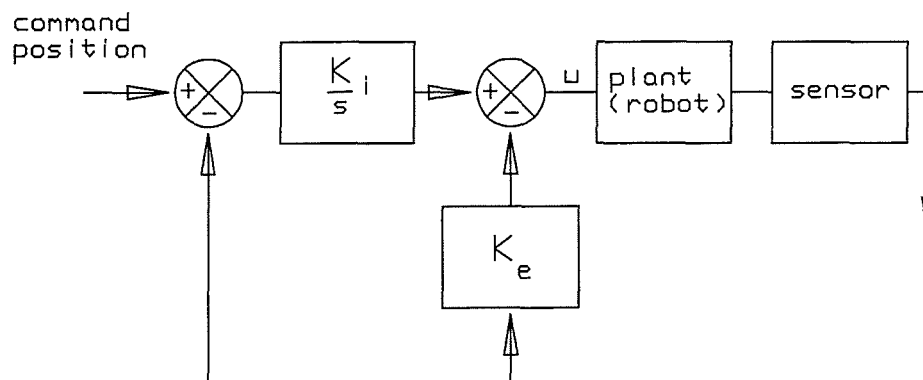


Figure 6.18 - PDF control

The PDF algorithm significantly resembles PD in terms of behaviour. Besides the proportional and derivative functions it has feedback of the control signal as a parameter. It provides an alternative method to integral control against steady state error. PDF, being a simpler algorithm than PID, is more suitable for fast digital implementation. PDF control systems are found to be advantageous when the ability to ignore loads is desirable. The pseudo derivative effect is created by subtracting the present error from the integral of the error.

The signal in a continuous system is :-

$$u(t) = k_i \int_{t_0}^{t_1} e(dt) - k_e e \quad (6.12)$$

and in digital implementation :-

$$u(nt) = k_i * (e_0 + e_1 + \dots + e_n) - k_e e_0 \quad (6.13)$$

where the error is taken to be equivalent to the beam tracker output signal.

6.6.2 Step Response - Implementation

The step response of a system is a standard measure that describes a system's performance. The swiftness of the response is measured by the rise time T_r from 10% to 90% of the final value. The settling time is the time when the error transient fluctuation settles within $\pm 5\%$ of the step amplitude.

Two methods were devised for creating a fast step :-

- rapid laser rotation actuated through a linear solenoid,
- displacing the arm 2 mm vertically down from the laser beam set point on the beam tracker surface (equivalent to a -10 V beam tracker signal with the 5 mm ϕ spot) and starting the slave control abruptly.

The first method did not produce a satisfactory step as vibrations were set up in the positioning head (see figure 6.19). It was difficult to synchronise the starting of the

solenoid and slave systems, giving poor repeatability. The second method, adopted for all tests, produced the equivalent of an instantaneous step and enabled easy superimposition of results sets. Sampling was synchronised so that the results could be compared directly.

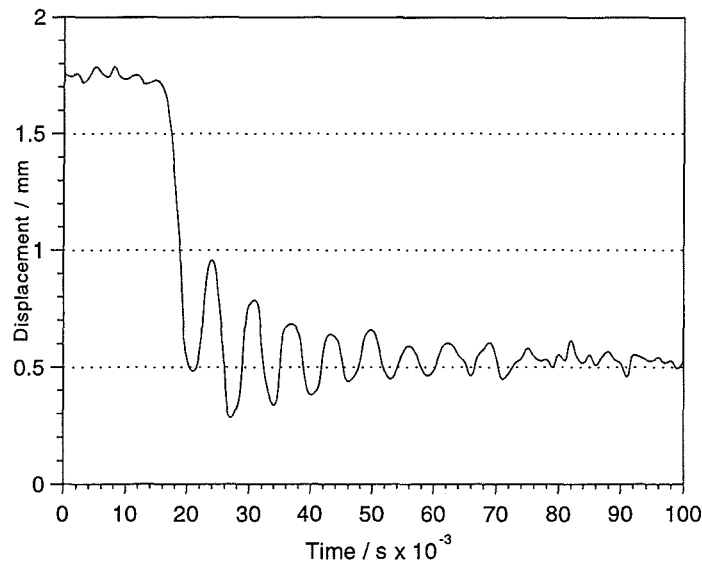


Figure 6.19 - Linear solenoid step showing excessive oscillations

Test conditions

Tests were carried out on an aluminium arm, the measured parameters for which were used by Surdhar (1995) for his simulation studies of the robot (see Section 6.6.3).

Table 6.3

Measured arm and actuator parameters - Pape (1995)				
Mass at tip / kg	Arm length / m	ρ / (kg/m ³)	J_m / (kgm ²)	$E \cdot I$ / (Nm ²)
0.1564	1.037	0.755	0.224	2.9×10^7

ρ , J_m , E and I are the mass per unit length of the arm, the moment of inertia of the motor and the product of Young's modulus and the axial moment of inertia of the arm respectively. Control gains were tuned experimentally to obtain the best step response, parameter values for each algorithm are listed in table 6.4.

Table 6.4

Control parameter values for step input tests			
	k_p	k_d	k_i
P	0.35	*	*
PD	0.55	0.4	*
PID	0.4	0.3	0.05
	k_e		k_i
PDF	0.2	*	0.3

The vertical actuator was not biased to counteract gravity effects as, to be effective at all angles of arm elevation, an adaptive bias system would have been needed. This would have unduly increased the complexity of the control algorithms and made interpretation of the arm response under a given controller more difficult. Loop times for all algorithms were set at 150 Hz to enable direct comparison between different algorithm performances.

Step response with proportional control

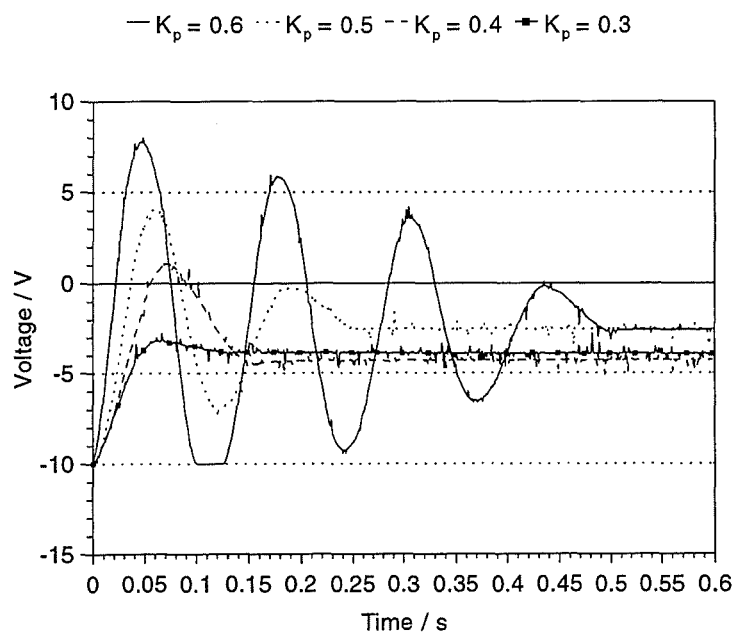


Figure 6.20 - Slave response to step input - proportional control

With proportional control the step response behaved as expected - the damping factor decreasing when the gain was increased. Figure 6.20 shows that the steady state error is large (-4 V at the beam tracker, equivalent to 0.8 mm steady state error at the tip) within the gain range that produced a stable response. Above $k_p = 0.6$, the rise time did not improve, only the settling time was extended and overshoot increased.

Step response with PD control

Adding derivative gain to the algorithm reduced the settling time without noticeably increasing the system response time. Proportional gain, k_p , could be increased from 0.3 to 0.55 producing a reduction in steady state error - the damping factor, k_d , reducing the tendency of the arm to overshoot and oscillate (see figure 6.21). Steady state error was still significant (- 1.5 V) as when both the error and arm velocity were small, the control signal was too small to produce actuator movement.

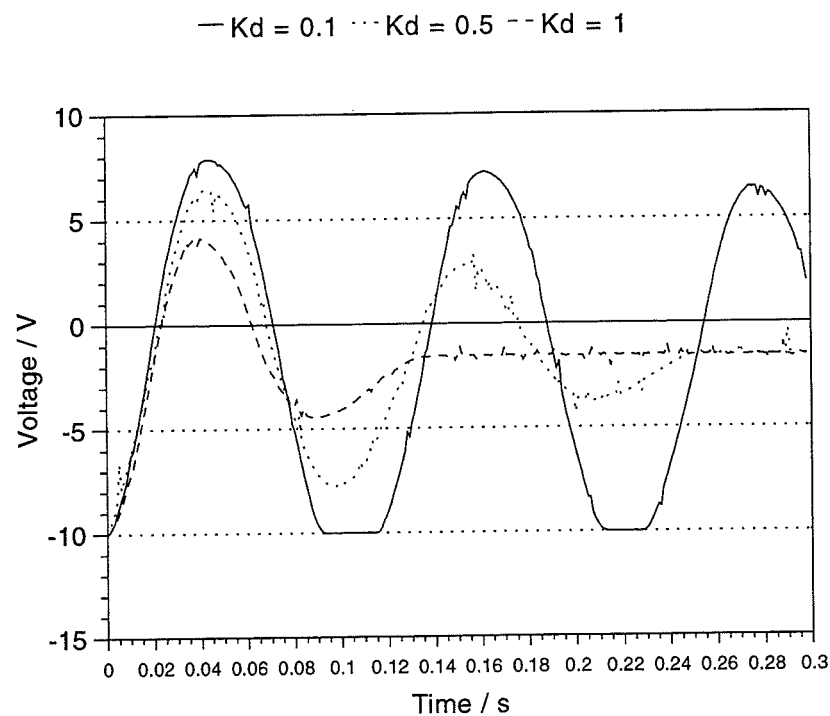


Figure 6.21 - Slave response to step input - PD control

Step response with PID and PDF controllers

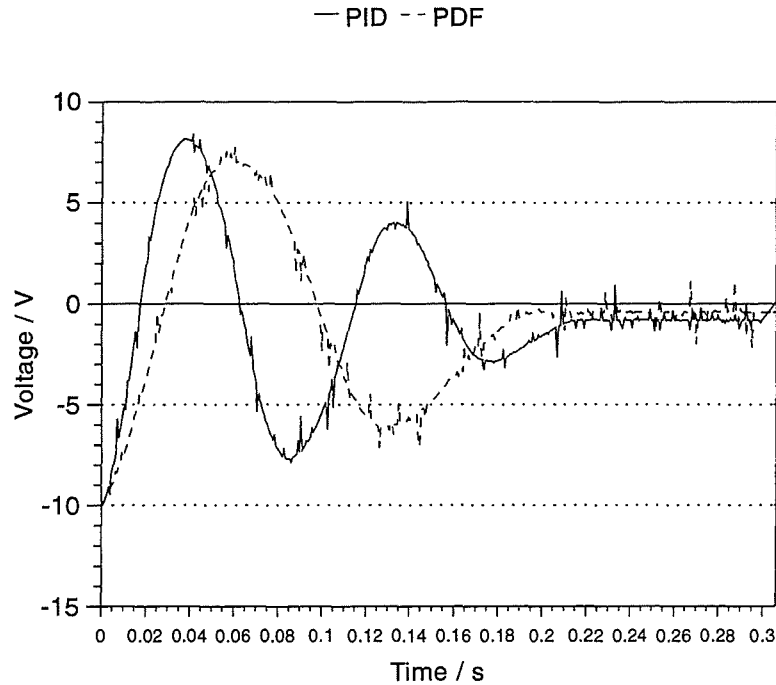


Figure 6.22 - Comparison of step response with PID and PDF control

PID and PDF control were expected to produce a reduction in steady state error, with PDF producing less overshoot. However, both produced severe oscillations in the arm, the integral term in each case introduced a response lag. Stable control was only achieved if the controller gains were reduced significantly, producing longer rise times than found with other algorithms. If the gains were reduced so that oscillation did not occur, the response was so slow that arm control was lost. The mainly-integral based PDF algorithm was apparently too slow to control the experimental system, introducing considerable lag in the system response.

6.6.3 Step Response - Conclusions

The tests showed that proportional control induced overshoot and produced large steady state errors at the arm tip. PDF control gave poor performance, the derivative term producing far too damped a response to the extent that it had to be virtually removed to produce controllable action. PD and PID controllers showed better response characteristics yet, with PID, stability could only be obtained when the integral term was small compared with the proportional and derivative gains - the PID then resembling PD.

Of the four control types implemented, PD control produced the best slave performance in terms of fastest settling time and least overshoot with permissible gains for k_p and k_d within the region of 0.5 to 0.6 and 0.35 to 0.45 respectively.

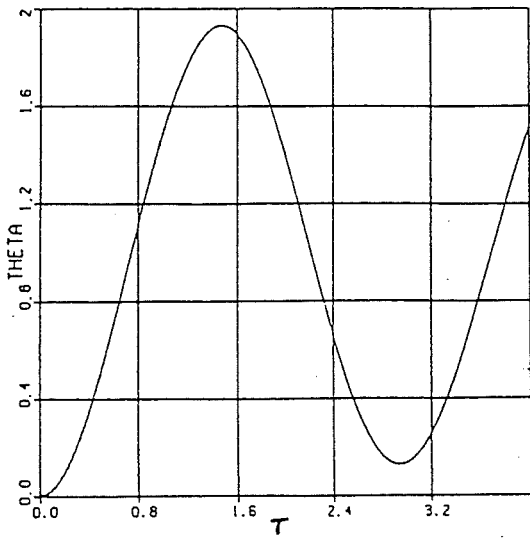
Supporting evidence for PD selection

The suitability of PD control for non-collocated systems is reported in recent publications by Grieco *et al* (1995) and Smith *et al* (1995) as described in Chapter 2.

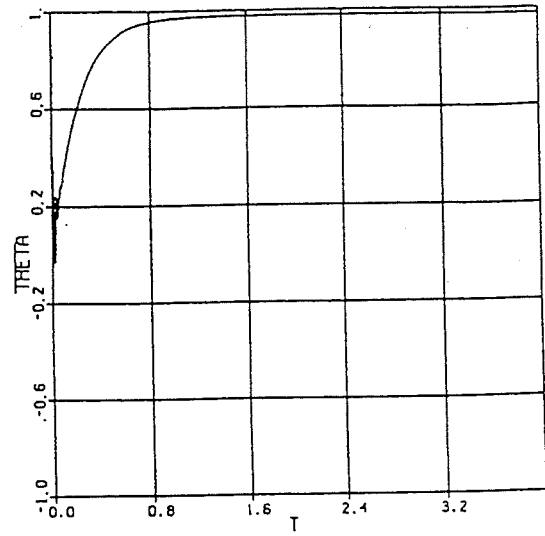
The PD approach is further validated by Surdhar (1995) and Surdhar *et al* (1995a, 1995b) in his PhD research into the simulation, modelling and adaptive control of the dual-axis robot. The parameters used in his model (written in Advanced Continuous Simulation Language) have been taken from values obtained from direct measurements on the practical robot by Pape (1994). The simulated control is based on the incorporation of a tip feedback parameter and the beam tracker characteristics defined in Chapter 5.

The performance of P, PD, PID and PDF controllers were tested on the model. Tip responses to a step input for the different controllers are shown in figure 6.23.

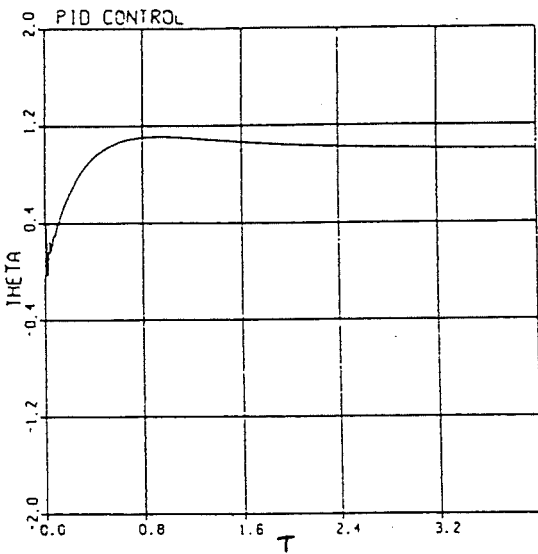
Surdhar has shown P control to be unsuitable. Arm position cannot be controlled in a reasonable timescale as tip oscillations are slow to decay. PDF control proved the hub to be unstable although vibrations were reduced quite significantly. PID and PD control produce similar rise times of 0.05 s, yet PD control gives a faster settling time of 1.6 s compared with 2.4 s for PID. PD control therefore gives the best settling time and rise time to an input step in comparison with the other controllers. These simulated results compare favourably with those obtained experimentally in confirming PD as the most effective of the four slave system controllers investigated. A PD slave control was therefore used during operational performance tests on the robot.



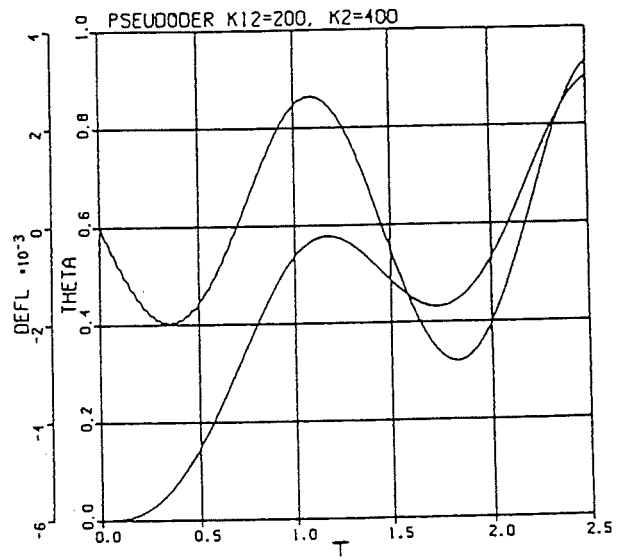
P control



PD control



PID control



PDF control

Figure 6.23 - Simulated tip responses for P, PD, PID and PDF controllers
- (Surdhar, 1995)

6.7 SIMULATION

The tip feedback based control system was simulated for the case of a rigid arm using Matlab (See Appendix F). The results are compared with those obtained experimentally on the prototype robot under proportional and PD controllers to show the effect that arm flexibility arm has on system behaviour.

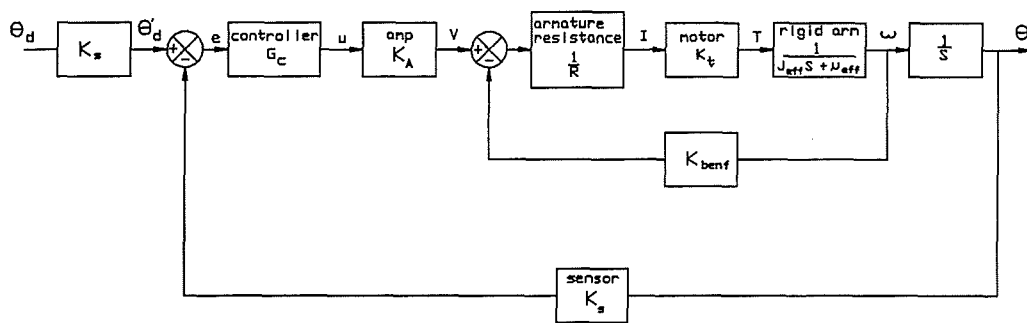


Figure 6.24 - The block diagram for the rigid arm system with tip feedback based control

The model was tested with a step input of amplitude 0.003 radians, corresponding to the limits of the linear range of the tip sensor (0-10 V). This is equivalent to a 3.3 mm vertical movement at the tip for the 1 m arm. The model did not account for gravity effects. The model used the following input parameters, the values matching those of the experimental system (Pape, 1995):

Effective inertia $J_{\text{eff}} = 0.224\text{-}0.492 \text{ kgm}^2$	Amplifier gain $k_A = 1$
Effective friction $\mu_{\text{eff}} = 0.39 \text{ kgm}^2\text{s}^{-1}$	Motor torque constant $k_t = 21 \text{ Nm/A}$
Proportionality constant $k_p = 0.3\text{-}1$	Motor back EMF $k_{\text{bemf}} = 20.53 \text{ V/rad s}^{-1}$
Motor armature resistance $R = 3.4 \ \Omega$	Gearbox ratio = $N = 1000:1$

From the block diagram it can be deduced that:

$$\text{Applied torque } T = (V - k_e \omega) k_t / R \quad (6.14)$$

Using Laplace transformed quantities:

$$\text{Hub angular velocity } \omega = \frac{T}{J_{eff} s + \mu_{eff}} \quad (6.15)$$

where

$$\mu_{eff} = \mu_{arm} + \frac{\mu_{mot}}{N^2} \quad (6.16)$$

$$J_{eff} = J_{arm} + \frac{J_{mot}}{N^2} \quad (6.17)$$

as $N = 1000$,

$$\mu_{eff} \approx \mu_{arm} = 0.39 \text{ (measured)} \quad (6.18)$$

$$J_{eff} \approx J_{arm} = 0.224-0.492 \text{ (measured)} \quad (6.19)$$

From (1) and (2):

$$\omega = \frac{k_t(V - k_e \omega)}{RJ_{eff} s + R\mu_{eff}} \quad (6.20)$$

by rearrangement:

$$k_t V = \omega(RJ_{eff} s + R\mu_{eff} + k_t k_e) \quad (6.21)$$

As:

$$\theta = \frac{1}{s} \omega \quad \text{and} \quad V = k_A G_c e = k_A G_c (\theta'_d - k_s \theta) \quad (6.22)$$

where

$$\theta'_d = k_s \theta_d \quad (6.23)$$

therefore, from (8):

$$s\theta(RJ_{eff} s + R\mu_{eff} + k_t k_e) = k_t k_A G_c (\theta'_d - k_s \theta) \quad (6.24)$$

or

$$\theta[RJ_{eff} s^2 + (R\mu_{eff} + k_f k_e)s + k_f k_A k_s G_c] = k_f k_A G_c \theta'_d \quad (6.25)$$

The transfer function is therefore:

$$\frac{\theta}{\theta'_d} = \frac{1}{[RJ_{eff} s^2 + (R\mu_{eff} + k_f k_e)s + k_f k_A k_s G_c] k_f k_A G_c} \quad (6.26)$$

which defines the transfer function for a second order system under proportional control.

For the PD controller the transfer function is modified as, in this case:

$$G_c = k_p(1 + T_d s) \quad (6.27)$$

therefore:

$$\begin{aligned} & \theta[RJ_{eff} s^2 + (R\mu_{eff} + k_f k_e)s + k_f k_A k_s k_p(1 + T_d s)] \\ & = k_f k_A k_p(1 + T_d s)\theta'_d \end{aligned} \quad (6.28)$$

$$\frac{\theta}{\theta'_d} = \frac{1}{[RJ_{eff} s^2 + (R\mu_{eff} + k_f k_e)s + k_f k_A k_s k_p(1 + T_d s)] k_f k_A G_c} \quad (6.29)$$

6.7.1 Simulation Results

Figures 6.25 and 6.26 show the simulated response of the rigid arm under proportional control to a 10 V step input at the tip sensor, the graphs being superimposed upon those obtained experimentally.

There is a poor match between the experimental and simulated results, the simulation showing faster rise and settling times with no overshoot. This can be attributed to the fact that the model does not account for the flexibility of the arm, unlike the simulation studies being carried out by Surdhar (1996) which include arm flexibility and match the experimental results to within 5%.

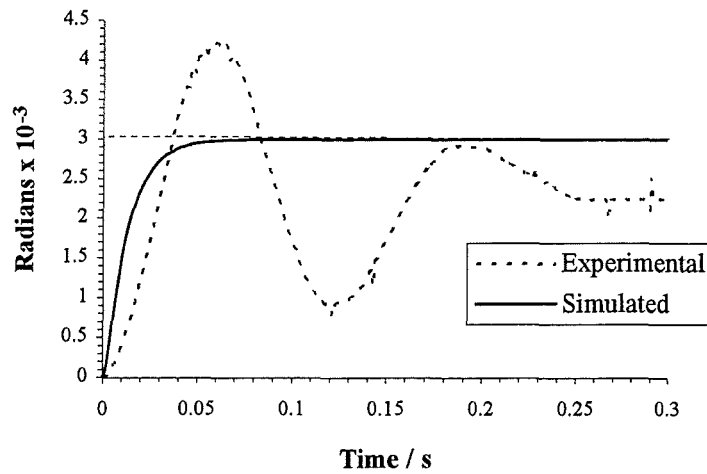


Figure 6.25 - Simulated step response, $J_{\text{eff}} = 0.492$ and $\mu_{\text{eff}} = 0.39$, proportional control

As shown in figure 6.26, a closer match is obtained for an effective inertia value of 3.0, the simulated response resembling that found in the experimental system due to arm flexing which is sensed at the tip.

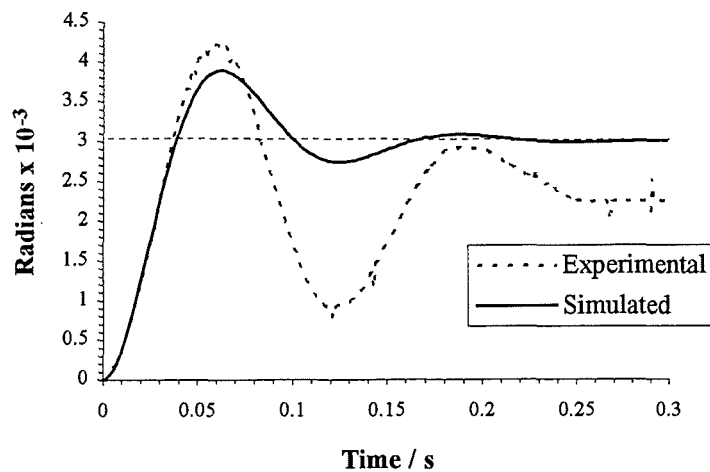


Figure 6.26 - Simulated step response at $J_{\text{eff}} = 3$, proportional control

The value of k_d used in the PD control simulation was 0.002, as compared with a value of 0.5 in the real system (k_p being 0.5 in both cases). The real system with the flexible arm, requires considerably more damping to achieve a fast settling time with minimal overshoot compared with the simulated system as shown in figure 6.27.

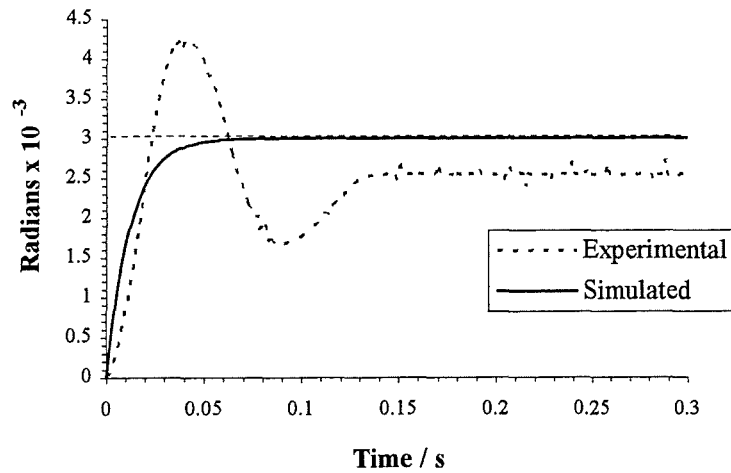


Figure 6.27 - Step response simulation, $k_d = 0.002$, PD control

Figure 6.28 shows the affect of increasing the value of J_{eff} from 0.492 to 4. The simulation then behaving more like the experimental system. The natural frequency of the arm in the experimental system was 13 Hz. An 8 Hz frequency of oscillation is shown in fig 6.e. This indicates that the controller acts so as to damp the natural arm oscillations.

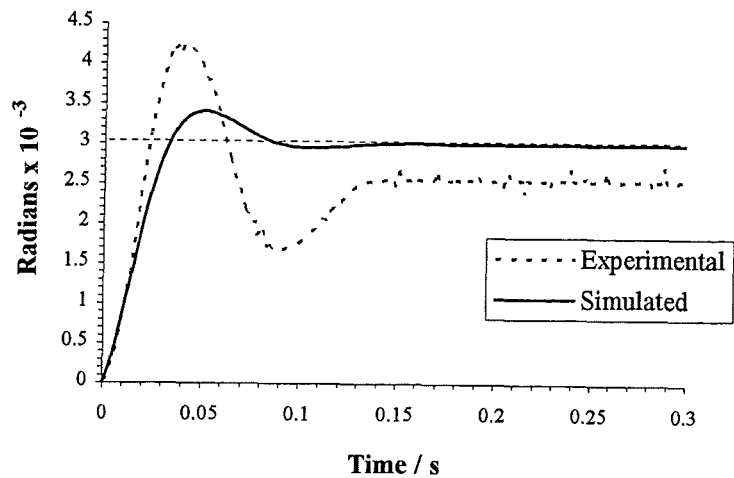


Figure 6.28 - Step response simulation, $k_d = 0.002$, $J_{eff} = 4$, PD control

The most likely cause of variations in behaviour between the experimental and simulation results can be attributed to the influence of arm flexibility on the real system. For both proportional and PD controlled simulated systems, faster settling times and less overshoot are found compared with the experimental version. No steady state errors are observed in the simulations gravity effects were not included, there being no requirement for a holding torque which, in the real system, is generated through a tip sensed position error.

6.8 OPERATIONAL PERFORMANCE

Investigations were conducted into both the deflection compensation and tip tracking ability of the robot. Gains for the PD control parameters are shown in table 6.4.

Spot size and beam tracker output

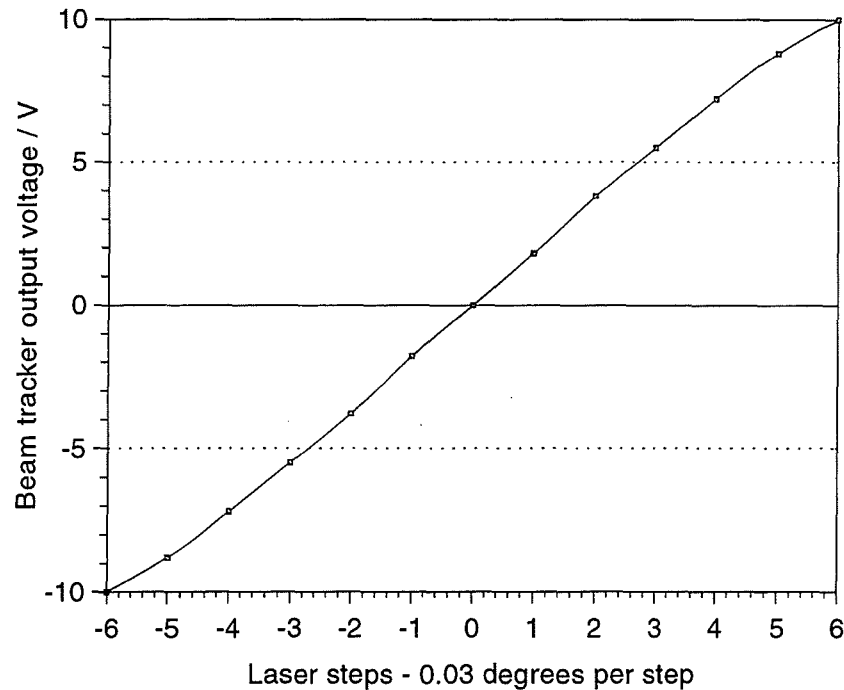


Figure 6.29 - Beam tracker output against laser positioning steps - 6 mm ϕ light spot

From Chapter 5, figure 5.10, it is shown that the deflection range sensed by the beam tracker depends upon incident light spot size. For the tests conducted, the laser was focused to give a 6 mm ϕ spot on the sensor surface. This produced a near linear response over a 3 mm range either side of centre, giving a ± 10 V change in output. Single positioning head steps caused a laser angle change at the hub of 0.03° (see Chapter 3, Section 3.3.1.3). With the 1.037 m long arm 13 steps (6 steps either side of the centre) caused the laser to traverse the sensor (see figure 6.24). For the beam tracker, this equates to a $0.018^\circ/\text{V}$ change in angle at the hub or a $0.3 \text{ mm}/\text{V}$ vertical displacement at the tip.

6.8.1 Deflection Compensation

Severe tip disturbance

Figure 6.30 give a comparison of uncontrolled and controlled arm response (in terms of beam tracker signals) to a severe tip disturbance produced by the sudden release of a 4.2 kg load from the end of the arm. With the load and under control, the actuator supplied a 42 Nm torque to hold the arm stationary. On releasing the load, the torque was reduced to a much smaller value.

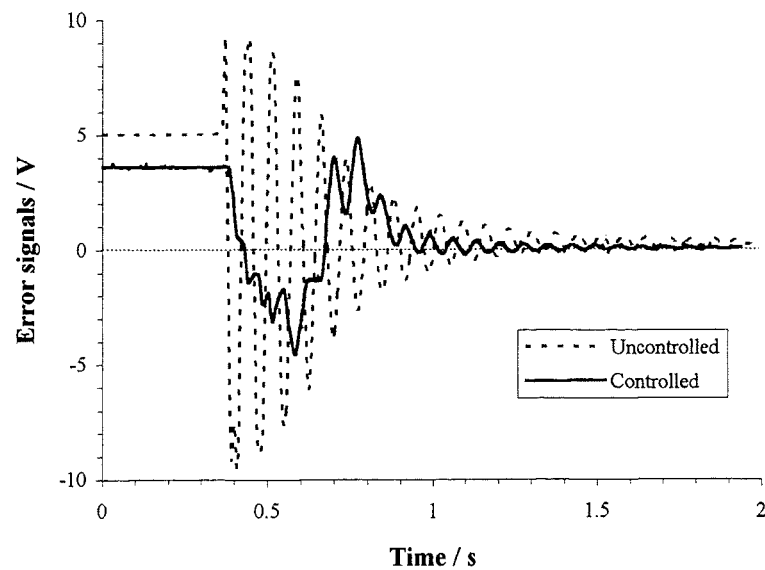


Figure 6.30 - Tip error in response to sudden release of a 4.2 kg load

Figure 6.30 shows that a holding torque error of 3.5 V (1.05 mm initial error) was required to support the load. On release of the load, at $t = 0.4$ s, the tip initially sprung up vertically by 2.85 mm (9.5 V total error). After 0.25 s the arm was pulled in the opposite direction by the actuator, overshooting the demand position by 1.35 mm before finally being brought to rest after a total settling time of 0.8 s with near zero steady state error.

For uncontrolled response, the arm oscillated at a frequency of 14 Hz with an initial amplitude of 3 mm (see table 6.5), the oscillations dying off exponentially over a 1.12 s period.

Although the controlled action could not completely suppress the link vibrations (as can be seen by the 14 Hz arm vibrations superimposed upon the error signal), the maximum amplitude of the vibrations was reduced by 52%, settling time was decreased by 28% and a near zero steady state was recorded. Under these conditions, where tip vibrations were so violent that they were uncontrollable, the system behaved as a steady state rather than dynamic controller.

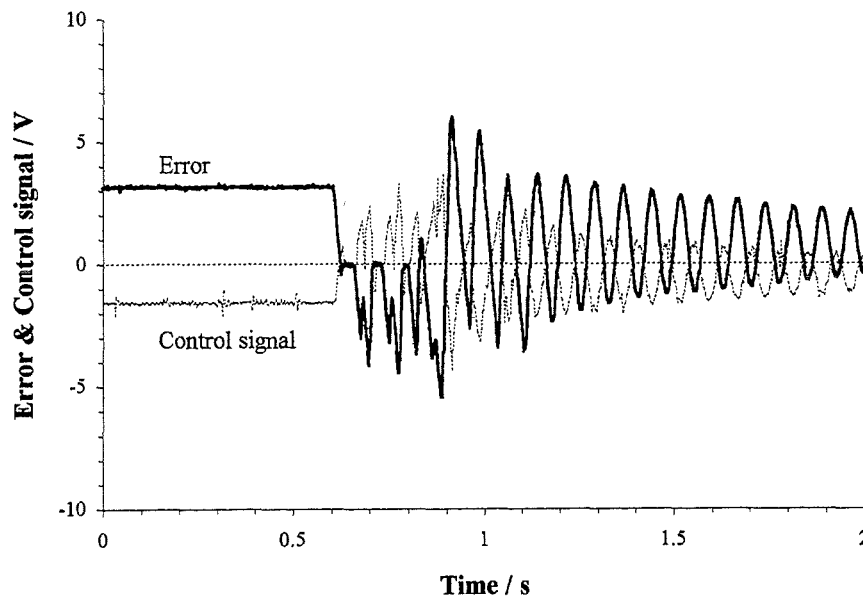


Figure 6.31 - Error and control signals with small integral contribution

Figure 6.31 shows the effect on controlled behaviour caused by the inclusion of a small amount of integral ($k_i = 0.02$) in the control algorithm. Below 0.02 the integral contribution had no appreciable effect. Above this value instability was produced.

The arm oscillated at its natural frequency of 14 Hz, the amplitude of the oscillations was 1.35 mm, these died away after 3 s. The effect of the integral term was more dramatic in the case of the unloaded arm, loading the arm with increased the damping of the system.

Table 6.5

Vertical tip displacements (mm) for uncontrolled and controlled tip disturbance		
	Without control	With control
Maximum	3.00	1.50
Minimum	-3.00	-1.50
Mean	-0.348	-0.156
Steady state errors / mm		
Initial position	1.50	1.05
Steady state	0.10	0.025
Difference	1.40	1.025

The difference between the initial and steady state tip position for the uncontrolled arm (1.4 mm) shows the amount of arm bend caused by the applied load. Under control, a smaller initial error of 1.05 mm (3.5 V at the beam tracker) was recorded as a sufficiently large error signal was needed to cause a holding torque to be supplied through the actuator. On release of the load, with the arm under control, a 1.025 mm reduction in tip error was seen producing a steady state error of only 0.025 mm.

Gradual tip weight reduction

This test was designed as a dramatic demonstration of the active deflection compensation component of the control strategy. A perforated container holding 2.1 kg of dry sand was hung from the end of the 1.2 m long arm such that the sand fell out at a rate of 1.75 g/s.

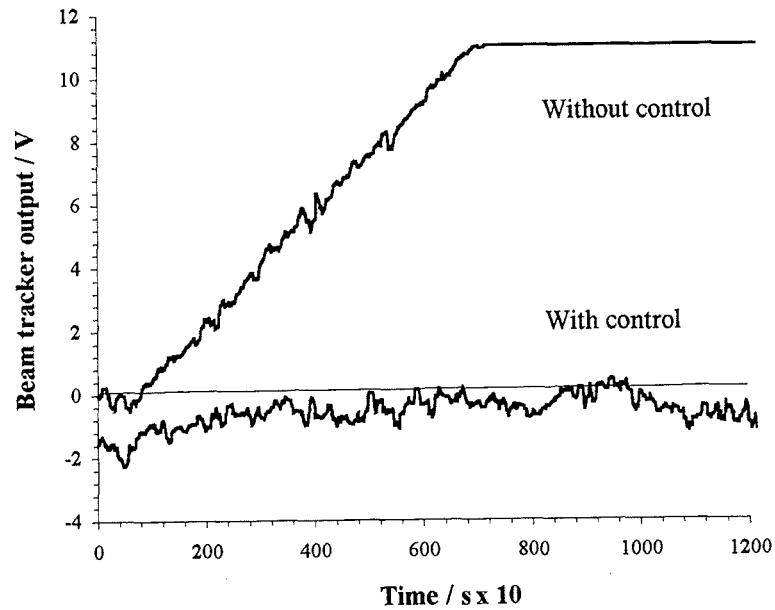


Figure 6.32 - Beam tracker tip position errors for gradual weight reduction with and without control

Figure 6.32 shows the effect on arm tip position with and without control being applied. With the full weight suspended from the arm, the laser was aimed such that the spot was centred upon the beam tracker. Without control and as the weight was reduced, the arm deflected upwards in a near linear fashion to a point where the beam tracker was out of range of the laser spot. By extrapolation, the maximum displacement caused by the release of the full load would be 6.1 mm. With control (from table 6.6) it can be seen that tip position is held to within a mean value of 0.16 mm of its original position.

Table 6.6

Vertical tip displacement (mm) for controlled gradual load reduction			
Maximum	0.925	Start mean	-0.258
Minimum	-1.709	End mean	-0.111
Mean	-0.163	Difference	-0.148

6.8.2 Tracking Response

Tracking tests were performed under PD control and PD control with a small continuous integral contribution. For each test, the arm was moved upwards through 30° from the horizontal. Tracking performance is shown in figure 6.33 and compared in table 6.7.

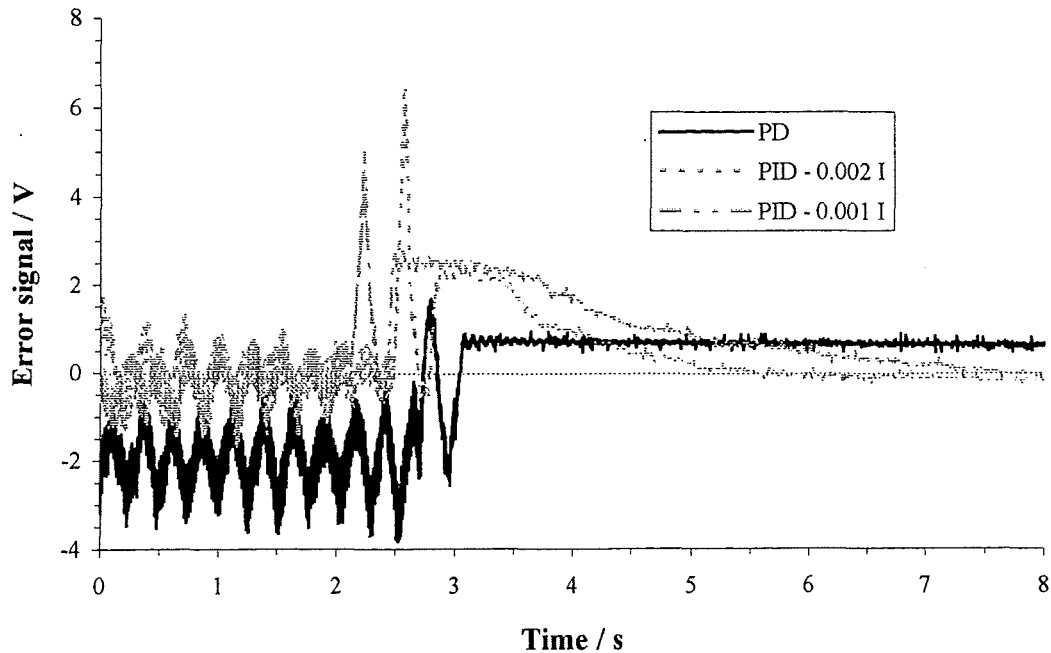


Figure 6.33 - Tracking response with and without integral control

The effect of the integral term in the control algorithm was beneficial in that it reduced both tracking and steady state errors, yet was disadvantageous in that integral 'bump' was introduced and settling times were increased considerably.

To enable both deflection compensation and tracking to be actioned simultaneously, the robot was operated under PD control. This produced a satisfactory response in both cases. With the integral contribution included, tip control was improved during tracking yet caused instability during deflection compensation tests.

Table 6.7

Tracking test results with and without a small integral contribution			
	PD	PD (0.001 I)	PD (0.002 I)
Average tracking error / mm	0.6	0.075	0.025
End-point overshoot / mm	0.49	1.5	1.9
Settling time / s	0.4	5.5	2.5
Steady state error / mm	0.45	0.01	0.005

During tracking tests, use was made of the hub motor position encoders as well as the tip feedback signals, so that hub and arm tip positions could be measured simultaneously. The positioning head was programmed to move the laser through both square and circular paths. Plots were made of hub position on which the corresponding arm tip position was superimposed.

6.8.2.1 - Tracking response - squares

Results are given for the arm following a $30^\circ \times 30^\circ$ square at a tip speed of 60 mm/s.

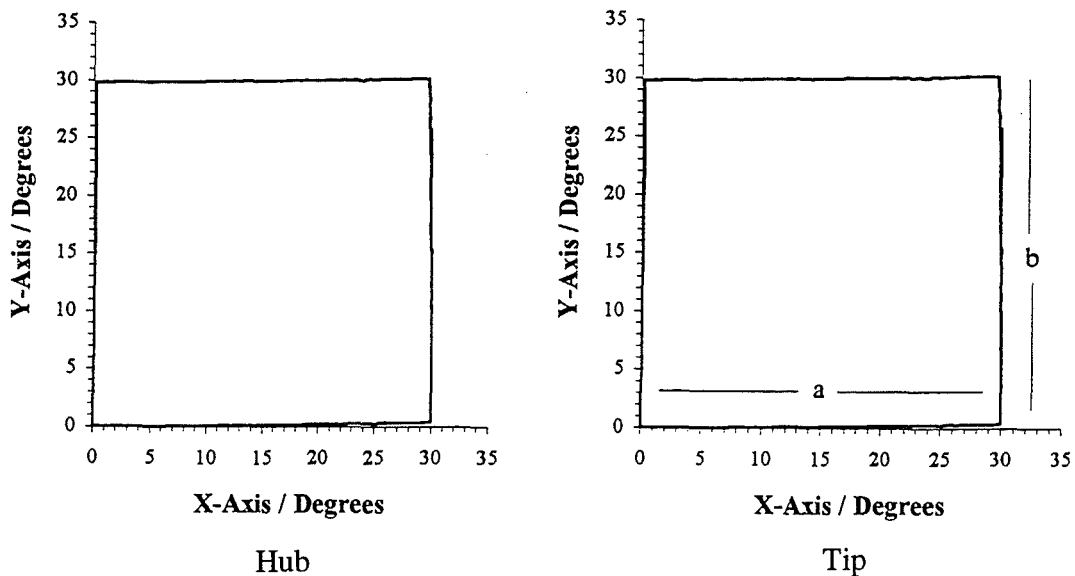


Figure 6.34 - Tracking response at hub and tip for a $30^\circ \times 30^\circ$ square

In figure 6.34, tip angle is plotted as the sum of hub angle and tip position angular error measured from the hub. As can be seen by the similarity in the plots, the system tracking ability is high. To emphasise this, figure 6.35 shows a section in which 10 (of 470) hub and tip data points are superimposed.

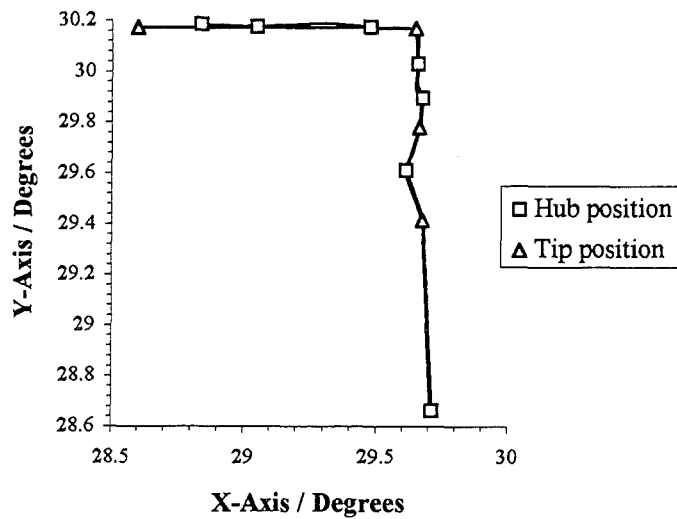


Figure 6.35 - Superimposed hub and tip angular positions - 10 data points

Tracking error in terms of tip translations is shown in table 6.8. The detectable error, as defined by the limits of the detector range, is ± 3 mm. For horizontal tracking, the tip lagged behind the laser by an average of 0.85 mm. During vertical tracking the lag increased to 1.32 mm due to the additional effort required to lift the arm against gravity.

Table 6.8

Tip position error (mm) for the 30° x 30° square tracking test						
	Full square		Section (a) (Horizontal)		Section (b) (Vertical)	
	X-Axis	Y-Axis	X-Axis	Y-Axis	X-Axis	Y-Axis
Max	2.047	1.651	1.910	0.475	0.248	-0.246
Min	-2.987	-2.653	-0.430	-1.442	-2.679	-2.653
Mean	-0.282	-0.233	-0.830	-0.846	-0.903	-1.326

6.8.2.2 Tracking response - circles

The positioning head was programmed to map out a circular path for the arm to track. Results are given for 3.5° and 17° circles with a 1 m arm. Speed of tip travel for the circles was 3.2 mm/s and 15 mm/s respectively.

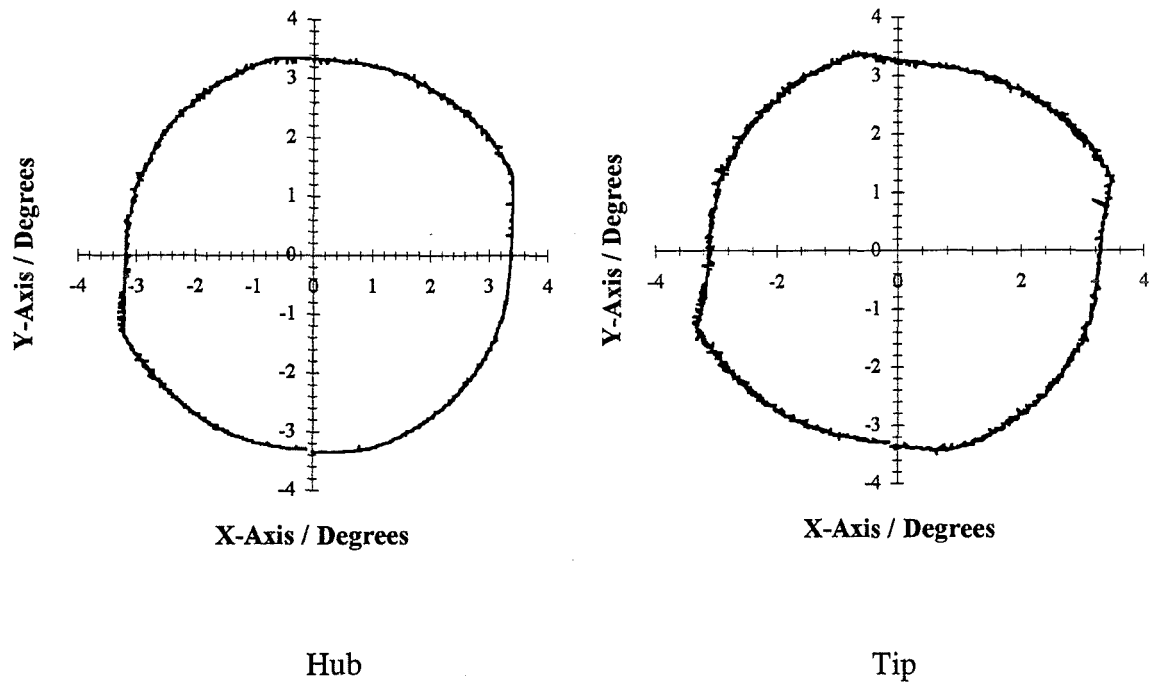


Figure 6.36 - Tracking response at hub and tip for a 3.5° circle

Mechanical imperfections (evident as friction and gear backlash) within the positioning head produced a less than perfect circle as shown in the hub angle position plot. Figure 6.37 shows how the tip position was always offset below the demand position due to the vertical axis motor's requirement for a holding torque signal to counteract the effect of gravity.

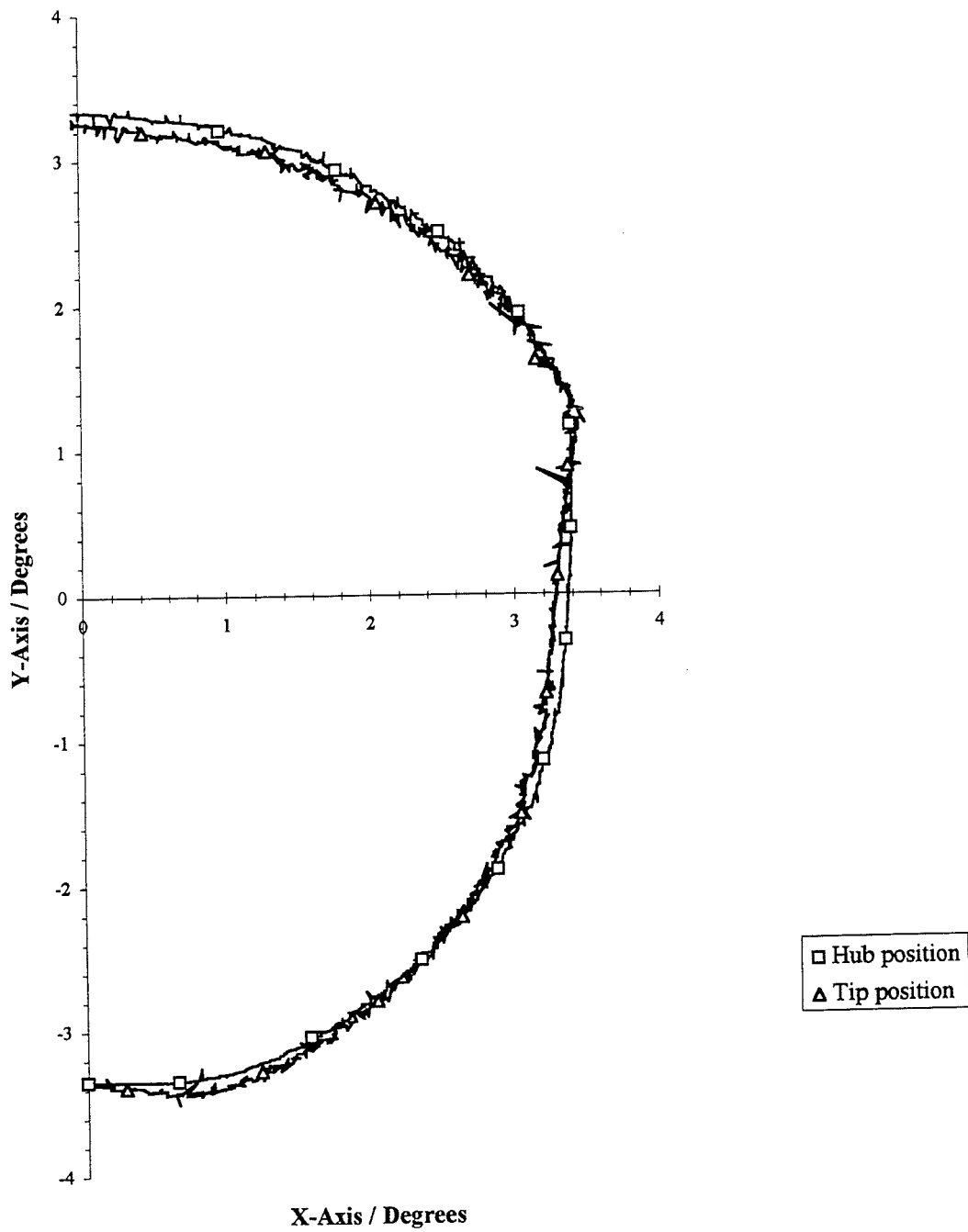


Figure 6.37 - Superimposed hub and tip angular positions for 3.5° circle
 - half circle shown for clarity

In figure 6.38 a plot is shown of 50 superimposed hub and tip points on a section of the circle showing the greatest tracking error. The difference between hub and tip positions show that gravity offset compensation is required for more accurate tracking.

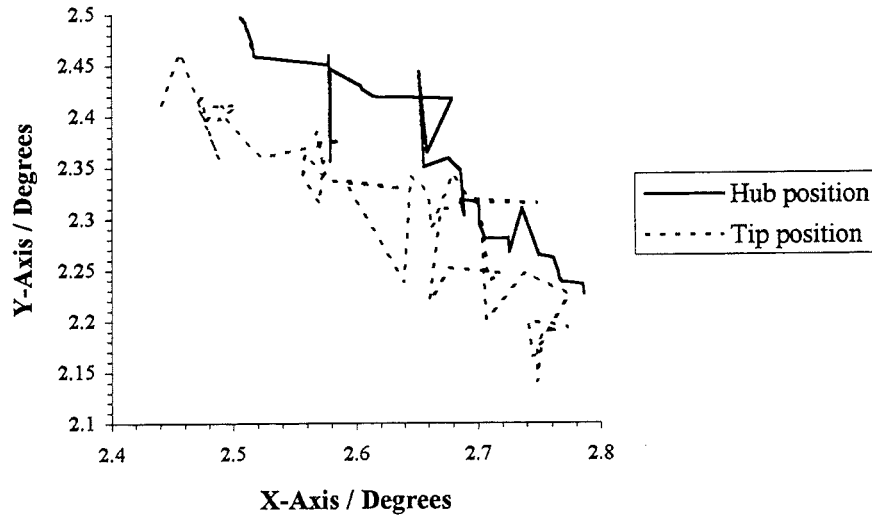


Figure 6.38 - Hub and tip positions superimposed for a section of the 3.5° circle

Figure 6.39 shows the hub and tip tracking profiles for the full 17° circle. 100 (of 3311) superimposed hub and tip data points are shown in figure 6.40.

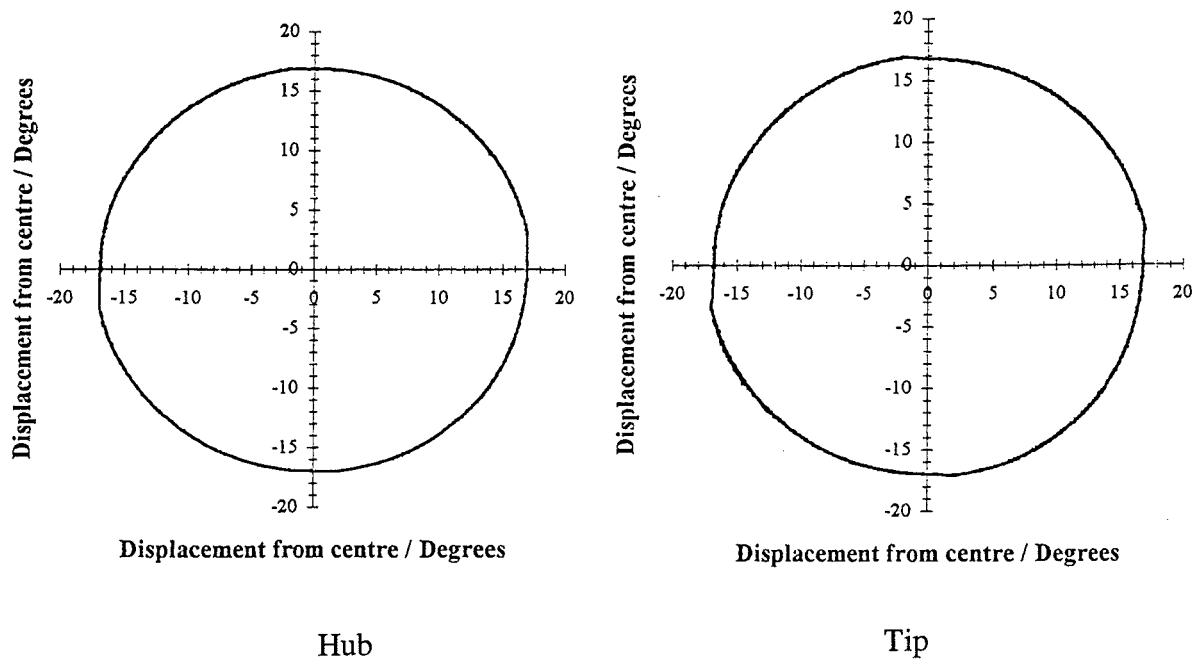


Figure 6.39 - Tracking response at hub and tip for a 17° circle

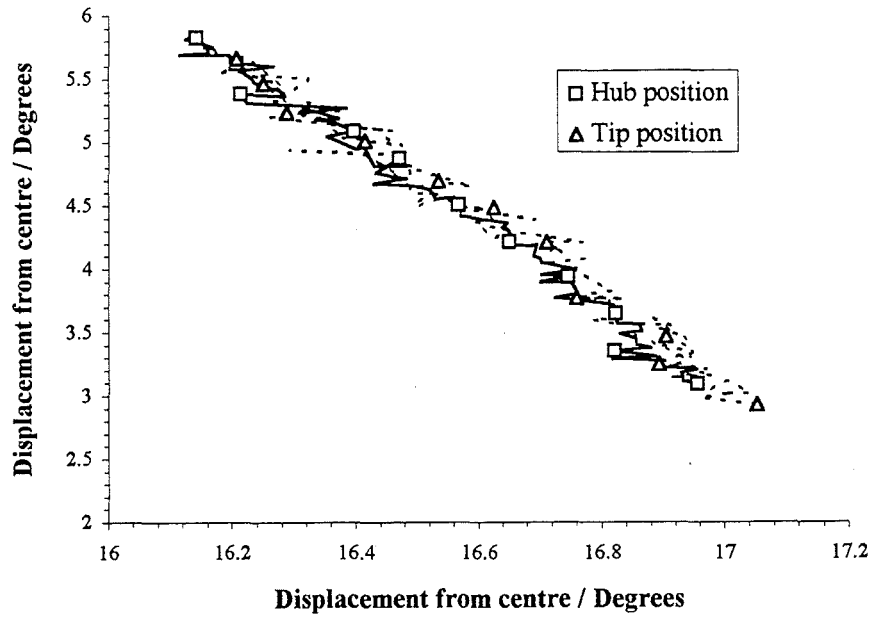


Figure 6.40 - Hub and tip positions superimposed - 100 data points

Table 6.9 shows the tracking error in terms of tip translations. For the 3.5° circle it can be seen that a mean tracking error of -0.37 mm is found for both the horizontal and vertical axes. With the 17° circle a greater tracking error is found for the vertical axis, again due to the requirement for a sufficiently large signal to counteract the effect of gravity on the arm.

Table 6.9

Tip tracking error / mm				
	3.5° circle		17° circle	
	X-Axis	Y-Axis	X-Axis	Y-Axis
Max	2.333	1.888	2.896	2.985
Min	-2.987	-2.987	-2.896	-2.986
Mean	-0.363	-0.366	-0.458	-0.864
Std dev	0.510	0.290	0.751	0.125

6.8.3 Tracking Results - Analysis

As stated, the beam tracker produced a linear output proportional to a spot displacement over a 3 mm range either side of centre. Outside of this region, saturation occurred giving a constant + or - 10 V signal. Table 6.10 gives percentage figures of data points outside the linear range for the tracking tests described.

Table 6.10

Percentage of data points falling outside the ± 10 V beam tracker linear region											
Square (938 data points)				3.5° circle (5024 data points)				17° circle (6622 data points)			
Horizontal		Vertical		Horizontal		Vertical		Horizontal		Vertical	
10V	-10V	10V	-10V	10V	-10V	10V	-10V	10V	-10V	10V	-10V
0	0.21	0	0	0	0.56	0	0.56	0	7.94	0	8.97

Only *negative* positioning error signals are found outside of the linear region. Tracking imbalance towards the negative quadrant of both the vertical and horizontal beam tracker pairs was caused by a direction bias within the Harmonic Drive actuators. A greater frequency of errors in the -10 V region was found when tracking the large 17° circle, big error signals occurring most frequently in regions where the arm tracked in an upwards vertical direction where additional actuator effort (and therefore a larger position error signal) was required to lift it against gravity.

One source of trajectory definition error, seen during tracking tests, can be attributed to the poor performance of the stepper motor driven positioning head. The stepping action did not produce smooth movement of the laser spot at the arm tip, each laser step producing the equivalent of a sudden 2 V change in output in the beam tracker signal - the effect being most noticeable with the large circle.

During fast movement, chatter within the gearboxes caused the laser to vibrate. This was observed as repetitive signals in the beam tracker as shown in figure 6.41.

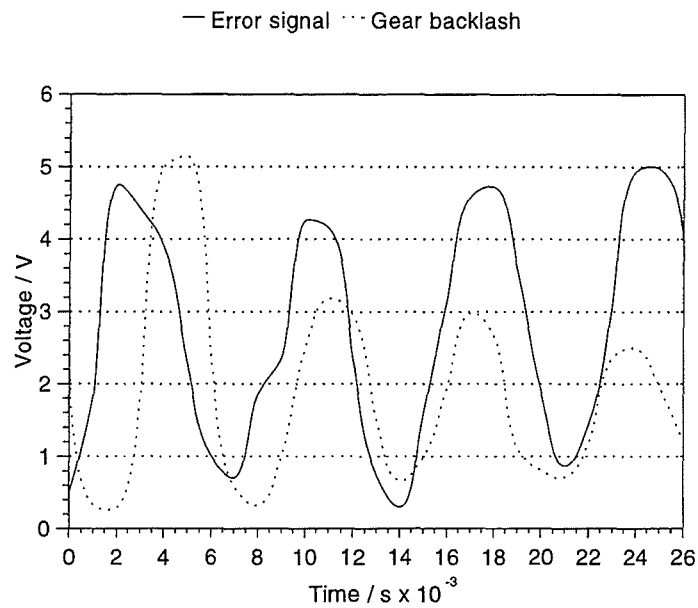


Figure 6.41 - Gearbox vibrations detected at the beam tracker

The maximum operating frequency of the stepper motors is 1000 Hz, giving a theoretical laser movement of $30^\circ/\text{s}$ at the head. In practice it was found that the maximum rate of angle change obtainable was only $15^\circ/\text{s}$ for single-axis movement and between $6.5 - 10^\circ/\text{s}$ for dual-axis movement. This was due to inefficient programming of the slow (12 MHz) 286 computer. An improved positioning head design is required, details of which are given in Chapter 8.

For the 17° circle, where greatest tracking error was seen, 92% of data points fell within the ± 3 mm sensor range, 68.3% of which were within ± 0.2 mm of the demand position, thus meeting the specifications given in Section 6.5. These figures show that, even though tracking ability was directly effected by the poor performance of the positioning head, the slave control system prevented excessive tip oscillations building up during arm movement.

Summary

Under proportional control, the arm could only track the laser at slow speed yet tip deflection compensation was handled well - the load at the tip providing sufficient extra damping to prevent tip oscillation.

For improved tracking ability additional damping was required. Three algorithms with damping terms were tested - PDF, PID and PD :-

- PDF control was found to behave unsatisfactorily on such a highly non-linear system as the flexible robot arm.
- Stable response with PID control could only be obtained when the integral gain was small compared with that of the proportional and derivative gains. Too great an integral contribution caused poor tracking behaviour and unstable tip response to step inputs.
- Under PD control the robot operated well, the additional damping term counteracting tip oscillations found with P control alone. As position errors were detected *directly at the tip*, small steady state errors could be obtained without the cost on performance of using an integral term.

Evidence as to the enhanced slave system performance when operated under PD control is given in the form of step input and tracking tests. Tracking errors at the tip of a 1 m arm were on average no greater than -0.43 mm. This performance compares well with results published for methods, described in Chapter 2, where tip position measurements are used as additional parameters for hub based control. Grieco *et al*, using a very flexible arm, report errors as big as 60 mm with their PD based controller using externally mounted cameras to detect tip position. Jiang *et al* and Uchiyama *et al* give figures in the region of 0.6 mm for an arm tracking a circular path, where tip position was measured using a laser/position sensing detector attached directly to the arm.

In the next chapter, conclusions are drawn as to the findings of this research.

References

- Cicalese, F., (1993) 'The implementation of the control algorithm for the laser guided robot', Middlesex University, Final year project report - 1993.
- Fu, K. S., Gonzales, R.C. and Lee, C.S.G., (1987) 'Robots: sensing, vision and sensing', McGraw-Hill International, Chapter 5, pp. 201-266.
- Holtzer, P., (1991) 'Error detection and correction for the end effector of a six axis robot', Middlesex Polytechnic, Final year project report - 1991.
- Houpis, H. and Lamont, G.B., (1985) 'Digital control systems, theory, hardware, software', McGraw Hill.
- Korhonen, J., (1995) 'The control and testing of a laser guided robot arm', MSc project, Middlesex University, July 1995.
- N-Nagy, F. and Siegler, A., (1986) 'Engineering foundations of robots', Prentice Hall International.
- Pape, M., (1995) 'An investigation of the structural and dynamic properties of an optically guided robot arm', Middlesex University, Final year project report - 1995.
- Phelan, M.P., (1977) 'Automatic control systems', Cornell University Press.
- Smith, E.S., (1995) 'An application of fuzzy-logic control to a classical military tracking problem', Naval Engineers Journal, Vol. 107, Part 1, pp. 99-108.
- Snyder, W.E., (1985) 'Industrial robots: computer interfacing and control', Prentice-Hall International.
- Surdhar, J.S., (1995) 'The control of a laser guided long reach robot', Middlesex University PhD Transfer Report.

Surdhar, J.S., Korhonen, J., White, A.S. and Gill, R., (1995a) 'A fuzzy PD controller applied to a long reach manipulator', MUCORT'95 - 1995 Conference on Research in Technology, Middlesex University, 6 pp.

Surdhar, J.S., White, A.S., Stoker, M., Gill, R. and Korhonen, J., (1995b) 'A transputer implementation of a fuzzy PD controller applied to a flexible link manipulator', In Proc. DARS'95 - Workshop on Human Oriented Design of Advanced Robotic Systems, Vienna, Austria, 5 pp.

Swevers, J., Torfs, F., Demeester, F. and Van Brussel., (1992) 'Fast and accurate tracking control of a flexible one-link robot based on real-time link deflection measurements', Mechatronics, Vol. 2, No. 1, pp. 29-41.

White, A.S. and Kelly, C., (1994) 'Optimisation of a control algorithm using a simulation package', Microprocessors and Microsystems, Vol. 18, No. 2, March 1994, pp. 89-94.

De Schutter, J. and Van Brussel, H., (Eds) (1992) 'Lecture notes of the short course on computer controlled motion', Katholieke Unniversiteit Leuven, Faculty of Applied Sciences, Department of Mechanical Engineering, Production Engineering, Machine Design and Automation (PMA), Celestijnenlaan 300 B, 3001 Heverlee, Belgium, June 1992, pp. 79-112.

Chapter 7

CONCLUSIONS

Control of long reach robots, based on direct tip position sensing through optical means, has shown to be feasible.

7.1 The Tip Position Control Strategy

A novel position control strategy has been developed in which the tip trajectory of a long reach robot is marked-out by the controlled movement of a laser beam. This beam passes through a hollow single link and impinges on an optical sensor at the tip. The sensor is designed to detect the laser spot position on its surface and outputs a position error signal corresponding to link deformation. By responding to this signal, the arm controller causes movement of the arm so that the sensor is re-centred on the laser beam. As a result, the arm control system causes the arm to 'slave' to the 'master' positioning system. The tip therefore constantly tracks the laser irrespective of arm bending with the slave system providing active tip position correction.

This approach is supported by Smith *et al* (1995) where a laser/quadrant detector combination are used in a military target tracking system. A tracking platform 'slaves' to a moving laser so that the quadrant detector is continuously 'locked on' to its target.

There are a number of major differences that distinguish the new system from others that use optical tip position sensing techniques.

Mechanical design

- The positioning head, from which arm tip trajectory is defined, is mechanically isolated from the load bearing robot frame and arm on a structure known as the endoskeleton. This ensures that trajectory definition is unaffected by load-induced distortion or mechanical misalignment of the

arm and actuators.

- The laser beam is projected up inside the hollow arm where it impinges on a sensor at the tip. The sensor is therefore shielded from external interference, such as ambient light, and the positioning head is protected from mechanical damage by the surrounding robot frame.

Control strategy

- Trajectory generation does not rely on a model of the physical system : tip trajectory is generated through movement of the laser alone.
- The output from the beam tracker is the primary, rather than an additional, position controlling parameter for the arm slave control system.
- Tracking accuracy is defined by the beam tracker characteristics in contrast to model based systems where accuracy is dependent upon the manipulator kinematics and dynamics.

7.2 Robot Design and Construction

Initially a single axis prototype robot was constructed. It proved adequate for 'proof of concept' validation, but its performance was limited by poor actuation and the manner in which tip position errors were detected through a linescan camera. Distinct improvements were achieved with a more powerful and responsive actuator and through the addition of a purpose-built beam tracker. From the results of test trials on this version, it was shown that even faster actuation was needed. This led to the construction of a dual-axis version operating through hub servo motors.

A series of laser positioning heads were produced, a stepper motor driven version operating through a dedicated PC was used with the dual-axis robot. Three joints were built - two revolute and one prismatic. Although tested, none have as yet been incorporated into an arm as the control system is not yet sufficiently developed to warrant their inclusion.

7.3 The Beam Tracking Systems

In the initial prototype, a linescan camera was adapted as a beam tracking system to enable single-axis control. Although successful, its use as a position sensor was hindered by its limited resolution and by the costs incurred in terms of time and computation needed to indirectly derive a position error from its output signals. For dual-axis movement, a device was required that could simultaneously detect arm position error about two orthogonal axes. A beam tracker was developed based upon a quadrant detector photodiode sensor. Through built-in electronics, position error signals could be directly generated corresponding to the displacement of the light spot from the detector centre in horizontal and vertical planes. These signals formed the basis of the error inputs to the arm position controller.

Performance characteristics of the beam tracker were measured on a purpose-built test rig, the results showing a close match with the theoretical behaviour. Light source characteristics, such as incident light intensity, spot profile and size were investigated. From these results, optimum light source parameters were established.

In operation, the dual-axis beam tracker was shown to give considerable tracking and step response improvement over the original linescan camera based device. Not only did it give improved accuracy and much higher resolution, it also formed a 'stand alone' sensing means in that position errors in two axes were determined in real-time with no signal post-processing being required.

7.4 Robot Performance Testing

The initial single-axis 'proof of concept' robot, operating under proportional control alone, demonstrated the ability of the optical system to both control primary arm positioning and correct for arm bending. As the speed of actuation of the robot was increased, limitations of the proportional control system became evident as uncontrollable oscillations appeared at the arm tip. PD, PID and PDF algorithms were investigated to improve damping and to reduce steady state error. Neither PID or PDF control proved successful due to the response lag associated with the integral term. Substantially better performance was

obtained through PD control alone giving robust behaviour with little steady-state error, the damping term reducing the tendency of the tip to oscillate at high gains. This experimental evidence for PD control as a favoured control method is backed up by the results of simulation tests on the dual-axis robot obtained by Surdhar (1995) and contemporary research into the control of long, flexible robot arms by Grieco *et al* (1995).

Results for step input and tracking response tests confirm the validity of the control concept as originally conceived. With a step input, the settling time at the tip of a 1 m arm was less than 0.9 s, giving a steady state error of 0.45 mm. For tracking tests, the robot was programmed to follow both square and circular trajectories, giving an average tracking error of less than 0.43 mm at the arm tip.

Summary

The following have been achieved

- formulation of the optically sensed tip position control strategy,
- construction of a two-axis prototype robot,
- development of a two-axis positioning head,
- the design, development and testing of a dual-axis beam tracker,
- the design and construction of revolute and prismatic joints,
- implementation and testing of arm position controllers, and
- robot performance analysis.

Chapter 8

FUTURE WORK

The work in this chapter is divided under four headings

- mechanical modifications,
- optical system improvement,
- slave controller development, and
- tip six degrees of freedom measurement.

8.1 MECHANICAL MODIFICATIONS

The positioning head - A smoother and faster operating positioning head is required, such as that using mirror galvanometers as described in Chapter 3, Section 3.3.1.1. Recent innovations in scanner technology have led to the introduction of integrated position sensors within the scanner mechanisms. These, in conjunction with the scanner driver, form a closed position regulating circuit giving a position resolution of 0.2 mrad and a repeatability to within 0.10 mrad (LSK Scanners, 1995). Heating effects within the galvanometer coils are now automatically compensated for and slow scanning speeds can be used making these devices most suitable for this application.

The endoskeleton - To insulate the positioning head further, the endoskeleton should be fixed directly to the floor rather than to the lower portion of the robot structure, a damping device separating the head from the column. Pneumatic and pendulum damper combinations can be used to provide high performance vertical and horizontal damping (Newport Ltd, 1995).

8.2 - OPTICAL SYSTEM IMPROVEMENT

There are three variable parameters associated with beam tracker behaviour: signal gain, sensor diameter and light spot characteristics.

Signal gain - Software control of signal gains would enable the error signal magnitude to be varied according to robot operating conditions. The error signal could be amplified as the arm approached a desired position so that arm actuator response is increased and steady-state error is reduced. This adaptive control of the beam tracker signal gains is achievable within the slave control algorithm or through direct software control of the programmable instrumentation amplifiers used within the beam tracker.

Quadrant detector diameter - For a given diameter sensor, detectable tip deflection angle reduces proportionally as arm length increases. A bigger detector will make the feedback from the tip larger in magnitude, not because the gain is increased, but because the range of deflection sensed will be larger. It is envisaged that a bigger sensor will be beneficial for arms with greater flexibility and length.

Light source and spot shape - Gas lasers give a more circular spot profile than is obtainable with a laser diode but their large size has prevented their incorporation within the restricted space available on the stepper motor driven positioning head. An advantage of the mirror galvanometer head is that the light source is not physically moved. A large gas laser can therefore be used. It can be mounted within the endoskeleton column, with the laser beam aimed along the desired trajectory by rotation of the galvanometer mirrors alone.

Spot size - As shown in Chapter 5 figure 5.10, a light spot with a diameter equal to half that of the sensor produces the most linear proportional output, but it limits the detectable deflection range to a distance equal to that of the sensor diameter. In operation it was found that better tip control was achieved when the spot diameter equalled approximately 3/4 that of the sensor. This gave a proportional increase in detectable movement at the tip before sensor saturation occurred - See Chapter 5, section 5.3.5.

The actual spot size will not affect the sensor output gain as this is configured as a differential amplifier circuit which amplifies the current imbalance on the diode array. However, by increasing both spot and detector sizes, bigger deflections can be measured.

Simultaneous 2-D calibration experiments are required to fully investigate the affects that changing the light spot parameters has on beam tracker performance.

8.3 SLAVE CONTROLLER DEVELOPMENT

System validation - hub verses tip control - Through simulation, Surdhar (1995), has shown that tip control gives settling times eight times faster than those of a hub encoder based method. This has not yet been verified practically as hub based control requires an accurate model of the physical system which is still undergoing continuous improvements.

Slave control algorithms - Surdhar *et al* (1995) have reported that a fuzzy logic based PD controller proves to be successful in controlling step response, yet at present it has only been applied to a single axis in the vertical plane. Control will need to be extended to the second axis. It is expected that the computational overheads as a result of the incorporation of the controller for a second axis will cause the control updates to become slower. Parallel processing techniques, via transputers, will enable control of each axis to be performed concurrently. Fuzzy PD control has produced excellent step responses with little overshoot, short settling times and near zero steady-state errors. This demonstrates that the robot can be controlled better with adaptive control than with fixed algorithms.

8.4 TIP SIX DEGREE OF FREEDOM MEASUREMENT

For true tip position control, the optical system must be able to define the required end-point position in terms of all three major axes, i.e. the system must be able to define an actual 'point' in space to which the end of the arm will travel. To account for arm distortion, twist about these axes must be measured and corrected by the controller.

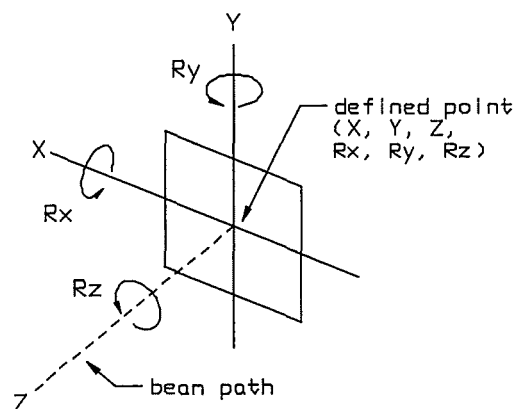


Figure 8.1 - The six degrees of freedom of the point defined in space

X and Y translational coordinates are established via the positioning head, the Z coordinate via the prismatic joint controller. Torque twist about each axis requires active correction to keep the detector surface normal to the axis of the incident beam.

8.4.1 Z-Axis Rotation

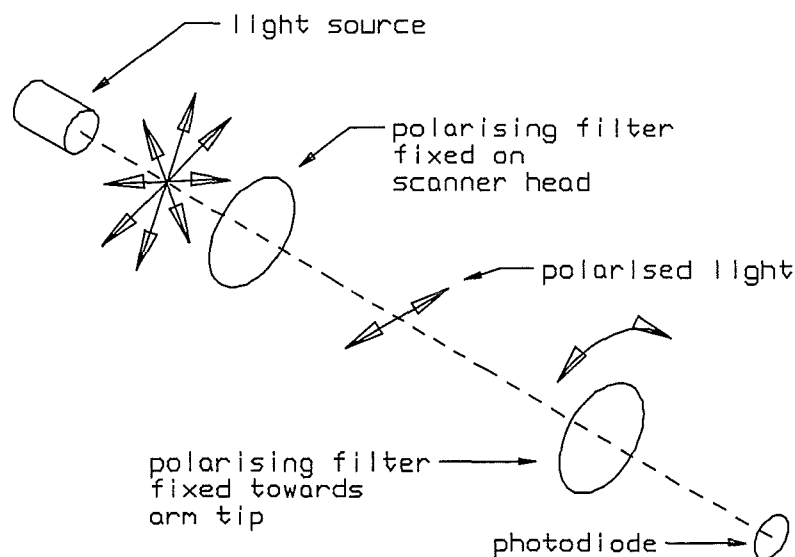


Figure 8.2 - Apparatus to measure twist about the Z axis

Small angles of twist about the Z axis can be measured accurately using polarimetry techniques. The light emitted from the laser consists of electromagnetic waves at right angles to one another emanating in all possible planes. The polarisation at this point is considered random and has no preferred direction. If a polarising filter is positioned in front of the laser the planes in which the electromagnetic waves travel can be controlled such that only a single plane is transmitted. A second polarising filter, attached inside the far end of the arm, is orientated so that its transmission axis is set at 15° to the first when the arm is not subjected to load. On loading the arm, the amount of twist will change, causing a variation in the angle between the transmission axes of the filter pair. Using a photodiode to measure the intensity of the light transmitted through the second filter, the degree and direction of twist can be measured.

8.4.2 X and Y Axis Rotations

Twist about the X and Y axes causes the beam tracker to rotate so that the detector surface is no longer held at right angles to the laser beam. For a single link arm this effect is negligible when compared with the positional errors incurred through arm bending and Z axis twist. If joints are included along the arm, the overall effect becomes more pronounced as the twist in each link will show as a cumulative error at the arm tip.

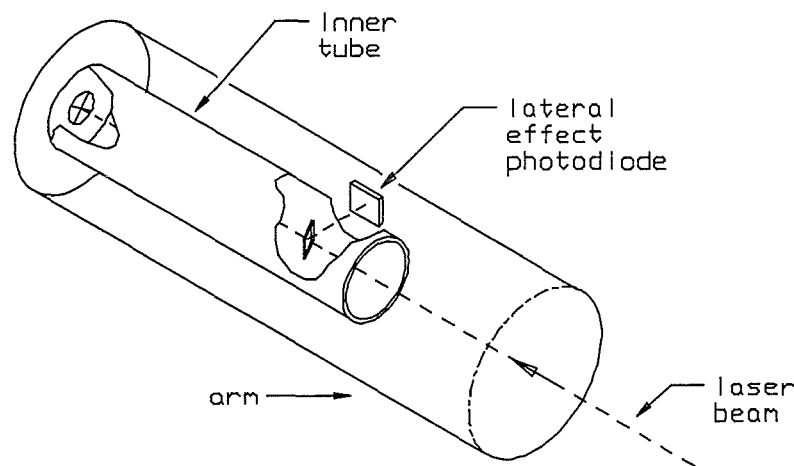


Figure 8.3 - Proposed apparatus for simultaneous X and Y axis twist measurement

Once twist about the Z axis has been corrected, twist about the X and Y axes can be measured using the apparatus shown in figure 8.3. A tube, attached around the beam tracker, extends down inside the arm. Two beam splitters, set at an angle of 45° to the laser beam, are positioned towards the end of the tube such that portions of the beam are reflected through holes in the tube towards the inner wall of the arm. The beam splitters are arranged mutually at right angles so that one reflects the beam vertically, the other horizontally. Both beams pass through cylindrical lenses mounted about the holes in the tube. The lenses change the beam into fine slits of light which impinge upon single-axis lateral effect position sensing photodiodes attached to the wall. The light slits need to be fine enough to give high resolution, yet be of sufficient length to ensure that both detectors remain exposed at maximum degrees of twist about both axes.

Rotation of the beam tracker will produce movement of the inner tube and beam splitters, which in turn will cause the reflected portions of the laser beam to be displaced along the

detectors. Position error signals are generated through the associated electronics which give the measured displacement of the light slit from the central null positions on both diodes simultaneously.

As torque-induced distortion is expected to be small when compared to load-induced arm bending along a wide diameter box or tubular section arm, corrective movements could be made using a pair of piezo-electric actuators mounted on a gimble at the base of the link. This system is designed to therefore re-orientate the beam tracker so that the beam tracker is maintained at right angles to the incident laser beam. Optical system accuracy will depend upon the resolution of the detectors, tube length and tube diameter.

8.4.3 Z-Axis Extension

A more economically viable method than that of using expensive laser interferometry techniques to measure prismatic joint extension (see Chapter 3, Section 3.5.3) is described here. The method, commonly used in compact disk players to focus the laser spot on the disk surface, uses the property of astigmatism to define the required distance. Astigmatism is a defect within optical systems which, instead of producing pin-point focused images, causes lines to be formed at different distances blurring the image in a particular plane. This is caused by a lens bending light more in one plane than in the other.

This effect can be used to advantage with a laser that has a focal point that is adjustable through movement of an objective lens. An optical block containing a cylindrical lens, is placed in front of the laser beam to introduce an astigmatic error which brings the focal point closer in only one plane.

Two focal points are produced, one in the vertical and one in the horizontal plane. The beam at the natural focal point is focused in one plane and out of focus in the other causing the beam to be a long narrow slit of light. At the near focal point the opposite occurs, giving a beam that is the same shape but revolved by 90°. Between these two extremes is a point where the spot is out of focus by the same amount in each plane forming a large circular spot.

A quadrant detector, fixed towards the end of the arm, will detect the beam shape impinging upon it. If the end of the arm is at the correct distance from the laser the beam is circular. Any focus error, equivalent to a positional error along the Z axis, will cause the beam to turn elliptical in one direction. The orientation of the detector causes the beam shape to illuminate diagonal quadrants when the spot is elliptical.

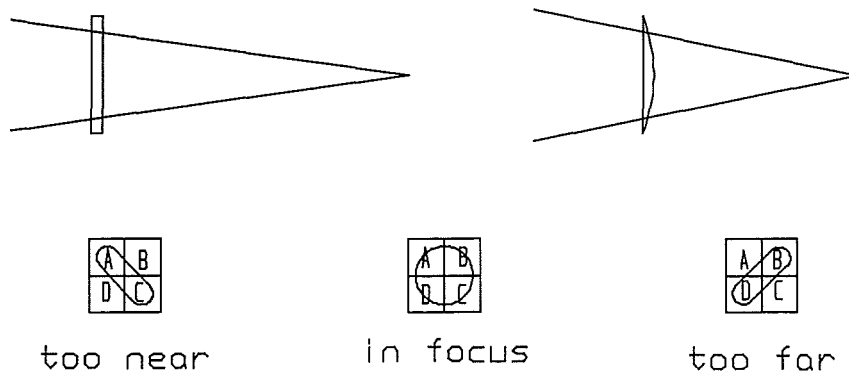


Figure 8.4 - Details of the astigmatic distance measuring system

When in focus equal amounts of light fall on each quadrant, but variations of focus causes more light to fall on two of the sectors than the others. This imbalance in diode output is extracted using operational amplifiers and an error signal, that can be used to move the prismatic joint, is produced. With a circular beam the (A+C) signal and the (B+D) signal cancel out producing a zero error signal. An elliptical spot causes either (A+C) or (B+D) signals to be larger, producing an error signal that can be used to cause corrective movements of the prismatic joint. These systems are effective at monitoring distances to within ± 0.01 mm.

8.4.4 Simultaneous Six Degree Of Freedom Measurement

The devices described above could be combined into a single multi-function position detecting unit. The system could be operated from a single laser, the beam being split into three parallel components through the use of a diffraction grating and a pair of fixed mirrors.

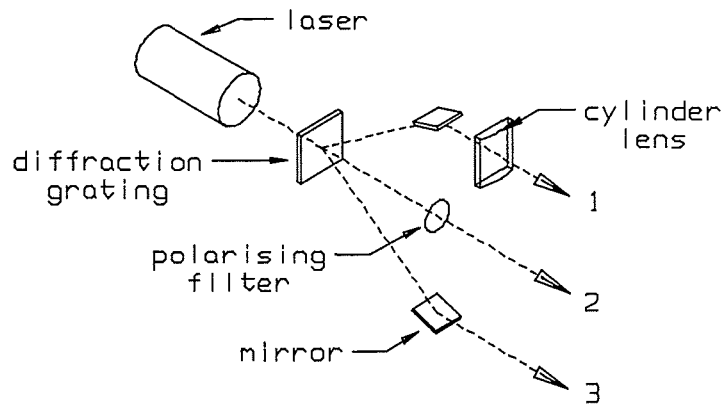


Figure 8.5 - Proposed modification to the positioning head required to establish tip position in terms of six degrees of freedom

The three light beams would monitor different arm translational and rotational movements. Beam 1 could be used with the astigmatic distance measuring method to determine the Z-axis arm translation. Beam 2 could be used to monitor twist about all three major axes. Beam 3 would impinge on the translational movement beam tracker.

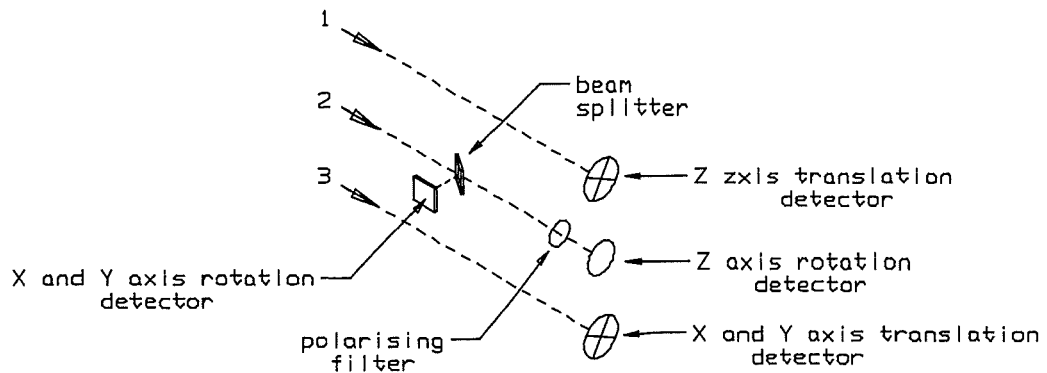


Figure 8.6 - The complete six degree of freedom position detection system

Translational movements would be determined according to the programmed path. Correction for load-induced arm twist would be through an automatic system. To function successfully, correction for twist about the Z axis must take priority over that about both the X and Y axes to prevent Z axis twist affecting X and Y axis twist measurements.

Summary

As the robot's performance has been progressively improved through the software implementation of control algorithms, inherent weaknesses in the mechanical components have been found to exist. Further development of the control concept requires upgrading of some of the mechanical sub-systems. This chapter has outlined some suggested modifications to specific components along with methods that can be used to extend the sensing range of the beam tracking systems.

Details are given of proposed methods that, in combination, can be used to build a beam tracking system which will measure arm end-point position in terms of six degrees of freedom.

- X and Y-axis translations - using the existing beam tracker,
- Z-axis translation - by the method using the astigmatic properties of cylindrical lenses,
- X and Y-axis rotation - torque twist measurement using a position sensitive detector, and
- Z-axis rotation by polarimetry techniques.

These systems can be added to the existing sensor arrangement in any order once the mechanical upgrading of the robot sub-components has been completed.

References

LSK Scanners (1995), 'LSK - The future of laser scanning', supplied by Optilas Ltd, Mill Court, Featherstone Road, Wolverton Mill, Milton Keynes MK12 5RE, U.K.

Newport Ltd (1995), 'Precision laser and optics products', Pembroke House, Thompsons Close, Harpenden, Herts U.K., pp. A-5 - A-6.

Surdhar, J.S., Korhonen, J., White, A.S. and Gill, R., (1995) 'A fuzzy PD controller applied to a long reach manipulator', MUCORT'95 - 1995 Conference on Research in Technology, Middlesex University, 6 pp.

Appendix A

Mechanical Inaccuracies in Robots

Information about the sources, effects and methods of accommodating for the mechanical inaccuracies in robots can be found in the following :-

Azhdari, A., Chalhoub N.G. and Gordaninejad, F., (1991) 'Dynamic modelling of a revolute-prismatic flexible robot arm fabricated from advanced composite materials', Journal of Nonlinear Dynamics, Vol. 2, pp.171-186.

Becquet, M., (1989) 'Analysis of flexibility sources in robot structure', Distributed Parameter Systems:Modelling and Simulation - IMACS 1989, pp.375-380.

Kiedrzyński, A., (1966) 'Mass stiffness analysis of robot links', Proceedings of the 16th ISIR (Brussels), pp.151-158.

McCallion, H., (1979) 'A compliance device for inserting a peg in a hole', The Industrial Robot, Vol. 6, No. 2.

Oppermann, R. and Salesse, C., (1990) 'Device for balancing forces, in particular weight, acting on a robot arm or the like', United States Patent, Number 4,901,591, Feb. 20, 1990.

Redford, A.H. and Lo, E., (1986) 'Robots in assembly', Open University Press.

Rivin, I.E., (1988) 'Mechanical design of robots', McGraw-Hill Book Company.

Sridhar, B., Aubrun. J.N. and Lorell, K.R., (1985) 'Identification experiments for control of flexible structures', IEEE Control Systems Magazine, Vol. 5, May 1985, pp. 29-35.

Whitney, D.E. and Nevins, J.L., (1979) 'What is remote centre compliance and what can it do?', Proceedings of the 9th International Symposium on Industrial Robots, Washington D.C., pp. 135-152.

Appendix B

Circuit diagram showing interconnections between the PC30 I/O board, the HCTL-1000 quadrature decoder and the UDN-29538 motor driver for the DC motor actuated positioning head.

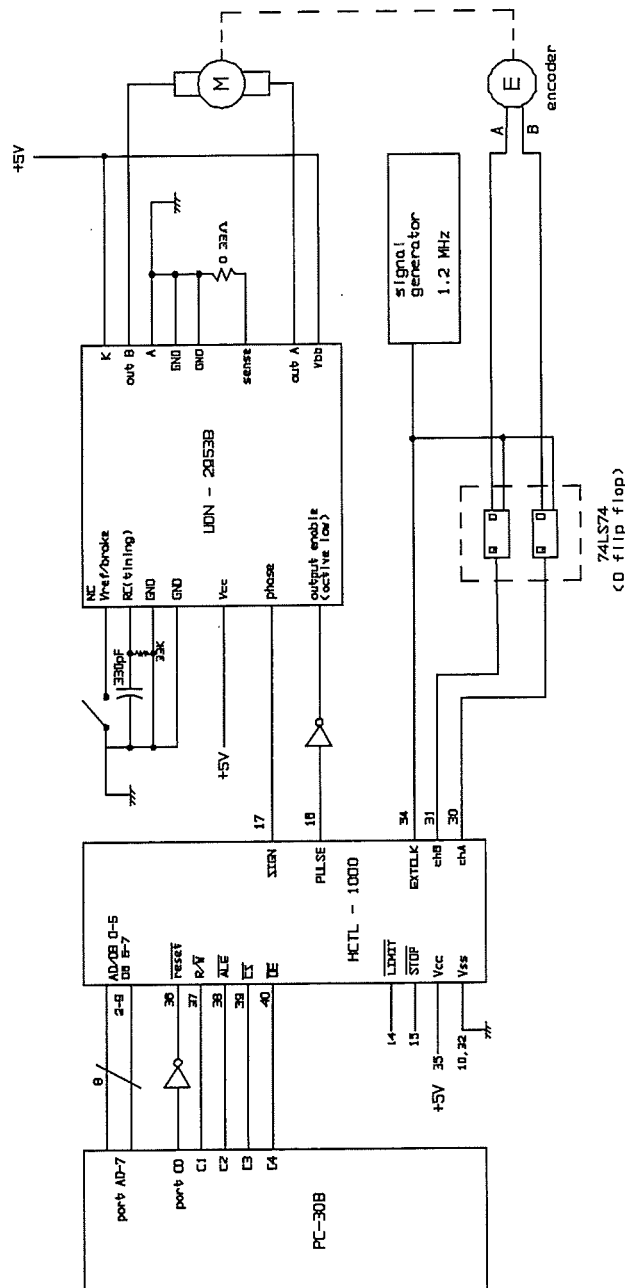


Figure A.1 - The DC motor driven positioning head circuitry

The Stepper Motor Driven Positioning Head Program (Petit, B. and Korhonen, J.)

This program controls the stepper motor driver circuits via the parallel port. It provides simultaneous X and Y axis movements, single axis and step by step movement.

```
#include <stdlib.h>
#include <stdio.h>
#include <dos.h>
#include <conio.h>
#include <math.h>

/*****
/*Subroutine in the case of the x value      */
/*is not the same that the y value      */
*****/

int rectangle (float x, float y, int address)
{
int i;

float degreesx;
float degreesy;

float rapport1;
float rapport;

float mem;
int mod;
int mod1;
int mem1;

int numberx;
int numbery;
int reset;
int freq;
int freq1;
rapport=1;
rapport1=0;

mem1=0;
mod1=0;

degreesx=abs(x*250)/7.5;
degreesy=abs(y*250)/7.5;
if (x!=0)
{
rapport = y/x;
}

if (rapport<0)
{
rapport=-rapport;
```

```

}
if ((x<=0)&& (y<=0))
{ numberx = 57; numbery = 177;reset=49;}
if ((x<=0)&& (y>=0))
{ numberx = 25; numbery = 145;reset=17;}
if ((x>=0)&& (y<=0))
{ numberx = 59; numbery = 179;reset=51;}
if ((x>=0)&& (y>=0))
{ numberx = 27; numbery = 147;reset=19;}

freq=4;/*7*/
freq1=10;/*20*/

if (fabs(degreesy)>fabs(degreesx))
{
rapport = 1/rapport;
mem = degreesx;
degreesx=degreesy;
degreesy=mem;
mem1 = numberx;
numberx = numbery;
numbery = mem1;
}

if (x==0)
{
rapport=0;
}

for (i=1;i<=degreesx;i=i+1)
{

/*****/
/*Change of the delay          */
/*****/

if (i>= (degreesx-20))
{
freq1=freq1+1;
}
else
{
if (freq1>freq)
{
freq1 = freq1-1;
}
else
{
freq1=freq;
}
}

rapport1 = rapport1 + rapport;
mod = rapport1;

```

```

/*****
/*send out the largest value of x or y */
/*****
/* */
/*delay(10);*/
/* */
output(address,reset); /* This is a new resetting */
output(address,numberx);

/*****
/*send out only if ...*/

/*****

if (mod1 != mod) /*to not send out if it's the same value*/
{
delay(freq1);
mem1=mem1+1;
output(address,numbery);
}
delay (freq1);
/* */
/*delay(10);*/
/* */
output (address,reset);
mod1=mod;
}
/*****
/*send out to correct the position */
/*****

if ((degreesy-mem1)>= 1)
{
for (i=mem1;i<=degreesy;i=i+1)
{
output (address,numbery);
delay(3);
output (address,reset);
}
}
output(address,0);
return 0;
}

/*****
/*Subroutine to give out data to the Parallel port*/
/*****

int WriteOut(void)
{
int adres=956 ;
char direction;
int numbsend,resetx;
float xvalue,yvalue;
float memx,memy;
float memx1,memy1;

```

```

/*****
/*  Choice of the direction      */
*****/

xvalue=1;
yvalue=1;
memx=0;
memx1=0;
memy=0;
memy1=0;
do
textcolor(2);
cprintf("To enter the number of degrees, press 's'\n");
printf("\n");
direction='0';
while (direction!='s')
{
if (kbhit()!=0)
{
direction=getch();
if (direction=='u')
{numbsend=144;resetx=17;}
if (direction=='d')
{numbsend=176;resetx=51;}
if (direction=='l')
{numbsend=9;resetx=17;}
if (direction=='r')
{numbsend=11;resetx=51;}
if (direction=='s')
{numbsend=17;resetx=17;}
/* Extra resetting here */
outport(adres,resetx);
delay(7);
outport (adres,numbsend);
delay(7);
outport (adres,resetx);
}
}
textcolor(15);
do
{
memx=memx1;
cprintf ("Give the X degrees : ");
cscanf("%e",&xvalue);
printf("\n");
printf ("  ");
memx=memx+xvalue;
}
while ((memx>90)||(memx<-90));
do
{
memy=memy1;
cprintf ("Give the Y degrees : ");
cscanf("%e",&yvalue);
printf("\n");
printf("  ");
memy=memy+yvalue;
}

```

```

}
while ((memy > 60) || (memy <-30));
printf("\n");

if ( ( xvalue<0) || (xvalue>0) || (yvalue<0) || yvalue>0)
{
memy1=memy1+yvalue;
memx1=memx1+xvalue;

}
else
{
xvalue=-memx1;
yvalue=-memy1;
memx1=0;
memy1=0;
}

rectangle(xvalue,yvalue,adres);

}
while ((xvalue <0) || (yvalue <0) || (xvalue >0) || (yvalue >0));

return 0;
}
/*****
/*Main Program */
*****/

int main (void)
{
clrscr();
textcolor(12);
cprintf("      This program is for the Incremental coordinates \n");
printf("\n\n");
textcolor(5);
cprintf(" You can use the keyboard to adjust the position of the spot");
printf("\n");
printf("\n");
textcolor(14);
cprintf("Press 'u' : UP");
printf("\n");
cprintf("      'd' : DOWN");
printf("\n");
cprintf("      'l' : LEFT");
printf("\n");
cprintf("      'r' : RIGHT\n");
printf("\n\n");

WriteOut();
outport(888,0);
clrscr();
return 0;
}

```

Appendix C

The Fast Laser Tracking/Deflection Compensation Program for Operating the Linescan Camera as a Beam Tracker (Holtzer, 1991).

This program reads in the linescan camera signal and computes a position error signal as a voltage, the magnitude and sign of the voltage being proportional to the displacement of the illuminated photosite from the central photosite (No. 128) of the photodiode array.

```
int cam ()
{
asm mov dx,70Bh
asm mov al,12h
asm out dx,al

st1:
asm mov dx,709h
asm in al,dx
asm and al,80h
asm jz st1

st2:
asm mov dx,709h
asm in al,dx
asm and al,80h
asm jnz st2

asm mov bx,00h
st3:
asm mov dx,709h
asm in al,dx
asm and al,40h
asm jnz exit
asm inc bx
asm jmp st3

exit:
return(_BX)

int res
int a=225
int b=15
int c=0

typedef unsigned char BYTE

BYTE lo,hi;
```

```

main()

while (c==0)
{
res=(cam()*15);
if (res>4095) res=4095;
else if (res<=0) res=0;
else

{
lo=res & b;
hi= (res>>4) & a;
asm mov dx,70Ch
asm mov al,lo
asm out dx,al
asm mov dx,70Dh
asm mov al,hi
asm out dx,al
}
}
}

```

The Linescan Camera/Computer Interfacing Electronics

(1) The clock pulse spreader circuit

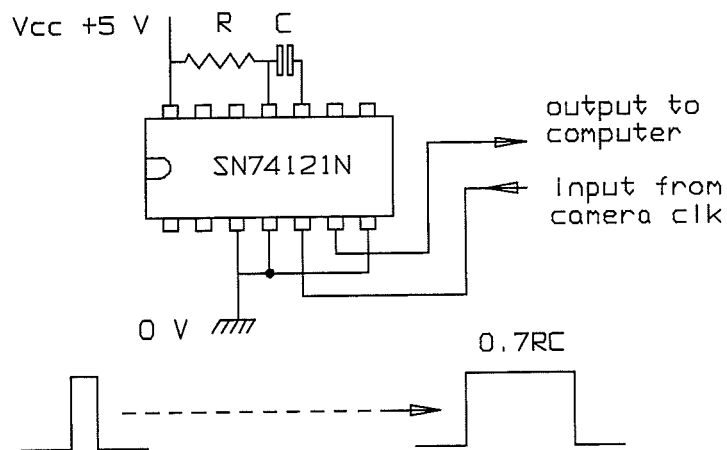


Figure A.2 - The clock pulse spreader circuit

I.C. = SN74121 monostable, $R = 12 \text{ K}\Omega$, $C = 0.1 \mu\text{F}$. The pulse duration is given by :-

$$t = RC \ln 2 \approx 0.7RC$$

(2) The camera signal squaring/TTL conversion circuit

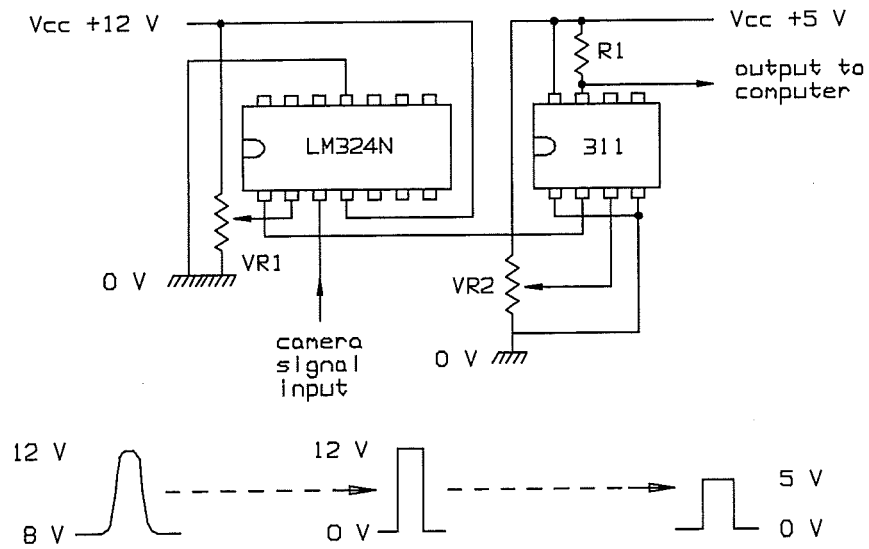


Figure A.3 - The camera signal squaring/TTL conversion circuit

I.C.'s = LM324N and 311 comparators, R1 = 1 K Ω , VR1 & VR2 = 3K3 pots

Appendix D

The Beam Tracker Performance Testing Apparatus

(1) The interferometer/PC interfacing electronics

The output pins of the Laser Display unit indicate the BCD digits, the sign and error. These were connected to five 74AS151, 8 into 1, multiplexer-data selector IC's. The five multiplexer serial data outputs were individually connected to the parallel port printer status input lines. On selecting the multiplexer inputs via the parallel port data output lines, the Laser Display BCD output could be recovered from the parallel port status register using masking software.

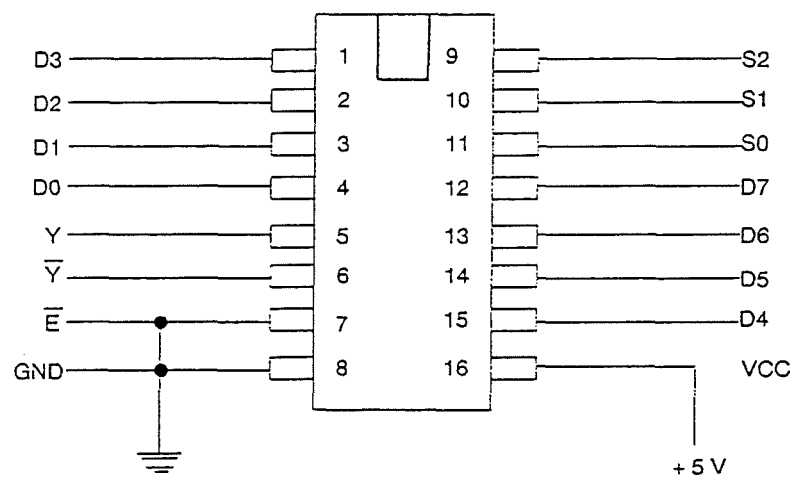


Figure A.4 - The 74AS151 multiplexer

This is a logical implementation of a single 8-pole switch, where the switch position is determined by the binary input to the select (address) inputs S_0 , S_1 and S_2 . The single output Y carries data from whichever input is selected from D_0 to D_7 . When no input is required the enable input is taken high (+ 5 V).

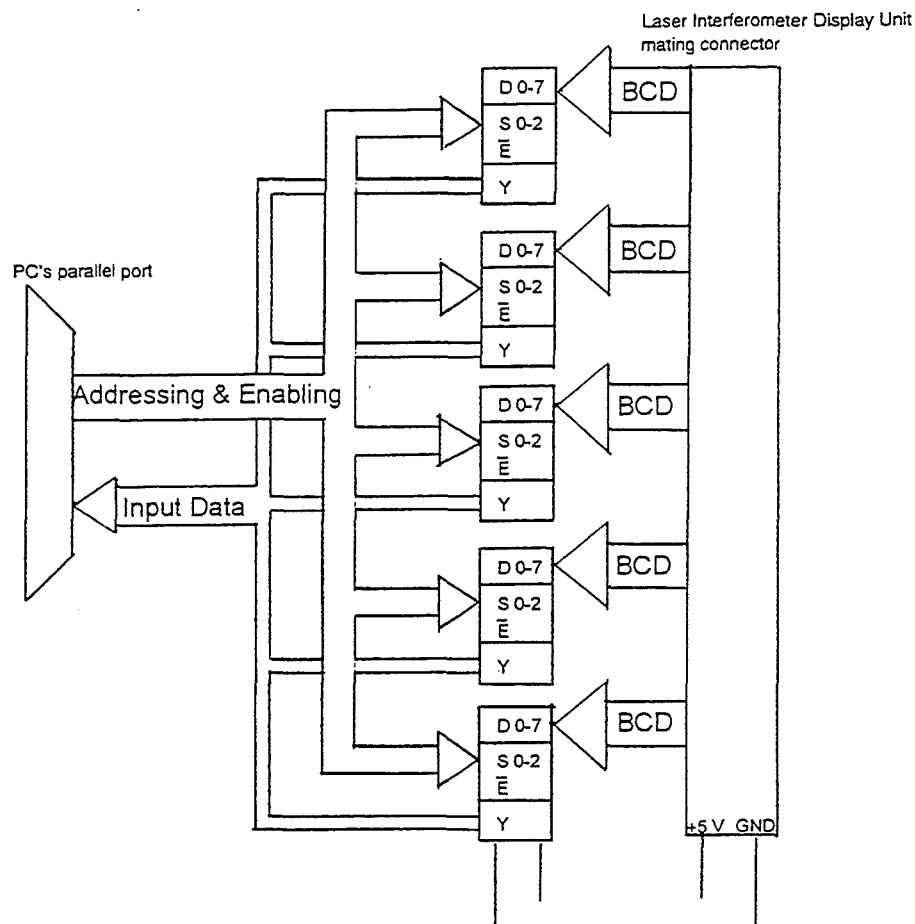


Figure A.5 - Block diagram of the interferometer/PC interfacing circuitry

(2) The interfacing software

The Hewlett-Packard 5500C Laser Head and 5505A Laser Display systems produce position data in BCD (Binary coded decimal) form. BCD is a way of expressing a denary number with 4 bits. The number of bits output from the 5505A printer port is 37 - supporting 9 digits and the sign.

The parallel Centronics port was chosen as the input port to the PC - therefore enabling connection of the interferometer unit to all PC's. The parallel port can be used to input 5 bits and output 12 bits at TTL levels (0 and 5 V).

The program's core is a loop which records the BCD coded digits. The multiplexers are first addressed with the port address 888's bits and then the data from the laser display is read to and masked out from the port address 889.

The data is then formatted into text strings so that it can be manipulated and displayed in a spreadsheet package, then data then being stored in the form of a text file.

```
//      This program the gets the reading of Hewlett-Packard laser interferometer with the help of a
//      multiplexer card. The program also reads analog voltages with the aid of an A/D card and produces
//      an Excel compatible file of the displacement/voltage readings.
/*****/

#include <stdio.h>
#include <stdlib.h>
#include <dos.h>
#include <conio.h>
#include <math.h>
#include <time.h>
#include <graphics.h>

#include "C:\w\include\DATAACQ.h"
#include "C:\LWINCLUDE\formatio.h"
#include "C:\LWINCLUDE\lwsystem.h"
#include "C:\LWINCLUDE\dataacq.h"

static int type_board;
static double volt;

void print_out(long output)
{
    outportb(888,output);
    outportb(890,1);
    outportb(890,0);
}

//      With freeze and defrost interferometer display can be stopped so that it does not change while being
//      read.

void freeze_display()
{
    outportb(888,5);
    outportb(890,1);
    delay(10);
    outportb(890,3);
    while(!(8&inport(889))); // Wait until ready
}

void defrost_display()
{
    outportb(888,0);
    outportb(890,1);
    while((8&inport(889)));
}

```

```

double readvolts()
{   while(AI_VRead (1, 0, 1, &volt));
    return volt;
}

main(void)
{
char buffer[13];
char *voltagebuf;
char volts[13];
int result;
int i=0;
char sign;
int digit1=0,digit2=0,digit3=0,digit4=0;
int digit5=0,digit6=0,digit7=0,digit8=0,digit9=0;
char out=13;
int count=0;
FILE *output_file;
int vdec,vsign;
char filename[35];
char answ='n';
int del_time;

    clrscr();
    Init_DA_Brds (1, &type_board);
    while(kbhit())
        getch();

    printf("Please give the delay time ?\n");
    scanf("%i",&del_time);

    while(answ=='n' || answ=='N')
    {   clrscr();
        if(answ==27)
            exit(1);
        printf("Please give the filename\n");
        scanf("%s",&filename);
        printf("Is the filename right ? Y / N\n");
        answ=getch();
        if ((output_file = fopen(filename,"wt"))== NULL)
        {   answ='n';
            printf("Cannot open file with this name\n");
            printf("Try another name or hit ESC to abort\n");
        }
    }
    while(out!=27)
    {   if(kbhit())
        out=getch();
        outportb(888,i);           // Address the right pins
        result = inport(889);     // Read in the address

        // When address = 0...3; digits 1,3,5,7,9
        // correspond pins in following way:
        // 11,12,13,15,10
        // digit1= $\Sigma$  (logic state of pin_n:0 11 (16)  $\cdot$ (2address))

        if(i<4)

```

```

    {   if(!(result&128))
        digit7+=pow(2,i);
        if((result&64))
            digit5+=pow(2,i);
        if((result&32))
            digit3+=pow(2,i);
        if((result&16))
            digit1+=pow(2,i);
        if((result&8))
            digit9+=pow(2,i);
    }

    if(i>3)
    {   if((result&32))
        digit4+=pow(2,(i-4));
        if((result&16))
            digit2+=pow(2,(i-4));
        if(!(result&128))
            digit8+=pow(2,(i-4));
        if((result&64))
            digit6+=pow(2,(i-4));
    }
    if(i==4&&(result&8))
        sign='-';
    if(i==4&&!(result&8))
        sign='+';
    i++;
    // All the needed data gathered
    if(i==8)
    {   i=0;

    sprintf(buffer, "%c%i%i%i%i%i%i.%i%i%i%i", sign, digit9, digit8, digit7, digit6, digit5
, digit4, digit3, digit2, digit1);
        // Remember to initialize the digits
        digit1=0;
        digit2=0;
        digit3=0;
        digit4=0;
        digit5=0;
        digit6=0;
        digit7=0;
        digit8=0;
        count++;
        printf("%s\n", buffer);
        voltagebuf = ecvt(readvolts(), 5, &vdec, &vsign);
        if(vsign)
            volts[0]='+';
        else
            volts[0]='-';

        sprintf(volts+1, "%s", voltagebuf);
        volts[vdec+1]='.';
        sprintf(volts+vdec+2, "%s", voltagebuf+vdec);
        printf("%s", volts);
        fputs(buffer, output_file);
        fputc(9, output_file);
        fputs(volts, output_file);
        fputc('\n', output_file);
    }
}

```

```

        delay(del_time);
    }

}
fclose(output_file);
return 0;

}

```

(3) Beam tracker to Lab-PC Plus I/O card attenuating circuits

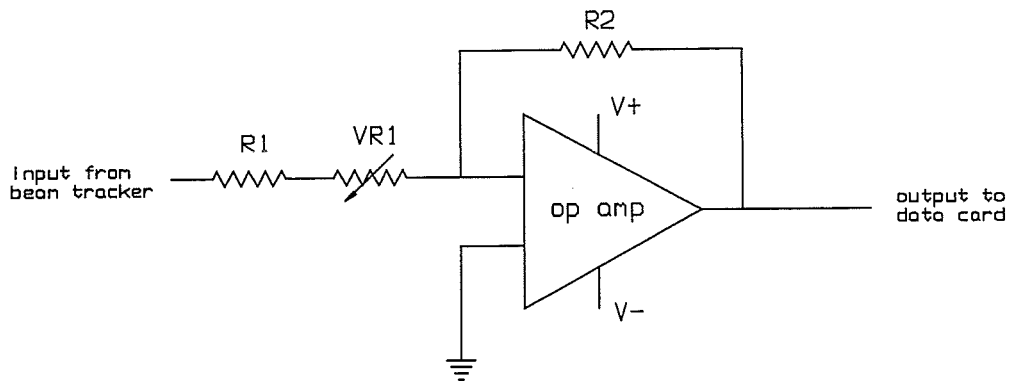


Figure A.6 - The beam tracker to Lab-PC Plus attenuating circuitry

The beam tracker outputs (± 10 V) were attenuated to ± 5 V for input to the Lab-PC Plus I/O card through 741 operational amplifier IC's configured as inverting amplifiers with half gain.

$$Gain = V_o = -V_i \frac{R_2}{R_1 + VR_1}$$

For half gain the following resistance values were used :-

$$R_1 = 19 \text{ k}\Omega, VR_1 = 2 \text{ k}\Omega, R_2 = 10 \text{ k}\Omega$$

The variable resistance, VR_1 enabled the gain to be accurately tuned and calibrated.

Appendix E

The Modified Single-Axis Robot - Slave Control Software

The software controllers for the robot arm were developed using Borland Turbo 'C' on an IBM 80486 DX 33 MHz PC equipped with an AMPLICON PC30B D/A, A/D interface board. The controller used only two of several I/O channels present on the board. The output channel to the actuator amplifier was 'DAC3', corresponding to the pin 1 on the connector of the board; the input channel from the beam tracker was 'CH1', corresponding to the pin 8 on the connector.

The choice of the input channel does affect the behaviour of the program because of the different resolution of the 4 DA channels: DAC0 and DAC1 are connected to 12-bit D/A converters whilst DAC2 and DAC3 are connected to the 8-bit D/A converters; changing resolution involves changing the way of coding voltage values in the digital code used by the board.

The I/O channel is selected adding a '#define' statement on the top of the program after the '#include "nando.h"' which is always required, so the top part of a general program should appear as: -

```
#include    "nando.h"  
#define    OUTPUT    outputchannel  
#define    INPUT    inputchannel
```

Where *outputchannel* and *inputchannel* numbers are between 0-3 and 0-15 respectively. To change the system configuration attention must be paid to the right setting of the board jumpers. For ± 10 V I/O settings jumper settings are :-

Output channels :-

DAC1: Jumper1-out, Jumper2-in; DAC0: Jumper3-in, Jumper4-out; DAC3: Jumper5-out,

Jumper6-in; DAC2: Jumper7-in, Jumper8-out.

Input channels :-

Jumper22-in; Jumper23-out; Jumper24-out; Jumper25-in.

The software was written as a series of functions under the library heading 'NANDO.LIB' which includes :-

PID control -

pid - which allows the user to choose the values of the gains

fixpid - using fixed values for the gains (the best found)

PD control -

pd - which allows the user to choose the values of the gains

fixpd - using fixed values for the gains (the best found)

Each function is described together with a program to drive the control functions.

Description of the function-library NANDO.LIB

PID control

Name pid

Usage double pid(double error, double *gain, int f)

Description This function performs a PID control algorithm using the array *gain* as gains of the pid loop. The integration involved in the pid loop is carried out using the trapezoidal approximation; the derivation is performed using four-point central-difference technique. To keep memory of the last four values of the error, a sort of circular queue is used; it is implemented in the array *double err[4]*. The index of the actual error in the array is the static variable *int time*, so the previous error is obtained, using the modulus operator, as *err[(time+3)%4]*, the one before the previous as

err[(time+2)%4]. The function provide to desaturate the integral when required. The value *f* is used as a flag when the function participate to simulation, otherwise it must be set to the value 1.

Return value The output of the PID loop.

PID with fixed gains

Name fixpid

Usage double fixpid(double error)

Description This function presents exactly the same features of pid, but the values of the gains are not changeable. The default value is the best found in this project.

Return value The output of the PID loop

PD control

Name pd

Usage double pd(double error, double *gain, int f)

Description This function performs the PD control algorithm. As for the other algorithm the flag *f* must be set to 1.

Return value The output of the control loop.

PD with fixed gains

Name fixpd

Usage double fixpd(double error)

Description The values of the constants are fixed to the best ones evaluated experimentally.

Return value The output of the PD loop.

*****THE LIBRARY NANDO.LIB*****

```
void  prepare_board() /* sets the PC30B */
{
    int  i;
    void  stopmotor();

    set_base(B_ADD);
    set_type(THIRTY_B);
    init();
    for(i=1; i<=15; i++)
        set_gain(i, 0);
    stopmotor();
    clrscr();
}

double  get_position() /* to read the error sensed by the camera */
{
    int    dig_error;
    double volt_error;

    ad_in(INPUT, &dig_error); /* reading */
    volt_error=(dig_error-2048.0)/204.8; /* Translation from digital-code to voltage */

    return( volt_error );
}

void  stopmotor() /* produce the 0-volts signal */
{
    da_out(OUTPUT, 128 << 4);
}

double  pd(error, gain, f)
double  error;
double  gain[];
int  f;
{
    int    temp;
    double  derivative;
    static double old_error = 0, signal = 0;

    if(f == 0)
        old_error = 0;
    derivative = error - old_error;

    signal = gain[0]*signal + gain[1]*error + gain[2]*derivative;

    if(signal > 9.5)
        signal = 9.5;
    else if(signal < -9.5)
        signal = -9.5;
    old_error = error;
    return(signal);
}
```

```

double pid(error, gain, f)
double error;
double gain[];
int f;
{
    double f_derivative, f_proportional;
    static double signal = 0, f_integral = 0;
    static int time = 3;

    if( f == 0 )
    {
        f_integral = 0;
        err[0] = 0.0; err[1] = 0.0; err[2] = 0.0; err[3] = 0.0;
        time = 3;
    }

    time = (time + 1) % 4;
    err[time] = error;
    f_derivative = (err[time]+3*err[(time+3)%4]-3*err[(time+2)%4]-err[(time+1)%4]);
    f_integral = f_integral + 0.5*(err[time] + err[(time+3)%4]);
    f_proportional = err[time];
    signal = gain[0]*f_proportional + gain[1]*f_integral + gain[2]*f_derivative;

    if(signal > 9.5)
        signal = 9.5;
    else if(signal < -9.5)
        signal = -9.5;
    return(signal);
}

```

```

double fixpid(error) /* pid using default gains */
double error;
{
    double f_derivative, f_proportional;
    static double signal = 0, f_integral = 0;
    static int time = 3;

    time = (time + 1)%4;
    err[time] = error;
    f_derivative = (err[time]+3*err[(time+3)%4]-3*err[(time+2)%4]-err[(time+1)%4]);
    f_integral = f_integral + 0.5*(err[time] + err[(time+3)%4]);
    f_proportional = err[time];
    signal = PID1*f_proportional + PID2*f_integral + PID3*f_derivative;

    if(signal > 9.5)
        signal = 9.5;
    else if(signal < -9.5)
        signal = -9.5;
    return(signal);
}

```

```

double fixpd(error)
double error;
{

```

```

int      temp;
double   derivative;
static double old_error = 0, signal = 0;

derivative = error - old_error;

signal = PI1*signal + PI2*error + PI3*derivative;

if(signal > 9.0)
    signal = 9.0;
else if(signal < -9.0)
    signal = -9.0;
old_error = error;
return(signal);
}

```

*****THE HEADER FILE NANDO.H*****

```

# define tcc
# include <stdio.h>
# include <conio.h>
# include <math.h>
# include <pc30.h>
# define B_ADD      0x700
# define THIRTY_B  2
# define INPUT      1
# define OUTPUT     3
# define PID1      0.6
# define PID2      0.00015
# define PID3      10
# define PI1       0.6
# define PI2       0.35
# define PI3       2.45
# define EPS       0.00001      /* solution-accuracy required */
# define ALSTEP    0.001        /* first change for alpha */
# define MAXNUMITER 20
# define NUM_OF_PAR 3
# define SIMULATION_SAMPLES 30000

double err[4] = { 0.0, 0.0, 0.0, 0.0 };

double startposition = 0;

double get_position(); /* Returns the error signal coming from the camera */

double fixpd(); /* PD algorithm using fixed values for the gains */

double fixpid(); /* PID algorithm using fixed values for the gains */

void stopmotor(); /* Sends the stop signal to the actuator */

void prepare_board(); /* Sets the PC30B */

double pid( double error, double *gain, int f);

double pd( double error, double *gain, int f);

```

Appendix F

The Dual-Axis Robot

Slave control algorithms - P, PD, PID and PDF software listing

This program includes P, PD, PID and PDF functions for both X and Y axes. When used, the inappropriate control functions are commented out.

```
# define tcc
# include <stdio.h>
# include <dos.h>
# include <math.h>
# include <pc30.h>
# include <pc30.h>
# include "c:\pc30\libutil\reg_30.h"
# include <time.h>
# include <bios.h>
# include <graphics.h>
#include <conio.h>

# define B_ADD 0x700
# define THIRTY_B 2
# define INPUT 1
# define OUTPUT 3

#ifdef tpc
static int board_num;
#else
static int board_num = 0;
#endif

// This initialises the I/O card and must be done before anything else

void prepare_board()
{   int i;
    set_base(B_ADD);
    set_type(THIRTY_B);
    init();
    for(i=1;i<=15; i++)
        set_gain(i, 0);
}

double integral_v[7]={0},integral_h[7]={0}; // Arrays for integrals

// PID; PD and PDF are all listed here

double controlvert(double error)
{   int k;
```

```

double derivative;
static double old_error=0.0, integ=0.0,signal;
derivative = error - old_error;

integ=0.0;
for(k=0;k<4;k++)
{   integral_v[k]=integral_v[k+1];
    integ+=integral_v[k];
}
integ/=4.0;           // Integral becomes 1/4 of the sum of the last 4 errors
integral_v[k]=error;

// The negative multiplier here just changes polarity
// PID control signal           // Comment if not being used
signal = (-0.1*error + 0.3*derivative - 0.05*integ);
// Stable values for PID

// PD control signal           // Comment if not being used
signal = (-0.15*error - 0.2*derivative);

// PDF control signal           // Comment if not being used
signal = (-0.3*integ + 0.2*error);

// P control signal           // Comment if not being used
signal = - 0.35*error;

    if(signal > 9.5)           // Limits the maximum control signal
        signal = 9.5;
    else if(signal < -9.5)
        signal = -9.5;
old_error = error;
//printf("%f\n",signal);
return(signal);
}

double controlhor(double error)
{   int k;
    double derivative;
    static double old_error=0.0,integ=0.0,signal;
    derivative = error - old_error;
    integ=0.0;
    for(k=0;k<4;k++)
    {   integral_h[k]=integral_h[k+1];
        integ+=integral_h[k];
    }

    integ/=4.0;
    integral_h[k]=error;

// PID control signal
signal = (-0.1*error + 0.3*derivative - 0.05*integ);

// PD control signal
signal = (-0.15*error + 0.2*derivative);

// PDF control signal
signal = (-0.3*integ + 0.2*error);

```

```

// P control signal
signal = - 0.35*error);

if(signal > 9.5)
    signal = 9.5;
else if(signal < -9.5)
    signal = -9.5;
old_error = error;
return(signal);
}

double get_positionvert()
{
    int dig_error;
    double volt_error;
    ad_in(INPUT, &dig_error);
    volt_error = (dig_error-2048.0)/204.8; // Converts the 12 bit integer into a double
    return(volt_error);
}

double get_positionhor()
{
    int dig_error;
    double volt_error;
    ad_in(0, &dig_error);
    volt_error = (dig_error-2048.0)/204.8;
    return(volt_error);
}

main()
{
    clock_t start, end;
    char key=0;
    int i, digital_code;
    long loop=0;
    double driver_signal, error;
    void prepare_board();
    float drive=0.0;
    prepare_board();
    clrscr();
    da_out(OUTPUT, 128 << 4); // Write zero volts to the outputs
    da_out(2, 128 << 4);
    start=clock();
    while (!kbhit()) // Do until key hit
    {
        loop++;
        driver_signal = pdfcontrolvert(get_positionvert());
        digital_code = floor(128.0-(driver_signal*12.8));
        digital_code = digital_code << 4;
        da_out(OUTPUT, digital_code);

        driver_signal = pdfcontrolhor(get_positionhor());
        digital_code = floor(128.0-(driver_signal*12.8));
        digital_code = digital_code << 4;
        da_out(2, digital_code);
    }

    end=clock();
    printf("The time was: %f\n", (end - start) / CLK_TCK);
    printf("\nThe nmbr of loops: %i\n", loop);
}

```

```

    da_out(OUTPUT, 128 << 4);
    da_out(2, 128 << 4);
    printf("DONE");
    getch();

    return(0);
}

```

The PC-30B 4 Channel Data Recording Program (Korhonen, J., 1995)

Program for recording four data channels simultaneously, 850Hz, 1000 samples. For greater sampling range increase the arrays dig-error and the length of the loops.

```

# define tcc
# include <stdio.h>
# include <dos.h>
# include <math.h>
# include <pc30.h>
# include "c:\pc30\libutil\reg_30.h"
# include <time.h>
# include <bios.h>
#include <conio.h>
#include <stdlib.h>
#include <sys\stat.h>
#include <fcntl.h>
#include <io.h>
# define B_ADD          0x700
# define THIRTY_B 2
#ifdef tpc
static int board_num;
#else
static int board_num = 0;
#endif

void prepare_board();
void prepare_board()
{
    int i;
    set_base(B_ADD);
    set_type(THIRTY_B);
    init();
    for(i=1;i<=15; i++)
        set_gain(i, 0);
}
main()
{
    FILE *out;
    int handle;
    clock_t start, end;
    long loop=0;
    int dig_error[4][1000];
    //int dig_error1[1000];
    int simple;
    int z,k;
    char *string,filename[30];
    float volt_error;
}

```

```

int dec, sign;
clrscr();
prepare_board();
while(kbhit())
    getch();
printf("HIT A KEY TO START");
getch();
start=clock();
k=0;
while (!kbhit())&&loop<1000
{
    while(k<4)
    {
        ad_in(k,&simple);
        dig_error[k+][loop]=simple;
    }
    k=0;
    loop++;
}
end=clock();
printf("The time was: %f\n", (end - start) / CLK_TCK);
printf("\nThe nmbr of loops: %i\n", loop);
printf("\nPLEASE INPUT THE FILENAME\n");
scanf("%s",&filename);
if ((out = fopen(filename, "wt")) == NULL)
{
    fprintf(stderr, "Cannot open output file.\n");
    return 1;
}
loop=0;
k=0;
while(loop<1000)
{
    while(k<4)
    {
        volt_error = ((float)(dig_error[k][loop])-2048.0)/204.8;
        string = ecvt(volt_error, 5, &dec, &sign);
        if(sign!=0)
            fputc('-', out);
        if(dec<0)
        {
            fputc('0', out);
            fputc('.', out);
            for(z=0;z>dec;z--)
                fputc('0', out);
            for(z=0;z<5;z++)
                fputc(string[z],out);
        }
        if(dec==0)
        {
            fputc('0', out);
            fputc('.', out);
            for(z=0;z<5;z++)
                fputc(string[z],out);
        }
        if(dec>0)
        {
            for(z=0;z<dec;z++)
                fputc(string[z],out);
            fputc('.',out);
            for(z=dec;z<5;z++)
                fputc(string[z],out);
        }
        k++;
        if(k<4)
            fputc(9,out);
    }
}

```

```

        if(k==4)
            fputc('\n',out);
    }
    k=0;
    loop++;
}
fclose(out);
return(0);
}

```

Matlab Simulation Programs

Rigid arm model - Proportional control

```

% Motor + Link Control - Rigid arm model - Proportional control
kp=0.5;
kA=1;
kt=21;
kbemf=20.35;
Jeff=0.492;
R=3.4;
μeff=0.39;

fprintf('Model of single joint manipulator\n\n\n')
fprintf(' Direct system :          \n')
fprintf('      omega(s)          Km          \n')
fprintf(' G(s)=----- = ----- \n')
fprintf('      Volt(s)  (Jeff*R)s + (Kt*Kbemf+R*μeff) \n')

num= Kt ;
den=[(Jeff*R) (Kt*Kbemf+R*μeff)];
printsys(num, den,'s');
fprintf(' \n\n Kp(1) controller in series :\n\n')

[num1,den1]=series(Kp*KA, 1, num, den);
printsys(num1, den1, 's');
[num2,den2]=series(num1, den1, 1, [1 0]);
printsys(num2, den2, 's');
[num3, den3]=feedback(num2, den2, 3000, 1);
printsys(num3, den3, 's');
[num4,den4]=series(3000, 1, num3, den3);
printsys(num4, den4, 's');

t=0:0.001:0.3;
[y,x]=lsim(num4, den4, ones(length(t),1)*0.003, t);
tt=t';
fid=fopen('robotpf.txt','w');
for I=1:300
fprintf(' \n\n Kp(1) controller in series :\n\n')
[num1,den1]=series(Kp*KA, 1, num, den);
printsys(num1, den1, 's');

[num2,den2]=series(num1, den1, 1, [1 0]);
printsys(num2, den2, 's');
[num3, den3]=feedback(num2, den2, 3000, 1);

```

```

printsys(num3, den3, 's');
[num4,den4]=series(3000, 1, num3, den3);
printsys(num4, den4, 's');

t=0:0.001:0.3;
[y,x]=lsim(num4, den4, ones(length(t),1)*0.003, t);
tt=t';
fid=fopen('robotpf.txt','w');
for I=1:300

fprintf(fid,'%10.5f %10.5f\n',tt(i),y(i));
end
fclose(fid);
lsim(num4, den4, ones(length(t),1)*0.003,t)
[End of file]

```

Rigid arm model - PD control

```

% Motor + Link Control - Rigid arm model - PD control.
Kp=0.5;
KA=1;
Kd=0.002;
Kt=21;
Kbemf=20.53;
Jeff=0.492;
R=3.4;
μeff=0.39;

fprintf('Model of single joint manipulator\n\n\n')
fprintf(' Direct system : \n')
fprintf('      omega(s)          Km          \n')
fprintf(' G(s)=-----= ----- \n')
fprintf('      Volt(s)  (Jeff*R)s + (Kt*Kbemf+R*μeff) \n')

num= [KA*Kt*Kd KA*Kt*Kp] ;
den=[(Jeff*R) (Kt*Kbemf+R*μeff)];
printsys(num, den,'s');

[num1,den1]=series(num, den, 1, [1 0]);
printsys(num1, den1, 's');
[num2, den2]=feedback(num1, den1, 3000, 1);
printsys(num2, den2, 's');
[num3,den3]=series(3000, 1, num2, den2);
printsys(num3, den3, 's');

t=0:0.001:0.3;
[y,x]=lsim(num3,den3, ones(length(t),1)*0.003,t);
tt=t';
fid=fopen('robotpdf.txt','w');
for I=1:300
fprintf(fid, '%10.5f %10.5f\n',tt(i),y(i));
end
fclose(fid);
lsim(num3, den3, ones(length(t),1)*0.003, t)
[End of file]

```

Appendix G

Published Work

Journal - Copy attached

- [1] Lewis, J., Gill, R. & White, A.: 'Heavy load robot', Industrial Robot, Vol.19, No.4, pp. 28-31, 1992.

Conference

- [2] Lewis, J., Gill, R. & White, A.: 'The development of a long reach flexible robotic arm', Proceedings of the 9th International CAD/CAM, Robotics and Factories of the Future Conference, Newark, New Jersey, USA., August 18-20 1993.
- [3] Lewis, J., Gill, R. & White, A.: "Development of an optical system for robot control", Proceedings of the IEEE/RSJ International Conference on Intelligent Robots and Systems, Yokohama, Japan, pp. 723-726, July 26-30 1993.
- [4] Lewis, J., Gill, R. & White, A.: 'Active optical sensing for the control of flexible robots', Proceedings of the 9th National Conference on Manufacturing Research, Bath, September 7th-9th, 1993.
- [5] Lewis, J., Gill, R. & White, A.: 'An optical end-point position control system for long reach, flexible link robots', 11th ISPE/IEE/IFAC International Conference on CAD/CAM, Robotics and Factories of the Future. Universidad de Pereira, Pereira, Colombia, August 1995.